



University  
of Glasgow

Chintapalli, Venkateswara Rao (2012) *An integrative and systems biology approach to Drosophila melanogaster transcriptomes*. PhD thesis  
<http://theses.gla.ac.uk/3361/>

Copyright and moral rights for this thesis are retained by the author

A copy can be downloaded for personal non-commercial research or study, without prior permission or charge

This thesis cannot be reproduced or quoted extensively from without first obtaining permission in writing from the Author

The content must not be changed in any way or sold commercially in any format or medium without the formal permission of the Author

When referring to this work, full bibliographic details including the author, title, awarding institution and date of the thesis must be given.

**An Integrative and Systems Biology Approach  
to *Drosophila melanogaster* Transcriptomes**

A thesis submitted for the degree of  
Doctor of Philosophy at the University of Glasgow

By

Venkateswara Rao Chintapalli

Institute of Molecular, Cell and Systems Biology  
College of Medical, Veterinary and Life Sciences

University of Glasgow

Glasgow

G12 8QQ

UK

January 2012

## Summary

The availability of fully sequenced genomes of the model organisms including *Drosophila*, and their subsequent annotation has afforded seamless opportunities for reverse genetics in a complex model organism. With the advent of DNA microarrays to assay the levels of tens of thousands of genes in a single sample, functional genomics has been significantly aided to understand the functions in systems context. These microarrays have been employed predominantly on the RNA samples that are extracted from the whole animals for example at different developmental stages or in response to external stimuli. However, these approaches relied on the expression patterns that represent the sum of transcription coming from all the organs, which do not estimate the tissue-specificity of transcription.

The purpose of this thesis is to provide tissue-specific transcriptomes of *Drosophila melanogaster* that were generated as part of the large FlyAtlas project using Affymetrix *Drosophila* GeneChips® (or microarrays). These chips, one at a time interrogate the levels of 18,500 transcripts (that represent all known genes) using 18,880 distinct probe sets in a single, total RNA sample. For each tissue, four biological replicates were analysed using the chips and the normalised signal intensities were obtained that represent the relative levels of mRNA expression. Using the transcriptomes, a general analysis was performed for potential novel insights into tissue-specific functions (Chintapalli et al., 2007) (Chapter 3). Then, a comparative analysis of epithelial tissues was performed to understand how the epithelia are organised in terms of their transcriptomes (Chapter 4).

The Malpighian tubules are the *Drosophila* epithelial counterparts of the human kidney. They show asymmetric organisation in the body cavity. FlyAtlas segment-specific tubule transcriptomes allowed the comparison of their potential functional similarities and differences, thus to understand the asymmetry in function (Chapter 5)(Chintapalli, 2012). This identified a human Best vitelliform macular dystrophy (BVMD) disease homolog, *Best2* in only the anterior pair of tubules that have the morphologically and functionally distinct enlarged initial (or distal) segment, a storage organ for  $\text{Ca}^{2+}$ . *Bestrophins* were accordingly selected as candidate genes to analyse organismal functions, and thus to

validate previous two theories that implicated bestrophins as  $\text{Ca}^{2+}$ -activated  $\text{Cl}^-$  channels and/or  $\text{Ca}^{2+}$  channel regulators (Chapter 6).

The confocal microscopy analysis of bestrophin YFP fusion proteins revealed interesting and novel localisations of bestrophins, in that Best1 was found in the apical plasma membranes, Best2 localised to peroxisomes, Best3 and Best4 were found intracellular. The salt survival analysis showed that Best1 is essential in regulating extra salt levels in the body. Furthermore, the fluid secretion analysis showed Best1's potential role in  $\text{Ca}^{2+}$ -dependent  $\text{Cl}^-$  function. Interestingly, the flies with reduced levels of *Best2* expression showed increased ability to survive on extra salt food; the basis for this was investigated further in Chapter 7. *Best2* was also found abundant in the eyes than anywhere else in the head. A comparative analysis of anterior tubule- and eye-specific transcriptomes revealed a potential overlap of  $\text{Ca}^{2+}$  signaling components, in that the PLCB signaling was one.

A neuropeptide  $\text{Ca}^{2+}$  agonist, *capa1* evoked secondary cytosolic  $\text{Ca}^{2+}$  responses were found high in *Best2* knockdowns. A quantitative PCR (qPCR) analysis of candidate  $\text{Ca}^{2+}$  signaling and homeostasis genes in *Best2* mutants revealed their gene expression upregulation, under control-fed and salt-fed conditions than their wildtype controls, fed on similar diet regimes. The *norpA* that encodes PLCB was found significantly enriched in the mutants. *Cyp6a23* is another gene that was highly upregulated in *Best2* mutants; it is a *Drosophila* homologue of human *Cyp11b*, a  $\text{Ca}^{2+}$ -responsive gene implicated in renal salt wasting. Upon the downregulation of *Cyp6a23*, flies became sensitive to salt diet feeding. Other genes investigated and found to be upregulated in the mutants include *transient-receptor-potential (trp)*  $\text{Ca}^{2+}$  channel and *retinal degeneration C (rdgC)*. Together, these results strongly suggest Best2 as a potential  $\text{Ca}^{2+}$  channel regulator, and provide fascinating insight into bestrophin function.

Peroxisomal localisation of Best2 in line with the implication that peroxisomes act as dynamic regulators of cell  $\text{Ca}^{2+}$  homeostasis led to another aspect of the project (Chapter 8). This study identified two *peroxins* that are most abundant in the tubules and play essential roles in the novel cyclic nucleotide-regulated peroxisomal  $\text{Ca}^{2+}$  sequestration and transport pathway and that are detrimental for peroxisome biogenesis and proliferation.

# Table of Contents

Summary .....	1
Table of Contents .....	3
List of Tables.....	8
List of Figures.....	9
Contributions from this work .....	11
Preface.....	12
Acknowledgements.....	13
Definitions.....	15
1. Introduction.....	21
1.1 Systems Biology .....	21
1.1.1 Functional genomics for systems biology .....	23
1.1.2 A case for model organisms use in functional genomics.....	24
1.1.3 DNA microarrays for functional genomics .....	25
1.1.4 Where integrative physiology meets systems biology .....	26
1.2 <i>Drosophila</i> as a model organism.....	27
1.2.1 Introduction and History .....	27
1.2.2 Reverse Genetics .....	28
1.2.2.1 GAL4/UAS system.....	28
1.2.3 Transgenesis.....	29
1.3 Tubules as a model epithelium in transport and signaling .....	32
1.3.1 General mechanisms of second messenger signaling.....	35
1.3.1.1 Second messenger signaling in the tubules .....	37
1.3.1.2 Second messenger signaling in tubules via capa peptides.....	38
1.3.1.3 The final targets of capa signaling in tubules .....	38
1.3.1.4 Second messenger signaling in tubules via Drosokinin .....	40
1.3.1.5 Ca <sup>2+</sup> handling by tubules.....	40
1.3.2 Weiczorek model for fluid secretion by tubules .....	41
1.3.3 Neuroendocrine control of tubule fluid secretion .....	43
1.4 Molecular Physiology of Cl <sup>-</sup> ion transport.....	44
1.4.1 Cl <sup>-</sup> channels.....	45
1.4.2 Cl <sup>-</sup> channel functions and associated channelopathies.....	47
1.4.3 CaCCs.....	48
1.4.3.1 Mechanisms of Ca <sup>2+</sup> -dependent Cl <sup>-</sup> secretion in epithelia.....	49
1.4.3.2 Ca <sup>2+</sup> -dependent Cl <sup>-</sup> secretion in epithelia .....	51
1.4.3.3 Disease relevance of CaCCs .....	52
1.4.3.4 Functional features and Molecular identity of CaCCs .....	52
1.4.3.4.1 ClCA family.....	53
1.4.3.4.2 Tweety family .....	54
1.4.3.4.3 Bestrophin family .....	54
1.4.3.4.4 Anoctamins.....	54
1.5 Peroxisome dynamics in the living organism .....	55
1.5.1 Peroxisome biogenesis.....	56
1.5.2 How is peroxisome number controlled? .....	57
1.6 Project aim .....	59
2. Materials and Methods.....	61
2.1 Fly stocks .....	61
2.2 Normal fly husbandry .....	63
2.3 Tissue dissections.....	63
2.4 Total RNA extraction.....	65
2.5 Complementary DNA (cDNA) synthesis .....	65

2.6	Oligonucleotide (primer) synthesis .....	66
2.7	Polymerase chain reaction (PCR).....	66
2.7.1	Standard PCR.....	66
2.7.2	Pfu-based Herculase II Fusion polymerase PCR .....	67
2.8	Quantitative reverse-transcriptase PCR (qPCR) .....	67
2.9	Agarose gel electrophoresis .....	69
2.10	PCR/Gel purification .....	69
2.11	Quantification of nucleic acids.....	69
2.12	Quality control of nucleic acids .....	70
2.13	Affymetrix microarrays.....	70
2.14	Microarray data analysis .....	72
2.14.1	Data processing.....	72
2.14.2	Normalisation .....	72
2.14.3	Grouping.....	72
2.14.4	Interpretation.....	72
2.14.5	Quality control.....	73
2.14.6	Principal Component Analysis (PCA).....	73
2.14.7	Statistical analysis.....	75
2.14.8	Functional annotation .....	75
2.15	Fold change (FC) analysis .....	75
2.16	Ingenuity pathway analysis (IPA) .....	75
2.17	Molecular cloning .....	76
2.17.1	Competent bacterial strains and plasmids.....	76
2.17.2	Gateway® cloning .....	77
2.17.2.1	Primer design and PCR amplification .....	77
2.17.2.2	Entry clones .....	77
2.17.2.3	Destination vectors .....	77
2.17.2.4	Gateway® recombination using LR-clonase.....	77
2.17.3	Transformation of <i>E. coli</i> .....	77
2.17.4	Purification of plasmid DNA.....	78
2.17.5	Validation of cloning products.....	78
2.17.5.1	PCR.....	78
2.17.5.2	Restriction enzyme digestion .....	78
2.17.5.3	Sequencing.....	78
2.17.6	Normal cDNA constructs .....	78
2.17.7	YFP fusion cDNA constructs .....	79
2.17.8	Double-stranded RNA constructs .....	79
2.17.9	DES® constructs .....	79
2.17.10	Dual promoter constructs for in situ hybridization.....	80
2.17.11	Normal cloning procedure .....	80
2.18	<i>Drosophila</i> S2 cell culture .....	81
2.18.1	Passaging .....	81
2.18.2	Transient transfection .....	81
2.19	Peroxisome Isolation.....	82
2.19.1	Tissue preparation .....	82
2.19.2	Gradient centrifugation .....	82
2.20	Protein analysis.....	83
2.20.1	Extraction .....	83
2.20.2	Bradford assay .....	83
2.20.3	SDS-PAGE separation.....	83
2.20.4	Western blotting.....	84
2.21	Production and purification of antibodies .....	84
2.21.1	Production.....	84

2.21.2 Purification .....	85
2.21.2.1 Isolation of IgG fraction from immune-serum .....	85
2.21.2.2 Preparation of affinity columns.....	85
2.21.2.3 Affinity purification of antibodies.....	86
2.22 Immunocytochemistry (ICC) .....	87
2.22.1 ICC of S2 cells.....	87
2.22.2 ICC of intact <i>Drosophila</i> tissues .....	87
2.23 Imaging .....	88
2.24 mRNA <i>in situ</i> hybridization .....	88
2.25 Fluid secretion assay .....	90
2.26 $[Ca^{2+}]_i$ measurements using recombinant aequorin.....	91
2.27 Diet regimes .....	92
2.28 Metabolomic analysis .....	93
2.28.1 Metabolite extraction.....	93
2.28.2 Liquid chromatography (LC)-Mass spectrometry (MS).....	93
2.28.3 Data capture and analysis.....	94
3. FlyAtlas, a gene expression database .....	95
Summary .....	95
3.1 Introduction .....	95
3.2 Results .....	97
3.2.1 Tissue-specific transcriptomes .....	97
3.2.2 Meta-analysis.....	100
3.2.3 New transcription units.....	100
3.2.4 An ontogenetic perspective.....	101
3.2.5 Surprising expression.....	103
3.2.6 Organotypic disease models .....	104
4. A transcriptomic view on epithelial structure and function .....	110
Summary .....	110
4.1 Introduction .....	111
4.2 Results .....	113
4.2.1 Differential expression and coregulation .....	114
4.2.2 Epithelial signatures .....	117
4.2.2.1 Salivary glands .....	118
4.2.2.2 Malpighian Tubules .....	123
4.2.2.3 Midgut .....	127
4.2.2.4 Hindgut.....	130
4.2.2.5 Functional compartmentalisation of the epithelia .....	132
4.2.3 Adult-specific functions .....	134
4.2.4 Direct comparison: adult tissue vs. larval tissue .....	135
4.2.5 Ingenuity pathway analysis (IPA).....	137
4.2.5.1 Biological functions.....	137
4.2.5.2 Toxicology functions .....	139
4.2.5.3 Canonical pathways .....	141
4.2.5.4 Molecular networks.....	142
4.3 Discussion .....	144
4.3.1 Limitations of the IPA.....	148
4.4 Conclusion .....	149
5. Microarray analysis of positional asymmetry of renal tubules in <i>Drosophila</i> ...	150
Summary .....	150
5.1 Introduction .....	151
5.2 Results .....	153

5.2.1	Left vs. right: genes upregulated in right-side tubules suggest an ..... interplay with the gut .....	153
5.2.2	A mechanism for asymmetric Ca <sup>2+</sup> handling .....	158
5.3	Discussion .....	159
6.	Functional studies on <i>Drosophila</i> bestrophins .....	161
	Summary .....	161
6.1	Bestrophins as candidate CaCCs .....	162
6.1.1	Identification in human disease .....	162
6.1.2	Structural aspects .....	164
6.1.3	Cl <sup>-</sup> channel function of bestrophins .....	166
6.1.4	Bestrophins as CaCCs .....	167
6.1.5	Physiological functions of bestrophins .....	168
6.1.6	<i>Drosophila</i> bestrophins .....	169
6.2	Results .....	171
6.2.1	Bestrophins in <i>Drosophila melanogaster</i> .....	171
6.2.2	Gene expression .....	171
6.2.3	<i>Best1</i> & <i>Best2</i> are differentially expressed in Malpighian tubules ..	175
6.2.4	<i>Best1</i> & <i>Best2</i> show differential localisation both <i>in vitro</i> and <i>in vivo</i> . .....	177
6.2.4.1	<i>In vitro</i> localisation.....	178
6.2.4.2	<i>In vivo</i> localisation.....	180
6.2.5	Making of transgenic fly lines and their validation .....	183
6.2.6	Salt and fluid regulation.....	185
6.2.6.1	<i>Best1</i> .....	185
6.2.6.2	<i>Best2</i> .....	189
6.2.7	<i>Best3</i> & <i>Best4</i> show high mRNA expression in the testis.....	191
6.2.8	<i>Best3</i> and <i>Best4</i> localisations .....	191
6.2.8.1	<i>In vitro</i> localisation.....	191
6.2.8.2	<i>In vivo</i> localisation.....	192
6.3	Discussion .....	194
6.4	Conclusion .....	201
7.	Further studies on <i>Drosophila</i> bestrophin 2 .....	203
	Summary .....	203
7.1	What is the link between increased secondary Ca <sup>2+</sup> elevations in <i>Best2</i> ... mutants and salt resistance? .....	205
7.2	Results .....	206
7.2.1	Further validations of <i>Best2</i> transgenics .....	206
7.2.2	<i>Best2</i> is an essential gene in <i>Drosophila</i> .....	207
7.2.2.1	<i>Best2</i> is confined to the Ca <sup>2+</sup> storing initial segment .....	208
7.2.3	<i>Best2</i> is highly abundant in the eyes .....	209
7.2.4	<i>Best2</i> mediates organismal oxidative stress responses .....	210
7.2.5	<i>Best2</i> regulates stimulated [Ca <sup>2+</sup> ] .....	211
7.2.6	Characterisation of <i>Best2</i> mutants.....	213
7.2.7	Ca <sup>2+</sup> -dependent gene expression is changed in <i>Best2</i> mutants under .. stress .....	215
7.3	Discussion .....	219
7.4	Conclusions .....	224
8.	Cell-specific peroxisome dynamics in the living organism .....	225
	Summary .....	225
8.1	Novel roles of peroxisomes in Ca <sup>2+</sup> homeostasis .....	227
8.1.1	<i>Drosophila</i> Malpighian (renal) tubules as an <i>in vivo</i> model to study .... peroxisome Ca <sup>2+</sup> homeostasis .....	229
8.1.1.1	Morphology and functional domains .....	229

8.1.1.2	Tubule peroxisomes .....	229
8.1.2	Aequorin probes for $[Ca^{2+}]$ measurements in vivo .....	232
8.1.3	Purpose of this study.....	233
8.2	Results .....	234
8.2.1	Renal peroxisomal targeting and validation of aequorin probes ....	234
8.2.1.1	Immunocytochemical localisation <i>in vitro</i> .....	234
8.2.1.2	Immunocytochemical localisation <i>in vivo</i> .....	235
8.2.1.3	$[Ca^{2+}]_{\text{perox}}$ measurements in S2 cells.....	237
8.2.1.4	$[Ca^{2+}]_{\text{perox}}$ measurements in tubules.....	239
8.2.2	Identification of novel peroxins <i>CG11919</i> and <i>CG13827</i> as the .....	
	<i>Drosophila</i> orthologues of human <i>PEX6</i> and <i>PEX11</i> .....	243
8.2.2.1	Renal peroxins are functional in adult tubules.....	245
8.2.2.1.1	Cell-specific <i>G11919</i> and <i>CG13827</i> knockdown depletes.....	
	peroxisomes and increases peroxisome abundance respectively in.....	
	tubules .....	245
8.2.2.1.2	Cell-specific renal peroxin knockdown deregulates $[Ca^{2+}]_{\text{perox}}$ ..	
	buffering .....	247
8.2.3	Identification of novel peroxisomal $Ca^{2+}$ sequestration and transport .	
	pathway in tubules.....	248
8.2.3.1	cGMP regulates $[Ca^{2+}]_{\text{perox}}$ buffering .....	249
8.2.3.1.1	Peroxisomes buffer $Ca^{2+}$ in the course of sustained $[Ca^{2+}]_{\text{cyto}}$ ....	
	elevations .....	249
8.2.3.1.2	Peroxisomes uptake $Ca^{2+}$ in response to external cGMP .....	250
8.2.3.1.3	Downregulation of <i>PDE1c</i> , a $Ca^{2+}$ /calmodulin-dependent PDE .	
	induces peroxisomal $Ca^{2+}$ uptake.....	250
8.2.3.1.4	Zaprinast, a PDE inhibitor increases stimulated peroxisomal ..	
	$Ca^{2+}$ uptake .....	250
8.2.3.1.5	<i>Best2</i> knockdown increases peroxisome $Ca^{2+}$ uptake .....	251
8.2.3.2	Spherite formation was affected in <i>CG13827-RNAi</i> knockdowns ..	
	.....	252
8.3	Discussion .....	253
8.1.1	Renal peroxins .....	255
8.3.1	A mechanism for $[Ca^{2+}]_{\text{perox}}$ buffering and $Ca^{2+}$ spherites.....	257
8.3.2	The significance of $Ca^{2+}$ in terms of peroxisome function.....	259
8.4	Conclusion .....	260
9.	General discussion and Future work .....	262
9.1	General discussion.....	262
9.1.1	FlyAtlas .....	262
9.1.2	Epithelial transcriptomes .....	263
9.1.3	Renal asymmetry in <i>Drosophila</i> .....	263
9.1.4	Functional studies on bestrophins and the identification of <i>Best2</i> as a	
	modulator of $Ca^{2+}$ signaling and homeostasis .....	264
9.1.5	Peroxisome dynamics in the living organism .....	265
9.2	Future work .....	266
Appendices	.....	268
References	.....	275

## List of Tables

Table 2-1 Fly stocks used in this study. ....	61
Table 2-2 FlyAtlas tissue descriptions. ....	63
Table 2-3 Typical cyclic conditions for PCR. ....	67
Table 2-4 <i>Pfu</i> -based Herculase II fusion polymerase PCR reaction mix and ..... protocol. ....	67
Table 2-5 Fly strains and plasmids used. ....	76
Table 2-6 Antibodies used for western blotting and immunocytochemistry. ....	86
Table 3-1 Genes that show extreme specificity of expression and that serve to ... validate the quality and discrimination of the data set. ....	98
Table 3-2 Genes expressed uniquely in specific tissues. ....	99
Table 3-3 Are the genes identified in embryonic tissues by <i>in situ</i> analyses also .. expressed in adult tissues? ..	102
Table 3-4 Some genes that are predominantly expressed in unexpected places. ... .....	103
Table 3-5 <i>Drosophila</i> genes expressed in tissues analogous to those involved in ... human disease. ....	105
Table 4-1 The top 50 genes enriched in salivary glands. ....	120
Table 4-2 The top 50 genes enriched in Malpighian tubules. ....	125
Table 4-3 The top 50 genes enriched in midgut. ....	129
Table 4-4 The top 50 genes enriched in hindgut. ....	131
Table 4-5 GO functional classification of epithelial signatures. ....	133
Table 4-6 The known genes that are consistently enriched across epithelia..	135
Table 4-7 Direct comparison of adult vs larval epithelial tissue. ....	136
Table 4-8 Top 5 IPA networks for each epithelium. ....	144
Table 5-1 Genes with significant expression differences between right (anterior) and left (posterior) tubules. ....	153
Table 6-1 Microarray gene expression data for all four bestrophins in various ..... tissues of <i>Drosophila melanogaster</i> . ....	173
Table 7-1 The fold change (FC) mean differences and associated statistics of the data in Figure 13. ....	217
Table 8-1 Genes related to peroxisomes and their relative abundance in tubules. .....	231
Table 8-2 <i>PEX6</i> and <i>PEX11</i> gene expression across <i>Drosophila melanogaster</i> ..... tissues. ....	244

## List of Figures

Figure 1-1 Schematic of heritable induction of transgenes using GAL4/UAS bipartite system. ....	29
Figure 1-2 Germline transformation of <i>Drosophila</i> . ....	30
Figure 1-3 Tubules of <i>Drosophila melanogaster</i> . ....	34
Figure 1-4 Cyclic nucleotide-dependent signaling components (in intracellular $Ca^{2+}$ mobilisation). ....	36
Figure 1-5 Human G-protein coupled receptor signaling pathway components in tubules. ....	39
Figure 1-6 Peroxisome disorders in humans. ....	55
Figure 1-7 Peroxisome biogenesis machinery. ....	59
Figure 2-1 <i>Best2</i> qPCR product melting curve. ....	68
Figure 2-2 Overview of the GeneChip 3' IVT express labelling assay. ....	71
Figure 2-3 Quality control using hybridization controls. ....	73
Figure 2-4 Quality control of biological replicates of each individual tissue of the FlyAtlas using PCA. ....	74
Figure 2-5 DES® TOPO®TA vector map. ....	80
Figure 2-6 Fluid secretion assay schema. ....	91
Figure 2-7 A schematic of calcium measurements. ....	92
Figure 3-1 <i>Drosophila</i> tissues typically express around half the computed transcriptome. ....	97
Figure 3-2 Evidence for novel transcription units in the <i>Drosophila</i> genome. ....	101
Figure 3-3 Calculating the equation of the fly. ....	108
Figure 4-1 Differential expression of epithelial transcriptomes. ....	115
Figure 4-2 Hierarchical clustering of epithelial transcriptomes. ....	116
Figure 4-3 Number of genes enriched (at least 5-fold) in larvae, adult or in both epithelia. ....	118
Figure 4-4 The commonly enriched genes in both adult and larval epithelia in the adult context. ....	134
Figure 4-5 Mammalian ortholog/paralog mapping of <i>Drosophila</i> epithelial signatures. ....	137
Figure 4-6 Mammalian biological functions enriched in <i>Drosophila</i> epithelia. ..	138
Figure 4-7 Mammalian toxicology functions enriched in <i>Drosophila</i> epithelia. .	140
Figure 4-8 Mammalian canonical pathways enriched in <i>Drosophila</i> epithelia. ..	141
Figure 4-9 Network analysis of epithelial enriched genes. ....	143
Figure 4-10 Network analysis of salivary gland enriched, protein trafficking function. ....	143
Figure 5-1 Internal asymmetry in <i>Drosophila</i> . ....	152
Figure 5-2 Ammonia is high at the back end of the fly. ....	156
Figure 6-1 Human retina in health and disease. ....	163
Figure 6-2 Transmembrane topology of hBest1. ....	165
Figure 6-3 Protein sequence alignment and putative protein sequence features of <i>Drosophila</i> bestrophins. ....	172
Figure 6-4 <i>Best1</i> is more abundant in female than male tubules. ....	176
Figure 6-5 <i>Best2</i> is highly enriched in both male and female anterior tubules than their posterior counterparts. ....	176
Figure 6-6 The absolute quantification of <i>Best1</i> & <i>Best2</i> mRNA expression, in the tubules and heads, using qPCR. ....	177
Figure 6-7 Bestrophin translational fusion constructs. ....	178
Figure 6-8 <i>Best1</i> localisation in S2 cells. ....	179
Figure 6-9 <i>Best2</i> colocalises with native peroxisomal SPoCk-C in S2 cells. ....	179

Figure 6-10 Best1::YFP localises in the apical plasma membrane of the tubules...	181
Figure 6-11 Best2::YFP colocalises with peroxisomal SPoCk-C in tubules.....	182
Figure 6-12 Best2 is peroxisomal <i>in vivo</i> . ....	182
Figure 6-13 Western blot of Best2-Aeq from the protein extracted from the..... purified peroxisomes.....	183
Figure 6-14 qPCR validation of <i>Best1-RNAi</i> and deletion flies. ....	184
Figure 6-15 qPCR validation of <i>Best2-RNAi</i> knockdown.....	184
Figure 6-16 Salt sensitivity of <i>Best1-RNAi</i> knockdowns driven using Act5C-GAL4... .....	187
Figure 6-17 Salt sensitivity of <i>Best1</i> deletion. ....	188
Figure 6-18 Ca <sup>2+</sup> agonist, capa1 inhibits fluid secretion in <i>Best1</i> deletion flies.	188
Figure 6-19 <i>Best2</i> knockdowns show increased salt resistance. ....	190
Figure 6-20 Genomic organisation of <i>Best3</i> & <i>Best4</i> . ....	191
Figure 6-21 Best3::YFP and Best4::YFP show distinct localisations in S2 cells. .	192
Figure 6-22 Best3::YFP and Best4::YFP fluorescence was specifically found in the probable cyst cells of the testis <i>in vivo</i> . ....	193
Figure 6-23 Overexpression of <i>Best3</i> causes morphologically defective testis. .	193
Figure 7-1 Cell-specific knockdown of <i>Best2</i> expression.....	206
Figure 7-2 qPCR validation of <i>Best2</i> overexpression flies. ....	206
Figure 7-3 <i>Best2</i> is an essential gene in <i>Drosophila</i> . ....	208
Figure 7-4 <i>Best2</i> expression is confined to the Ca <sup>2+</sup> storing anterior initial ..... segment.....	209
Figure 7-5 <i>Best2</i> is highly abundant in the eyes. ....	209
Figure 7-6 <i>Best2</i> is antagonistic to survival on oxidative stress. ....	211
Figure 7-7 Best2 modulates secondary Ca <sup>2+</sup> responses. ....	213
Figure 7-8 The genomic location of transposon insertions of <i>Best2</i> .....	214
Figure 7-9 <i>Best2</i> insertional mutants are salt resistant.....	214
Figure 7-10 Flies eat salt food.....	215
Figure 7-11 Best2 regulates Ca <sup>2+</sup> -dependent transcription. ....	217
Figure 8-1 Schema of the peroxisomal targeting construct. ....	234
Figure 8-2 Targeting of Aequorin <sub>perox</sub> and immunocytochemical localisation with . native catalase in S2 cells.....	235
Figure 8-3 Validation of Aequorin <sub>perox</sub> targeting <i>in vivo</i> .....	237
Figure 8-4 [Ca <sup>2+</sup> ] measurements in S2 cells.....	239
Figure 8-5 Basal and stimulated [Ca <sup>2+</sup> ] <sub>perox</sub> in tubules.....	241
Figure 8-6 Comparison of quantitative [Ca <sup>2+</sup> ] <sub>cyto</sub> and [Ca <sup>2+</sup> ] <sub>perox</sub> measurements.	242
Figure 8-7 Typical resting [Ca <sup>2+</sup> ] <sub>cyto</sub> and [Ca <sup>2+</sup> ] <sub>perox</sub> measurements. ....	242
Figure 8-8 Equilibration of cytosolic and peroxisome targeted aequorin. ....	242
Figure 8-9 Renal peroxins are functional. ....	246
Figure 8-10 Mistargeting of Aequorin <sub>perox</sub> in different parts of the tubules in ..... C42-GAL4>CG11919-RNAi knockdowns. ....	246
Figure 8-11 Aequorin <sub>perox</sub> targeting in the initial segment of the CG13827-RNAi ... knockdown tubule. ....	247
Figure 8-12 [Ca <sup>2+</sup> ] <sub>perox</sub> buffering is impaired in the PEX mutants. ....	248
Figure 8-13 cGMP stimulates peroxisome Ca <sup>2+</sup> uptake. ....	249
Figure 8-14 [Ca <sup>2+</sup> ] <sub>perox</sub> buffering in <i>Best2-RNAi</i> knockdowns is altered. ....	251
Figure 8-15. Spherite formation was affected in PEX knockdowns.....	252
Figure 8-16. A model for peroxisomal Ca <sup>2+</sup> sequestration and transport excretion. .....	258

## Contributions from this work

Chintapalli, V., Wang, J., and Dow, J. (2007). Using FlyAtlas to identify better *Drosophila melanogaster* models of human disease. *Nat Genet* 39, 715-720.

Venkateswara R. Chintapalli, Selim Terhzaz, Jing Wang, Mohammed Al Bratty, David G. Watson, Pawel Herzyk, Shireen A. Davies and Julian A. T. Dow (2012). Functional correlates of positional and gender-specific renal asymmetry in *Drosophila*. *PLoS ONE* 7(4): e32577.

Venkateswara R. Chintapalli, Jing Wang, Pawel Herzyk, Shireen A. Davies and Julian A. T. Dow (2012). A transcriptomic view on epithelial structure and function. (in prep).

Venkateswara R. Chintapalli, Shireen A. Davies and Julian A. T. Dow. *Drosophila* bestrophins: Best2 regulates calcium signaling. (in prep).

Venkateswara R. Chintapalli, Shireen A. Davies and Julian A. T. Dow. Identification of two renal peroxins that encode *Drosophila* orthologs of human Pex6 and Pex11g in a novel cGMP-mediated peroxisome calcium sequestration pathway. (in prep).

## **Preface**

It is a great opportunity to do a research degree like Ph.D. which opens up a window of opportunity. I sincerely thank Professor Julian A.T. Dow for giving me such an opportunity.

One of the wonderful happenings of the universe is our own earth that created our destiny in the cosmic system. Beginning to understand this universal creation became the habit of the human being that endowed with intellectual power. I am genuinely privileged to be a small part of the scientific discovery process.

I dedicate this Ph.D. to my family.

## Acknowledgements

I am utmost grateful to my supervisor Professor Julian A.T. Dow for allowing me to do this Ph.D. I am grateful for all his advice and kind support, at all levels, during all these years. I am utmost grateful to Professor Shireen A. Davies for all the help and advice during all these years.

I thank both Julian and Shireen for their warm hospitality and the tasteful food during the festive periods.

I thank the University of Glasgow for the wonderful and supportive environment. I thank Professor Alan Taylor and Alastair Whitelaw of the graduate school of biomedical and life sciences and Dr. David Martin, the registrar of the University for their kind help with my Ph.D. matters.

I also thank my first assessors Dr. Kevin O' Dell and Dr. Stephen Goodwin for their advice.

I thank Dr. Jing Wang for her personal advice and helpful discussions. I thank Pablo Cabrero, Dr. Selim Terhzaz, Sujith Sebastian, Rujuta Sahani, Dr. Jenny Evans, Louise Henderson and Dr. Anthony Dornan for their help and helpful discussions. I am also thankful to all the members of media preparation room, specifically, Linda and Tracey for providing me with fly food to the highest quality.

I am thankful to Dr. Pawel Herzyk for allowing me to use their bioinformatics facility at the Polyomics facility of the University. I am thankful to Julie Galbraith at the Polyomic facility for her warm welcome at all times. I am thankful to Mohammed Albratty and Dr. David Watson for the useful collaboration to do Metabolomics and pursue some of the novel ideas.

Last but not least, I am utmost grateful for my wife, Deepthi for being such a wonderful partner to pursue this dream. I owe a lot to her and my son, Shreyash for their sacrifice all these years. I thank my family for all their love.

The research reported within this thesis is my own work  
except where otherwise stated, and has not been  
submitted for any other degree

Venkateswara Rao Chintapalli

## Definitions

Aequorin <sub>perox</sub>	peroxisomal-targeted aequorin
[Ca <sup>2+</sup> ]	calcium concentration
[Ca <sup>2+</sup> ] <sub>cyto</sub>	cytosolic calcium concentration
[Ca <sup>2+</sup> ] <sub>i</sub>	intracellular calcium concentration
[Ca <sup>2+</sup> ] <sub>perox</sub>	peroxisomal calcium concentration
°C	degrees Celsius
5-HT	5-hydroxytryptamine
ANO	anoctamin
APS	ammonium persulphate
ATP	adenosine triphosphate
ATPase	adenosine triphosphatase
BCIP	5-bromo-4-chloro-3-indoyl phosphate
BDGP	Berkeley <i>Drosophila</i> Genome Project
Best	bestrophin
BK	big potassium
BLAST	basic local alignment search tool
bp	base pairs
BSA	bovine serum albumin
C-	carboxy-
Ca <sup>2+</sup>	calcium
CaCC	Ca <sup>2+</sup> -activated Cl <sup>-</sup> channel
cADPR	cyclic adenosine diphosphate ribose
CAM	calmodulin
CAMK	calmodulin kinase
cAMP	adenosine 3'-5' cyclic monophosphate
CAP <sub>2b</sub>	cardioacceleratory peptide 2b
cDNA	complementary DNA
CF	cystic fibrosis
CFTR	cystic fibrosis transmembrane regulator
cGK	cGMP-dependent kinase
cGMP	guanosine 3'-5' cyclic monophosphate
Cl <sup>-</sup>	chloride ion
ClC	chloride channel
CNG	cyclic nucleotide gated channel
CPA	cation proton antiporter
CRF	corticotropin-releasing factor
CYP	Cytochrome P450
DAB	3,3-diaminobenzamidine

DAG	diacylglycerol
DAPI	4,6-diamidino-2-phenylindole
dATP	2' deoxyadenosine triphosphate
dCTP	2' deoxycytosine triphosphate
DEPC	diethyl pyrocarbonate
DES	<i>Drosophila</i> expression system
dGTP	2' deoxyguanosine triphosphate
Dh	diuretic hormone
DIDS	4,4'-Diisothiocyano-2,2'-stilbenedisulfonic acid
DIG	digoxigenin
DMF	dimethylformamide
DMSO	dimethylsulphoxide
DNA	deoxyribonucleic acid
dNTP	2' deoxy (nucleotide) triphosphate
dsRNA	double strand RNA
DTT	dithiothreitol
dTTP	2' deoxythymidine triphosphate
dUTP	2' deoxyuridine triphosphate
E <sub>Cl</sub>	Cl <sup>-</sup> equilibrium potential
EDTA	ethylenediamine tetra acetic acid
EGTA	ethylene glycol bis tetracetic acid
ER	endoplasmic reticulum
EST	expressed sequence tag
EtBr	ethidium bromide
FC	fold change
FCS	foetal calf serum
FDR	false discovery rate
FRET	fluorescence resonance energy transfer
g	gram
g	centrifugal force equal to gravitational acceleration
GABA	γ-Aminobutyric acid
GAL4	yeast transcription factor
GCOS	GeneChip® Operating Software
GFP	green fluorescent protein
GO	gene ontology
GPCR	G-protein-coupled receptor
G-protein	guanine nucleotide-binding protein
GST	glutathione-S-transferase
GTP	guanosine triphosphate
h	hours
HBS	HEPES buffered saline

HC	hierarchical clustering
HCO <sub>3</sub> <sup>-</sup>	bicarbonate
HEK	human embryonic kidney
HEPES	N-((2-hydroxyethyl) piperazine-N'-(2-ethanesulphonic acid))
HPSF	high purity salt-free
hs	heat shock
HSD	Hydroxysteroid (17-beta) dehydrogenase
IBMX	3-isobutyl-1-methylxanthine
ICC	immunocytochemistry
I <sub>ClCa</sub>	Ca <sup>2+</sup> -activated Cl <sup>-</sup> current
I <sub>HCO3<sup>-</sup></sub>	bicarbonate current
InsP <sub>4</sub>	inositol 1,3,4,5-tetrakisphosphate
IP <sub>3</sub>	inositol 1,4,5-trisphosphate
IP <sub>3</sub> K	inositol 1,4,5-trisphosphate kinase
IP <sub>3</sub> R	inositol 1,4,5-trisphosphate receptor
IPA	Ingenuity® pathway analysis
IPTG	isopropyl B-D-thiogalactoside
IVT	<i>in vitro</i> transcription
K <sup>+</sup>	potassium ion
Kb	kilobases
K <sub>d</sub>	an equilibrium constant for dissociation
kDa	kilo Dalton
L.D.	light/dark
lacZ	β-galactosidase
LC-MS	liquid chromatography-mass spectrometry
M	molar
mAChR	muscarinic M3 receptors
MALDI-TOF	matrix assisted laser desorption ionisation - time of flight
MBSU	Molecular Biology Support Unit
mg	milligram
μg	microgram
min	minutes
ml	millilitre
μl	microlitre
mm	millimetre
mM	millimolar
μM	micromolar
Mn <sup>2+</sup>	manganese
MOPS	3-(N-morpholino)propane-sulphonic acid
mRNA	messenger RNA

N-	amino-
Na <sup>+</sup>	sodium ion
NAADP	Nicotinic acid adenine dinucleotide phosphate
NBT	nitroblue tetrazolium
ng	nanograms
NHA	Na <sup>+</sup> /H <sup>+</sup> antiporter
NHE	Na <sup>+</sup> /H <sup>+</sup> exchanger
nm	nanometre
nM	nanomolar
NO	nitric oxide
NOS	nitric oxide synthase
OD	optical density
ORF	open reading frame
OSN	olfactory sensory neuron
P	probability
PAGE	polyacrylamide gel electrophoresis
PAT	PBS, Triton X-100, BSA
PBD	peroxisomal biogenesis disorder
PBS	phosphate buffered saline
PBT	PBS, Triton X-100
PCA	principal component analysis
PCR	polymerase chain reaction
PDE	phosphodiesterase
PEX	peroxin
Pfu	<i>Pyrococcus furiosus</i>
pH <sub>i</sub>	intracellular pH
PIP <sub>2</sub>	phosphatidylinositol 4,5-bisphosphate
PKA	cyclic AMP-dependent protein kinase
PKC	protein kinase C
PLC	phospholipase C
PMSF	phenylmethylsulphonylfluoride
PPA	peroxisome proliferating agent
PRA	prenylated Rab acceptor protein
PTS	peroxisomal targeting sequence
qPCR	quantitative reverse transcriptase polymerase chain reaction
r.h.	room humidity
rdg	retinal degeneration
rGC	receptor guanylate cyclase
RLU	relative light unit
RNA	ribonucleic acid
RNAi	RNA interference

RNase	ribonuclease
RPE	retinal pigment epithelia
RT	room temperature
RT-PCR	reverse transcriptase polymerase chain reaction
RYR	ryanodine receptor
s	second
SDS	sodium dodecyl sulphate
SED	single enzyme disease
SEM	standard error of the mean
SERCA	sarco/endoplasmic reticulum Ca <sup>2+</sup> -ATPase
sGC	soluble guanylate cyclase
SLC	solute carrier
SPoCk	secretory pathway Ca <sup>2+</sup> -ATPase
TAP	tandem affinity purification
TBE	tris-borate EDTA
TE	tris-EDTA
TEMED	N,N,N',N'-tetramethylethylenediamine
TEP	trans-epithelial potential
TMD	transmembrane domain
TRH	Thyrotropin-releasing hormone
Tris	2-amino-2-(hydroxymethyl)-1,3-propanediol
TRP	transient receptor potential
TRPL	transient receptor potential-like
U	unit
UAS	upstream activating sequence
UTP	uridine triphosphate
UTR	untranslated region
UV	ultraviolet
VASP	vasodilator-stimulated phosphoprotein
V-ATPase	vacuolar-type H <sup>+</sup> adenosine triphosphatase
VDCC	voltage-dependent Ca <sup>2+</sup> channel
X-gal	5-bromo-4-chloro-3-indolyl-β-D-galactopyranoside
YFP	yellow fluorescent protein
ZSS	zellweger spectrum syndrome

**One and three letter  
amino acid codes:**

A	Ala	Alanine
C	Cys	Cysteine
D	Asp	Aspartic acid
E	Glu	Glutamic acid
F	Phe	Phenylalanine
G	Gly	Glycine
H	His	Histidine
I	Ile	Isoleucine
K	Lys	Lysine
L	Leu	Leucine
M	Met	Methionine
N	Asn	Asparagine
P	Pro	Proline
Q	Gln	Glutamine
R	Arg	Arginine
S	Ser	Serine
T	Thr	Threonine
V	Val	Valine
W	Trp	Tryptophan
Y	Tyr	Tyrosine
*	Stop	

# 1. Introduction

The 'central dogma of life' explains the flow of genetic information from DNA to RNA to protein. The foundation for the theory was the discovery of the DNA double helix structure that changed the world forever (Watson and Crick, 1953). Then 'the invention of polymerase chain reaction (PCR) technique', revolutionised molecular biology (Saiki et al., 1988). Later, completely sequenced genomes, from bacteria to higher eukaryotes including humans are made readily available to the scientific community (Mardis, 2011). Furthermore, comparative analysis of fully sequenced genomes provided further definition and annotation to the genomes sequences (Rubin et al., 2000; Ureta-Vidal et al., 2003), in addition to providing information about the relative conservation of functional elements (Flicek et al., 2011). This led to the concept of functional genomics to functionally characterise the fully sequenced genomes. The integrative approach of functional genomics necessarily includes genomics, transcriptomics, proteomics and metabolomics to study genomes, and to assay the levels of RNAs, proteins, and metabolites at a genomic scale, respectively. This integrative approach draws upon the rapid advances in complementary technologies which range from such diverse fields as molecular biology to the silicon wafers within the field of information technology, and is seen as a holistic approach to understand biological complexity at the systems level. This holistic approach became an emerging field, the so called systems biology, in particular to explain biology at the systems level, and consequently the *Science* journal presented a special issue to mark systems biology's potential staying power as a new modern scientific field (Chong, 2002).

## 1.1 Systems Biology

Systems theory was first introduced in a compilations book of writings by a biologist, Ludwig von Bertalanffy that dates back to the 1940's (Bertalanffy, 1969). In this book von Bertalanffy argued that the constitutive characteristics of a system open to its environment are not explainable from the characteristics of the isolated parts. In addition, he argued that these systems qualitatively acquire new properties through emergence in their environmental interactions, thus they are in a continual evolution.

'Systems biology' theory has evolved from the general systems theory as a holistic approach to describe and understand the mechanisms of complex biological systems. The ultimate goal of systems biology from a biologist point of view is to develop predictive models of biological systems at healthy and diseased states (Hood et al., 2004).

Systems biology as a discipline tries to integrate systems from several levels from technology to biology and seeks to understand biological processes in quantitative terms (Albeck et al., 2006). In contrast to the traditional reductionist approach that aims to study functions of genes or proteins to gain broad knowledge, systems biology focuses towards more systems-level functions in networks and interactions between individual components of networks.

The systems biology asks the question in the context of a whole system rather than in isolation as mentioned earlier. For example, it tries to understand how an organism works at systems level, and how disruption of a single component causes a system-wide change through a complex set of interactions among the interconnected networks of genes, proteins, and metabolites (Mustacchi et al., 2006; Stuart et al., 2007). Thus, constructing meaningful and possibly accurate models of molecular, cell and tissue, and whole organism functions from a systems point is of utmost important. This envisaged to eventually allow, for example, the translation of systems level understanding of genes to drugs at a faster rate with more precision.

The need for a systems biology approach becomes clearer in multicellular organisms. Because, for example, increased complexity in multicellular organisms poses problems in fully comprehending the phenotypic consequences of a genetic intervention. In the post genomic era, genetic analysis using gene knockdown, over expression, deletion or knockout need precision. This is because to understand the phenotypes of genetic intervention depends on a variety of factors in multicellular organisms including developmental stages, cells types, and cellular processes in which it functions. In addition, highly sophisticated compensatory mechanisms exist in multicellular organisms unlike single celled yeast and bacteria that allow the former to overcome the genetic perturbation.

Moreover, second-site mutations in *Drosophila*, for example, often partially suppresses the phenotypes of genetic perturbation by the way of accumulating modifiers if they were maintained as homozygous stocks (Ashburner, 1989; Miklos and Rubin, 1996).

### **1.1.1 Functional genomics for systems biology**

Systems biology needs high quality functional data sets. The omics technologies augmented systems biology approaches by means of providing semi-quantitatively modelled data at gene, protein and metabolite levels (Ge et al., 2003). Genomic level quantification of genes using microarrays and high parallel sequencing technologies has been more reliable than the quantification of proteins and metabolite levels. This is due to increased biological complexity at protein and metabolite level and inherent technical difficulties in extraction to identification of proteins and metabolites.

For example, protein microarrays are limited in number of proteins that a single protein array can profile (Albeck et al., 2006). Analysis of metabolite flux needs more refined datasets with advanced mathematical models as the diversity and dynamics of the molecules increase many-fold from genes to metabolites. Nonetheless, the data from omics technologies has been allowing constructive and predictive biological models at various stages of a biological system, for example, at various stages of development, environmental conditions, disease states, genetic perturbations, physiological states, cells, tissues, and pharmacological interventions (Joyce and Palsson, 2006).

Systems biology aims to integrate a multitude of information rich systems to build mathematical models to eventually predict, for example, a biological response to a particular drug or environmental stimuli. In addition, omics approaches have been dramatically accelerating hypothesis generation and testing in biological models; for example tissue-specific transcriptomics allowed to annotate probable tissue-specific functions in *Drosophila* (Chintapalli et al., 2007).

With the advent of information technologies, computer simulations are made possible for biological information obtained through omics technologies (Joyce and Palsson, 2006), allowing to integrate the information to build informative models for example to prioritize drug targets and design clinical trials.

### **1.1.2 A case for model organisms use in functional genomics**

Model organisms serve the need of systems biology in the form of providing large-scale omics data sets that provide systems level measurements for virtually all types of cellular components in a model organism (Joyce and Palsson, 2006). The model organisms from Yeast to *Drosophila* have been instrumental in aiding a systems biology approach for greater understanding biological systems (Mustacchi et al., 2006; Stuart et al., 2007). This is crucial for functional genomics.

Fully sequenced genomes for *Drosophila* species have now reached 12 (Adams et al., 2000; Celniker et al., 2002; Clark et al., 2007; Richards et al., 2005). This allows comparative analysis and functional annotation of genomes using both computational and experimental approaches (Shoemaker et al., 2001). Whole genome and tissue-specific gene expression quantification using DNA microarrays further provided information to draw parallels between the species of interest. For instance, a case for *Drosophila* suitability to study human disease in a cognate fly tissue of human disease was presented (Wang et al., 2004). In addition, a pioneering study into the tissue-specific gene expression patterns not only provided a wealth of information regarding tissue functions, but also yielded important insights into gene expression in its own right (Chintapalli et al., 2007). This data are now in the form of an online expression database called FlyAtlas, which can be easily mined for genome-wide gene expression patterns across multiple tissues.

By the time that fully sequenced genomes from different organisms became available to the scientific community, it was calculated that only 20% of the genome had been characterised, or at least named, in the well-studied model organism *Drosophila*. Not surprisingly, most of the previously annotated genome had been implicated in developmental functions of the organism.

The comparative analysis and computer annotations of the genomes revealed surprising numbers of genes, and without any functional information. This has been called the 'phenotype gap', where there is clear difference in functional phenotypes and the number of genes annotated (Dow, 2007; Dow and Davies, 2003; Wang et al., 2004).

However, in retrospect, it has been long calculated using the data from a range of organisms including yeast, worms, flies, and mice that one third of genetic loci are essential for fly survival. The rest of the two thirds of the genome when mutated may not show any instantly lethal phenotypes (Miklos and Rubin, 1996).

### ***1.1.3 DNA microarrays for functional genomics***

DNA microarrays, that have the capacity to assay the expression of tens of thousands of genes at a time, have become a routine use to analyse systems level functions (Bammler et al., 2005; Schena et al., 1995). Although, understanding protein levels may be more informative than understanding RNA levels, genome wide high throughput methods like mass spectrometry can identify only a fraction (0.2%) of proteins from a given sample because of technical difficulties and increased biological complexity from RNA to protein (Mirza and Olivier, 2008). This means that a global picture of the levels of proteins is much harder to obtain from a single MS experiment using current approaches than to obtain global RNA levels using DNA microarrays.

Transcriptomics detail high throughput genomic scale measurements of mRNA expression. The DNA microarrays allow quantifying the levels of tens of thousands of genes in a single mRNA sample and pioneered the way for analysing transcriptomes at a massive scale. As the disruption in mRNA levels is one of the indicators of the protein function, studying the function of genes at the mRNA level became a powerful technique for functional genomics (Adams, 2008). The microarrays have been employed for many of the experimental scenarios to study the global levels of mRNA changes, to analyse and compare transcriptomes of cells, tissues, whole organisms, under normal and disease, drug-treated and non-treated states.

The microarrays are the solid surfaces on to which thousands of small DNA products, cDNA or short oligonucleotide sequences are immobilised in sets (as probesets) in an orderly fashion (as an array) and are given a unique identifier. The solid surfaces can be either small glass slides that are regularly used in the labs or they can be compact silicon chips.

The DNA is printed, spotted, or directly synthesized on the support which is mostly accomplished by the help of advanced engineering fields such as robotics and photolithographic printing (Nuwaysir et al., 2002).

Different kinds of commercial microarrays exist depending on the species and length of the DNA probe. In particular, oligonucleotide microarrays, designed using Affymetrix technology are the first of their kind and are widely used ([www.affymetrix.com](http://www.affymetrix.com)). These Affymetrix DNA microarrays are also called GeneChips®. The GeneChip of *Drosophila* Genome v2.0 provides comprehensive coverage of the *Drosophila melanogaster* genome for surveying gene expression for more than 18,500 transcripts. This GeneChip is based on the content from the release 3.1 of the *D. melanogaster* genome by Flybase ([www.flybase.org](http://www.flybase.org)) and the Berkeley *Drosophila* Genome Project (BDGP) ([www.fruitfly.org](http://www.fruitfly.org)). The v2 GeneChip® of *D. melanogaster* is the second generation GeneChips® and covers 30 percent more content than the first generation *D. melanogaster* design. These arrays have been used in generating the FlyAtlas tissue-specific transcriptomes.

#### **1.1.4 Where integrative physiology meets systems biology**

‘Physiology’ is asking the bigger question of how an organism works at various states and levels. However, the classical physiological approaches were eroded by ethical issues in animal experimentation and increased belief in the analytical or reductionist approach to understand the complexity at cellular and molecular level (Dow, 2007). Physiology thus transformed into integrative physiology to accommodate the reductionism that had evolved in the form of cellular and molecular physiology. In the post-genomic era, systems biology approach with its powerful arsenal of techniques and modalities brought back the physiology as integrative and systems biology.

## 1.2 *Drosophila* as a model organism

### 1.2.1 Introduction and History

Thomas Hunt Morgan was the first to observe the *white* mutation in *Drosophila* in 1910. Since then *Drosophila* has been instrumental in genetic studies regarding a variety of biological questions that span development to physiology.

*Drosophila* has been so successful as a model organism because it offered powerful genetics, in addition to its smaller size, short developmental cycles, and the relative ease and affordability in maintaining them in the lab. Furthermore, *Drosophila* has a less complicated genome with just 2-fold higher redundancy of protein than the unicellular eukaryote, *Saccharomyces cerevisiae* (Rubin et al., 2000). In addition, integrated online genetic and genomic resources (such as Flybase.org) provide a wealth of functional information and stock centres that may have over a million different flies, send them at free or nominal costs. Fly genetics is enriched with the powerful genetic markers and balancer chromosomes that allow marking genes of interest and trace the lineages over the generations. The fully sequenced genomes with detailed genome annotations (so far for 12 different species) and transposon mediated transgenesis and powerful induction of RNAs at a precise spatiotemporal resolution offered enormous power to reengineer the entire genome of *Drosophila* (Golic and Golic, 1996; Ryder et al., 2007).

Developmental biology has so much dominated *Drosophila* research that even genes which are now known to be expressed specifically in adults have been described in developmental roles (Chintapalli et al., 2007). In light of this and rapid developments in *Drosophila* genetic and genomic tools such as GAL4/UAS system, *Drosophila* now has become a valuable model organism for studying molecular physiology of post-embryonic functions (Dow and Davies, 2003). A case for *Drosophila* as a model for studying human genes became more clear with the implication that about 75% of *Drosophila* genes have human counterparts (Chien et al., 2002), including those involved in genetic disorders and cancer (Bier, 2005; Vidal and Cagan, 2006).

## 1.2.2 Reverse Genetics

Reverse genetics is a powerful approach to elucidate gene function by analysing corresponding mutant phenotypes (Lewin, 1986; Orkin, 1986; Ruddle, 1982). This has been proposed to be a quickest and most promising way of inferring function for a novel gene (Dow and Davies, 2003). A variety of model organisms that are equipped with powerful genetic and genomic and physiological tools serve the need of the reverse genetics.

In *Drosophila* it is much simpler to create a gene knockout or a hypomorph than potentially in any multicellular organism in addition to the existing hundreds of thousands of stock lines.

### 1.2.2.1 GAL4/UAS system

The transposon mediated transgenesis enabled the development of the GAL4/UAS binary system for tissue-specific expression of introduced DNA sequences (Figure 1-1). The two components of the system were derived from the yeast and widely used in *Drosophila* transgenesis (Duffy, 2002). The GAL4/UAS system was first developed for targeted gene expression in *Drosophila* (Brand and Perrimon, 1993).

As part of the bipartite system, the enhancer traps flies that express the yeast GAL4 transcription factor (that is not found in *Drosophila*) in a tissue and cell specific manner, and are crossed to the flies that are harbouring upstream activating sequence (UAS) -downstream fused cDNA sequences. The UAS is the high affinity binding site of the transcriptional activator GAL4. The F1 generation of the cross will have both UAS and GAL4 elements and GAL4 is produced under the regulation of native enhancer consequently driving the expression of the genes or cDNA sequences of interest. This system is generally used to ectopically express transgenes of interest including double-stranded RNAs (for RNAi) or cDNAs (for wildtype overexpression). More refined versions of the targeted expression tools are constantly evolving that are keeping the promise of '*Drosophila* as a valuable model organism' (Pfeiffer et al., 2010).

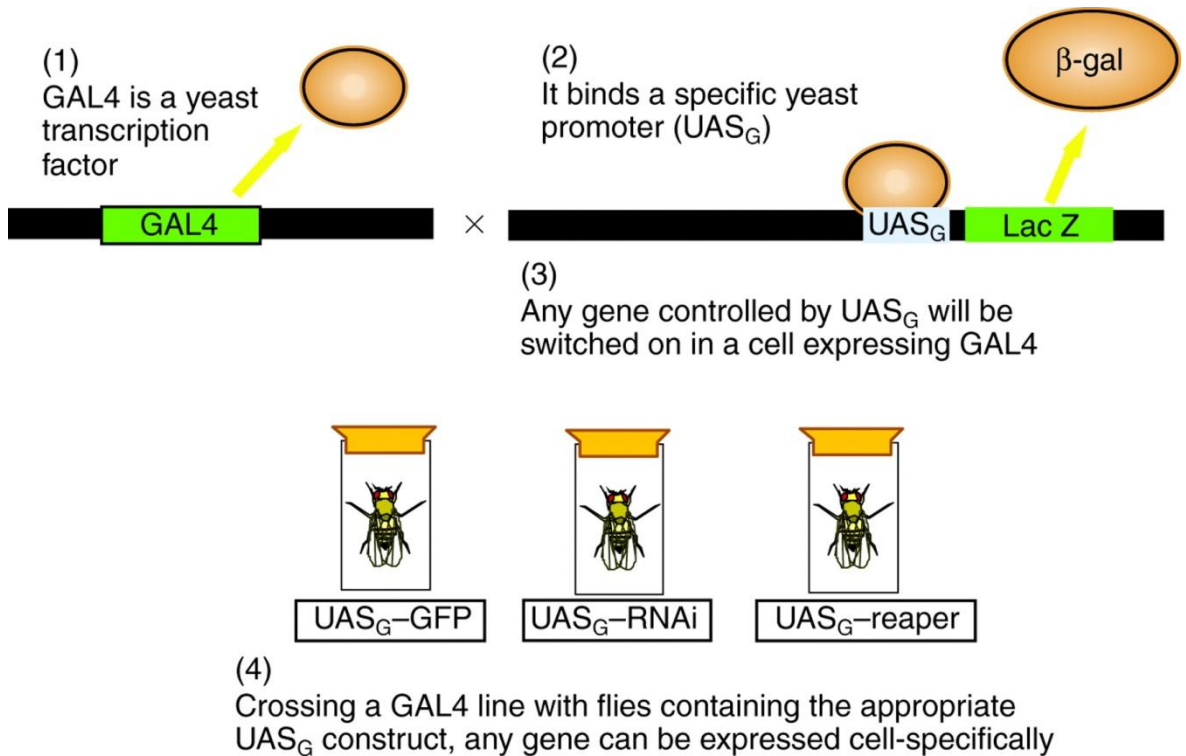


**Figure 1-1 Schematic of heritable induction of transgenes using GAL4/UAS bipartite system.** The first part of the system includes flies harbouring GAL4 in their genome under the control of genomic enhancers or promoters or cloned promoters of interest. The second part of the system includes the flies harbouring UAS (upstream activating sequence) fused to the DNA sequence of interest. When the flies from two systems crossed they produce F1 progeny harbouring both GAL4 and UAS elements. GAL4 upon its expression (depending on the control of regulatory element) binds to the UAS drives the expression of the downstream DNA sequences. This way ectopic expression of a transgene (GFP, RNAi or cDNA) is achieved cell- and tissue-specifically using the appropriate regulatory elements. Figure adopted from (Dow, 2007).

### 1.2.3 Transgenesis

Efficient transgenesis techniques are an absolute necessity of reverse genetics. The transgenesis can be defined as a group of technologies for manipulating DNA or introducing a foreign DNA into an organism of interest (Venken and Bellen, 2007).

Transposons are semi-autonomous DNA sequences that move around in all genomes. They can be adopted by experimenters to ‘jump around’ DNA of choice far more efficiently than any direct attempts to insert DNA into the genome. Transposon-mediated germline transformation is an efficient transgenesis technique in *Drosophila* that allows a piece of a foreign DNA to integrate into the genome and transmit into the successive generations (Figure 1-2).

The transgenesis in *Drosophila* can be achieved through transposon-mediated integration. Specifically, the *P*-element transposon mediated transposition has been relatively more successful than other transposons fairly due to the disadvantages of the later in *Drosophila*. Spradling and Rubin first used a genetically engineered *P*-elements to re-introduce the *rosy* gene back into the *rosy* mutant flies (Spradling and Rubin, 1982).

The first generation *Drosophila* enhancer traps utilised *P*-element mediated transposition and is employed to possibly identify genomic enhancers (O'Kane and Gehring, 1987). This technique employs the fusion of *lacZ* (that encode the  $\beta$ -galactosidase) with *P*-element, and a minimal promoter, germline transformed into *Drosophila*. The subsequent analysis of  $\beta$ -galactosidase expression allows the assessment of cell-type- and tissue-specific patterns of genomic enhancer elements.

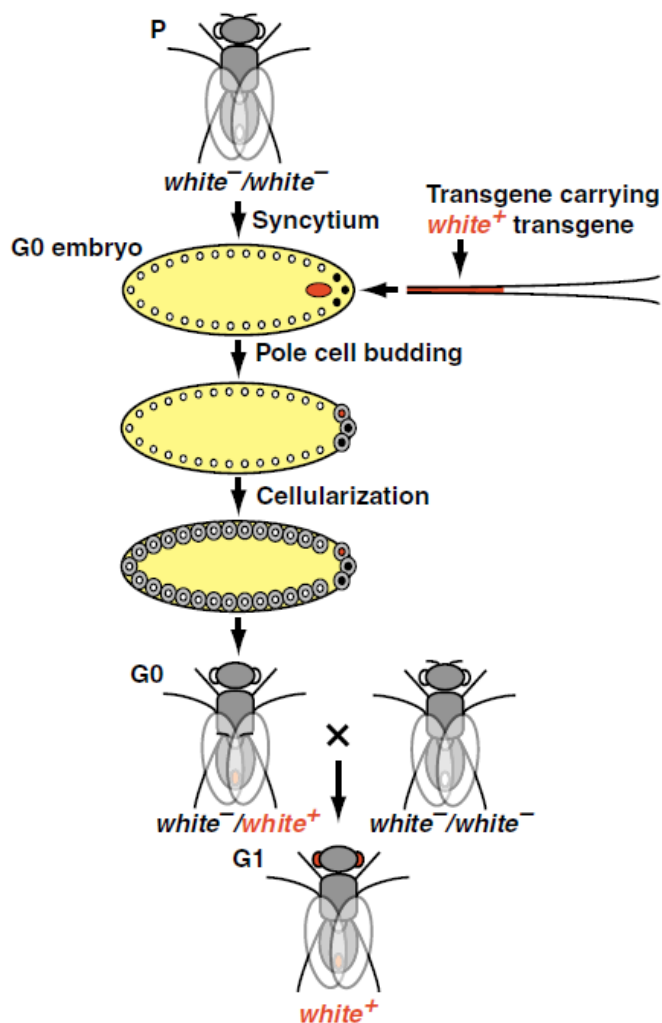


Figure 1-2 Germline transformation of *Drosophila*. [taken from (Venken and Bellen, 2007)]

*P*-elements are introduced into *white*- fly by the simultaneous microinjection into the syncytial blastoderm stage embryo of a plasmid encoding a transposase, allowing its transient expression. In this way, the transposon is stably incorporated into the genome with no further transposition events. The *P*-element carries the *mini-white* gene, so the injected flies are *white*<sup>+</sup> and easily scored for successful insertions.

This technique alone has revolutionised the already hugely successful *Drosophila* genetic enterprise and allowed tissue-specific gene silencing using heritable RNAi (Kalidas and Smith, 2002; Kennerdell and Carthew, 2000), mis-expression screens to create dominant phenotypes (Rorth, 1996; Rorth et al., 1998) and the identification of the sub-cellular localisation of tagged proteins.

Gene knockdown using double-stranded RNA (dsRNA), or RNAi has been instrumental (Hunter, 1999). Particularly, in *Drosophila*, RNAi became a routine after devising a GAL4/UAS bipartite system (explained in the following sections) to conditionally ablate gene expression at a single cell resolution within a systems context.

The dsRNAs can be introduced in two ways in *Drosophila*, exogenous, and endogenous (Carthew, 2003). The exogenous approach involves the introduction of a small interfering RNAs (siRNA) directly into the embryos or cultured cells. The more widely used endogenous method depends on the GAL4/UAS system where a long inverted repeat RNA sequence is expressed *in vivo*. Upon the expression, they form hairpin-like dsRNAs in the cell, and are recognised by the RNAi pathway, leading to the inhibition of mRNA expression (Kennerdell and Carthew, 2000). The former method is more convenient and particularly suited for developmental studies; the later approach is convenient for one to express the RNAis of interest conditionally. Thus the endogenous method allows the study of adult functions of the genes of interest without intervening for example, in the organismal developmental functions.

A novel transformation vector, pRISE was used to construct RNAis for making transgenic flies for this study (Kondo et al., 2006). This vector contains a characteristic Gateway™ cassette, attR1-ccdB-attR2 as an inverted repeat sequence between an intron for *in vitro* recombination and a pentameric GAL4 binding sequence for conditional expression.

This cassette allows recombination of entry clones containing the target sequence of interest into the pRISE for the subsequent germline transformation. More detailed information is provided in Materials and Methods chapter.

Malpighian (renal) tubules (tubules, from now onwards) of *Drosophila* have been instrumental in elucidating cell-specific signaling and molecular physiology of ion transport mechanisms. The first microarrays ran on tubules provided a basis for generating FlyAtlas tissue-specific transcriptomes (Wang et al., 2004). In the following section, the tubules as model test beds for functional genomics to further our understanding of cell signaling and transport physiology mechanisms, is presented.

### **1.3 Tubules as a model epithelium in transport and signaling**

*Drosophila* tubules are functionally analogous to mammalian kidneys (Dow and Romero, 2010; Wang et al., 2004). *Drosophila* has two pairs of tubules: one ramifies anteriorly in the body and the other towards posteriorly, and each pair is joined by a common ureter, which opens up into the hindgut of the alimentary canal (Figure 1-3, upper panel). Each pair of tubules consisting of around 150 cells shows morphological and functional domains.

Each anterior tubule has an enlarged initial segment, the organ that titres haemolymph  $\text{Ca}^{2+}$ . In contrast, the posterior tubules show a smaller initial segment. In addition, each pair of the tubules has a distinctly narrower transitional segment and a fluid secreting main segment that leads to the ureter. In addition, GAL4 enhancer trap analysis revealed six distinct genetic boundaries in tubules (Figure 1-3, upper panel) (Sozen et al., 1997).

The main segment is composed of two cell-types including principal (type I) and stellate (type II) cells (Figure 1-3, lower panel). The principal cells are columnar, with deep basal infoldings and long microvilli, whereas stellate cells are star-shaped, smaller in shape with less basal infoldings with shorter apical microvilli. Other cells, including stem cells and mechano-sensory or chemosensory cells have also been shown using lineage tracing and molecular marker analysis and the enhancer trap analysis, respectively (Singh et al., 2007; Sozen et al., 1997).

Because of the extensive genetic, genomic, and physiological characterisation of this simple epithelia, it has become a unique tool for analysing the molecular physiology of ion transport to dissecting cell signaling pathways that may have biomedical relevance in an organotypic context (Chintapalli et al., 2007; Dow et al., 1994b; Dow and Romero, 2010; Dow and Davies, 2003).

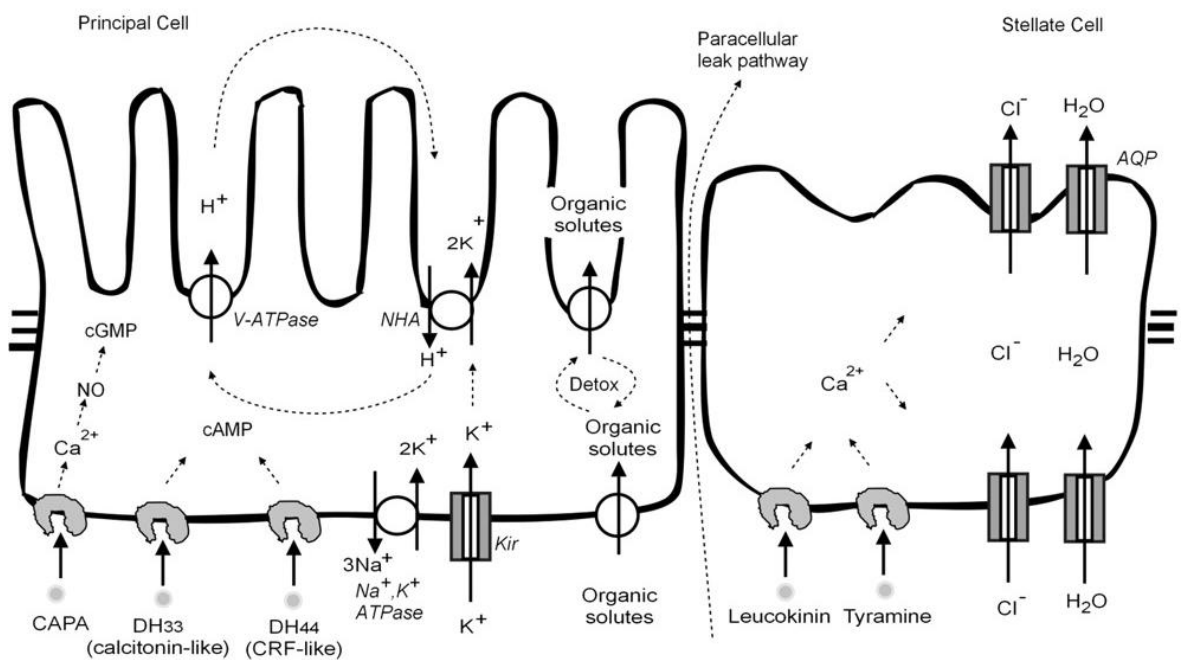
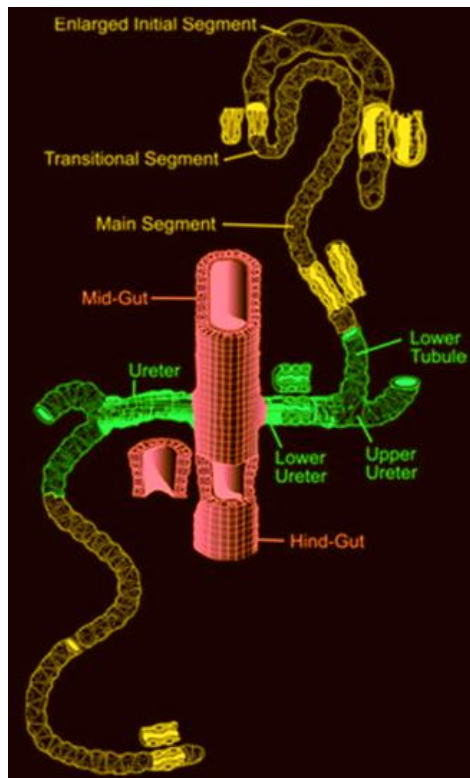


**Figure 1-3 (Upper panel) Tubules of *Drosophila melanogaster*.**

*Drosophila* has two pairs of tubules namely anterior and posterior tubules that ramify anteriorly and posteriorly in the body respectively. Morphologically and functionally distinct domains are labelled for anterior tubules; their posterior counterparts have the equivalent domains except that they don't have the enlarged initial segment. (adopted from (Wessing A, 1978))

(Lower panel: taken from (Dow and Romero, 2010)) **Two major cell types of tubules.**

**The larger principal and smaller stellate cells are joined together with septate junction.**

**These two cells intercalate tubule lumen thus separating the lumen from hemolymph.**

**Detailed cell-specific signaling and physiological functions are depicted for both the cells.**

### 1.3.1 General mechanisms of second messenger signaling

Second messengers including  $\text{Ca}^{2+}$ , cAMP and cGMP play important roles in signal transduction thereby regulating many physiological processes from neuronal excitability, muscle contraction to fluid secretion upon the activation of a variety of primary messengers.  $\text{Ca}^{2+}$  is a universal second messenger that transmits signals across the length and breadth of a cell (Berridge et al., 2000). Fundamentally,  $\text{Ca}^{2+}$  signaling is initiated in two ways starting either from a G protein-coupled receptor (GPCR), or receptor tyrosine kinase activation by a variety of primary messengers. Activation of both receptors leads to the production of  $\text{IP}_3$  from the conversion of phosphatidylinositol (4,5)-bisphosphate ( $\text{PIP}_2$ ) to diacylglycerol (DAG) (Berridge and Irvine, 1989).  $\text{IP}_3$  at stimulated concentrations binds to  $\text{IP}_3$  receptors on the ER, leading to the influx of  $\text{Ca}^{2+}$  into the cytosol at times leading to 10-times more  $[\text{Ca}^{2+}]_{\text{cyto}}$ . However, the  $\text{Ca}^{2+}$  response kinetics differ, in that the tyrosine kinase receptor mediated PLC $\gamma$  activated  $\text{Ca}^{2+}$  release is slower and longer than the G-protein receptor mediated, PLC $\beta$  activated release. Another route for  $\text{Ca}^{2+}$  entry from the extracellular space in nonexcitable cells is hyperpolarization of plasma membrane where  $\text{K}^+$  entry through  $\text{K}^+$  channels changes the membrane potential to negative, leading to  $\text{Ca}^{2+}$  influx from voltage-independent  $\text{Ca}^{2+}$  channels. But, in excitable cells,  $\text{Ca}^{2+}$  transients occur with fast kinetics through voltage-dependent  $\text{Ca}^{2+}$  channels.

The second messenger signaling through cAMP and cGMP has been extensively studied in *Drosophila*, following the discovery and implication of *dunce*, a cAMP-specific phosphodiesterase (PDE), in learning and memory (Davis and Kiger, 1981; Dudai et al., 1976). The two components of the cyclic nucleotide signaling, cAMP and cGMP have their distinct mechanisms and pathways of regulation and signaling initiated by activation of a variety of hormone and neurotransmitter receptors as discussed earlier (Figure 1-4). The cAMP is synthesized by adenylate cyclases. The synthesis is stimulated in response to a primary messenger, such as adrenaline, leading to the activation of downstream effector proteins at high concentrations.

A variety of primary messengers can initiate a cAMP signal involving G proteins in a given cell type reflecting the specificity of downstream signaling cascade

activation. The binding of the primary messenger to G-protein coupled receptor induces a conformational change in the receptor leading to the activation of the  $\alpha$ -subunit of the G-protein. Depending on the G-protein that is activated, ( $G_s$  stimulates and  $G_i$  inhibits) adenylate cyclase is either activated or inhibited. Activated adenylate cyclase then produces cAMP from the cytosolic ATP, and at stimulated concentrations cAMP activates cAMP-dependent protein kinases (e.g., PKA). Then the kinases transduce the signals by catalysing the phosphorylation (activation or deactivation) of intracellular enzymes, eliciting a wide array of metabolic and functional processes.

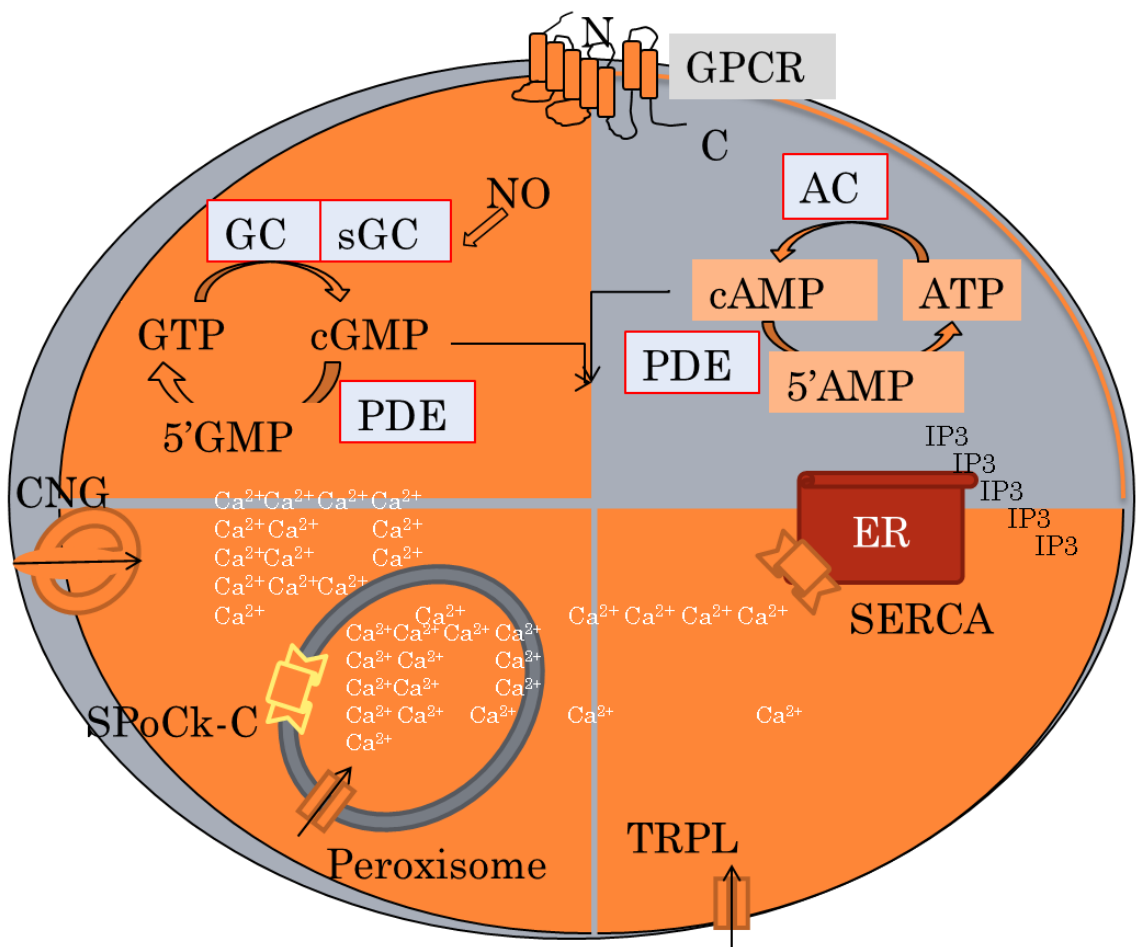


**Figure 1-4 Cyclic nucleotide-dependent signaling components (in intracellular  $Ca^{2+}$  mobilisation).**

Intracellular second messenger system, cyclic nucleotide (cGMP and cAMP) signaling cascade is activated by the upstream first messengers (for example, neuropeptides). At both resting and activated states (in other words, spatiotemporal) cyclic nucleotide concentrations are regulated by PDEs.

For example, in blowfly salivary glands, two 5-hydroxytryptamine (5-HT) receptors with homologues in their Dipteran counterpart *Drosophila melanogaster* (Chapter 4) are found. The two receptors act through two independent second messenger signaling systems one involving cAMP and the other  $\text{Ca}^{2+}$  to drive potassium transport and to open  $\text{Ca}^{2+}$ -activated  $\text{Cl}^-$  channels respectively leading to salivary gland secretion (Berridge, 2005). This is a classic example of how the second messenger systems are evolved to regulate similar physiological processes via distinct mechanisms.

cGMP signaling has an added layer of complexity in that a cGMP signaling event can be initiated either by a primary messenger, via a receptor guanylate cyclases or by the gaseous signaling molecule nitric oxide (NO), which activates soluble guanylate cyclase, perhaps binding to its heme moiety in an autocrine or paracrine manner (Davies, 2006). In either ways, receptor activation leads to the production of cGMP from guanosine triphosphate (GTP).

Then the cGMP at effective concentrations mediates its intracellular effects through the activation of specific cGMP-dependent protein kinases (e.g., PKG).

PDEs negatively regulate cyclic nucleotides by hydrolytic catalysis, giving rise to adenosine- and guanosine-5'-monophosphate (5'-AMP or GMP) thus controlling the spatiotemporal aspects of the signaling (Baillie, 2009; Day et al., 2005; Zaccolo and Movsesian, 2007). A variety of PDEs can control either cAMP or cGMP or both. For example, PDE I activity depends on  $\text{Ca}^{2+}$ /calmodulin-dependent kinase, perhaps through phosphorylation by PKA.

#### **1.3.1.1 Second messenger signaling in the tubules**

The fruit fly tubules provided a wealth of information in regards to the regulation of both cytosolic and organellar  $\text{Ca}^{2+}$  signaling and transport mechanisms (Davies and Terhzaz 2009). Furthermore, cGMP signaling mechanisms are well documented at a single cell resolution (Day et al., 2005; Kerr et al., 2004). This has been achieved via the identification and isolation of neuropeptides capa and leucokinin (Dow and Davies, 2003).

Particularly, the capa mediated GPCR signaling mechanisms are well characterised by combining the power of *Drosophila* classical and modern genetics (GAL4 enhancer trapping), physiological techniques (fluid secretion assays) with pharmacological approaches in tubules. The GAL4 enhancer trapping provided a panel of fly lines that express GAL4 in a cell-specific manner including principal and stellate cells (Sozen et al., 1997).

### 1.3.1.2 Second messenger signaling in tubules via capa peptides

The capa family of peptides consists of capa1, capa2 and CAP<sub>2b</sub> (Davies and Terhzaz, 2009; Predel and Wegener, 2006). All these have been shown to mobilise Ca<sup>2+</sup>, nitric oxide and the cGMP in tubules with similar kinetics in only the principal cells of tubules thereby initiating the fluid secretion response (Broderick et al., 2004; Davies and Terhzaz, 2009; Sozen et al., 1997). In *Drosophila* tubules, CAP2b of *Manduca sexta* stimulates intracellular cGMP levels via the activation of nitric oxide synthase (Davies et al., 1995). Furthermore, the increased cGMP levels can be rescued by the NO scavenger methylene blue.

Although, NO seems to act as an autocrine signal via tubule localised dNOS, the ectopic expression of the dNOS, specifically in principal cells, did not appear to increase fluid secretion levels (Broderick et al., 2003). However, when the PDE activity was inhibited by the cGMP-PDE inhibitor zaprinast, it did increase the secretion.

### 1.3.1.3 The final targets of capa signaling in tubules

The [cGMP] increase via capa peptide may have two potential targets in tubules, including cyclic GMP-dependent protein kinases (cGKs) cGMP-gated ion channels that allow Ca<sup>2+</sup> ions. *Drosophila* encode two cGKs namely *dg1* and *dg2* (or foraging), and are expressed in tubules (MacPherson et al., 2004b). It has been proposed in tubules that cGK may control cGMP levels via phosphorylation of cGMP phosphodiesterases (MacPherson et al., 2004a). These have been further confirmed by transgenic expression of *cGK* genes in tubules, and expression of cGK-DG1 and DG2P2 in principal cells increases fluid secretion upon cGMP or capa1 stimulation respectively.

Previous observations suggest that cGMP treatment of the tubules increases the transepithelial potential (TEP) possibly by the activation of vacuolar-type ATPase (V-ATPase) (O'Donnell and Maddrell, 1995). The second sought after targets of cGMP are CNG channels. CNG channels like TRPs play important role in signal transduction. A *Drosophila* cGMP-specific CNG channel has been cloned and shown to be highly permeable to  $\text{Ca}^{2+}$  ions (Baumann et al., 1994). This channel has been shown to be approximately 50-fold more sensitive to cGMP than to cAMP. The mRNA expression was found in tubules (MacPherson et al., 2001).

The cGMP transport role of the famous *white* gene, that encodes an ATP binding cassette G2 (ABCG2) sub-family member, has recently been revealed in the tubules in consistent with its high mRNA expression in these organs other than eyes (Evans et al., 2008). Transport assays demonstrated defective transport of cGMP in *white* mutants (partial deletion and loss of function) leading to increased levels of cGMP which can be rescued upon expression of wildtype *white* transgene. This is another example of cGMP's role in the tubule function.

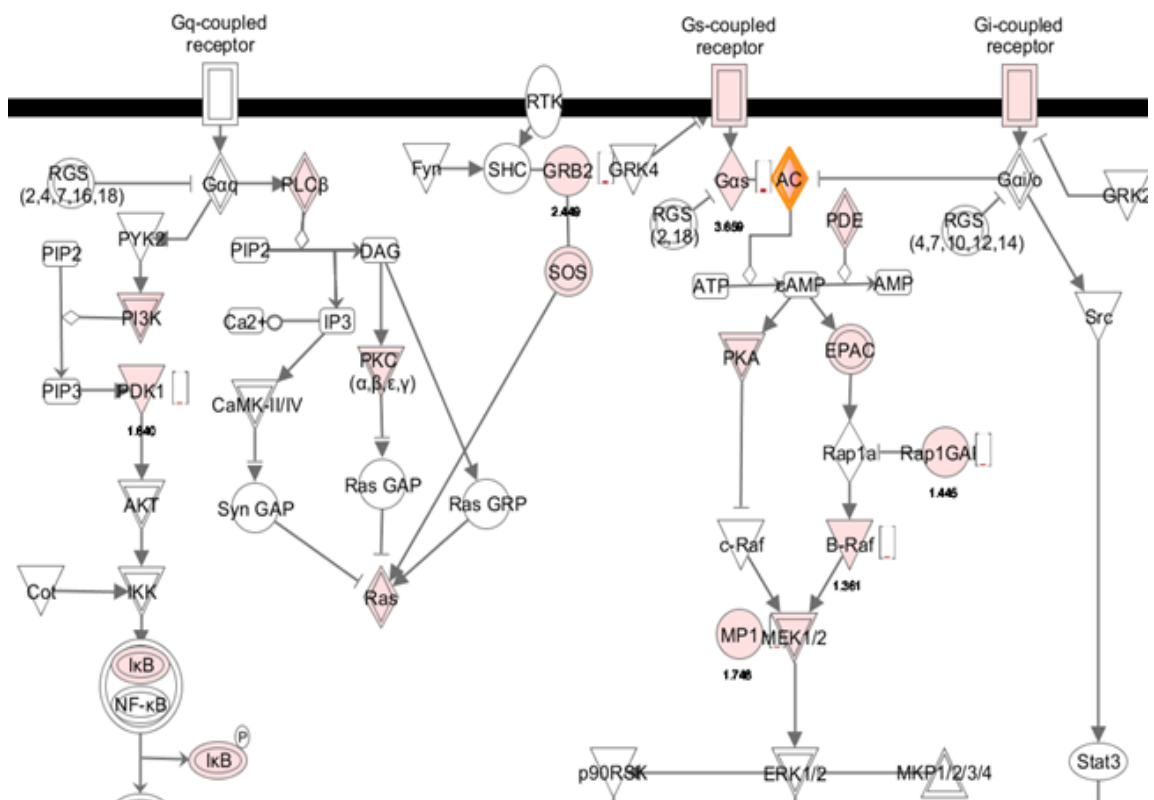


**Figure 1-5 Human G-protein coupled receptor signaling pathway components in tubules. *Drosophila* tubule transcriptome was overlaid on to the mammalian pathway to show conservation of function. The shapes shaded in red colour are the mapped mammalian orthologues of *Drosophila* genes.**

Mammalian network analysis of *Drosophila* epithelial tissue transcriptomes also revealed that there are many components that are orthologous to humans, are faithfully expressed in *Drosophila* tissues such as tubules (Figure 1-5).

#### 1.3.1.4 Second messenger signaling in tubules via Drosokinin

On the other hand, *Drosophila* leucokinin (Drosokinin) acts upon the stellate cells and elevates intracellular  $\text{Ca}^{2+}$  and regulates fluid secretion. Besides these observations, in  $\text{Ca}^{2+}$ -free conditions, thapsigargin, an endoplasmic reticulum (ER)  $\text{Ca}^{2+}$ -ATPase inhibitor, elevates  $[\text{Ca}^{2+}]_{\text{cyto}}$  in only the tubule smaller stellate cells but not principal cells. Taken together, this data strongly demonstrates the existence of cell-specific  $\text{Ca}^{2+}$  signaling mechanisms in tubules.

#### 1.3.1.5 $\text{Ca}^{2+}$ handling by tubules

In a simple epithelium like tubule, regulatory mechanisms for  $\text{Ca}^{2+}$  handling are highly sophisticated in that several pumps and channels are involved under the control of multiple regulatory cascades (Davies and Terhzaz, 2009). The plasma membrane  $\text{Ca}^{2+}$  channels in tubules include L-type  $\text{Ca}^{2+}$  channels (voltage-gated), cyclic nucleotide-gated (CNG) channels, and transient-receptor-potential (TRP) channels. The organellar  $\text{Ca}^{2+}$  pumps that respond to  $\text{Ca}^{2+}$  upon  $\text{IP}_3$  stimulation include SERCA, or sarco/endoplasmic reticulum  $\text{Ca}^{2+}$ -ATPase and SPOck or secretory pathway  $\text{Ca}^{2+}$ -ATPase.

Tubules have been investigated for the *Drosophila* homologues of human L-type  $\text{Ca}^{2+}$  channels. The  $\alpha$ -subunits, *Dmca1A*, *Dmca1D* are found to express in these non-neuronal tissues (MacPherson et al., 2001) in consistent with pharmacological studies on vertebrates that provided evidence for functional L-type  $\text{Ca}^{2+}$  channels in the kidneys (Hayashi et al., 2007).

In tubules, these channels were observed to be sensitive to the channel antagonists, verapamil and nifedipine, and found to inhibit stimulatory fluid secretion responses by tubules. Verapamil seems to inhibit thapsigargin induced  $[\text{Ca}^{2+}]_{\text{cyto}}$  increase; indicating an alternate route for thapsigargin action (probably via plasma membrane channels), and is consistent with previous observations.

The localisations of these channels in the tubules found to be apical and basolateral and segment specific in that the dihydropyridine-sensitive channels occur in the apical membranes of the  $\text{Ca}^{2+}$  storing initial segment suggesting the transepithelial transport route in these segments.

The pharmacology of plasma membrane  $\text{Ca}^{2+}$  channels seems to overlap. Verapamil and nifedipine have also been shown to modulate cGMP induced  $[\text{Ca}^{2+}]_{\text{cyto}}$  response in tubule principal cells that can be abolished by a reduction in extracellular  $\text{Ca}^{2+}$ . This possibly suggests a role for CNG channels in mediating  $\text{Ca}^{2+}$  influx into the cells (MacPherson et al., 2001). According to the FlyAtlas mRNA signal, the CNGs are better candidates than L-type calcium channels in tubules as the former express more abundantly than the later. Given the kinetics of voltage-gated  $\text{Ca}^{2+}$  channels, CNG channel-mediated  $\text{Ca}^{2+}$  influx mechanisms may lead to the slow transient uptake by organelles that are seen in mitochondria for example (Terhzaz et al., 2006).

In tubules, transient receptor potential-like (TRPL) channels, rather than the TRPs in photoreceptor cells, are required for normal epithelial function (MacPherson et al., 2005). However, the novel TRP members that are found in the FlyAtlas to be abundant in tubules and may also play roles in epithelial function.

The famous intracellular  $\text{Ca}^{2+}$ -release channels include  $\text{IP}_3$  and ryanodine receptors ( $\text{IP}_3\text{R}$  and  $\text{RyR}$ ) that facilitate the release of  $\text{Ca}^{2+}$  from internal stores. The function of  $\text{IP}_3\text{R}$  in ER calcium release mechanisms have been extensively studied; and  $\text{RyR}$  is known in the sarcoplasmic reticulum (SR) and mediates skeletal muscle contraction through its allosteric activation by the conformational change in L-type  $\text{Ca}^{2+}$  channels, alpha subunit 1 (Cav1.1) (Proenza et al., 2002).

### ***1.3.2 Weiczorek model for fluid secretion by tubules***

It has been widely believed that the  $\text{Na}^+$ -motive force generated by  $\text{Na}^+/\text{K}^+$  ATPase energises animal plasma membranes. This has been an established route that allows secondary active transport of amino acids, glucose and several other nutrients.

In contrast, the 'Wieczorek model' conclusively presented evidence for an apical V-ATPase in energizing insect plasma membranes (Harvey and Wieczorek, 1997). Furthermore, this model argues a case for an apical alkali metal ( $\text{Na}^+$  and  $\text{K}^+$ ) exchanger as a functional partner for V-ATPase function.

The strongest evidence for an apical V-ATPase came from the lepidopteran midgut goblet cell apical membranes where  $\text{K}^+$  stimulated ATPase activity was localised (Wieczorek et al., 1986). In addition, the apparent 10, 000-fold proton gradient across the goblet cells was found to be balanced by a voltage of -240 mV (Dow, 1989). This voltage difference later was conclusively demonstrated to be caused by a V-ATPase (Harvey and Wieczorek, 1997; Schweikl et al., 1989).

In *Drosophila*, V-ATPase increases luminal positive transepithelial potential (TEP) in principal cells where it is found, and drives fluid secretion. Furthermore, the secretion can be pharmacologically abolished by both bafilomycin A1, and amiloride, the potential V-ATPase and  $\text{Na}^+/\text{H}^+$  exchanger inhibitors respectively (Dow et al., 1994a; Giannakou and Dow, 2001).

In the V-ATPase functional model, the apical NHE was thought to transport alkali metals, predominantly  $\text{K}^+$ , into the lumen in exchange for  $\text{H}^+$ . This will not only allow the membrane potential equilibrium, but it in turn drives the water flow into the lumen along its osmotic gradient. However, until recently, no plausible candidate for an apical antiport/exchanger partner for the V-ATPase (as required for the Wieczorek model) could be identified in *Drosophila*. Recently, two candidates including Nha1 and Nha2 have been shown to be the *Drosophila* representatives of the newly-discovered CPA2 branch of the cation proton antiporter family (also known as NHAs). These were proposed as better candidates for Wieczorek exchangers than the better known CPA1 branch that includes the classical  $\text{Na}^+/\text{H}^+$  exchangers (or NHEs) (Day et al., 2008).

However, as the name suggest, V-ATPases are predominantly found in the endomembrane vesicles in the endolysosomal pathway translocating protons into the vesicular compartments in expense of an ATP at the cytoplasmic side (Anraku et al., 1989; Jentsch, 2007).

Classically, this inward movement of  $H^+$  ions thought to be accompanied by a  $Cl^-$  influx leading to acidification of the compartments. However, ClC exchangers instead of  $Cl^-$  channels have been proposed to compensate the electrical currents generated by the V-ATPases (Scheel et al., 2005).

Although the insect Wieczorek model offers an exciting avenue for plasma membrane energization via apical V-ATPases, it still remains to be seen whether  $Cl^-$  channels or exchangers offer anything to explain apical V-ATPase function.

### **1.3.3 Neuroendocrine control of tubule fluid secretion**

Neuroendocrine signaling mechanisms are well characterised in tubules. Particularly, secretion physiology of tubules via neurohormone peptide modulation by the development of fluid transport assays (Dow et al., 1994b). Several short stretches of peptide sequences including *Manduca sexta* cardio-acceleratory peptide CAP2b, *Anopheles* leucokinin, *Drosophila* capa, leucokinin, and calcitonin-like peptides stimulate fluid secretion via distinct or overlapping G-protein coupled receptor signaling mechanisms (Iversen et al., 2002; Radford et al., 2002).

For example, CAP2b (*Drosophila* capa1 and capa2 (Kean, 2002 #200)) stimulates *Drosophila* tubule fluid secretion and cation conductance via principal-cells with an increase in intracellular  $Ca^{2+}$  (Rosay et al., 1997) and [cGMP] (Davies et al., 1995).

Drosokinin, in contrast, specifically stimulates intracellular  $[Ca^{2+}]$  and fluid secretion in stellate cells leading to the activation of  $Cl^-$  conductance (Terhzaz et al., 1999b); (O'Donnell et al., 1998; Rosay et al., 1997); (Radford et al., 2002). Furthermore, cyclic nucleotide levels do not seem to change in stellate cells (Davies et al., 1995). CRF-like peptide diuretic hormone or Dh is another neurohormone that stimulates [cAMP] and tubule secretion (Cabrerero et al., 2002). The external addition of cGMP and cAMP to tubules also increases fluid secretion (Dow et al., 1994a). Taken together, neurohormone regulation of tubule diuretic responses via G-protein coupled receptor signaling mechanisms should prove useful for molecular physiological analysis using tubules as an organotypic test bed.

In the following sections the remaining two key areas will be introduced including the molecular physiology of  $\text{Cl}^-$  ion transport and peroxisome dynamics in the living organism, as these have been investigated as part of this thesis.

## 1.4 Molecular Physiology of $\text{Cl}^-$ ion transport

Organisms must respond to their surrounding environmental variations to sustain their life. They have evolved methods of maintaining their internal environments independently of external variations; this is called homeostasis. The homeostasis is achieved by sophisticated cellular physiological mechanisms, and the 'molecular physiology' explains the basis for physiological functions of organisms at the molecular level.

Ion channels are fundamental to the organismal homeostasis and survival. They are integral membrane proteins that facilitate the transport of ions across biological membranes. Several classes of ion channels are involved in the transport of inorganic ions such as  $\text{Cl}^-$ ,  $\text{Na}^+$ ,  $\text{K}^+$  and  $\text{Ca}^{2+}$ .

The channel proteins have a marked difference from the transporters in that the latter form 'alternate access' thereby preventing the formation of a continuous pore that cannot generate a continuous ionic gradient like the channels. In contrast, the channels through their selectivity filters for different ions catalyse the specific downhill movement of the ions into and out of the cells or cellular compartments. Unlike ion pumps, channels facilitate ions into and out of a cell (ionic flux) in a passive manner at very high ion conduction rates with a selectivity sequence for different ions.

The selectivity sequence depends on the ability of a channel to conduct one ion over other. Channels play a fundamental role in modulating electrochemical gradients generated by ion pumps and exchangers. The direction of the ionic flux is dictated by the concentrations of various ions within the cell, and its external milieu leading to the voltage differences across the membrane, and so ions move down their electrochemical gradient. The movement of ions across the membranes produces electrical currents ( $I$ ) leading to changes in membrane potential. The membrane potential changes can influence the activity of other types of channels in the membrane.

### 1.4.1 Cl<sup>-</sup> channels

Cl<sup>-</sup> channels are a structurally and functionally diverse group of ion channels that conduct Cl<sup>-</sup>, and other anions. These channels reside both in the plasma membrane and in intracellular organelles and regulate the passive movements of Cl<sup>-</sup> along its electrochemical gradients. Often, anion channels are called Cl<sup>-</sup> channels despite their capacity to conduct other anions, because of the abundance of Cl<sup>-</sup> in biological systems (Duran et al., 2010).

The low abundant anions such as bicarbonate (HCO<sub>3</sub><sup>-</sup>) and reactive oxygen species, superoxide (O<sub>2</sub><sup>-</sup>) produced from biological redox reactions are also transported through the channels. Accordingly, these anions are detrimental in cellular physiology and signaling. For example, HCO<sub>3</sub><sup>-</sup> secretion is important in CF pathology, although it is not fully clear CFTR itself can code for I<sub>HCO3-</sub> or whether it modulates putative members of Cl<sup>-</sup> / HCO<sub>3</sub><sup>-</sup> exchangers like SLC26A3 (Duran et al., 2010; Stewart et al., 2009). The transport of O<sub>2</sub><sup>-</sup>, that plays essential roles in cellular signaling, has been shown to be mediated by ClC-3 (Miller et al., 2007; Mumbengegwi et al., 2008). Although, the molecular identity of Cl<sup>-</sup> channels remains obscure, they have been best categorised depending on the basis of their gating mechanisms into five broad classes as shown below (Verkman and Galletta, 2009).

1. cAMP- or ATP-activated (cystic fibrosis (CF) transmembrane regulator or CFTR channels)
2. Voltage-activated (Cl<sup>-</sup> channels or ClC channels)
3. Ligand-activated (γ-Aminobutyric acid or GABA channels)
4. Volume- or swelling-activated (Tweety or Maxi channels)
5. Ca<sup>2+</sup>-activated (bestrophins and anoctamins)

The above classification is limited by the available data, thus overlapping gating mechanisms may exist. In addition, Cl<sup>-</sup> channels may also be regulated by pH, anions and phosphorylation by proteins kinases, or on the binding or hydrolysis of ATP (Jentsch et al., 2002).

Moreover, the potential diversity of  $\text{Cl}^-$  channels has often been revealed in the patch-clamp experiments. Despite differences in experimental conditions, the diversity of  $\text{Cl}^-$  channels is widely accepted in terms of their single-channel conductance, anion selectivity, and mechanism of their regulation.

Some of the well-known  $\text{Cl}^-$  channels like CFTR and ClC have been well studied. These studies provide some fascinating insights into  $\text{Cl}^-$  channels as a whole in terms of their mechanisms of regulation and physiological roles that can be used to study their molecular counterparts.

The CFTR encoded channels are multifunctional channels that not only act as an anion channel but also act as a regulator of other ion channels including  $\text{Ca}^{2+}$ -activated  $\text{Cl}^-$  channels (CaCCs) (Nilius and Droogmans, 2003).

These channels are predominantly gated by cAMP and are involved in fluid transport processes across various epithelia including the airways. The  $\Delta 508$  mutation causes impaired trafficking of CFTR thus reducing its incorporation into the plasma membrane. This was thought to be the major cause of the lethal airway lung disease, cystic fibrosis (Cuthbert, 2011).

The ClC family has nine members that are grouped into three classes according to their sequence homology. These include ClC-1, ClC-2, hClC-Ka (rClC-K1) and hClC-Kb (rClC-K2); ClC-3 to ClC-5, and ClC-6 and ClC-7. The first crystal solved for a  $\text{Cl}^-$  channel was of a ClC from bacteria at 3 Å resolution. It revealed the homodimer structure of the ClC channel with a two-fold axis perpendicular to the membrane plane (Dutzler et al., 2002).

Moreover, each of the subunits of the dimer forms its own ion-conduction pore. The ClC-1, ClC-2, ClC-Ka and ClC-Kb are plasma membrane channels. The other members of the ClC family are predominantly found in the intracellular vesicles in the endolysosomal pathway and may compensate currents of  $\text{H}^+$ -ATPases thus facilitating their luminal acidification of these membranes. As such, impaired synaptic vesicle acidification is seen upon disruption of intracellular ClC-5 and ClC-3 channels (Piwon et al., 2000; Stobrawa et al., 2001).

However, upon heterologous expression, CLC-4 and CLC-5 have been found in the plasma membranes and mediated  $\text{Cl}^-$  currents at positive intracellular voltages (Friedrich et al., 1999; Steinmeyer et al., 1995). In contrast, the Thomas Jentsch lab provided compelling evidence for  $\text{Cl}^-/\text{H}^+$  exchanger activity for CLC-4 and CLC-5 that provide neutralising anion currents for V-type  $\text{H}^+$ -ATPases that pump protons into the compartments (Jentsch, 2007; Jentsch et al., 2005). The significance of the electrogenic exchange mechanism however is unclear, as it needs additional metabolic energy, unlike  $\text{Cl}^-$  channels that mediate passive  $\text{Cl}^-$  movements.

Nevertheless, it has been hypothesized that intracellular CLCs are not only important for facilitating vesicular acidification, but may also contribute the regulation of  $\text{Cl}^-$  concentrations in these compartments (Scheel et al., 2005).

In line with this hypothesis, Jentsch and colleagues obtained some fascinating insight into the mystery of CLC-5 and CLC-7 function using knock-in mouse models; separately published in 2010 (Novarino et al., 2010; Weinert et al., 2010). The knock-in mouse models that have a single point mutation that uncouples  $\text{H}^+$  transport from inward  $\text{Cl}^-$  transport still show the same pathology as in both CLC-5 and CLC-7 knockout mouse. These findings emphasise the mysteries still surrounding CLC proteins in terms of their physiological functions.

### ***1.4.2 $\text{Cl}^-$ channel functions and associated channelopathies***

$\text{Cl}^-$  channels are implicated in a plethora of cellular and physiological functions including regulation of  $\text{pH}_i$ , cell volume,  $[\text{Ca}^{2+}]_i$ , and membrane potential (resting and depolarization).  $\text{Cl}^-$  channels, thus mediate transepithelial transport of solutes, secretion of hormones, bone metabolism, cell proliferation, differentiation to neuronal signal propagation (Jentsch et al., 2002; Planells-Cases and Jentsch, 2009).  $\text{Cl}^-$  channels mediate these functions through the transport of charge, the current flowing through the channel or transport of matter. The important distinction between  $\text{Ca}^{2+}$  and  $\text{Cl}^-$  a decade ago has been that the non-belief in  $\text{Cl}^-$  role in cellular signaling (Jentsch et al., 2002). However, a paradigm shift is currently seen in the  $\text{Cl}^-$  channel field, as the  $\text{Cl}^-$  movements, now, are clearly associated with cellular signaling events (Duran et al., 2010).

Diseases caused by dysfunction of channel proteins are collectively known as channelopathies, so the dysfunction in  $\text{Cl}^-$  channel function is responsible for  $\text{Cl}^-$  channelopathies. The famous  $\text{Cl}^-$  channelopathies include cystic fibrosis, Best disease, myotonia congenita, osteopetrosis, Bartter syndrome (with deafness), and Dent's disease. These channelopathies are caused by their respective channel defects in CFTR, Best1,  $\text{ClC-1}$ ,  $\text{ClC7/Ostm1}$ , Barttin, and  $\text{ClC-5}$ . The functional defects are manifest in  $\text{Cl}^-$  secretion in the airways, RPE  $\text{Cl}^-$  transport, decreased  $\text{Cl}^-$  conduction, acid secretion in osteoclasts, renal salt loss and endolymph secretion and endosomal acidification.

Even the subtle functional disturbances in  $\text{Cl}^-$  channel functions can cause the diseases like myotonia congenita, a skeletal muscle disorder where decreased muscle contractility or muscle stiffness is seen. In the muscle cells and in various other systems, the interplay between  $\text{Na}^+$ ,  $\text{K}^+$  ATPase and the inwardly rectifying  $\text{K}^+$  channels establish the resting membrane potential. However, during muscle activity, the relatively large  $\text{Cl}^-$  conductance keeps the resting membrane potential near  $\text{Cl}^-$  equilibrium potential ( $E_{\text{Cl}}$ ) thus contributing to the equilibrium of the membrane potential. This equilibrium is disrupted in myotonia congenita patients where decreased  $\text{Cl}^-$  conductance is observed (Bryant, 1969; Lipicky and Bryant, 1971; Lipicky et al., 1971).

As this thesis deals with the characterisation of possible contributions of bestrophins as CaCCs or, the regulators of other channel functions, the literature surrounding these channels has been reviewed in Chapter 6 and Chapter 7. However in addition to these main chapters, the general rules of CaCCs are reviewed below.

### **1.4.3 CaCCs**

In electrophysiological experiments,  $\text{Ca}^{2+}$  was found to activate  $\text{Cl}^-$  currents, thus these currents were called as  $\text{Ca}^{2+}$ -activated  $\text{Cl}^-$  currents ( $I_{\text{ClCa}}$ ). The  $I_{\text{ClCa}}$  were described about three decades ago in *Xenopus levis* oocytes. However, the molecular identity of the channels responsible for the  $I_{\text{ClCa}}$  phenomenon has long been elusive until the bestrophins and more recently anoctamins have been proposed to be the candidates (Barish, 1983; Hartzell et al., 2008; Hartzell et al., 2009; Miledi, 1982).

In the *Xenopus* oocytes, the activation of  $I_{ClCa}$  was found to occur upon fertilization that depolarizes the membrane, and prevents additional sperm entry into the oocytes. Later,  $I_{ClCa}$  were found in salamander photoreceptor inner segments, and suggested to be playing a role in transmitter release (Bader et al., 1982; MacLeish and Nurse, 2007). Further studies demonstrated that  $I_{ClCa}$  in many cell types including cardiac, skeletal and vascular smooth muscle cells, endothelial and epithelial cells, as well as neurons. Accordingly, the candidate channels proposed to be encoding the currents have been shown to be important in epithelial secretion, excitability of cardiac and neuronal membranes, olfactory transduction, vascular tone regulation and photoreception (Kunzelmann et al., 2007). However, unambiguous identification of the molecular components responsible for the  $I_{ClCa}$  still remains elusive due to interfering native  $I_{ClCa}$  when studying a foreign protein in a heterologous electrophysiology experiment.

#### 1.4.3.1 Mechanisms of $Ca^{2+}$ -dependent $Cl^-$ secretion in epithelia

In glandular secretion, from acinar cells of various secretory glands including salivary, pancreatic and lachrymal glands, activated via muscarinic receptors,  $Ca^{2+}$ -activated  $Cl^-$  secretion plays important role. This occurs via the primary neurotransmitter messenger during parasympathetic stimulation via basolateral muscarinic M3 receptors (mAChR) (Kunzelmann et al., 2007; Melvin et al., 2005). Activation of G-protein coupled mAChR or purinergic P2Y receptors is mediated by  $Ca^{2+}$ -dependent  $Cl^-$  secretory mechanism in the airways and intestine.

In all the above cases, intracellular  $Ca^{2+}$   $[Ca^{2+}]_i$  is mobilised through various routes mentioned earlier leading to the activation of CaCCs. In addition, other cellular signaling pathways that act on ryanodine receptors elicit repetitive local  $Ca^{2+}$  spikes near apical membrane. Furthermore, acidic stores like lysosomes and secretory granules act in concert with  $IP_3$ -mediated ER and ryanodine receptor pathways (Menteyne et al., 2006). Activation of CaCCs via phosphorylation by the multifunctional calmodulin-dependent kinase II (CAMKII) depending on inositol tetrakisphosphate ( $InsP_4$ ) levels was shown to be one of the regulatory mechanisms in T84 epithelial cells (Ho et al., 2001). However, this was ruled out in other tissues like salivary glands (Kunzelmann et al., 2007).

The above reports suggest the diversity of activation of CaCCs in different cells and tissues. Thus suggesting differential regulation and function in secretion via CaCCs. In vascular smooth muscle cells, for example, the regulation of native CaCCs mediated by CaMK II and calcineurin and involved in vascular tone (Leblanc et al., 2005). In *Drosophila*, CaMKII expression is not that significantly found in the salivary glands according to the FlyAtlas suggesting the coregulation of different modules in signaling is also an important factor.

CaCCs are activated upon increases in the  $[Ca^{2+}]_i$ . The elevation in  $[Ca^{2+}]_i$  possibly occurs through an extracellular primary messenger that acts on a membrane receptor, triggering the activation of  $Ca^{2+}$  mobilising events.

The subsequent activation of  $Cl^-$  channels may dependent on multiple  $Ca^{2+}$  mobilising events including from intracellular stores, through the activation of plasma membrane  $Ca^{2+}$  channels (such as voltage-, cyclic nucleotide- or volume-activated  $Ca^{2+}$  channels) or through store-operated  $Ca^{2+}$  channels. Thus, the events coupled to the activation of CaCCs in various cell types have the potential in regulating multiple cellular events (Leblanc et al., 2005). Moreover, CaCCs provide a triggering mechanism in cellular signaling, as they are normally closed at resting, free intracellular  $Ca^{2+}$  concentration (~100 nmol/L) in most cell types, during signal transduction for membrane excitability, osmotic balance, transepithelial chloride movements, or fluid secretion (Leblanc et al., 2005).

Heterologous expression and characterisation of a non-native protein channels often hampered by the associated endogenous channel activation in the system (Jentsch et al., 2002). In the case of CaCCs, questions have been raised regarding the activation of  $I_{ClCa}$  under experimental conditions that use  $Ca^{2+}$  ionophores such as ionomycin and in patch clamp experiments in which  $I_{ClCa}$  is activated independently of receptor stimulation (Kunzelmann et al., 2007). Often, very little activation of  $I_{ClCa}$  was observed in native airway epithelial cells with even at high concentrations of ionomycin, comparatively with the stimulation of P2Y2 receptors, for example (Kunzelmann et al., 2007). These observations led to the suggestion that methods using ionomycin and high external  $Ca^{2+}$  concentrations in excised membrane patches may be nonphysiological.

Furthermore, intracellular  $\text{Ca}^{2+}$  elevations by basolateral membrane stimulation via mAChR receptors in airways or distal colon does not directly activate  $\text{Cl}^-$  channels in the luminal membrane but enhances the driving force for luminal  $\text{Cl}^-$  secretion by activation via  $\text{K}^+$  channels in the basolateral membrane (Kunzelmann et al., 2007; Mall et al., 1998).

#### 1.4.3.2 $\text{Ca}^{2+}$ -dependent $\text{Cl}^-$ secretion in epithelia

The mammalian airways show  $I_{\text{ClCa}}$  (Yang et al., 2008). CF pathology linked to altered  $\text{Cl}^-$  secretion in human airways and other secretory epithelia is a life threatening disease. CF is caused by a cAMP-activated CFTR encoded  $\text{Cl}^-$  channel dysfunction (Schwiebert et al., 1999).

In contrast,  $\text{CFTR}^{-/-}$  transgenic mouse do not develop CF lung disease. Instead, it does show pronounced  $\text{Ca}^{2+}$ -activated  $\text{Cl}^-$  secretion in the airway epithelia probably mediated by  $\text{ClCa}$  (Grubb et al., 1994). This  $\text{Cl}^-$  secretion in the airways was thought to compensate for the CFTR under pathological conditions in mouse airways; although such compensation was not observed in human airways. Interestingly, the purinergic receptor agonist treatment with UTP activates latent  $I_{\text{ClCa}}$ , and compensates for CFTR loss of function (Knowles et al., 1991). These observations led to designing modified purine nucleotides for human CF therapeutic intervention. The airway surface liquid essentially is maintained by CFTR mediated  $\text{Cl}^-$  secretion rather than  $\text{Ca}^{2+}$ -activated  $\text{Cl}^-$  secretion. Because the activation of CaCCs seems to result in transient  $\text{Cl}^-$  secretion partly due to the basolateral  $\text{Cl}^-$  uptake by  $\text{Na}^+ / 2 \text{Cl}^- / \text{K}^+$  cotransporter. But, how this explains disease pathology is still not resolved.

The colonic epithelium plays an important role in the absorption of nutrients. In the luminal membranes of the colonic rectal and distal segments, CFTR seems to be a predominant luminal  $\text{Cl}^-$  channel and an essential component in transient  $\text{Ca}^{2+}$ -activated  $\text{Cl}^-$  secretion (Kunzelmann and Mall, 2002).

The roles of CaCCs in intact renal tubules, a major transporting and fluid secreting epithelia, in the electrolyte transport have not been shown conclusively. However, the  $I_{\text{ClCa}}$  have been clearly presented for primary cultures of renal cells (Barro Soria et al., 2009).

The same study suggested that CaCCs in the renal epithelia may have essential roles in the re-absorption of large quantities of salt filtered by the mammalian glomerulus.

As mentioned earlier, secretory stimulants such as acetyl choline and cholecystokinin clearly stimulates  $\text{Cl}^-$  secretion upon the activation of  $\text{Ca}^{2+}$  that is distinct from the cAMP pathway in the pancreatic ducts both *in vivo* and *in vitro* studies unlike the renal epithelium. However, the CFTR knockout mouse does not display pathological ductular secretion similar to airways that are not affected in the pathology. These results suggest alternative mechanisms or roles for CaCCs for example in modulating other channels or in regulating cell proliferation and controlling cell volume (Hartzell et al., 2005a).

#### 1.4.3.3 Disease relevance of CaCCs

There is currently a lack of understanding of how CaCCs dependent  $\text{Cl}^-$  secretion can cause the pathological conditions of CFTR, Best disease, in the epithelia, making the disease relevance of these channels somewhat ambiguous. Although, these genes are implicated in the diseases, the functional studies so far are not conclusive to explain the defective contribution of  $\text{Cl}^-$  secretion via these channels. A proper elucidation of the functional roles of these proteins that explain the pathologies is necessary. This can only be achieved using relevant animal disease models as for example the  $I_{\text{ClCa}}$  seen in *in vitro* models cannot be recapitulated *in vivo*. However, model organisms including *Drosophila*, where there is a wealth of genetic and genomic tools available could be useful to understand the molecular mechanisms involved in the pathological conditions.

#### 1.4.3.4 Functional features and Molecular identity of CaCCs

$I_{\text{ClCa}}$  have been observed and studied in detail within several systems, however the molecular identity of the channels responsible for these currents has yet remained inconclusive. However, several candidate genes that may encode CaCCs have been cloned and characterised. Some common biophysical characteristics seems to be shared by CaCCs in different tissues in terms of their voltage dependence, degree of outward rectification  $I^- > \text{Cl}^-$  permeability and pharmacological inhibition.

They also show differences in single channel conductance and regulation; for example phosphorylation by CaMKII in different tissues. The fact that they may be variably regulated by cell volume, pH, voltage and  $\text{Ca}^{2+}$ , suggests that they should exist in a complex bioenergetic framework. This diversity in regulation and function can be achieved by variable expression of different CaCCs, and their functional coregulated partners such as CaMKs in a cell- and tissue-specific manner and their potential impact on the other channels. In addition, the arrangement of CaCCs with different proteins seems to determine their function. For example, the interaction of large conductance potassium channel BK-subunit with the putative  $\text{Ca}^{2+}$ -activated  $\text{Cl}^-$  channel protein ClCA1 has been shown (Greenwood et al., 2002).

Some of the details regarding the ambiguity in molecular identity of CaCCs have been presented in the sections below.

#### **1.4.3.4.1 ClCA family**

ClCA1 was first cloned from a bovine tracheal expression library encoding DIDS- and DTT-sensitive anion channel (Cunningham et al., 1995). The same study also showed that the ClCA1 was sensitive to ionomycin and DTT in COS-7 cells using whole-cell patch clamp experiments. Later, the first human counterpart of the bovine ClCA1 was identified in  $\text{Ca}^{2+}$ -activated  $\text{Cl}^-$  secretion and proposed to form an intermediate conductance chloride channel (Gandhi et al., 1998; Gruber et al., 1998).

As mentioned earlier,  $\text{Ca}^{2+}$ -activated  $\text{Cl}^-$  secretion via ClCA compensate for CFTR dysfunction in the mouse models and accordingly, they have been shown to be expressed in various epithelial tissues (Ritzka et al., 2004). However, ClCA and ClCA2 show different biophysical properties putting them under suspicion to be real candidates for CaCC (Yang et al., 2008). The potential functions of bovine ClCA2 in endothelial cell adhesion in tumour growth, and the human ClCA3 protein' secretory nature further supported the above notion (Yang et al., 2008). However, mouse ClCA1 when co-expressed with KCNMB1 (BK-subunit, a regulatory subunit of  $\text{Ca}^{2+}$ -activated  $\text{K}^+$  channel) seem to produce  $I_{\text{ClCa}}$  that resemble those of endogenous CaCCs (Greenwood et al., 2002).

The human ClCK channels like the rodent ClCK1 have also been shown to be modulated by extracellular  $\text{Ca}^{2+}$  and protons (Gradogna et al., 2010). However, the activation of ClCKa channel was not completely abolished in the absence of  $\text{Ca}^{2+}$ , demonstrating that  $\text{Ca}^{2+}$  is not strictly essential for the channel activation. Moreover, hydrophobicity analysis revealed one or two transmembrane segments in ClCK, a structure that seem to be unusual for  $\alpha$ -subunits of ion channels and therefore may not be feasible as single entity  $\text{Cl}^-$  channel (Suzuki, 2006).

Other members of ClC superfamily of  $\text{Cl}^-$  channels that are implicated in CaCC function include ClC-3, a homologue of the voltage-gated  $\text{Cl}^-$  channel ClC-0. Although this has been suggested to form a CaCC, the general biophysical characteristics differ substantially from those of native CaCCs. Moreover, mice lacking ClC-3 does show normal  $\text{Ca}^{2+}$ -activated  $\text{Cl}^-$  conductance thus may contribute to  $\text{Ca}^{2+}$ -activated  $\text{Cl}^-$  secretion with other channels (Arreola et al., 2002; Huang et al., 2001).

#### **1.4.3.4.2 Tweety family**

Tweety family has been long standing as a candidate for CaCC that form large conductance CaCCs (maxi  $\text{Cl}^-$  channels) in the excitable tissues including heart, brain and skeletal muscle (Suzuki, 2006). However, a role for these channels in non-excitabile, epithelial tissues was not seen as a potential, since epithelial  $\text{Cl}^-$  channels show small conductance.

#### **1.4.3.4.3 Bestrophin family**

Bestrophins are discussed in detail in Chapters 6 and 7 as these have been chosen for the functional characterisation as part of this thesis.

#### **1.4.3.4.4 Anoctamins**

While the ambiguity has been increasing in bestrophins as a candidate CaCC hypothesis, novel members came into picture in the form of anoctamins. Anoctamins first got attention from the gene expression studies where first family member, *ANO1*, has been identified as upregulated in squamous cell carcinoma cells of the head and neck (Carles et al., 2006), and in gastrointestinal stromal tumours (Espinosa et al., 2008).

## 1.5 Peroxisome dynamics in the living organism

Peroxisomes are single membrane-bound, ubiquitous and diverse organelles that perform key metabolic functions in almost all eukaryotic cells (Visser, van Roermund et al. 2007; Islinger, Cardoso et al. 2010). They can house as many as 100 enzymes and perform a range of essential metabolic functions within a variety of cells from the  $\alpha$ - and  $\beta$ -oxidation of fatty acids, synthesis of ether lipids (plasmalogens), and oxidation of bile acids and cholesterol and degradation of  $H_2O_2$ . Defects in peroxisomal formation and function in humans result in a spectrum of peroxisomal disorders which are broadly classified into two groups, peroxisome biogenesis disorders (PBDs), and single enzyme deficiencies (SEDs) (Figure 1-6).

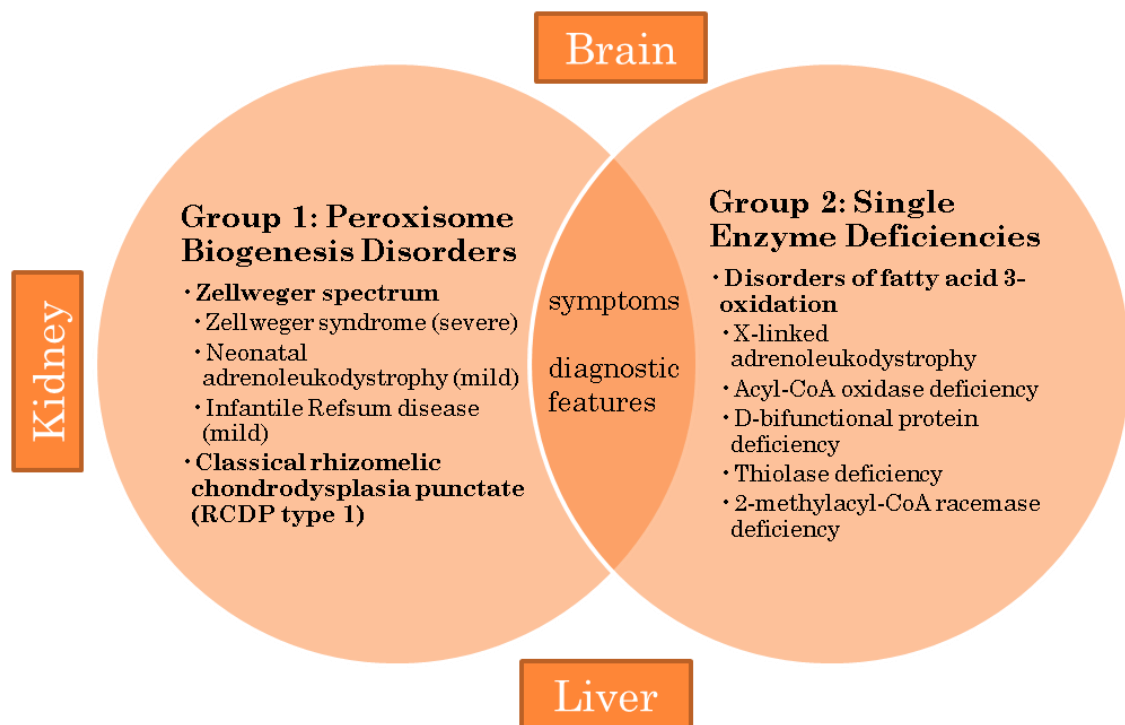


**Figure 1-6 Peroxisome disorders in humans.**

Peroxisome disorders are broadly categorised into two groups, peroxisome biogenesis disorders (PBDs) and single enzyme deficiencies (SEDs). Two groups have overlapping symptoms and diagnostic features with manifestations in the brain, kidney and liver.

Peroxisome biogenesis disorders show Zellweger spectrum syndrome (ZSS) including single enzyme deficiencies such as adrenoleukodystrophy (Reddy and Mannaerts 1994; Wanders 2004; Wanders and Waterham 2006) with severe to mild disease phenotypes.

ZSS patients show morphogenesis defects, severe neurological dysfunction, neurosensory defects, regressive changes, hepatodigestive involvement with failure to thrive leading to early death due to the absence of recognizable liver peroxisomes (Baumgartner et al., 1998; Poggi-Travert et al., 1995).

In ZSS and other single enzyme deficiencies, human patients show hypotonicity or reduced muscle contractility associated with other factors such as hyponatremia where reduced sodium levels are found in the serum. Some reports suggest that the hypotonia could prolong to the adult stages. The hypotonicity is also associated with poor feeding (including reduced food intake) and increased very long chain fatty acids (VLCFAs). In single enzyme deficiencies caused by acyl Co-A oxidase 1 (ACOX1) and the multifunctional hydroxysteroid (17-beta) dehydrogenase 4 (HSD17B4) consistently show neonatal hypotonia and neonatal seizures refractory to resistant for therapeutic intervention.

### **1.5.1 Peroxisome biogenesis**

The enigmatic biogenesis of peroxisomes can be divided into three conceptual steps including membrane formation, matrix protein import and proliferation. For de novo synthesis of peroxisomes, all proteins destined for peroxisomes should be transported to and assembled at the sites of peroxisome assembly as they are encoded by the nuclear genome, unlike for example mitochondrial proteins. The sequential formation of peroxisomes is achieved by peroxisome transport proteins, peroxins (or PEX) which can principally recognize two peroxisomal targeting consensus sequences (PTS) including PTS1, (S/A/C)-(K/R/H)-(L/M) and PTS2, (R/K)-(L/I/V)-X5-(Q/H)-(L/I/V) (Figure 8-3). Two types of proteins need to be delivered to peroxisome assembly sites and into their lumen. These include peroxisome membrane proteins (PMPs) and luminal proteins. It is well established that peroxisomal luminal proteins are synthesised on polyribosomes and post-translationally imported directly into the peroxisome lumen, though the PMP transport is still a controversial area (Nuttall et al., 2011).

Peroxins are well conserved throughout evolution (Gould et al., 1990; Neuberger et al., 2003b; Purdue and Lazarow, 2001). Some peroxins cause severe defects in humans.

For example, defects in the *PEX6* gene function are the second most common causes of ZSS disorders (Ebberink et al., 2010). The *PEX6* encodes a putative AAA ATPase (ATPases Associated with diverse cellular Activities).

*PEX6* along with *PEX1p* recycle *PEX5p* in the last steps of the cargo delivery into the peroxisomal matrix for the next round of import (Rucktaschel et al., 2011).

The *PEX11* family is another important family that promotes peroxisome division in multiple eukaryote species. Like mammals (and unlike yeast), there are three known *PEX11* genes in *Drosophila melanogaster* (mammalian counterpart is shown in brackets with the identification method) including *CG8315* (*PEX11B*; Homologene), *CG13827* (*PEX11γ*; Homologene) and *CG33474* (*PEX11γ*; BLASTN). All are annotated to be involved in peroxisome fission. Unlike its human counterpart, the *Drosophila* *PEX11γ* (*CG13827*) has a putative carbohydrate kinase, *FGGY*, conserved site that shows phosphotransferase activity (alcohol group as acceptor). This site is also found in glycerol kinase, xylulokinase, gluconate kinase, L-fuculokinase and carbohydrate kinase.

### **1.5.2 How is peroxisome number controlled?**

Peroxisomes, like many organelles, exist in defined copy numbers and sizes in a given cell type and its metabolic state (Chang et al., 1999; Thoms and Erdmann, 2005). They can be as few as 3 and as many as 100s in number and can be inducible by external environment. For example, yeast grown on high concentrations of glucose can have as few as 1-3 peroxisomes while the same yeast grown on oleic acid can have 10 large peroxisomes (Erdmann and Blobel, 1995). The peroxisome transitions between metabolic states of the cell should therefore be actively controlled. The molecular machinery driving membrane fusion and fragmentation on the organelle is key factor for this phenomenon where peroxins play well established roles in peroxisome formation and fission (Opalinski et al., 2011; Thoms and Erdmann, 2005). Two general classes of organelle division factors can be identified in organelle biogenesis including the one that has the components essential for division and directly participate in the vesicle budding event, and the other that has the recruitment factors, which helps bring the division machinery to the organelle membrane.

According to the available data, PEX11 proteins belong to the second class where they involve in the recruitment of the components required for the peroxisome division; VPS1/DLP1 the yeast and human dynamin-related GTPases respectively belong to the first class where they are directly involved in initiating the budding process.

These hypotheses come from the fact that the loss of PEX11 protein function had a less severe effect on peroxisome abundance while its overexpression promoted peroxisome division (Li and Gould, 2002). In contrast, the loss of VPS1/DLP1 blocks peroxisome division completely though the overexpression did not increase the division (Hoepfner et al., 2001).

A report by (Li et al., 2002) suggests *PEX11 $\gamma$*  to be different from *PEX11a* and *PEX11B* in that its overexpression does not induce peroxisome proliferation in mammalian fibroblasts. Its expression was neither altered by classical peroxisome proliferating agents (PPAs) that function as ligands for PPAR $\alpha$  (Reddy and Hashimoto, 2001), nor by the loss of PEX11 $\alpha$  or PEX11B. Thus, they concluded that the phenotypes caused by *PEX11 $\alpha$ <sup>-/-</sup>/PEX11B<sup>-/-</sup>/PEX11 $\gamma$ <sup>-/-</sup>* knockouts in human fibroblasts were the same as the phenotypes in *PEX11 $\alpha$ <sup>-/-</sup>/PEX11B<sup>-/-</sup>* knockouts.

They also showed that PPAs induce the expression of *PEX11a* and promote peroxisome division. The phenotypes of *PEX11 $\alpha$ <sup>-/-</sup>* mice indicate the same for a novel class of PPAs (e.g., 4-Phenylbutyrate) that act independently of peroxisome proliferator-activated receptor alpha (PPAR $\alpha$ ). But it is not the case for classical PPAs that act as activators of PPAR $\alpha$ . The cells lacking both *PEX11* genes have no defects in peroxisome abundance.



So the work plan was involved in identifying genes with highly specific expression patterns, ideally the genes that are enriched in tubules, because of the wealth of downstream phenotypes available in this tissue. Then, these genes were investigated using functional tools including heritable RNAi, overexpressors, GFP-fusions, fluid secretion, and other tools and techniques developed as needed.

## 2. Materials and Methods

### 2.1 Fly stocks

The original stocks used in this study are presented below (Table 2-1). The first column identifies the fly line, the second indicates the genotype, the third describes the line and the fourth shows whether it was obtained from stock centres or made in-house as part of the project.

**Table 2-1 Fly stocks used in this study.**

**Flies were either obtained from the stock centres or made in house. Fly ID, fly identification; genotype, genetic description; description, what is the fly for; reference, where it was obtained from (if it is so).**

Fly ID	Genotype	Description	Reference
$w^{1118}$	<i>white-</i> ( <i>w</i> -);+/+;+/+	Isogenic white - background was used for <i>P</i> -element mediated germline transformation of transgenes of interest. It is a loss of function allele for white and acts as the wild-type for flies generated in this background.	<a href="http://flybase.org/reports/FBaI0018186.html">http://flybase.org/reports/FBaI0018186.html</a>
Canton S	w+;+/+;+/+	Wild type - <i>Drosophila melanogaster</i>	<a href="http://flybase.org/reports/FBst0000001.html">http://flybase.org/reports/FBst0000001.html</a>
c42-GAL4	w-; +/+; c42-GAL4/c42-GAL4	GAL4 enhancer trap specific to the tubule principal cells.	(Sozen et al., 1997); <a href="#">Dow/Davies Labs</a>
c724-GAL4	w-;+/+;c724-GAL4/c724-GAL4	GAL4 enhancer trap specific to the tubule stellate cells.	(Sozen et al., 1997); <a href="#">Dow/Davies Labs</a>
UAS- <i>Best1</i>	w-;+/+;UAS- <i>Best1</i> /TM3	<i>Best1</i> wild-type cDNA fusion with upstream activating sequence (UAS) promoter originally derived from Yeast.	Venkat Chintapalli, Dow/Davies Labs
UAS- <i>Best1</i> -YFP	w-; +/+; UAS- <i>Best1</i> -YFP/TM3	<i>Best1</i> wild-type cDNA fusion with upstream UAS promoter and downstream yellow fluorescent protein (YFP).	Venkat Chintapalli, Dow/Davies Labs
UAS- <i>Best1</i> -RNAi	w-;+/+;UAS- <i>Best1</i> -RNAi/TM3	<i>Best1</i> double stranded RNA ( <i>dsRNA</i> ) fusion with upstream UAS.	Venkat Chintapalli, Dow/Davies Labs
UAS- <i>Best2</i>	w-; +/+; UAS- <i>Best2</i> /TM3	<i>Best2</i> wild-type cDNA fusion with upstream UAS promoter.	Venkat Chintapalli, Dow/Davies Labs
UAS- <i>Best2</i> -YFP	w-; +/+; UAS- <i>Best2</i> -YFP/TM3	<i>Best2</i> wild-type cDNA fusion with upstream UAS promoter and downstream yellow fluorescent protein (YFP).	Venkat Chintapalli, Dow/Davies Labs
UAS- <i>Best2</i> -RNAi	w-; +/+; UAS- <i>Best2</i> -RNAi/TM3	<i>Best2</i> <i>dsRNA</i> fusion with upstream UAS.	Venkat Chintapalli, Dow/Davies Labs
UAS- <i>Best3</i>	w-; +/+; UAS- <i>Best3</i> -YFP/TM3	<i>Best3</i> wild-type cDNA fusion with upstream UAS promoter.	Venkat Chintapalli, Dow/Davies Labs

UAS- <i>Best3</i> -YFP	w <sup>-</sup> ; UAS- <i>Best3</i> -YFP/CyO; +/+	<i>Best3</i> wild-type cDNA fusion with upstream UAS promoter and downstream yellow fluorescent protein (YFP).	Venkat Chintapalli, Dow/Davies Labs
UAS- <i>Best3</i> -RNAi	w <sup>-</sup> ; +/+; UAS- <i>Best3</i> -RNAi/TM3,Sb	<i>Best3</i> dsRNA fusion with upstream UAS	<a href="http://stockcenter.vdr.c.at/control/product/~VIEW_INDEX=0/~VIEW_SIZE=100/~product_id=8371">http://stockcenter.vdr.c.at/control/product/~VIEW_INDEX=0/~VIEW_SIZE=100/~product_id=8371</a>
UAS- <i>Best4</i>	w <sup>-</sup> ; +/+; UAS- <i>Best4</i> /TM3	<i>Best4</i> wild-type cDNA fusion with upstream UAS promoter.	Venkat Chintapalli, Dow/Davies Labs
UAS- <i>Best4</i> -YFP	w <sup>-</sup> ; UAS- <i>Best4</i> -YFP/CyO; +/+	<i>Best4</i> wild-type cDNA fusion with upstream UAS promoter and downstream yellow fluorescent protein (YFP).	Venkat Chintapalli, Dow/Davies Labs
UAS- <i>Best4</i> -RNAi	w <sup>-</sup> ; +/+; UAS- <i>Best3</i> -RNAi/UAS- <i>Best3</i> -RNAi	<i>Best4</i> dsRNA fusion with upstream UAS.	<a href="http://stockcenter.vdr.c.at/control/product/~VIEW_INDEX=0/~VIEW_SIZE=100/~product_id=5272">http://stockcenter.vdr.c.at/control/product/~VIEW_INDEX=0/~VIEW_SIZE=100/~product_id=5272</a>
UAS- <i>Aequorin</i> -SKL	w <sup>-</sup> ; UAS- <i>Aequorin</i> -SKL/CyO; +/+	Aequorin wild-type cDNA fusion with upstream UAS and downstream canonical peroxisomal tripeptide signal sequence: SKL (Serine-Lysine-Leucine) that targets the proteins to peroxisome lumen.	Venkat Chintapalli, Dow/Davies Labs
UAS- <i>Aequorin</i> -KVK-SKL	w <sup>-</sup> ; UAS- <i>Aequorin</i> -KVK-SKL/CyO; +/+	Aequorin wild-type cDNA fusion with upstream UAS and downstream hexapeptide sequence for KVK-SKL (Lysine-Valine-Lysine - Serine-Lysine-Leucine) that targets the proteins to peroxisomes. Additional tripeptide preceding SKL has been shown to enhance the peroxisome luminal targeting.	Venkat Chintapalli, Dow/Davies Labs
UAS- <i>Aequorin</i>	w <sup>-</sup> ; +/+; UAS- <i>Aequorin</i>	Aequorin wild-type cDNA fusion with upstream UAS.	Dow/Davies Labs
UAS- <i>pHluorin</i> -KVK-SKL	w <sup>-</sup> ; UAS- <i>pHluorin</i> -KVK-SKL; +/+	pHluorin fusion with upstream UAS and downstream hexapeptide sequence for KVK-SKL (Lysine-Valine-Lysine - Serine-Lysine-Leucine) that targets the proteins to peroxisomes. Additional tripeptide preceding SKL has been shown to enhance the peroxisomal targeting.	Venkat Chintapalli, Dow/Davies Labs
UAS- <i>pHluorin</i>	w <sup>-</sup> ; UAS- <i>pHluorin</i> ; +/+	pHluorin fusion with upstream UAS.	Venkat Chintapalli, Dow/Davies Labs
UAS- <i>CG11919</i> -RNAi	w <sup>-</sup> ; UAS- <i>CG11919</i> -RNAi; +/+	<i>CG11919</i> dsRNA fusion with upstream UAS.	<a href="http://stockcenter.vdr.c.at/control/product/~VIEW_INDEX=0/~VIEW_SIZE=100/~product_id=32430">http://stockcenter.vdr.c.at/control/product/~VIEW_INDEX=0/~VIEW_SIZE=100/~product_id=32430</a>
UAS- <i>CG13827</i> -RNAi	w <sup>-</sup> ; UAS- <i>CG13827</i> -RNAi; +/+	<i>CG13827</i> dsRNA fusion with upstream UAS.	<a href="http://stockcenter.vdr.c.at/control/product/~VIEW_INDEX=0/~VIEW_SIZE=100/~product_id=101466">http://stockcenter.vdr.c.at/control/product/~VIEW_INDEX=0/~VIEW_SIZE=100/~product_id=101466</a>

## 2.2 Normal fly husbandry

Wildtype, *Drosophila melanogaster* (Canton S strain) flies were normally raised on standard medium (Appendix I) on a 12:12 h L:D cycle, at 23°C, and at 55% room humidity. To facilitate the collection of accurately staged adults, a laying population of around 12 males and 12 females were transferred to fresh vials daily. When adults emerged, they were subsequently transferred to fresh vials on the day of emergence, and used 7 days later. Where larvae were used, they were of feeding third-instar.

## 2.3 Tissue dissections

Flies were anaesthetised briefly by chilling on ice, then immediately dissected for tissues in *Drosophila* Schneider's medium (Invitrogen UK). Sample preparation information is presented in Table 2-2, including the number of tissues dissected, their definitions, total amount of RNA and Affymetrix amplification protocol for microarrays (Affymetrix Inc. UK).

**Table 2-2 FlyAtlas tissue descriptions.**

Tissue	Definition	Number per sample	Total amount of RNA used (ng)	Affymetrix protocol
Adult Brain	Excludes eyes and head capsule.	200-250	1500	One-Cycle
Adult Head	Severed at the neck. Includes brain, eyes, cuticle and some fat body.	100-150	1500	One-Cycle
Adult Eye	Dissected from the brain and the rest of the head capsule. So includes plenty of cuticle.	40-60	100	IVT-Express
Adult Thoracicoabdominal ganglion	The fused thoracic ganglia that are easily dissected from the ventral surface of the thorax after removing the head.	250-300	1500	One-Cycle
Adult Salivary gland	The glands lying on the ventral lateral sides of the thorax.	80-100	1500	One-Cycle
Adult Crop	The round diverticulum of the foregut, including the stalk.	100-120	1500	One-Cycle
Adult Midgut	From (and including) the proventriculus, down to just in front of the insertion of the Malpighian tubules.	40-60	1500	One-Cycle
Adult Tubule	Both anterior and posterior tubules with their common ureters, severed at the junction with the gut.	20 each separately	100	Two-Cycle

Adult Hindgut	From the insertion of the tubules, back to and including the rectum.	80-100	1500	One-Cycle
Adult Heart	The Dorsal abdominal heart, necessarily including some adherent tissues (such as fat body)	30-40	100	IVT-Express
Adult Fat body	Identifiable fat body from the thorax and abdomen.	60-80	1500	One-Cycle
Adult Ovary	Ovaries from mated females, excluding the uterus and spermatheca.	20-30	1500	One-Cycle
Adult Testis	Testis excluding the accessory glands.	50-60	1500	One-Cycle
Adult Male accessory glands	Accessory glands excluding other parts of the male genital tract.	50-60	1500	One-Cycle
Adult Virgin spermatheca	Spermatheca (excluding ovaries and uterus) from 7-day old virgin females kept isolated from males from adult emergence.	40-50	100	Two-Cycle
Adult Mated spermatheca	Spermatheca (excluding ovaries and uterus) from 7-day old females allowed to mate from emergence.	40-50	100	Two-Cycle
Adult carcass	What's left of the thorax and abdomen after the gut and sexual tracts have been removed.	40-60	1500	One-Cycle
Larval CNS	The brain and thoracic ganglia.	60-80	1500	One-Cycle
Larval Salivary gland	Salivary glands including ducts.	80-100	1500	One-Cycle
Larval midgut	From (and including) the proventriculus, down to just in front of the insertion of the Malpighian tubules.	40-60	1500	One-Cycle
Larval tubule	Both anterior and posterior tubules with their common ureters, severed at the junction with the gut.	60-80	1500	One-Cycle
Larval hindgut	From the insertion of the tubules, back to and including the rectum.	80-100	1500	One-Cycle
Larval fat body	Prominent lateral fat bodies.	30-40	1500	One-Cycle
Larval trachea	The major tracheal trunks, excluding spiracles and obvious adherent tissues.	40-50	100	IVT-Express
Larval carcass	What's left after the other tissues have been removed.	40-50	1500	One-Cycle
<i>Drosophila</i> S2 cells (growing) (Invitrogen-UK)	S2 cells growing at 25°C in Schneider's medium, before confluence.	3-5 million cells	1500	One-Cycle
Whole fly	Whole animal.	15-20	1500	One-Cycle

Except for the ovary, testis and accessory gland, equal number of males and females contributed to each RNA sample. As the tubules are bilaterally asymmetric, additional care was taken to include equal numbers of anterior and posterior tubules in each sample. Sufficient tissues were dissected in Schneider's medium to obtain 2 µg total RNA. As this involves significant pooling for such tiny tissues, tissues were collected immediately after each dissection into RLT buffer for RNA extraction (Section 2.4). This procedure was repeated 4 times for each tissue; that is, each Affymetrix chip corresponds to an independent biological replicate. For whole fly RNA extraction at least 30 flies were used.

## 2.4 Total RNA extraction

RNA extraction was carried out in a nuclease-free environment using RNeasy Mini columns according to the manufacturer's protocol (Qiagen UK). After the dissections and/or collection of tissues or whole flies, they were immediately frozen at -80°C. Homogenizations were done manually using a small blue rod/pestle for whole flies and heads, or an ultrasonic cell disruptor (Misonix, Inc., USA) for other soft tissues.

Then the homogenate was centrifuged for 3 min and supernatant was collected into a fresh 1.5 ml microcentrifuge tube. The rest of the protocol was according to Qiagen kit. An on column DNA digestion step (using Qiagen DNAase kit) was included for reducing genomic DNA contamination. RNA was eluted using 20 µl of nuclease-free water from the column and it was stored at -80°C until further use.

## 2.5 Complementary DNA (cDNA) synthesis

cDNAs for PCR and qPCR were synthesised using 500 - 1000 ng of total RNA. Recombinant reverse transcriptase (SuperScript® II; Invitrogen UK) was used to reverse transcribe the RNA in a total of 20 µl of reaction volume. Firstly, Oligo (dT)12-18mers (500 µg/ml), 500 - 1000 ng total RNA, 1 µl dNTP (10 mM each of dCTP, dGTP, dATP and dTTP) and sterile distilled water to make up to 12 µl total volume were assembled in a PCR tube. This mixture was heated to 65°C for 5 min and chilled for 2 min on ice.

The contents were collected by brief centrifugation and mixed with 4 µl of 5x first-strand buffer, 2 µl of 0.1 M DTT and 1 µl of RNAaseOUT® (40 units/µl; Invitrogen). The reaction mixture was then incubated for 2 min at 42 °C. After the incubation, 1 µl (200 units) of SuperScript® II RT was added and mixed by pipetting gently up and down. Then incubated at 42 °C for further 50 min in a Hybaid PCR express thermal cycler (Thermo UK). Finally, the reaction was terminated by heating at 70 °C for 15 min and centrifuged briefly to collect the cDNA contents at the bottom. The cDNA made was used for normal PCR, qPCR or *Pfu*-based PCR as described in the following sections.

## 2.6 Oligonucleotide (primer) synthesis

Oligonucleotide primers were designed using MacVector 11.1.1 (MacVector, Inc. UK) or other web resources (Primer3, NCBI; Oligodesign, Invitrogen UK). The sequences were sent to the MWG Biotech custom primer service for synthesis on a 0.01 µmol scale. This includes purification using high purity salt-free (HPSF) technology (MWG) based on reverse phased chromatography and quality assessment by matrix assisted laser desorption ionisation - time of flight (MALDI-TOF) analysis. Primer stock concentrations at 100 µM were obtained for each primer by resuspending the lyophilised powder in ddH<sub>2</sub>O and a working concentration of 6.6 µM was prepared from the stocks. Primers were stored at -20 °C until further use.

## 2.7 Polymerase chain reaction (PCR)

### 2.7.1 Standard PCR

Standard PCR was performed using pre-aliquoted ready-to-use mastermix in a Hybaid thermal cycler (Thermo UK). This mix uses the *Taq*-Polymerase (modified) which has 5' to 3' polymerization and exonuclease activity but lacks 3' to 5' exonuclease (proofreading) activity. The mastermix includes Thermoprime plus DNA polymerase (1.24 U) (Thermo UK), Tris-HCl (75 Mm; pH 8.8 at 25 °C), (NH<sub>4</sub>)<sub>2</sub> SO<sub>4</sub> (20 Mm), MgCl<sub>2</sub> (1.5 Mm), Tween 20 (0.01%), dNTPs (0.2 mM each). PCR reactions were normally performed in a total of 25 µl volume. The cycling parameters used are presented in the table below. PCR products were separated by agarose gel electrophoresis described in section 2.9.

**Table 2-3 Typical cyclic conditions for PCR.**

Step	Number of cycles	Temperature	Duration	Principle
Initial denaturation	1	95°C	5 - 10 min	To denature secondary structures
Denaturation	30	95°C	30s	To denature the end products of each PCR cycle
Annealing		55 - 62°C	30s	Temperature is set depending on the melting temperature of the primers used; typically ~5°C lower than T <sub>m</sub>
Extension		72°C	30s - 5 min	Extension time is set at the rate of 20 basepairs/sec
Final extension	1	72°C	10 min	For the final extension of incomplete ssDNA

### 2.7.2 *Pfu*-based Herculase II Fusion polymerase PCR

*Pfu*-based Herculase II fusion polymerase (Agilent UK) was used for amplifying longer products. It has a high affinity double-stranded DNA binding domain that enhances the processivity and increases the yield. The protocol used is presented in the table below.

**Table 2-4 *Pfu*-based Herculase II fusion polymerase PCR reaction mix and protocol.**

Parameter	Targets <1 kb	Targets 1 - 10 kb	cDNA Targets
Input template DNA	100 - 300 ng genomic DNA or 1 - 30 ng vector DNA	100 - 400 ng genomic DNA or 1 - 30 ng vector DNA	1 - 2 µl cDNA from RT-PCR reaction
Herculase II polymerase	0.5 µl	1 µl	1 µl
DMSO	0 - 8% final concentration	0 - 8% final concentration	0 - 8% final concentration
Primers (each)	0.25 µm	0.25 µm	0.25 µm
dNTPs	250 µm each dNTP	250 µm each dNTP	400 µm each dNTP
Extension time	30s	30s per kb	60s per kb
Denaturing temperature	95°C	95°C	95°C
Extension temperature	72°C	72°C	68°C

## 2.8 Quantitative reverse-transcriptase PCR (qPCR)

QPCR was performed using SyberGreen® chemistry incorporating high-fidelity Taq-polymerase (Finnzymes GRI UK), and cycling was performed using DNA Opticon Engine (Bio-Rad UK) and amplification was monitored in real time using the Opticon III software.

QPCR was performed using either cDNA or RNA as the starting material. The negative controls (without Superscript II) and/or a blank (without cDNA) were maintained to monitor and subtract the genomic DNA contamination and background fluorescence respectively. The primer sequences for the specified gene amplifications are provided in Appendix VI. PCR conditions commonly used included denaturation at 94 °C for 30s, annealing for 30 s at primer-dependent temperature and extension for 30 s at 72 °C. An additional step (75-76 °C for 10s) was included to melt primer dimers before reading the SyberGreen fluorescence of amplification products. The total number of PCR cycles used was 30-40. Finally, a melting curve step from 70 °C to 90 °C was used to determine if the primers amplified one specific product. The right PCR product was identified using the melting curve. If the melting curve shows one single peak like that is shown in Figure 2-1, at the right melting temperature predicted for the PCR product, then the expression data were further analysed.

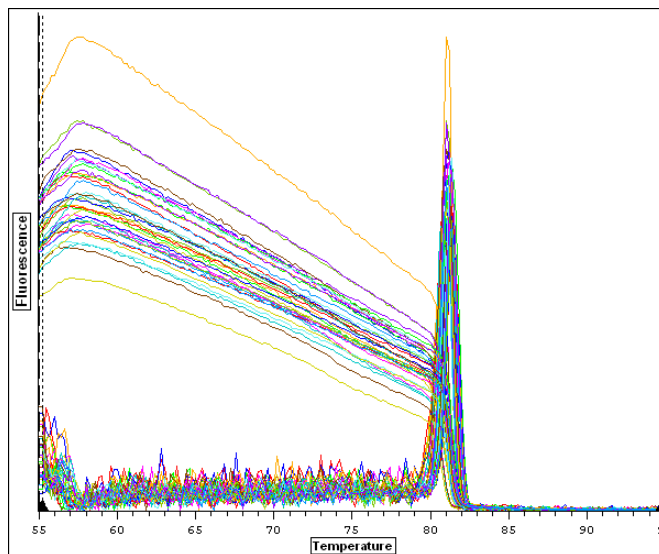


**Figure 2-1** *Best2* qPCR product melting curve.

The ribosomal *rp49* (or *rpl32*) or *alpha-Tubulin84B* genes were used as a reference controls (being house-keeping genes) to normalize the data. The data obtained was then expressed as fold difference on the basis of CT values using the  $2^{-\Delta\Delta CT}$  method (van Iterson et al., 2009). The standard error mean (SEM) and *P*-values for statistical significance were calculated using GraphPad Prism statistics software (GraphPad Software USA).

## 2.9 Agarose gel electrophoresis

PCR products were run on 1% agarose gel to assess quality and specificity. Gel was casted using 0.5x TBE [90 mM Tris, 90 mM boric acid (pH 8.3), 2 mM EDTA], containing 0.1 µg/ml EtBr as described in (Joseph Sambrook, 2001). 6x loading dye [0.25% (w/v) bromophenol blue, 0.25% (w/v) xylene cyanol, 30% (v/v) glycerol in water] was added to samples and a 1 kb ladder (Invitrogen) to a final concentration of 1x 5 µl (500 ng) of ladder and 10-20 µl samples were loaded into the wells.

Typically these were run at 100 V; the dye front was followed for electrophoresis termination and the DNA was visualised using high performance ultraviolet transilluminator (UVP UK) and compared against the ladder band size. Where needed gel extraction of PCR products was carried out as described in section 2.10 and quantified using NanoDrop, described in section 2.11.

## 2.10 PCR/Gel purification

PCR products and the products excised from the gels were purified using Qiagen PCR/Gel purification kit according to manufacturer guidelines. DNA was eluted in 20-30 µl of nuclease-free water.

## 2.11 Quantification of nucleic acids

DNA and RNA quantification was performed using a NanoDrop 1000 spectrophotometer (Thermo UK) in 1.5 µl sample volume. NanoDrop is a more robust spectrophotometer as the path lengths of 1.0 mm and 0.2 mm are used, compared to a standard 10.0 mm path spectrophotometer. This will allow it to quantify 50 times more concentrated samples than the normal ones.

Quantity was automatically calculated using the formulas below. First, background absorbance was read using the reference (water or the buffer in which the nucleic acid was diluted) and zeroed for background. Then the sample was read for absorbance at two wavelengths:  $A_{260}$  and  $A_{280}$  nm and their ratio ( $A_{260}/A_{280}$ ) was used to assess the purity of DNA and/or RNA. A ratio of ~1.8 for DNA and ~2.0 for RNA were used as a guide for sample purity.

If the ratio was appreciably lower or higher in either case, the samples were discarded. Quantities were calculated as ng/ $\mu$ l using a modified Beer-Lambert equation based on  $A_{260}$  and their respective analysis constants for both DNA and RNA.

$$C = (A * e)/b$$

Where  $c$  is the nucleic acid concentration in ng/ $\mu$ l,  $A$  is the absorbance in AU,  $e$  is the wavelength-dependent extinction coefficient in ng-cm/ $\mu$ l and  $b$  is the path length in cm. And the extinction coefficients used were 50, 33 and 40 for double-stranded DNA, single-stranded DNA (cDNA) and RNA respectively.

## 2.12 Quality control of nucleic acids

Due to environmental abundance of RNases, and the instability of RNA, integrity checks for quality control were performed before any RNA dependent application was carried out. In addition to NanoDrop  $A_{260}/A_{280}$  ratio, an Agilent 2100 Bioanalyzer (Agilent UK), based on the computer assisted nanogel electrophoresis for total RNA and complementary RNA (cRNA), was used for quality control.

## 2.13 Affymetrix microarrays

Total 2  $\mu$ g of RNA was reverse-transcribed and *in vitro* transcribed according to the standard Affymetrix protocol to produce biotinylated complementary RNA (cRNA). Prior to the reverse transcription, poly-A RNA controls were spiked into the RNA samples in known staggering concentrations which help to monitor the labelling process independently from the quality of starting RNA samples. The cRNA was then purified and checked for integrity (Section 2.12) and fragmented. Fragmented cRNA was hybridized on to *Drosophila* genome version 2 GeneChip® expression arrays (4 biological replicates per tissue). Hybridized probes were then stained using streptavidin phycoerythrin conjugate and scanned with an Affymetrix® GeneChip® Scanner 3000 7G. The overview of the GeneChip® 3' IVT express kit labelling assay is shown in Figure 2-2. An additional amplification step was used as necessary for RNA samples less than 2  $\mu$ g in the two-round

amplification protocol. The starting amount of RNA for the two-round amplification was 100 ng.

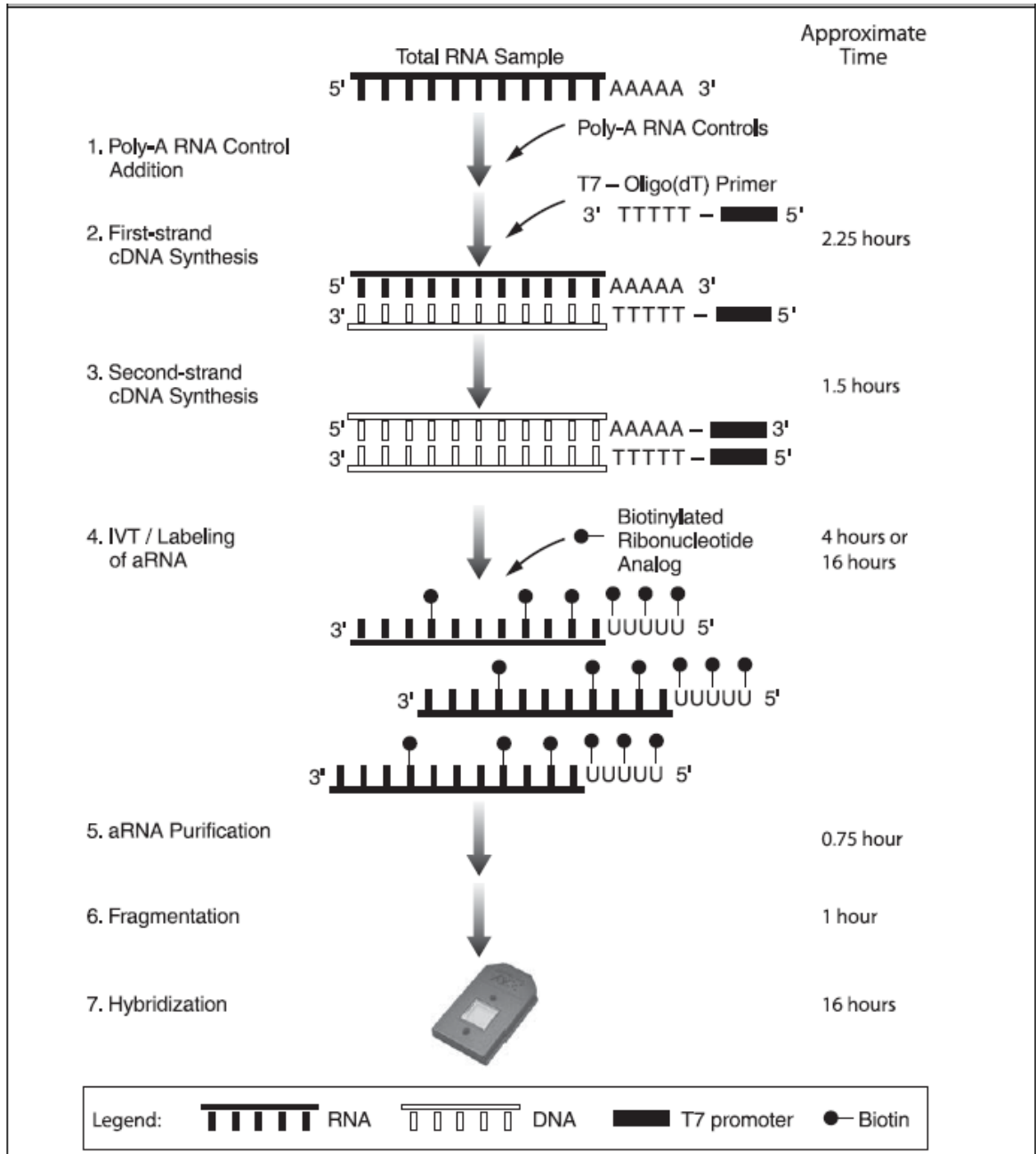


**Figure 2-2 Overview of the GeneChip 3' IVT express labelling assay (taken from [www.affymetrix.com](http://www.affymetrix.com)).**

For the FlyAtlas, data (signal intensity file or CEL file) were processed using Affymetrix® proprietary GCOS software (v 1.4) to obtain signal intensity values. Then these were exported into the data mining tool (v 3.1) and individual tissue specific transcriptomes were compared against the whole fly transcriptome to obtain *t*-test *P*-value for the statistical significance for differential expression of each probeset.

## **2.14 Microarray data analysis**

For advanced analysis and annotation, Partek<sup>®</sup> Genomics Suite™ (Partek Inc. UK) was used. Raw data (signal intensity) CEL files were obtained from the Affymetrix<sup>®</sup> GCOS and uploaded into GeneSpring for further data processing and analysis. In Partek<sup>®</sup>, data was analysed in several sequential steps which include data processing, normalisation, grouping, interpretation, quality control, statistical analysis and functional annotation.

### **2.14.1 Data processing**

Standard data processing includes summarization, log transformation and baseline transformation.

### **2.14.2 Normalisation**

Robust multi chip average method (RMA) was employed as the normalisation algorithm to normalise the signal intensity (Irizarry et al., 2003). The baseline to median of samples was chosen, in which, for each probe, the median of the log summarized signal intensity values from all the samples was calculated and subtracted from each of the samples.

### **2.14.3 Grouping**

As four biological replicates were used (for each tissue sample), they were grouped into one condition (e.g., tissue) to obtain the average and SEM. The fold change was obtained by comparing the averaged signal intensities of each individual tissue transcriptome against the average of their respective whole fly or feeding whole larvae transcriptomes.

### **2.14.4 Interpretation**

Replicate samples were grouped in the previous section as tissues. Tissue interpretation was used for sample analysis.

## 2.14.5 Quality control

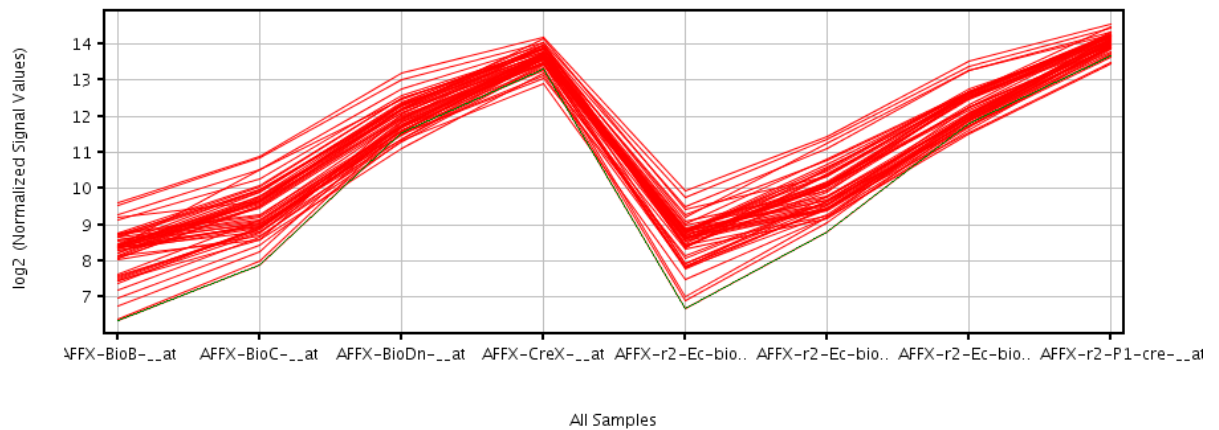


**Figure 2-3 Quality control using hybridization controls.**

**Log<sub>2</sub> transformed signal intensities of Affymetrix standard hybridization controls are plotted on the graph for quality control of mRNA hybridization. Each line shows a single biological replicate of a tissue for different hybridization controls that are spiked in during the cRNA preparation.**

Quality control of the microarray experiment was performed on the transcriptome data to assess the hybridization and labelling efficiency across replicates, interreplicate signal variations independently of the starting mRNA quality. Hybridization controls were composed of a mixture of biotin-labelled cRNA transcripts of bioB, bioC, bioD, and cre prepared in staggered concentrations (1.5, 5, 25, and 100 pm respectively). This mixture was spiked-in into the hybridization cocktail. bioB is at the level of assay sensitivity and should be present at least 50% of the time. bioC, bioD and cre must be Present all of the time and must appear in increasing concentrations. The hybridization controls show the signal value profiles of these transcripts (only 3' probesets are taken) where the X-axis represents the Biotin labelled cRNA transcripts and the Y-axis represents the log of the normalized signal intensity.

## 2.14.6 Principal Component Analysis (PCA)

Principal component analysis (PCA) reduces the dimensionality of the data by taking linear combinations of dimensions. The gene expression data for each tissue exist in the form of rows (genes) and columns (tissues). So the major trends in the data are identified on the basis of these. The dimensionality of the data was reduced to three principal components that represent the total variation in the data (Figure 2-4). The four biological replicates of each tissue (in most cases) show less variation.

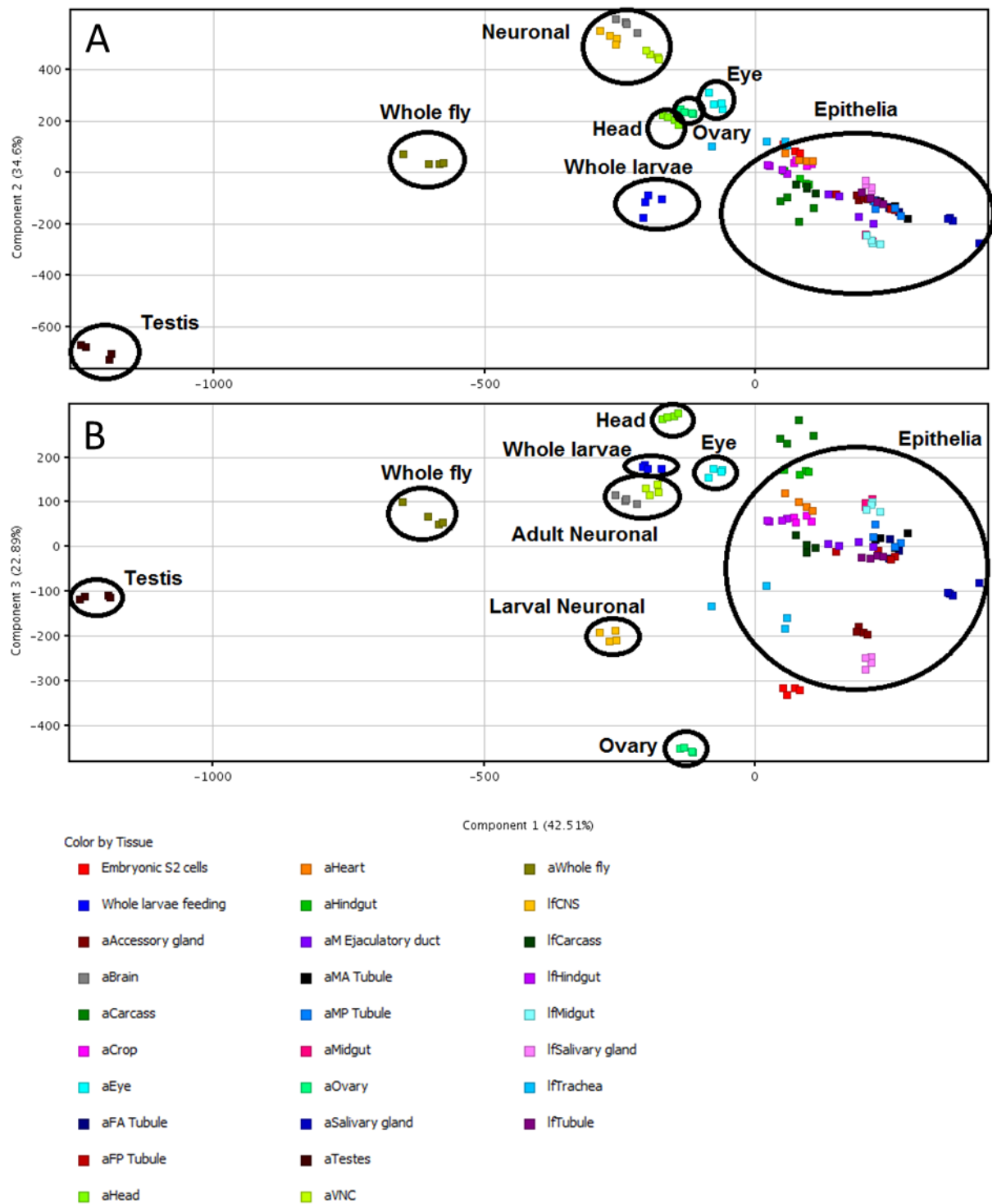


**Figure 2-4** Quality control of biological replicates of each individual tissue of the FlyAtlas using PCA.

PCA was performed on the replicated tissue transcriptomes. Similar tissue replicates are colour coded, and show the least variation (in most cases). (A) First two components capture the maximum variation. (B) The first and the third components correspond to the rest of the variation. Epithelial transcriptomes analysed as part of the Chapter 4 show less amount of variation.

### **2.14.7 Statistical analysis**

Each individual tissue transcriptome was compared against the whole fly transcriptome. The unpaired *t*-test was performed on two groups (tissue transcriptome versus whole fly transcriptome) and *P*-values were calculated. The multiple testing correction, Benjamini and Hochberg false discovery rate (FDR) being the least stringency method (Dudoit et al, 2000) was used for accounting false positives. The standard *P*-value cut-off 0.05 was used to obtain significantly 'differentially expressed genes'.

### **2.14.8 Functional annotation**

Hierarchical clustering (HC) and GO methods were used to represent the data on an intuitive heat map and to functionally annotate using ontology terms respectively. HC was performed using GeneSpring™ standard method (Eisen et al., 1998). HC was performed using the filtered entities with Pearson uncentered similarity measure and average linkage rule. GO-enrichment *P*-values, also known as the enrichment scores, signify the relative importance or significance of the GO term among the genes in the selection compared to the genes in the whole dataset. The *P*-value cut-off was set at 0.05. Corrected *P*-value was also calculated to correct for false positives using Benjamini and Hochberg FDR.

## **2.15 Fold change (FC) analysis**

Before the fold change analysis, all the entities (probe sets) filtered on expression on (10 - 100)<sub>th</sub> percentile in the raw data to filter for non-expressed probesets in any of the replicate. These were called 'filtered entities'. The ratio between condition 1 (tissue) and condition 2 (whole fly) was calculated which was called as the FC. FC analysis was used to identify genes with expression ratios or differences between two conditions, outside of a given cut-off or threshold fold change.

## **2.16 Ingenuity pathway analysis (IPA)**

The networks and functional analyses were generated through the use of Ingenuity Pathways Analysis or IPA (Ingenuity® Systems USA).

The datasets containing *Drosophila* Affymetrix probe set IDs and corresponding FCs were uploaded into the application. Each probe set ID was mapped to its corresponding gene object in the Ingenuity Pathways Knowledge Base via ortholog mapping (to their vertebrate counterparts including Human, Mouse, Rat and Canine). IPA considers Homologene clusters for the ortholog/paralog mapping (Wheeler et al., 2008). The genes significantly enriched in pathways, functions, lists were generated and compared to each other for specific, different and common functional themes.

## 2.17 Molecular cloning

### 2.17.1 Competent bacterial strains and plasmids

**Table 2-5 Fly strains and plasmids used.**

Strain	Genotype	Use
TOP10 competent cells (Invitrogen)	(F- mcrA, D(mrr-hsdRMS-mcrBC), f80lacZ DM15, DlacX74, recA1, deoR, araD139, D(ara-leu)7697, galU, galK, rpsL, (StrR), endA1, nupG).	For plasmid transformation and propagation of TOPO-related clones
DH5 $\alpha$ subcloning efficiency competent cells (Invitrogen)	(F- f80dlacZ DM15, D(lacZYA-argF), U169, deoR, recA1, endA1, hsdR17 (rK-, mK+), phoA, supE44, l-, thi-1, gyrA96, relA1).	For normal plasmid transformation and propagation
Plasmid	Use	
pP[UAST]	For germline transformation of cloned sequences under control of the UAS enhancer sequence (Brand and Perrimon, 1993).	
pCR <sup>®</sup> 2.1-TOPO <sup>®</sup>	For cloning poly adenylated PCR products according to the TOPO TA cloning kit protocol (Invitrogen).	
pMT/V5-His-TOPO <sup>®</sup>	For cloning of PCR products for expression in S2 cells (Invitrogen)	
pTW	Gateway cloning destination vector for recombining entry clones (in pENTR) to generate final clones for germline transformation of cDNA of interest under the control of the upstream UAS in the UAS/GAL4 binary induction of transgenes <i>in vivo</i> .	
pTWV	Gateway cloning destination vector for recombining entry clones (in pENTR) to generate final clones for germline transformation of cDNA of interest under the control of the upstream UAS. It also incorporates a C-terminal yellow fluorescent protein (YFP) sequence for fluorescent tagging.	
pRISE	Gateway cloning destination vector for recombining entry clones (in pENTR) to generate final clones for germline transformation of dsRNA of interest under the control of the upstream UAS (Kondo et al., 2006).	
pP[UAST Aequorin]	Used to append peroxisomal signal sequence to its C-terminal before the stop codon for germline transformation.	

## **2.17.2 Gateway® cloning**

The Gateway® cloning system (Invitrogen), which uses homologous recombination technique, was used to clone the cDNA or dsRNA amplicons for germline transformation of *Drosophila* embryos for GAL4/UAS system induction of transgene expression *in vivo* in the flies. The system uses entry (pENTR) and destination vectors (*P*-element containing germline transformation vectors).

### **2.17.2.1 Primer design and PCR amplification**

For Gateway® entry cloning, a forward primer was designed to contain a CACC sequence for directional cloning into the entry vector: pENTR. PCR amplifications were performed using Herculase® fusion polymerase according to the protocol in Section 2.7.2.

### **2.17.2.2 Entry clones**

Entry clones were made using pENTR vector according to the manufacturer's instructions (Invitrogen).

### **2.17.2.3 Destination vectors**

Destination vectors used include pRISE, pTW and pTWV for RNAi, normal overexpressor and tagged overexpressor constructs respectively.

### **2.17.2.4 Gateway® recombination using LR-clonase**

Gateway® recombination of entry and destination clones was performed using LR-clonase enzyme mix according to the manufacturer's protocol (Invitrogen). Essentially, the enzyme catalyses the *in vitro* homologous recombination between an entry clone (pENTR-attL-GENE OF INTEREST-attL) and a destination vector (containing attR sites) to generate an expression clone of interest.

## **2.17.3 Transformation of *E. coli***

Competent *E. coli* cells were transformed with the construct of interest according to the manufacturer's protocol. Briefly, cells were thawed on ice and the plasmid was mixed and incubated for 5 min on ice. The positive clones were identified using the antibiotic resistance markers of the clones generated.

### **2.17.4 Purification of plasmid DNA**

Purification of plasmid DNA was done using Qiagen mini or maxi kits (Qiagen UK). The overnight grown cultures were spun down to pellet the cells. The cells were lysed in the lysis buffer and DNA was either column eluted in 30 µl of water (for minipreps) or resuspended in 500 µl of water (for maxipreps).

### **2.17.5 Validation of cloning products**

The cloning products obtained using different cloning procedures were validated for sequence, direction and length using PCR, restriction enzyme digestion and/or sequencing.

#### **2.17.5.1 PCR**

For PCR validation, the clones were amplified using the combination of primers: one from the transgene, the other from the vector. This confirms whether it is inserted in the right direction and has the full length transgene. However, this approach was only employed for transgenes less than 2000 bp as the increase in length causes the cycling conditions greatly vary.

#### **2.17.5.2 Restriction enzyme digestion**

Restriction enzyme digestion was employed if the transgenes were inserted in the right direction and if they were right size.

#### **2.17.5.3 Sequencing**

Before they were sent off to be microinjected, DNA sequencing was done on the constructs for any possible errors in the proof reading of the polymerase.

### **2.17.6 Normal cDNA constructs**

pTW destination vector was used to recombine the pENTR entry clones for the normal overexpression constructs Table 2-5.

### **2.17.7 YFP fusion cDNA constructs**

pTWV destination vector with a C-terminal YFP tag was used to recombine the pENTR entry clones for the tagged constructs Table 2-5.

### **2.17.8 Double-stranded RNA constructs**

pRISE vector was used for making double stranded RNA constructs for transgenic RNAi flies for GAL4/UAS system induction of RNAi *in vivo*. Gateway recombination system was used for RNAi constructs where pRISE (Kondo et al., 2006) is used as donor and pENTR D TOPO® as an entry vector. RNAi constructs were made for *Best1* and *Best2*. These were sent for *Drosophila* embryo germ line transformation to BestGene Company (USA). *Best3* and *Best4* UAS RNAi stocks were obtained from the collection of Vienna *Drosophila* Research Centre (<http://stockcenter.vdrc.at/control/main>) and/or in NIG-Fly, Japan Stock centre (<http://www.shigen.nig.ac.jp/fly/nigfly/index.jsp>).

### **2.17.9 DES® constructs**

*Drosophila* expression system (DES®) constructs were designed for stable and transient expression of the protein of interest *in vitro* in S2 cells. A map is presented in Figure 2-5. PCR products (transgenes) with Adenine (A) overhangs produced using *Taq*-polymerase cloned into DES-TOPO-TA vector. Transient expression was induced using CuSO<sub>4</sub> to activate the metallothionein promoter. These constructs were used for subcellular localisation and quantitative Ca<sup>2+</sup> measurements.

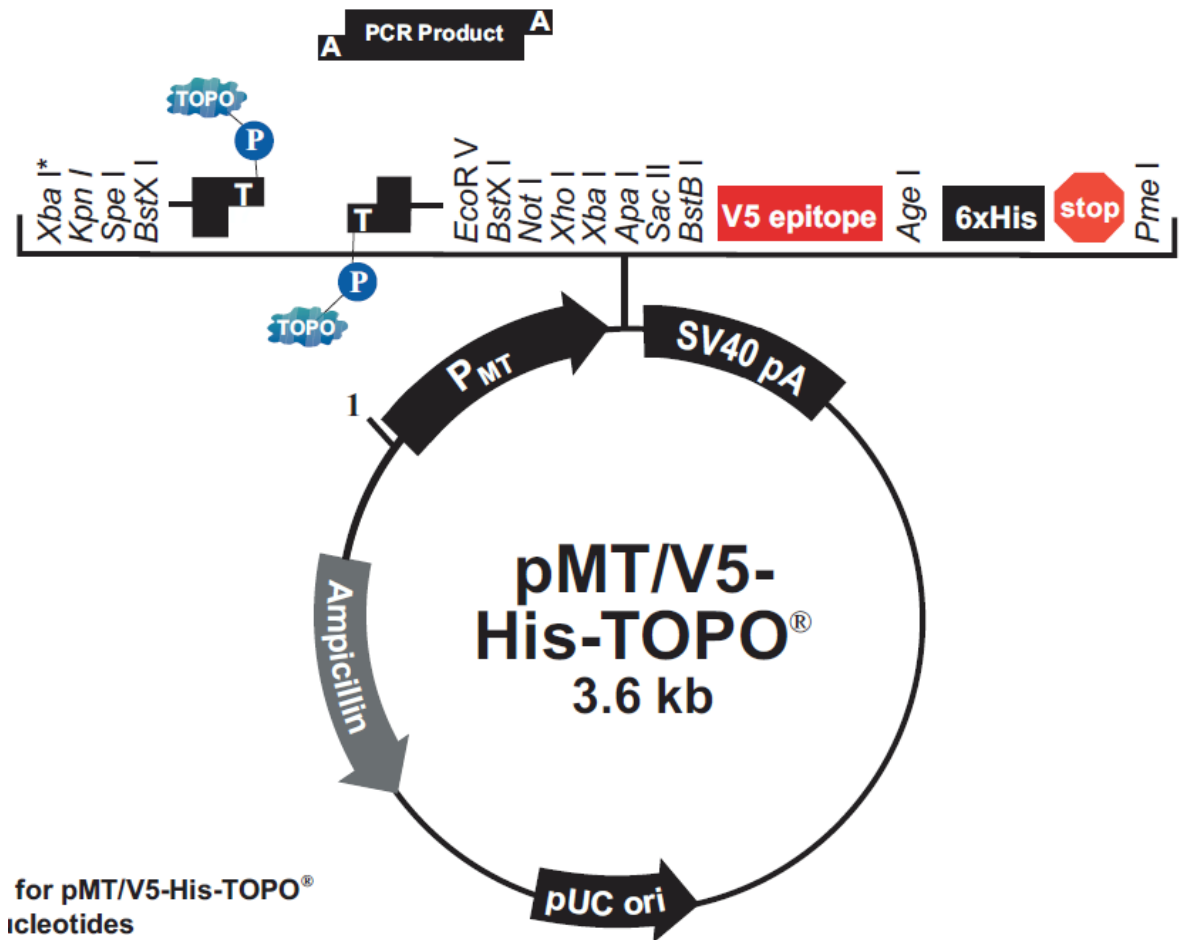


Figure 2-5 DES<sup>®</sup> TOPO<sup>®</sup>TA vector map.

This vector was used for cloning of transgenes of interest for transient expression *in vitro* in S2 cells. PCR products were generated to have Adenine (A) overhangs and cloned into the linearised covalently bound Topoisomerase (TOPO) containing vector that joins thymidines with adenosine overhangs of the product.

### 2.17.10 Dual promoter constructs for *in situ* hybridization

PCR II TOPO vector, with dual promoters either side of the multiple cloning site, was used for making RNA probe constructs for *in situ* hybridization.

### 2.17.11 Normal cloning procedure

PCR products were directly cloned, using the Invitrogen TOPO cloning kit into appropriate TOPO<sup>®</sup> vectors according to the manufacturers' instructions and transformed into TOP10 cells or DH5 $\alpha$ . 100  $\mu$ l of the transformed cells was then spread onto L-agar plates containing 100  $\mu$ g/ml ampicillin or the antibiotic appropriate to the resistant marker of the plasmid, and incubated overnight at 37°C.

The transformants were removed as single colonies and grown overnight (with shaking) at 37°C in 5 ml or 100 ml L-broth (Appendix II) using appropriate antibiotic for selecting the clones.

## **2.18 *Drosophila* S2 cell culture**

### **2.18.1 *Passaging***

*Drosophila* S2 cells (Invitrogen) were maintained in complete Schneider's medium or CSM [Schneider's medium supplemented with 10 % fetal calf serum (FCS)] at 28°C. 15 ml of cells were kept in T75 flasks. Cells were passaged when their density reached  $10^7$  cells/ml. The weakly adherent S2 cells were resuspended gently by pipetting and then diluted by adding 6 ml of cells into 9 ml of CSM in a fresh flask.

### **2.18.2 *Transient transfection***

Transient transfection was carried out in tissue culture six-well plates. 24 hours before transfection  $6 \times 10^6$  cells in a volume of 3 ml were seeded into individual wells. The calcium phosphate method of transfection was used. Plasmid DNA was prepared using a maxi-prep kit (Qiagen) and eluted in TE buffer. For each transfection a 1.5 ml microcentrifuge tube containing 19 µg of each plasmid DNA, 240 mM  $\text{CaCl}_2$  in a total volume of 300 µl was set up. This was mixed well and then added drop-wise over 1-2 min to 300 µl of 2x HEPES buffered saline (HBS) whilst bubbling air through to mix with a sterile Pasteur pipette. After mixing the DNA/calcium phosphate was allowed to precipitate for 30 min at RT before being added drop-wise to the seeded S2 cells whilst swirling continually to mix.

After overnight incubation at 28°C the cells were resuspended by pipetting, pelleted by centrifugation at 1500 g at RT for 1 min and resuspended in 3 ml fresh CSM to wash. This step was repeated twice more before cells were resuspended in 3 ml of CSM and returned to the six-well plates after residual cells had been carefully aspirated from the plates with a P200. If a plasmid encoding a metal inducible promoter was used,  $\text{CuSO}_4$  to 0.5 mM was added to the cells to induce expression and expression was allowed to proceed for 40-42 h.

Cells were then harvested by centrifugation at 1,500 g for 1 min at RT, washed once in PBS, pelleted and either frozen at -70°C before use or used immediately.

## **2.19 Peroxisome Isolation**

### **2.19.1 *Tissue preparation***

A total of 100 flies were collected for peroxisome isolation using gradient centrifugation using the Pierce peroxisome isolation kit (Pierce UK). First the whole flies were washed in sterile PBS and homogenised for 30 s at 8000 rpm (on ice) in 800 µl of peroxisome enrichment buffer A. Prior to the homogenisation, protease inhibitor cocktail (Sigma) was added (1:100) to the solutions. After centrifugation in buffer A, 800 µl of peroxisome enrichment buffer B was added and the tube inverted to mix 15 times. The mix was centrifuged at 500 g for 10 min at 4°C and supernatant was transferred to a new 2 ml tube by discarding the pellet. Lipids present after the centrifugation were removed from the surface using a pipette before the transfer of the supernatant.

### **2.19.2 *Gradient centrifugation***

Gradient centrifugation was performed using the Optiprep solution containing 60% iodixanol in water with a density of 1.32 g/ml. Optiprep solution was specified to be endotoxin-free, non-ionic, non-toxic to cells and metabolically inert. The high density facilitates the fractionation of cells by flotation from a dense load zone through a continuous gradient. Two gradients of the Optiprep media (35% and 30%) were made using gradient dilution buffer and overlaid one top of the other in ultracentrifuge tubes (Beckman UK) and the sample (prepared in section 2.19.1) on top of them. Then the samples were ultracentrifuged at 180,000 g for 90 min at 4°C in a Beckman Optima TL ultracentrifuge. The visible white band that appears at the bottom of the centrifuge was collected by pipetting for peroxisomes. And the samples were centrifuged for 20 mins at 18,000 g to get rid of the Optiprep™ media to obtain pure peroxisomes as the pellet. These were stored at -20°C until further use. The peroxisomes were resuspended in buffers according to the downstream application.

## **2.20 Protein analysis**

### **2.20.1 *Extraction***

Whole fly protein was extracted from about 10-50 flies. Flies were homogenised in 100 µl of Tris-Lysis buffer (2 % (w/v) SDS, 70 mM Tris, pH 6.8) containing 2 µl of Sigma protease inhibitor cocktail (Sigma) in a 1.5 ml microcentrifuge tube. Flies were homogenised using a hand-held pestle and then a Microson ultrasonic cell disrupter, until the sample appeared homogeneous. The sample was then centrifuged at 13 000 rpm for 10 min to remove debris, and the supernatant transferred into a new tube.

### **2.20.2 *Bradford assay***

The Bradford protein assay was used to quantify the protein concentration using Bovine serum albumin (BSA) protein standard interpolation. Assay carried out in a 96-well plate. Appropriate standard concentrations were used to obtain the sample concentrations. Typically, eight BSA standards of 0-5 µg in water were set up in triplicate in a 50 µl total volume. 5 µl of protein supernatant (approximately 3-4 µg of protein) was also set up in triplicate in a final volume of 50 µl. 200 µl of a 1 in 5 dilution of Bradford reagent concentrate (BioRad UK) was added to both standard and sample proteins in the wells. The absorbance at 590 nm was read using a plate reader and each standard absorbance was plotted against the known concentration to interpolate the unknown protein sample absorbance to calculate their quantities.

### **2.20.3 *SDS-PAGE separation***

Electrophoretic separation of proteins was performed using Novex NuPAGE™ electrophoresis system. Novex Xcell II™ kit was used with 12-well 4-12 % Bis-Tris-HCl (Bis(2-hydroxyethyl) imino-tris (hydroxymethyl) methane-HCl) buffered (pH 6.4) polyacrylamide gels were used. The 1x NuPAGE™ MOPS SDS running buffer was used: diluted from a 20x MOPS SDS running buffer stock solution (Appendix V). The gels were then run at 200 V constant with an expected current of 100-115 mA/gel at the start and 60-70 mA/gel at the end, for approximately 50 min.

Protein samples (20 µg) were prepared by adding 6x SDS-PAGE loading buffer to a 1X loading buffer final concentration. The samples were briefly vortexed, heated to 95°C for 5 min and pulse-spun to collect the samples at the bottom and loaded into the wells. Protein molecular weight marker: ECL Plex™ fluorescent Rainbow Marker (GE Life Sciences UK) was used for sizing the proteins on the gel.

#### **2.20.4 Western blotting**

Proteins along with the rainbow marker were separated on SDS-PAGE were transferred on to Hybond ECL membrane (GE Life Sciences, UK) for western blotting. Protein blots were then removed from the module and the efficiency of the transfer was checked by the fluorescent rainbow marker. After staining, the blots were washed with water to make the bands visible and after visualisation, washed with transfer solution before blocking. Blocking was done in PBS, 0.1 % (v/v) Tween 20, 5 % (w/v) Marvel milk powder for 1 h (at RT) to overnight (at 4°C). The blots were briefly washed for 15 min in PBS, 0.1 % (v/v) Tween 20. The primary antibody (at various concentrations) was then incubated in blocking solution for 3 h (at RT) to overnight (at 4°C). Washes followed in PBS, 0.1 % (v/v) Tween 20, 1x 15 min, 3x 5 min on a horizontal shaker at RT. The secondary antibody (at various concentrations) was then incubated in PBS, 0.1 % (v/v) Tween 20 for 1 h at RT and the blot washed well for at least 3 h at RT in PBS before detection. Cyanine fluorescent dyes Cy5- or Cy3-conjugated secondary antibodies were used as the secondary antibodies (Amersham UK).

### **2.21 Production and purification of antibodies**

#### **2.21.1 Production**

Peptide sequences consisting 14 amino acids were designed for the unique regions of each individual bestrophin using Invitrogen peptide Select online free software. A Cysteine (C) was added to the N terminus of the peptide so that they could be KLH conjugated. These peptide sequences were sent to Genosphere Biotechnologies (France) in order to synthesize the peptide *in vitro* and produce anti-rabbit polyclonal antibodies (<http://www.genosphere-biotech.com/>).

Fourteen amino acid peptide sequences were selected from the C-terminal regions of the PDE protein sequence. Sequences were selected on the basis of antigenicity using the Parker antigenicity option in MacVector. Modelling of the secondary structure of the proteins was also carried out to identify regions that were predicted to comprise turns and random-coils as these are most likely to reside on the solvent accessible surface of the protein. The chosen peptides were screened for low similarity to other proteins in the *Drosophila* database using BLAST searching; any peptide that had greater than 6 consecutive amino acids in common with another protein was rejected.

## **2.21.2 Purification**

### **2.21.2.1 Isolation of IgG fraction from immune-serum**

A 'HiTrap Protein A HP' column (Amersham UK) was equilibrated by passing 30 ml of PBS through at ~2ml/min. 5 ml of immune-serum was filtered through a 0.22  $\mu$ M filter, and then syringed through the column to bind. The column was washed with 30 ml of PBS and the IgG fraction was eluted with 17 ml of 0.1 M glycine, pH 3.0. The first 2 ml were discarded and 15 ml of IgG were collected in a 50 ml Falcon tube containing 1.5 ml 1 M Tris-HCl pH 8.0. The absorbance at 280 nm was read to check the yield and the IgG was dialysed overnight against PBS using a Slide-A-Lyzer dialysis cassette (Pierce).

### **2.21.2.2 Preparation of affinity columns**

The bottom cap was fitted to a 10 ml polypropylene column (Pierce) and the column filled with deionised water. A frit was pushed to the bottom of the column using the plunger from a disposable syringe. The water was drained by removing the end cap and 5 ml of Sulfolink slurry (Pierce) was added and allowed to sediment for 30 min. The slurry buffer was removed down to the surface of the gel and 25 ml of 50 mM Tris-HCl, 5 mM Na-EDTA pH 8.5 was added to the reservoir. The buffer was run through the column and a further 25 ml of buffer added when there was space and allowed to run through to the top of the gel. The end cap was replaced whilst 1 mg of antibody-specific peptide was dissolved in 4 ml of 50 mM Tris-HCl, 5 mM Na-EDTA. This was added to the column, mixed well, the cap fitted and placed on a rotator for 15 min. The column was set up right and left to settle for 45 min.

The caps were removed and the solution allowed to drain to the top of the gel. 15 ml of 50 mM cysteine in 50 mM Tris-HCl, 5 mM Na-EDTA were run into the column. The end caps were fitted, the contents mixed thoroughly and the column was placed on a rotator for 15 min. The column was set upright and allowed to settle for 45 min. The top cap was removed and the top frit fitted just above the level of the gel. The end cap was removed and the solution allowed to run out. 60 ml of 1 M NaCl was then run through the column followed by 50 ml of PBS and then 40 ml of 0.05 % (w/v) sodium azide in PBS keeping the level above the gel. The end caps were fitted and the column stored at 4°C until use.

### 2.21.2.3 Affinity purification of antibodies

The affinity column was brought to RT and the sodium azide was drained. The column was equilibrated by passing through 30 ml of PBS and the IgG fraction was passed through. Next followed a wash with 30 ml of PBS and finally the antibody was eluted with 0.1 M glycine, pH 3.0. 12 x 1 ml fractions were collected into 12 x 1.5 ml microcentrifuge tube containing 100 µl Tris-HCl pH 8.0. To determine the yield, the absorbance at 280 nm of each fraction was measured and fractions with readings greater than 0.05 were pooled and dialysed overnight against PBS with 0.01 % (w/v) sodium azide. The absorbance at 280 nm was again taken in order to ascertain the final yield using the following equation: Antibody concentration (mg/ml) =  $A_{280} \times 1.35$  mg/ml. Aliquots of the antibodies were made and frozen at -20°C until use.

**Table 2-6 Antibodies used for western blotting and immunocytochemistry.**

Antibody and Source	Dilution and Use
Anti-V5-tag (mouse monoclonal, Invitrogen)	1:500 (immunocytochemistry or ICC); 1:5000 (Western)
Anti-GFP (mouse monoclonal, ZYMED)	1:1000 (Western)
Alexa Fluor®568-labelled anti-rabbit IgG H & L (goat polyclonal, Molecular Probes)	1:500 (ICC)
Alexa Fluor®568-labelled anti-mouse IgG H & L (goat polyclonal, Molecular Probes)	1:500 (ICC)
FITC-labelled anti-rabbit IgG H & L (donkey polyclonal, Diagnostics Scotland)	1:250 (ICC)
Anti-Best2, affinity purified (rabbit polyclonal, this study)	1:200 (Western and ICC)
Anti-Aequorin (rabbit polyclonal, Abcam UK)	1:1000 (ICC)
Anti-LAMP (mouse polyclonal, Abcam UK)	1:1000 (ICC)

## 2.22 Immunocytochemistry (ICC)

Immunocytochemical staining of cells and tissues, described in the following sections was performed for *in vitro* and *in vivo* localisation studies.

### 2.22.1 ICC of S2 cells

S2 cells were resuspended and collected into 15 ml falcon tubes from the tissue culture flasks. And these were spun at 3000 g free rotating tabletop centrifuge and supernatant was removed and cells were washed with PBS two times. About 100  $\mu$ l of cells at a density of  $6 \times 10^6$  cells/ml were plated and left for 15 min to allow cells to settle and adhere. Excess solution was removed and the samples washed 3 times with PBS. Samples were then fixed by the addition of 4 % (w/v) paraformaldehyde in PBS for 15 min at RT. Samples were then washed 3 times with PBS, and blocked in PBS, 0.2 % (w/v) BSA, 0.1 % Triton X-100 for 10 min at RT.

They were then incubated overnight at RT in a humidified box with primary antibody diluted to the desired concentration in PBS/BSA/Triton X-100. Samples were then washed 3 times with PBS and incubated for 1 h at RT with the appropriate secondary antibody, diluted to the desired concentration in PBS/BSA/Triton X-100. Samples were then washed 3 times in PBS and, if required, DAPI stained as described in section 2.22.2. The coverslips to which samples were attached were then mounted on slides using VectaShield mounting medium (Vector Laboratories UK) and sealed with glycerol-gelatin. Samples were imaged by a confocal microscope system, as described in section 2.23.

### 2.22.2 ICC of intact *Drosophila* tissues

Intact tissues were dissected carefully in Schneider's medium and transferred into a 1.5 ml microcentrifuge tube containing PBS (pH 7.4). Then the tissues were washed with PBS 2 more times and the PBS was carefully removed. Tissues were then fixed in 4 % (w/v) paraformaldehyde in PBS at RT for 10-30 min. The tissues were washed three times in PBS and permeabilised using PBS, 0.3 % (v/v) Triton X-100 (PBT) for 30 min. This was followed by incubation with PBT with 10 % (v/v) goat serum (Sigma) (PBT-GS) for 3 h at RT.

Primary antibody, diluted to the desired concentration in PBT-GS, was then applied and the tubes incubated in a humidified box overnight at 4°C.

The following day the tubules were washed in PBT 5 x 30 min and incubated in PBT-GS (Sigma) for 3-4 h. Secondary antibody, diluted to the desired concentration in PBT-GS, was then applied and the tubes were incubated in a dark humidified box overnight at 4°C.

The tissues were then washed with PBT 3 x 1 h and in PBS 3 x 5 min. Then the nuclei were stained using 500 ng/ml DAPI for 2 min in PBS, diluted from a 10 mg/ml (in H<sub>2</sub>O) stock solution. Tissues were washed 3 times with PBS before mounting. They were mounted in Vectashield mounting medium on confocal microscopy slides (BDH UK) or plates (Matek corporation USA). For slides, a coverslip was used and sealed with glycerol/gelatin (Sigma UK). The samples were viewed using a confocal microscopy system.

## 2.23 Imaging

Fluorescent imaging was carried out using confocal microscope system: LSM510 Meta from Zeiss Technologies UK. A HeNe1 543nm laser and a 561-625 band pass filter were used for imaging the Alexafluor® 568 secondary antibody. An Argon 488 laser and a 505-530 band pass filter were used for imaging the FITC antibody or fluorescent proteins. For visualisation of DAPI, a pseudo-DAPI technique was used. The DAPI was excited using the standard UV source (mercury lamp) and the image captured using the confocal photomultipliers. The DAPI image was then merged with the other channels retrospectively using the proprietary LSM Meta software. A 40x objective was used in most cases.

## 2.24 mRNA *in situ* hybridization

The *in situ* protocol was adopted from those described by (Allan et al., 2005) and the Berkeley *Drosophila* Genome Project (BDGP) 96-well *in situ* protocol (<http://www.fruitfly.org/about/methods/RNAinsitu.html>). The same primers (Appendix VI) used for qPCR in the above-described method were used to generate *in situ* probes.

The sequences of all PCR products were analysed using National Centre for Biotechnology Information (NCBI) and BDGP databases with basic local alignment search tool (BLAST) to check the cross-hybridization potential of the sequences and found no significant matches with other *Drosophila melanogaster* sequences in the database.

PCR products were then cloned into the dual promoter PCR II TOPO vector (Invitrogen UK) and two types of DIG-labelled RNA in situ probes (sense and anti-sense) were generated by *in vitro* transcription. The sense probes were used as negative controls. To distinguish between sense and anti-sense, the orientation of the insert was checked using colony PCR with the combination of either M13 forward or reverse with a forward gene specific primer.

Adult tubules were dissected in Schneider's medium (Invitrogen UK) and placed into wells of a Millipore 96-well plate (MAGVN22 or MAGVS22) with 100 µl of Schneider's medium. Schneider's medium was removed by the use of a vacuum pump, and postfix solution [10 mM potassium phosphate buffer (pH 7.0) containing 140 mM NaCl, 0.1% (v/v) Tween-20, and 5% (v/v) formaldehyde] was added for 20 min, followed by three washes with PBT [10 mM potassium phosphate buffer (pH 7.0) containing 140 mM NaCl and 0.1% (v/v) Tween-20]. The tissues were incubated with proteinase K in PBT (4 µg/ml) for 3 min at RT; the reaction was stopped with two washes of PBT containing 2 mg/ml glycine. The samples were washed twice with PBT before incubation with postfix for a further 20 min at RT.

The tissues were washed with five changes of PBT, followed by one wash with 50% hybridization buffer [5x SSC containing 50% (v/v) formamide, 10 mM KH<sub>2</sub>PO<sub>4</sub>, 140 mM NaCl, 1 mg/ml glycogen, 0.2 mg/ml sheared salmon sperm DNA, and 0.1% Tween-20 (pH 7.0)] plus 50% (v/v) PBT. The samples were washed once with hybridization buffer before a 1 h preincubation with hybridization buffer at 55 °C and subsequently incubated for 43 h at 55 °C with 100 µl of hybridization buffer containing 200-300 ng of either the sense or anti-sense riboprobe, taking care to seal the wells with parafilm to prevent evaporation.

After hybridization, the samples were washed four times with hybridization buffer at 55°C, followed by a final wash overnight with hybridization buffer at 55°C. Samples were washed once with 50% (v/v) hybridization buffer and 50% (v/v) PBT, followed by four washes with PBT, and then incubated overnight at RT with 100 µl of preabsorbed alkaline phosphatase-conjugated anti-digoxigenin Fab fragment (Roche UK) diluted 1:2,000 with PBT. The unbound antibody was removed with extensive washing in PBT (at least 10 times for 5-10 min). The samples were incubated with DIG detection buffer (100 mM Tris-HCl, pH 9.5, 100 mM NaCl, 50 mM MgCl<sub>2</sub>) for 5 min and then repeated again. The colour reaction was initiated by the addition of DIG detection buffer 5-bromo-4-chloro-3-indolyl phosphate (BCIP) and nitro blue tetrazolium (NBT) and left to 10 min to 2 h at RT. Development was stopped with extensive washing with PBT containing 50 mM EDTA, and the tissues were removed from the wells and mounted on slides with 70% glycerol and viewed with the AxioCam imaging system (Carl Zeiss UK).

## 2.25 Fluid secretion assay

The miniaturised version of classical Ramsay assay for tubule fluid secretion was used for measuring rates of secretion (Dow et al., 1994b). The pairs of tubules were dissected along with the ureter. One end was wrapped around a metal pin under white, heavy mineral oil (Sigma UK) whilst the other tubule was immersed in 9 µl of *Drosophila* saline: Schneider's (50:50), containing trace amounts of the red dye, Amaranth, for easy viewing of the emerging bubbles, ensuring the ureter remains in the oil. Drops emerging from the ureter were removed with a fine glass rod every 10 minutes and measured under a microscope graticule. Drugs including antagonists and agonists were added to the Schneider:saline as a 10x stock in 1 µl when required.

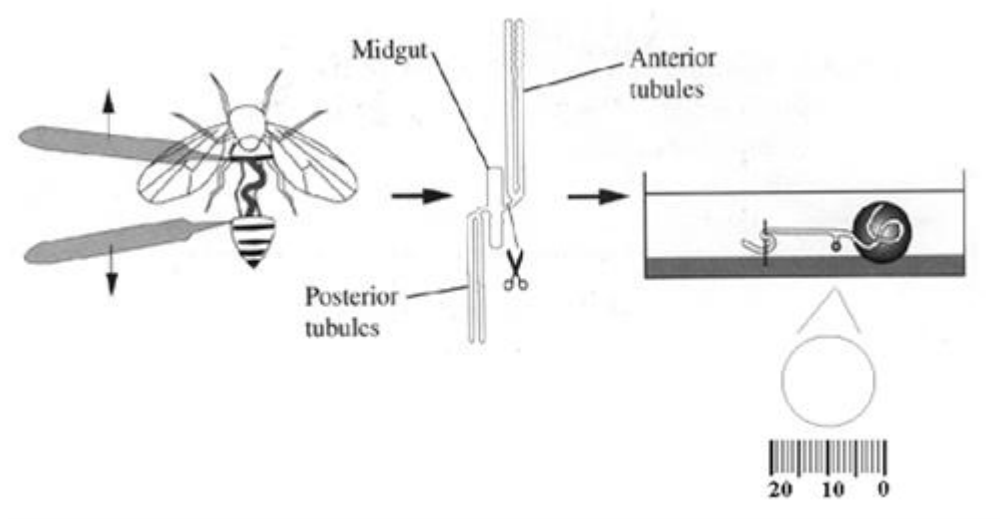
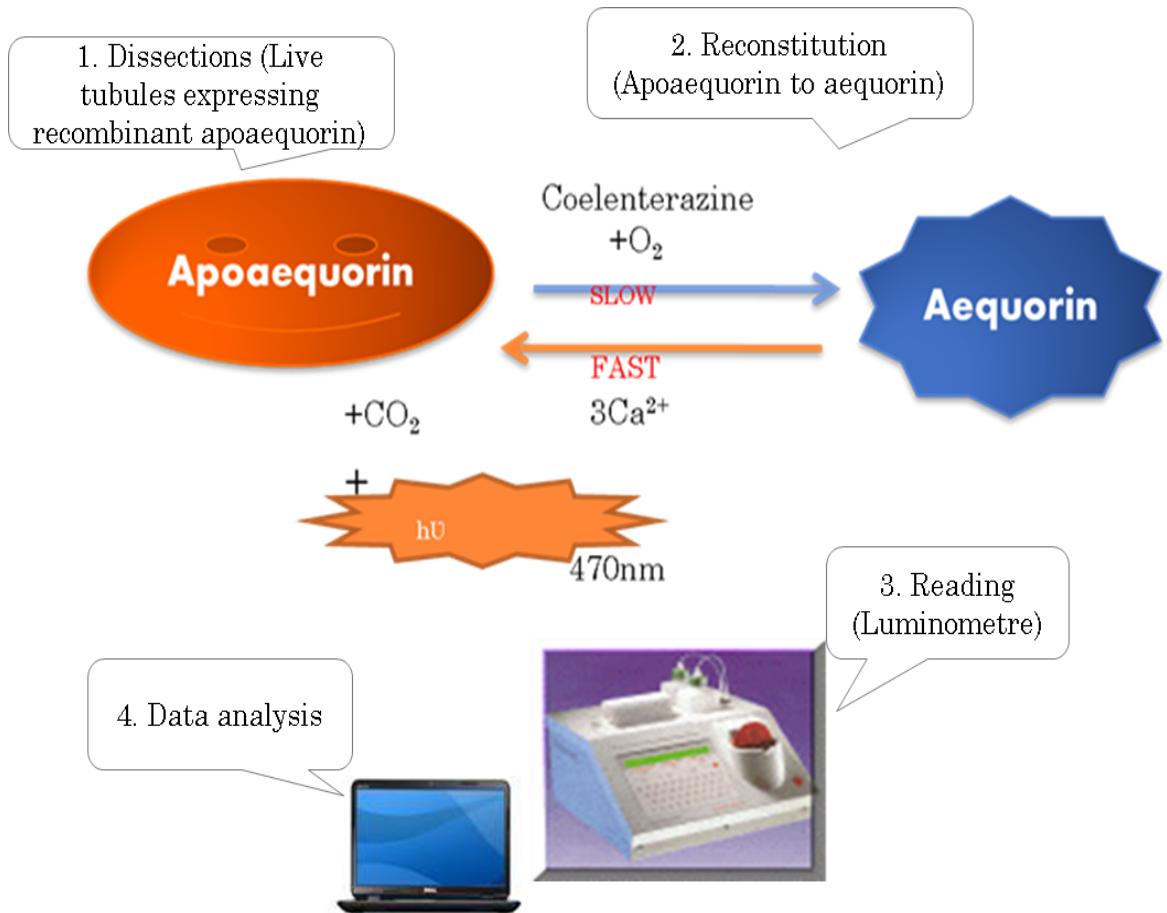


Figure 2-6 Fluid secretion assay schema (Dow et al., 1994b).

Intact tubules are dissected along with their common ureter from the flies in Schneider's medium using fine forceps (left panel). Tubule ureter is cut just before its joining with gut (middle panel). One tubule is wrapped around the needle and other tubule is in the Schneider:saline mix; all are immersed in the mineral oil (right panel; above). Finally tubule secreted droplets emanating from the ureter are measured using the microscope graticule and converted in to nl/min (right panel; below)

## 2.26 $[Ca^{2+}]_i$ measurements using recombinant aequorin

Intracellular  $Ca^{2+}$  concentrations  $[Ca^{2+}]_i$  were measured in tubules, using recombinant transgenic aequorin probes, according to the published protocols (Rosay et al., 1997; Southall et al., 2006). Briefly, 40 pairs of tubules ectopically expressing apo-aequorin were dissected, incubated at RT (in dark) with  $2.5 \mu M$  coelenterazine to reconstitute aequorin for 3 h in a volume of  $170 \mu l$  of Schneider's medium. Then the  $Ca^{2+}$ -dependent aequorin luminescence was measured using Lumat LB 9507 ultrasensitive luminometre (Berthold Technologies UK). At the end of each experiment, total aequorin was released using  $300 \mu l$  of lysis buffer (1% (v/v) Triton X-100,  $100 \text{ mM } CaCl_2$ ) from tubules in order to calculate the total luminescence; and data were back-integrated using a program written in Perl, based on the method described by (Button and Eidsath, 1996).



**Figure 2-7 A schematic of calcium measurements.**

For recording agonist/antagonist induced Ca<sup>2+</sup> transients, the following steps were inserted after reading the basal luminescence for 10-120 sec and before the lysis release of total aequorin. First mock injections were made with 25 µl of Schneider's for reading control transients due to mechanical disturbance from the injection. In the same way, agonist/antagonist was injected and recorded the luminescence Ca<sup>2+</sup> changes, and later compared with the mock changes.

## 2.27 Diet regimes

For salt feeding assays, 3 % or 4 % NaCl was added into the normal fly food media; in the same way, KCl (5 %) sorbitol (14.5 %) was added. About 20-30 males or females transferred after they were being raised in the same vial for one day at the age of 5 days. The flies were counted as they died at intervals of 12 hrs.

## 2.28 Metabolomic analysis

### 2.28.1 *Metabolite extraction*

Metabolites were extracted in the solvent mixture of methanol: chloroform: water in the ratio of 3:1:1. Briefly, 10 whole flies or 200 tubules (males and females separately) were collected into a 1.5 ml microcentrifuge tube containing the solvent mixture. They were crushed using a small blue rod and sonicated using ultrasonic cell disruptor. The suspension was then centrifuged for 10 min at 10, 000 rpm in a tabletop microcentrifuge at 4°C, and the supernatant was collected in a fresh tube. The precipitate was used for Bradford quantification of protein for normalisation of metabolite signal intensity arbitrary units where necessary.

### 2.28.2 *Liquid chromatography (LC)-Mass spectrometry (MS)*

LC-MS data were acquired using a Finnigan LTQ Orbitrap instrument (Thermo Fisher Scientific, UK) set at 30, 000 resolution at Strathclyde University metabolomic facility. Sample analysis was carried out under positive ion mode for small metabolites and negative mode for polar lipid compounds. The mass scanning range was  $m/z$  50-1200, while the capillary temperature was 200°C and the sheath and auxiliary gas flow rates were 30 and 10 arbitrary units respectively. The LC-MS system automated by XCalibur version 2.0 (Thermo UK) was run in binary gradient mode. Solvent A was 0.1 % formic acid in HPLC grade water and solvent B was 0.1 % formic acid in acetonitrile. Analysis was carried out on a ZICHILIC column (150 x 4.6 mm, 5 µm particle size, HiChrom UK) fitted with a guard column. A flow rate of 300 µl/min was used and the injection volume was 10 µl, the gradient used was as follows: 90% B at (0 min) - 50% B at (16 min) - 20% B at (18 min) - 20% B at (28 min) - 90% B at (36 min). Samples were kept in a vial tray which was set at a constant temperature of 3°C. The injection volume was 25µl. Mass measurement was externally calibrated according to the manufacturer's instructions just before commencing the experiment, and was internally calibrated by lock masses (positive ion mode  $m/z$  83.06037 and  $m/z$  195.08625, due to acetonitrile dimer and caffeine respectively and negative ion mode 91.00368 due to formic acid dimer).

Runs were carried out in negative ion mode using the conditions above after tuning in the negative ion mode and the assigning appropriate lock mass. Runs were also carried out on an Orbitrap Exactive™ instrument fitted with a HCD cell using the same mass spectrometry parameters and chromatographic conditions with a HCD cell energy of 20 eV.

### **2.28.3      *Data capture and analysis***

Data files were processed using Sieve 1.3 (Thermo UK). The parameters used in Sieve were: time range 4-30 min, mass range 75-700 amu, frame width 0.02 amu and Rt width 2.5 min. The output from Sieve was transferred into Sieve Extractor, an Excel spreadsheet and an in-house macro written in Visual Basic, used to search against a mass list of 65000 compounds taken from the KEGG, Metlin, Human Metabolome and Lipid Maps databases.

## 3. FlyAtlas, a gene expression database

### Summary

FlyAtlas, an online resource, provides the most comprehensive view yet of expression in multiple tissues of *Drosophila melanogaster*. Meta-analysis of the data shows that a significant fraction of the genome is expressed with great tissue specificity in the adult, demonstrating the need for the functional genomic community to embrace a wide range of functional phenotypes. Well-known developmental genes are often reused in surprising tissues in the adult, suggesting new functions. The homologs of many human genetic disease loci show selective expression in the *Drosophila* tissues analogous to the affected human tissues, providing a useful filter for potential candidate genes.

Additionally, the contributions of each tissue to the wholefly array signal can be calculated, demonstrating the limitations of whole-organism approaches to functional genomics and allowing modeling of a simple tissue fractionation procedure that should improve detection of weak or tissue-specific signals.

### 3.1 Introduction

Experimental reverse genetics is a powerful tool for understanding novel genes, a key goal of functional genomics (Kaiser, 1990), both for basic science and for the understanding of human disease (Orkin, 1986; Ruddle, 1982). Simple genetic models have vital roles in this endeavour because of the relative ease, power and cost of their reverse genetic techniques compared with mouse (Adams and Sekelsky, 2002) (Bargmann, 2001). The announcement of the *Drosophila* genome was accompanied by prediction of its utility in understanding human genetic disease, and this optimism was accompanied by the formation and subsequent closure or refocusing of several companies. Now, a more prosaic approach pertains. The case for *Drosophila* as a model of human disease is based on a gene-by-gene argument, and the powerful genetics associated with this tiny fly is starting to produce useful insights. It has also proved possible to 'humanize' the fly by introducing human genes of interest and studying them in an organotypic context that can prove more informative than studies in cell culture.

However, recent data suggest that to study novel genes by reverse genetics (that is, studying gene function by generating mutants and studying the phenotypes), the *Drosophila* community may need to broaden its focus. It has long been realized that functional genomics demands functional phenotypes, whereas most model organisms were adopted for studies of development. The mismatch between the range of functions of an organism's genes and the range of phenotypes available in that organism has been termed the 'phenotype gap' (Brown and Peters, 1996; Bullard, 2001; Dow, 2003). The utility of *Drosophila* in studies of development is beyond dispute, but it is salutary to note that perhaps a third of a million researcher-years spent studying *Drosophila* (predominantly its development) had led to the identification of only 20% of its genes (Dow, 2003) before the release of the genome sequence (Adams et al., 2000). So if most of the genes encoded by the *Drosophila* genome are not primarily developmental in function, where should one seek phenotypes for the rest?

As well as providing some clear messages about the utility of whole-fly arrays, the database also helps delineate the phenotype gap by identifying those tissues in which specific genes of interest (and thus, the homologs of human disease genes) can be studied. The online data set thus provides an instant entrée into the field, not just for Drosophilists but also for scientists who can identify a likely homolog in the fly, regardless of the organism they use.

FlyAtlas is composed of data covering 17 distinct adult tissues (brain, head, eyes, thoracoabdominal ganglion, salivary glands, crop, midgut, tubule, hindgut, heart, fatbody, ovary, testis, male accessory gland, virgin spermatheca, mated spermatheca, carcass), dissected from 7-day-old Canton S adults, and 8 larval tissues (CNS, salivary gland, midgut, tubule, hindgut, fat body, trachea and carcass), dissected from third-instar feeding larvae. Each tissue was processed with four biological replicates on Affymetrix *Drosophila* GeneChips® version 2 (with 18, 880 probe sets for 18,500 transcripts), and compared with a matched whole-fly sample (Materials and Methods). Thus, the FlyAtlas presents an excellent opportunity to study gene expression in multiple tissues and provides a complementary resource to published developmental data sets (Arbeitman et al., 2002).

## 3.2 Results

### 3.2.1 Tissue-specific transcriptomes

FlyAtlas data provide a good survey of gene expression for both adult and larval tissues. About half of the genome is expressed in each tissue calculated on the basis of the number of probe sets that were called significant. Total percentage of expressed genome among tissues accounts for about 85% of the computed *Drosophila* transcriptome in contrast to 67% the whole-fly sample (Figure 3-1).

Although the widespread practice of grinding up the whole organism for transcriptomic or proteomic studies is understandable, given the tiny size of the whole organism, the implication of this result, as we discuss later, is that a significant fraction of the genome will be missed or underrepresented in such samples.

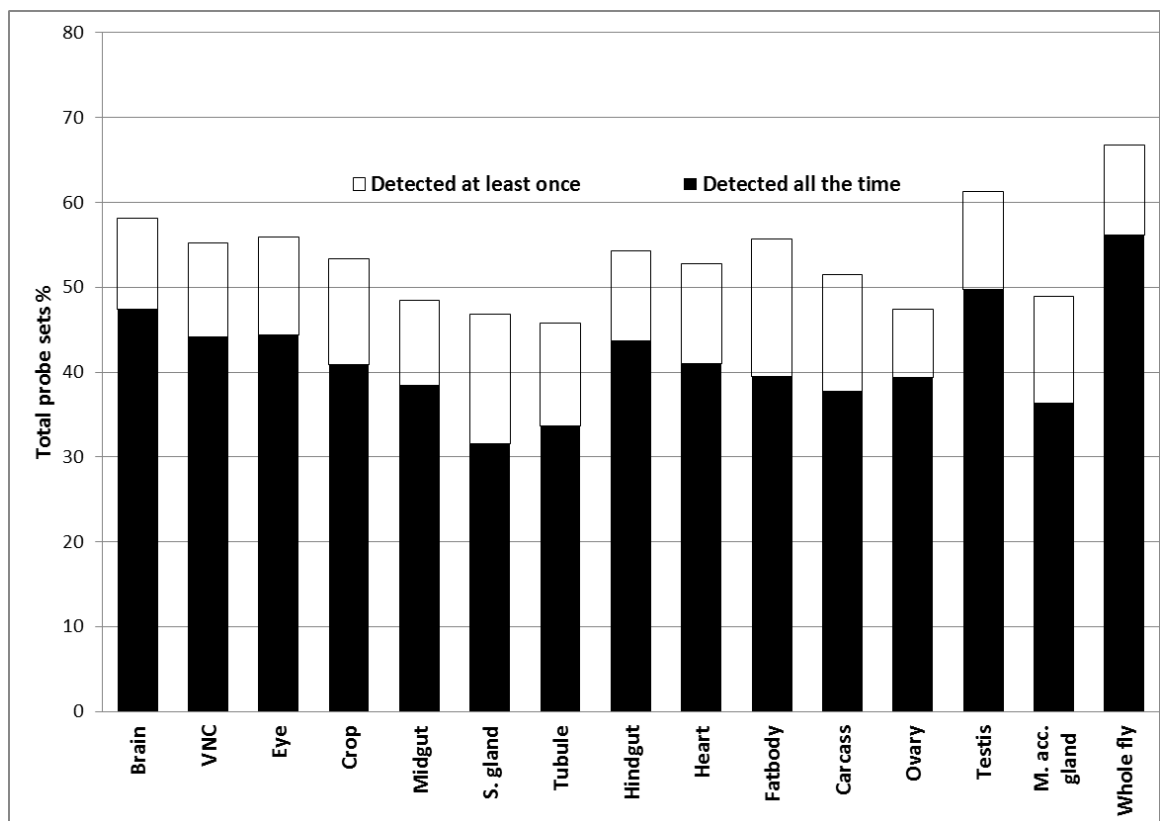


**Figure 3-1** *Drosophila* tissues typically express around half the computed transcriptome (updated on 26<sup>th</sup> January 2012).

For each tissue, the number of probe sets giving at least one 'present' call is shown, together with those meeting the stricter criterion of giving four present calls out of four chips.

Of course, the quality of the data set and the underlying tissue dissections is critical for such assertions. It is possible to perform an informal 'quality control' on the data set by seeking genes that are strongly enriched in particular tissues. For example, the photoreceptor channel *trp* should be enriched in the head sample but ideally should not show up strongly in the brain. The results (Table 3-1) confirm that there is excellent discrimination, even between physically adjacent tissues (such as brain and head; midgut, tubule and hindgut or testis and accessory gland).

**Table 3-1 Genes that show extreme specificity of expression and that serve to validate the quality and discrimination of the data set (updated on 26<sup>th</sup> January 2012). Errors are omitted for clarity; these are in the range of 5%-10% and are given online at <http://flyatlas.org/>. Boldface indicates the maximum signal for each gene. Abbreviation: S, salivary; M, male; Acc, accessory; VNC, ventral nerve cord or thoracoabdominal ganglion.**

Gene	Expected region	Mean signal level													
		Brain	VNC	Eye	Crop	Midgut	S.gland	Tubule	Hindgut	Heart	Fatbody	Carcass	Ovary	Testis	M.Acc. gland
<i>Crz</i>	Brain	<b>1102</b>	6	12	3	4	6	2	2	1	4	2	0	1	1
<i>Fmrf</i>	VNC	436	<b>3250</b>	0	0	0	3	2	0	0	3	17	1	3	3
<i>trp</i>	Eye	74	3	<b>6507</b>	2	5	5	2	2	5	1	1	0	3	2
<i>DmsR-1</i>	Crop	13	8	69	<b>364</b>	2	8	3	1	6	6	10	0	1	4
<i>ser99Dc</i>	Midgut	0	2	5	3	<b>6335</b>	255	5	4	1	4	6	0	2	3
<i>CG31202</i>	S.gland	3	13	0	63	6	<b>4838</b>	6	3	1	1	38	4	4	3
<i>CG15408</i>	Tubule	1	2	1	3	2	6	<b>4337</b>	3	4	13	5	1	7	5
<i>CG9993</i>	Hindgut	3	0	4	2	11	7	13	<b>2647</b>	<b>3</b>	<b>5</b>	<b>5</b>	2	2	9
<i>Hand</i>	Heart	10	23	1	8	148	37	41	77	<b>5003</b>	225	259	1	22	1
<i>arginase</i>	Fatbody	16	15	21	17	9	12	15	44	526	<b>1085</b>	474	4	5	6
<i>Cpr49Ab</i>	Carcass	2	12	0	8	4	6	7	6	57	189	<b>3200</b>	1	1	6
<i>Otu</i>	Ovary	4	5	4	7	7	18	14	4	4	19	27	<b>1353</b>	6	4
<i>Mst84Dd</i>	Testis	3	3	3	5	9	11	6	8	3	13	22	1	<b>2525</b>	46
<i>Acp76A</i>	M.Acc. gland	3	3	2	4	3	9	5	3	2	5	75	4	40	<b>11565</b>

Generalizing from these examples, although 25% of all probe sets are ubiquitously expressed ('housekeeping' genes), there is a significant fraction of the genome that is highly tissue-specifically expressed in the adult (Table 3-2). Although brain and testis are particularly distinctive (Andrews et al., 2000), every tissue has a population of tens to thousands of genes that are detected nowhere else.

**Table 3-2 Genes expressed uniquely in specific tissues.**

For each tissue 'unique expression' refers to the number of probe sets called 'present' at least twice but present nowhere else in the fly; 'predominant expression' refers to the number of probe sets called 'present' more often in a given tissue than in all other tissues combined.

Tissue	Unique expression	Predominant expression
Brain	292	779
Head	156	585
Crop	12	12
Midgut	117	316
Tubule	31	80
Hindgut	80	279
Testis	1,317	2,079
Ovary	81	241
Accessory glands	47	339
Total (out of 18,770)	2,121	4,698

The clear implication of this result is that, for over a quarter of *Drosophila* genes, there is a single tissue in which study should be focused. Indeed, it may be counterproductive to embark on a now-standard reverse-genetic workup of a novel gene unless that tissue is studied, because an informative phenotype may be missed. Analogous to the Krogh principle of comparative physiology that "for every physiological problem, there is an animal uniquely suited by nature to study it" (Krogh, 1929), we propose an analogous principle for functional genomics: for every novel gene, it is as sensible to study it where it is most abundantly expressed as to study it where it is first encountered. Thus, FlyAtlas is a first step toward connecting the researcher to the tissue.

These results also show the importance of taking an organismal (tissue) and ontogenetic (multiple-life stage) view of gene expression in order to prevent a danger we term 'shoehorning': the squeezing of a gene's declared functions into expected phenotypes (for example, assuming that a channel must be neural in function) or into the phenotypes familiar to a particular experimenter (behavioral or developmental, for example). Given that the vast majority of *Drosophila* research focuses on embryonic development, and most of the remainder on neurogenetics, there is a real danger that major functions might be overlooked because of the dearth of functional research outside these areas. Again, the availability of tissue-specific expression data should encourage a more global view of each gene's possible functions.

### 3.2.2 Meta-analysis

There are further useful meta-analyses possible for these data. For example, research in *Drosophila* has been revolutionized by the GAL4/UAS binary system for tissue-specific expression of transgenes (Brand and Perrimon, 1993). Many GAL4 drivers are derived from enhancer-trap screens and may not be absolutely specific to a particular tissue or cell type. Genes that are absolutely specific to a single tissue of those studied so far can be extracted from the data set (Chintapalli et al., 2007; Chapter 5); the control regions of these genes may prove ideal drivers for GAL4 expression in flies. Conversely, there is also a need to identify genes with abundant and relatively invariant expression. It has been shown that qPCR normalization is better performed with a basket of invariant genes, from which the best reference genes for a particular experiment can be deduced experimentally (Vandesompele et al., 2002). FlyAtlas offers good candidate reference genes for the adult (Chintapalli et al., 2007); interestingly, the *Drosophila* 'standard' reference gene rp49 (Rpl32) ranks 3,172nd.

### 3.2.3 New transcription units

There are 18,880 *Drosophila* probe sets on the Affymetrix *Drosophila* 2 expression chip, covering around 13,500 genes. This is because many genes have additional, transcript-specific probe sets. However, several thousand probe sets were designed against features that were not considered sufficiently authoritative to justify annotation as a *Drosophila* gene, usually because of lack of compelling data that the putative gene was transcribed. It is clear from FlyAtlas that many of these features are genuinely transcribed, frequently tissue-specifically; this may explain why they were not hit with multiple ESTs. For example, HDP feature 01001 has a prodigious signal of 9,570 in male accessory glands and is almost undetectable elsewhere, so it is not surprising that its expression was not previously validated. Furthermore, each class of feature has a characteristic hit rate (Figure 3-2). Across FlyAtlas, 85% of probe sets against documented genes were found to be transcribed in at least one tissue; whereas 18%, 60% and 21% of HDP, sim4 and FGENESH features were found to be transcribed. Indeed, of 3,000 undocumented features on the Affymetrix array, 665 detect significant expression somewhere in the adult.

Thus, microarrays of tissue-specific RNA samples may be useful tools in transcript discovery, even for a genome as well-documented as *Drosophila*.

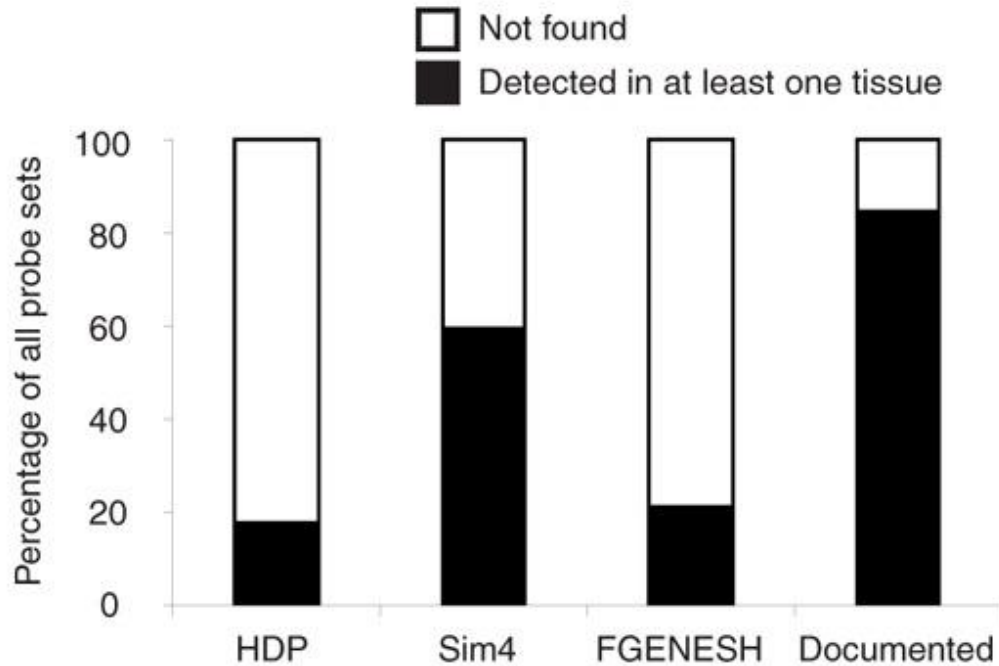


**Figure 3-2 Evidence for novel transcription units in the *Drosophila* genome.** Probe sets were classified according to their Affymetrix annotations; documented genes refer to probe sets that are annotated with a FBgn or CG reference number and are thus known to FlyBase. The remaining probe sets were then categorized by feature code (HDP, sim4 or FGENESH). To provide a strict test of expression, the number of tissues for which all four chips were called 'present' by Affymetrix software was scored for each probe set, and only those with at least one expressed tissue were scored as 'expressed'. Data are expressed as a percentage of all probe sets in that category.

### 3.2.4 An ontogenetic perspective

These data provide perhaps the clearest view yet of the transcriptional landscape of adult *Drosophila*; but does it bear any resemblance to other life stages? The Berkeley *Drosophila* expression database (<http://www.fruitfly.org/cgi-bin/ex/insitu.pl>) thus far contains information on the systematic determination of patterns of gene expression in *Drosophila* embryogenesis by RNA *in situ* for 6,138 genes. The Berkeley *Drosophila* Genome Project (BDGP) data set is searched by FlyAtlas so that users are notified if an embryonic expression pattern is available for a particular gene. Additionally, the BDGP *in situ* data have been annotated with gene ontology (GO) terms for distinct body parts, so we looked for persuasive overlap between embryonic and adult expression patterns.

There is very little reason to assert a priori that the same genes expressed in a given embryonic tissue are still expressed in the adult, but if around half the genome were expressed in an embryonic tissue (as in adult), and if there were no connection between embryonic and adult expression patterns, one would predict that only 25% of *in situ* hits would be expressed in the corresponding adult tissue. In fact, the concordance is far higher for the several tissues sampled (Table 3-3), with typically 90% of the genes identified by embryonic *in situ* analyses still expressed in adult flies, as measured by microarray. This result suggests intriguingly that the mature transcriptional profile of many tissues is substantially established by the late embryo.

**Table 3-3 Are the genes identified in embryonic tissues by *in situ* analyses also expressed in adult tissues?**

Adult regions selected were those for which there are recognizable late-embryonic precursors. A nonredundant list of CG numbers for genes called 'present' on four out of four chips was compared with CG numbers identified by embryonic *in situ* analyses to be either found in a given tissue, expressed ubiquitously or called 'faint ubiquitous' in stage 13-16 embryos. CG numbers common to both lists were counted.

Region	Number of genes		
	Adult array	Embryonic <i>in situ</i>	Common
Brain	8092	1218	1115
Midgut	6770	1452	1255
Tubule	5969	507	445
Hindgut	7588	827	759

In principle, *in situ* and microarray analyses are complementary; the former provides great spatial resolution (down to the single-cell level), whereas the latter is much more sensitive and quantitative. This can be seen in the relatively low numbers of genes detected by *in situ* analyses, even taking into account the 6,138 genes in the data set. However, it is clear that a joint *in situ*/array approach is powerful.

### 3.2.5 Surprising expression

FlyAtlas provides further provocative reminders that genes may not be expressed merely where they are expected. Table 3-4 shows some exciting insights into some well-known genes, selected to cover a range of gene class and function.

**Table 3-4 Some genes that are predominantly expressed in unexpected places. Bold face indicates the maximum signal for each gene.**

		Mean signal levels								
Gene	Described in	Brain	Head	Midgut	Tubule	Hindgut	Ovary	Testis	Accessory gland	
<i>cry</i>	Circadian behavior	279	575	267	<b>1,972</b>	868	7	25	205	
<i>fas2</i>	Neuronal fasciculation	129	66	49	<b>1,676</b>	78	5	9	53	
<i>obp56d</i>	Olfaction	71	4,045	1	1	<b>5,663</b>	1	106	5	
<i>kelch</i>	Nurse cell	181	<b>185</b>	22	16	22	5	6	6	
<i>rpk</i>	Sensory neurons	1	0	1	7	0	<b>904</b>	47	0	
<i>toe</i>	Eye, thorax	10	68	7	8	14	8	13	<b>3,725</b>	
<i>vnd</i>	Embryonic CNS	6	4	<b>289</b>	5	6	3	2	8	
<i>dsx</i>	Sex determination	21	119	89	<b>140</b>	106	9	1	8	

*Cryptochrome*, important in circadian function (Stanewsky et al., 1998), is functionally significant in peripheral tissues as well as in brain (Ivanchenko et al., 2001). However, the signals in the tubule and hindgut are much higher than in brain, supporting reports that in this simple organism, tissues run autonomous clocks (Giebultowicz et al., 2000). *Fasciclin2*, implicated in neural functions from axonal path finding to short-term memory, is predominantly expressed in the tubule. Given the importance of homeostasis to small organisms, the tubule enrichment could help to explain the low viability of some *fas2* alleles, and it serves as a reminder of the non-neuronal significance of cell junctions (Carthew, 2005).

The large family of odorant-binding proteins provides specificity to olfactory sensing in insects and, accordingly, has been described in the context of olfaction or gustation in the head (Graham and Davies, 2002; Hekmat-Safe et al., 2002). However, one of the odorant-binding protein genes (*Obp56d*) shows expression not just in the head but also at extremely high levels in the hindgut, providing an unexpected opening for olfactory research.

Another gene (*Obp56e*) is expressed in just the head and accessory gland, whereas *Obp56f* and *Obp22a* are expressed exclusively in the accessory gland but not in the head ([www.flyatlas.org](http://www.flyatlas.org)).

Several developmental genes are reused in very unexpected places in the adult: for example, *twin of eyegone*, important in visual and thorax development (Aldaz et al., 2003; Dominguez et al., 2004), is virtually specific to the male accessory gland in the adult.

Similarly, *ventral nerve system defective (vnd)* (Jimenez et al., 1995) is reused very specifically in the adult midgut. The sex determination gene *doublesex* is primarily an epithelial gene in the adult, suggesting that adult homeostasis may be sexually dimorphic.

*Kelch*, a component of the ring canal (Robinson and Cooley, 1997), is expressed at much higher levels in brain and head than ovary.

This is appropriate for a homolog of *gigaxonin*, a human gene associated with neuropathy (Bomont et al., 2000). *Kelch* may thus provide a better model for human disease than mere sequence similarity might predict.

### **3.2.6 Organotypic disease models**

Can this analogy be taken further? Are there other human genetic disease loci with *Drosophila* homologs that are expressed preferentially in tissues functionally analogous to the human target, increasing confidence in the validity of the *Drosophila* gene as a model? Combining the FlyAtlas data set with the Homophila database (Chien et al., 2002) provides a unique opportunity to test the idea. In fact, cursory examination uncovers multiple loci with this persuasive combination of evidence (Table 3-5).

**Table 3-5 *Drosophila* genes expressed in tissues analogous to those involved in human disease.**

The entire Homophila database was downloaded from <http://superfly.ucsd.edu/homophila/> and merged with the array database. We then selected probe sets against genes with Homophila annotations that showed signal enrichment in tissues analogous to those implicated in the human disease. Boldface indicates the maximum signal for each gene.

Tissue signals										
Gene	Brain	Head	Midgut	Hindgut	Tubule	Ovary	Testis	Accessory gland	Human gene	OMIM entry
<b>Brain</b>										
<i>kek2</i>	<b>156</b>	19	4	5	8	2	3	5	<i>SLITRK1</i> ( <i>KIAA1910</i> )	Tourette syndrome (137580)
<i>CG5594</i>	<b>2,267</b>	867	441	142	35	133	53	124	<i>Slc12a6</i>	Agenesis of the corpus callosum with peripheral neuropathy (218000)
<i>CG1909</i>	<b>1,265</b>	306	2	24	2	6	0	9	( <i>RAPSYN</i> )	Congenital myasthenic syndrome associated with AChR deficiency (608931)
<i>Lcch3</i>	<b>748</b>	173	2	3	3	2	8	5	Gaba-A receptor gamma-2	Myoclonic epilepsy, severe, of infancy (607208)
<i>CG7971</i>	<b>1,722</b>	437	117	62	70	31	23	171	<i>NIPBL</i> ( <i>delangin</i> )	Cornelia de Lange syndrome (122470)
<b>Midgut</b>										
<i>CG6295</i>	3	21	<b>5,461</b>	4	2	1	1	2	<i>LIPI</i> ( <i>PRED 5</i> )	Hypertriglyceridemia, susceptibility to (145750)
<i>CG31636</i>	2	19	<b>159</b>	2	1	1	7	1	<i>c17orf79</i> ( <i>T TPI</i> )	Ataxia with isolated vitamin E deficiency (277460)
<i>eTry</i>	2	5	<b>5,967</b>	6	6	3	5	3	Proenterokinase	Enterokinase deficiency (226200)
<b>Tubule</b>										
<i>CG3762</i>	441	1,213	4,665	5,497	<b>6,242</b>	1,906	354	1,170	Vacuolar proton pump	Renal tubular acidosis with deafness (267300)
<i>ry</i>	80	142	97	49	<b>770</b>	2	18	7	Xanthine oxidase	Xanthinuria type I (278300)
<i>Irk3</i>	328	123	4	48	<b>4,932</b>	1	1	11	Renal outer-medullary potassium	Bartter syndrome, antenatal, type 2 (241200)
<i>CG5284</i>	568	451	292	361	<b>1,334</b>	540	75	357	Chloride channel <i>CLCN5</i>	Dent disease 1, nephrolithiasis, X-linked (30008)
<i>CG17752</i>	1	1	2	1	<b>6,341</b>	1	2	3	<i>SLC22A12</i> ( <i>URAT1</i> )	Hypouricemia, renal (220150)
<b>Ovary</b>										
<i>PI3K92E</i>	283	171	182	188	108	<b>395</b>	92	185	PI 3-kinase, alpha	Ovarian cancer (604370)
<b>Testis</b>										
<i>bol</i>	104	19	1	9	6	1	<b>1,778</b>	82	<i>DAZL</i> ( <i>SPYGLA</i> )	Spermatogenic failure, susceptibility to (601486)
<i>Ubp64E</i>	294	221	238	514	334	196	<b>752</b>	367	<i>Drosophila</i> fat facets-related	Azoospermia (415000)
<i>CG17150</i>	2	2	5	3	5	2	<b>391</b>	6	<i>ITLN1</i> ( <i>HL1</i> )	Kartagener syndrome (244400)

Although these genes are plausible candidates for investigation, *Drosophila* is neither a mammal nor a vertebrate. Does a physiological approach to *Drosophila* yield insights into human gene function that are not obtainable in humans or mice? In fact, our understanding of many human genes (and not just those involved in development) has emerged from *Drosophila*. Behavioural screens in *Drosophila* identified the role of cyclic AMP in memory (Byers et al., 1981). They also identified the first clock genes (Konopka and Benzer, 1971) and found the prototype for the Shaker family of potassium channels (Salkoff and Wyman, 1981).

Of course, neurogenetics is an accepted area of functional similarity between human and fly, but the approach can extend to other tissues that are much less explored. The roles of the tubule, for example, are analogous to those of the human kidney, liver and innate immune system (Dow and Davies, 2006). As well as generating a primary urine, it is loaded with cytochrome P450s and glutathione transferases that imply a major role in detoxification (Yang et al., 2007), and it is capable of mounting a robust immune response independent of the cardinal insect immune tissue, the fat body (Kaneko et al., 2006; McGettigan et al., 2005). The tubule data set contains genes with homologs well-known in the mammalian renal literature.

The V-ATPase proton pump, for example, has been shown to be essential (Davies et al., 1996), and mutations in genes encoding all 13 V-ATPase subunits implicated in plasma membrane transport have resulted in a renal phenotype in *Drosophila* (Allan et al., 2005), presaging the discovery of a renal phenotype in humans with a similar mutation (Karet et al., 1999). All three inward-rectifier K<sup>+</sup> channel genes (analogous to the ROMK channel associated with a form of Bartter syndrome) are strongly enriched in the tubule and hindgut, implying an epithelial transport role rather than the neural role that is usually sought for channels in *Drosophila* (Evans et al., 2005). Perhaps most famously, *rosy*, the second mutant ever identified in *Drosophila* (Glassman and Mitchell, 1959), exactly recapitulates the symptoms of xanthinuria type I, the human disease associated with xanthine oxidase mutations (Dent and Philpot, 1954; Wang et al., 2004). Thus, there are ample scope and informative phenotypes to explore renal function in this simple organism (Dow and Davies, 2003).

The other tissues listed in Table 4 also show persuasive similarities, but the physiological study of other tissues is at an earlier stage. However, the data clearly illustrate the importance of a tissue-centered view in functional genomics, both a priori in the design of transcriptomic or proteomic experiments and post hoc in the central goal of functional genomics: the elucidation of the major functions of all the genes encoded by a genome. To this end, FlyAtlas provides a valuable tool to focus efforts directed at both goals.

We suggest an important and salutary meta-analysis of this data set. Many *Drosophila* microarray studies have used whole-organism RNA samples (from embryos, larvae or adults). Clearly, given the tissue specificity of expression we describe above, this is less than ideal. However, it is possible to demonstrate exactly how bad it is by modeling the whole-organism transcriptome from the transcriptomes of its constituent tissues—that is, drawing up an 'equation of the fly'. In principle, the whole-fly transcriptome is made up of the sum of the transcriptomes of each tissue, multiplied by a coefficient that is effectively the fraction of organismal mRNA contributed by that tissue:

$$\text{Signal}_{\text{Fly}} = \sum_{\text{Tissues}} \text{Signal}_n \times c_n$$

A set of hybridizations with tissue-specific mRNA preparations allows the coefficients to be calculated. In principle, for each gene with truly tissue-specific expression, the whole-fly signal represents the contribution of that tissue to the whole fly. However, this approach depends on the accurate identification of truly tissue-specific genes. A simpler approach (Figure 3-3) is to plot tissue signal against whole-fly signal for each tissue and take the lowest gradient through the experimental points; this represents the best estimate of the coefficient for that tissue. The resulting equation can be tested against the real whole-fly transcriptome. As each tissue is added, the average abundance of widely expressed genes approaches the theoretical 1:1 line, and highly tissue-specific genes disappear from the lower region of the plot as they reach the trend line. As can be seen, with 11 tissues, around 70% of the real signal can be modeled. The rest of the tissues may fill the gap between real and simulated fly signal.

The implication of the equation for whole-organism transcriptomics is severe; it shows that most tissues each contribute less than 5% to the organismal signal. So, considering a typical array signal of 100, and taking a 50% change as a threshold for detection, a gene expressed in a single tissue would have to change its signal by at least 1,000 for the change to be detected in a wholefly hybridization.

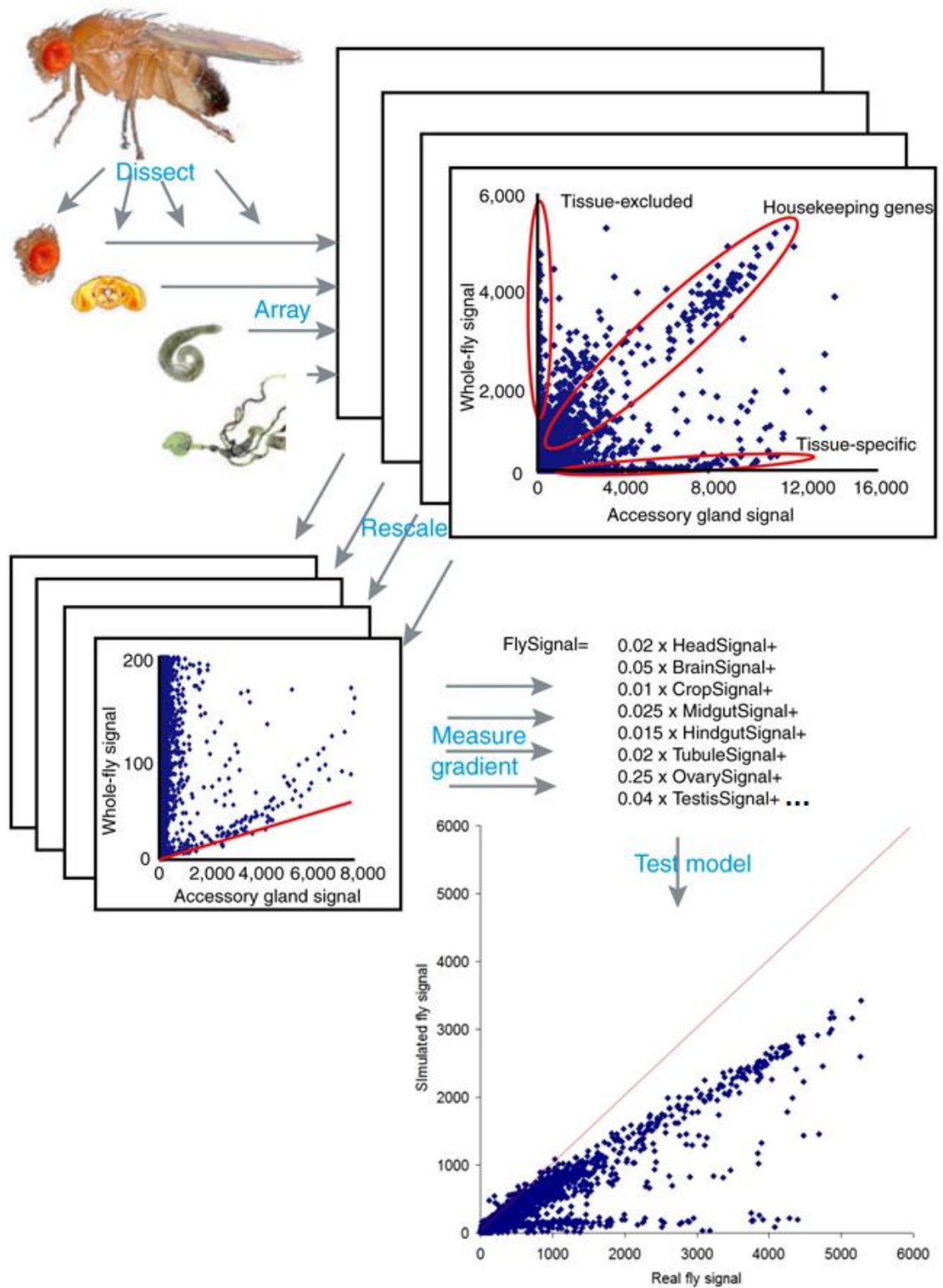


**Figure 3-3 Calculating the equation of the fly.**

Tissues are dissected from the adult fly, and their signals are plotted against the whole fly. Although all degrees of specificity are represented, most genes tend to be generally expressed, tissue excluded or tissue specific. By rescaling and plotting the lowest gradient that runs through experimental data, coefficients for the whole-fly array simulation can be estimated. These can then be tested iteratively against real-world results as new tissues are added. Calculated whole-fly signal = 0.02 x head + 0.05 x brain + 0.01 x crop + 0.025 x midgut + 0.015 x hindgut + 0.02 x tubule + 0.25 x ovary + 0.04 x testis + 0.06 x accessory gland + 0.015x thoracoabdominal ganglion + 0.17 x carcass

Thus, a whole-fly array is capable of detecting only orchestrated changes in widely expressed genes or truly exceptional changes in genes with more restricted expression patterns. Whole-fly arrays are thus a trade-off between convenience and sensitivity, reporting a severely attenuated subset of the true changes occurring between experimental groups. As the body plan and relative tissue sizes of the adult are largely established by the late embryo (with the conspicuous exception of those adult tissues generated by proliferation of the imaginal discs), the argument can be extended to whole-organism arrays or proteomic studies of other life stages.

Is there a strategy that would maximize the chances of detecting a spatially restricted change, at least in the adult, for finite extra effort? From the data available at present, perhaps a five-way split would provide a working compromise: head, alimentary canal, male and female genitalia (separately) and carcass. 'Whole-head' would report on head, brain and fat body, with perhaps a threefold drop in sensitivity for the individual tissues; similarly, 'alimentary canal' would report on midgut, tubule and hindgut, with similar performance. Gonads would combine the distinctive transcriptomes of (for example) testes and accessory glands, without swamping either, and the carcass would report on cuticle, muscle and associated tissues. The increased cost could then be balanced against hugely increased authority and utility of the data.

Thus, FlyAtlas hints at some exciting new directions for *Drosophila* functional genomics. Of course, this approach needs continual refinement; as new tissues and developmental stages are added to FlyAtlas, the authority of the data set will increase. Ideally, an atlas should include every domain that can be identified by a GAL4 enhancer trap, perhaps using poly-A binding protein technology to allow selective purification of mRNAs (Yang et al., 2005). Similarly, as the computational transcriptome of the fly is successively refined and the knowledge rolled out in new generations of array (such as tiling or exon arrays (Manak et al., 2006)), it will be useful to update the data iteratively. Overall, though, the emphasis on tissues and organ systems will help to redirect and focus efforts toward organism-level systems biology in this useful model organism.

## 4. A transcriptomic view on epithelial structure and function

### Summary

The previous FlyAtlas analysis provided general insight into tissue-specific transcriptomes. In this chapter, a comparative analysis of epithelial transcriptomes was performed to uncover similarities and differences in any of the two epithelia to elucidate epithelial function. The transcriptomes of four major epithelial tissues (salivary glands, Malpighian tubules, midgut and hindgut) for both adult and larvae are compared. Each epithelial transcriptome is compared against the whole fly for adult and whole larvae for the larval transcriptome. A gene expression signature for each individual epithelium was obtained using the upregulated fold change enrichment. These signature genes were used to identify common signatures in adult and larvae. The signature genes were then analysed for their potential mammalian ortholog/paralog functions/diseases, canonical pathways and networks using Ingenuity pathway analysis (IPA). The significantly enriched IPA functional classes for novel genes demonstrate how the analogous tissues in flies and humans could be compelling examples of molecular and functional convergent evolution. Taken together, the meta-analysis of tissue specific transcriptomes in *Drosophila* not only uncovered potential similarities of the epithelia but also unravelled functional similarities with their vertebrate counterparts.

## 4.1 Introduction

Molecular genetics and biochemical techniques extended our understanding of genes and their functions. The invertebrate model organism, the ‘fruit fly’ *Drosophila melanogaster* has been instrumental in this task. Advancements in molecular biology such as microarrays have provided a wealth of information-rich gene expression datasets. For example, our laboratory generated ‘FlyAtlas’ provided authoritative gene expression levels in many fly tissues, leading to our proposed hypothesis that the best place to study the functional role of a gene is in the tissue it’s abundantly expressed but not where it’s first studied (Chintapalli et al., 2007).

Developmental studies in *Drosophila* and several other model organisms have shed light on many of the molecular mechanisms that are conserved across species. Cell polarity is one of these processes that has been extensively modelled across epithelial cells and tissues (Gibson and Perrimon, 2003; Knust and Bossinger, 2002; Nelson, 2003). For example, planar cell polarity (PCP) is a highly conserved hallmark feature of epithelia, from flies to humans (Simons and Mlodzik, 2008). While the developmental functions and mechanisms are well studied for the epithelia, the adult functions of many novel genes still remain unexplored, because of the phenotype gap (Chintapalli et al., 2007; Dow, 2003; Wang et al., 2004).

The alimentary canal ramifies throughout the body and constitutes the major epithelial tissue of the fly. The complex developmental transitions form the adult epithelia that include the major transporting and secreting epithelia of the fly: salivary glands, midgut, hindgut, and Malpighian tubules. These are divided into two groups including primary and secondary epithelia. The primary epithelia originate from ectoderm and include epidermis, fore and hindgut, Malpighian tubules, and salivary glands (Beyenbach et al., 2010a; Hartenstein, 1993). The secondary epithelium, the midgut, originates from mesenchymal intermediates during mesenchymal-epithelial transition (Tepass and Hartenstein, 1994). During larval and pupal transition, epithelial tissues including gut and salivary glands undergo extensive reconstruction (metamorphosis).

However, the posterior gut or hindgut is only partly replaced; Malpighian tubules persist into the adult and the gastric caeca, and outgrowths of the anterior larval midgut are not replaced in the adult (Hartenstein, 1993). Thus, these changes from larval to adult may reflect the major gene expression changes between these two life stages.

Neuroendocrine control is the predominant mechanism of regulation of the epithelial tissues; in that insect tubules for example, share common endocrine mechanisms (G.M. Coast, 2002; Veenstra, 2009) such as the regulation of fluid secretion to excrete metabolic waste and to regulate stress resistance and insulin production (Soderberg et al., 2011). The stem cells and their niches have also been shown to be important in the tissue regeneration and repair in the epithelia (Micchelli and Perrimon, 2006; Ohlstein and Spradling, 2006; Singh et al., 2007). For hindgut, it is proposed that stem cell niches play a key role in the formation of adult tissue during larval and pupal phases (Takashima et al., 2008).

Epithelial tissues comprise distinct functional domains and multiple cell-types (Andrew et al., 2000; Micchelli and Perrimon, 2006; Sozen et al., 1997; Takashima et al., 2008). They perform wide ranging functions from transport, cell signaling, to immune sensing largely depending on their internal and external milieu and their opening and closing pose. While most of the epithelia are capable of doing functions related to one another, they must retain a functional theme. For example, salivary glands: secretion; midgut: nutrient uptake; Malpighian tubules: fluid transport and hindgut: excretion. Nutrient absorption, immune and endocrine functions are some that are predominantly performed and are shared by the epithelia. The molecular and functional understanding of some of the epithelia is better than the others because of their simplicity and adaptability to the manipulation that science requires in order to rapidly understand their biological and molecular complexity. The Malpighian (renal) tubules of the fly are the functionally analogous tissues to human kidneys and thus far best studied for their adult functions in ion transport (Dow and Davies, 2003); signalling through  $\text{Ca}^{2+}$ , NO, cAMP and cGMP (Davies and Terhzaz, 2009; Day et al., 2005); and host defence to xenobiotics and pathogens (McGettigan et al., 2005; Yang et al., 2007).

Here, a meta-analysis was carried out on four major epithelial tissue transcriptomes of the adult and the larval *Drosophila melanogaster*, generated as part of the FlyAtlas. A gene expression signature was obtained for each epithelium using the upregulated gene lists. Common signature lists were obtained for larval, adult and across both stages. Then, the signature genes were analysed using Ingenuity® Pathway Analysis (IPA) for their potential vertebrate enriched functions/diseases, canonical pathways and networks.

## 4.2 Results

The principal component analysis (PCA) was performed to account for variation among the biological replicates of the same tissue (Figure 2-4). This identified among the tissues, epithelial tissues altogether show less variation in the principal component that represented the most variation. I then sought to find the differences between the epithelial tissues against whole fly or whole larvae.

The first analysis (Section 4.2.1) includes the comparison of transcriptomes of each epithelium against their adult whole fly or whole larvae. The significantly differentially expressed (up and down regulated) ( $FDR \leq 0.05$ ) gene lists were generated. A list of upregulated genes (at least 2-fold) was obtained for each epithelium, and was called the 'epithelial signature'. The signature genes were then compared to each other (Section 4.2.2), first to uncover unique and common genes in adult versus larval transcriptomes of each epithelium; and second to uncover the commonality among adult and larval epithelia separately. In addition, a heatmap was constructed for all the epithelial tissues using a hierarchical clustering method to show possible relationships among the epithelia.

The second analysis (Section 4.2.3) includes the comparisons of the epithelial transcriptomes against the adult whole fly to get an epithelial transcriptomic signature in an adult functional context. This is because of the distribution of the adult whole fly and whole larvae transcriptomes against the rest of the epithelia on the PCA map; all the epithelia show less variation (Figure 2-4).

This analysis was to find out the genes that show high expression in both adult and larval tissues, which probably do post-embryonic functions, rather than simply being confined to developmental functions.

The third analysis (Section 4.2.4) includes the direct comparisons of adult versus larval tissue transcriptomes. This reveals the larval and adult abundant gene expression patterns.

Finally, using the 2-fold enriched lists ( $FDR \leq 0.05$ ) generated from the first analysis, Ingenuity Pathway Analysis (IPA) was performed for the potential vertebrate enriched functions/diseases, canonical pathways and networks (Section 4.2.5).

### ***4.2.1 Differential expression and coregulation***

The number of genes that were at least 2-fold differentially ( $FDR \leq 0.05$ ) expressed is shown in (Figure 4-1). They were divided into 2-5-, 5-10-, 10-20- and  $\geq 20$ -fold up- and down-regulated groups. The sum of the transcription of highly enriched (at least 5-fold) common genes is 60-70% higher in adult than the larval epithelia.

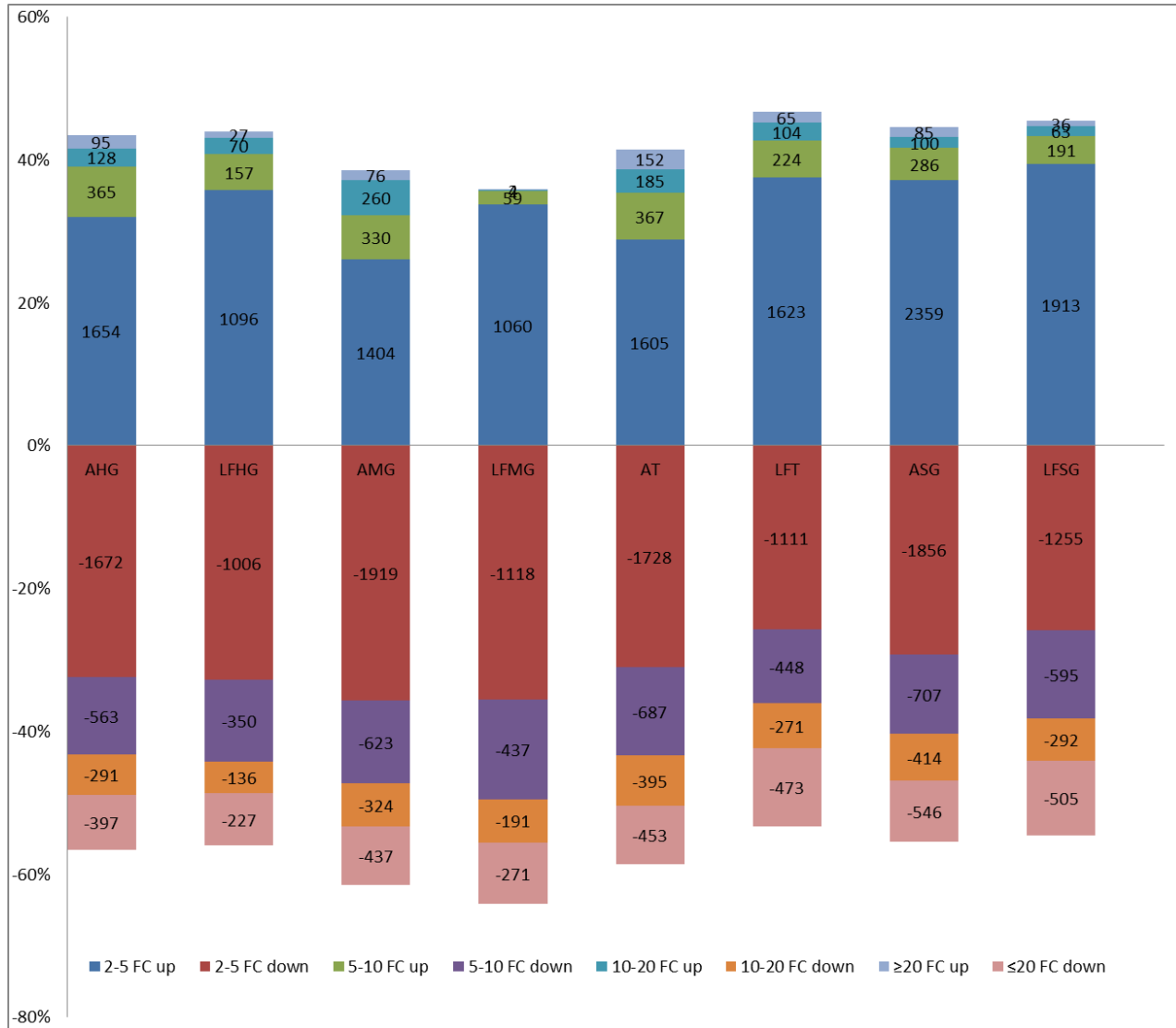


**Figure 4-1 Differential expression of epithelial transcriptomes.**

The distribution of 2-fold or higher differentially expressed genes across epithelia is shown. The significantly changed ( $FDR \leq 0.05$ ) genes are presented as 2-5, 5-10, 10-20 and  $\geq 20$  fold change up and downregulated groups. Abbreviations: A=adult, LF=larval feeding, HG=hindgut, MG=midgut, T=Malpighian tubules, SG=salivary glands.

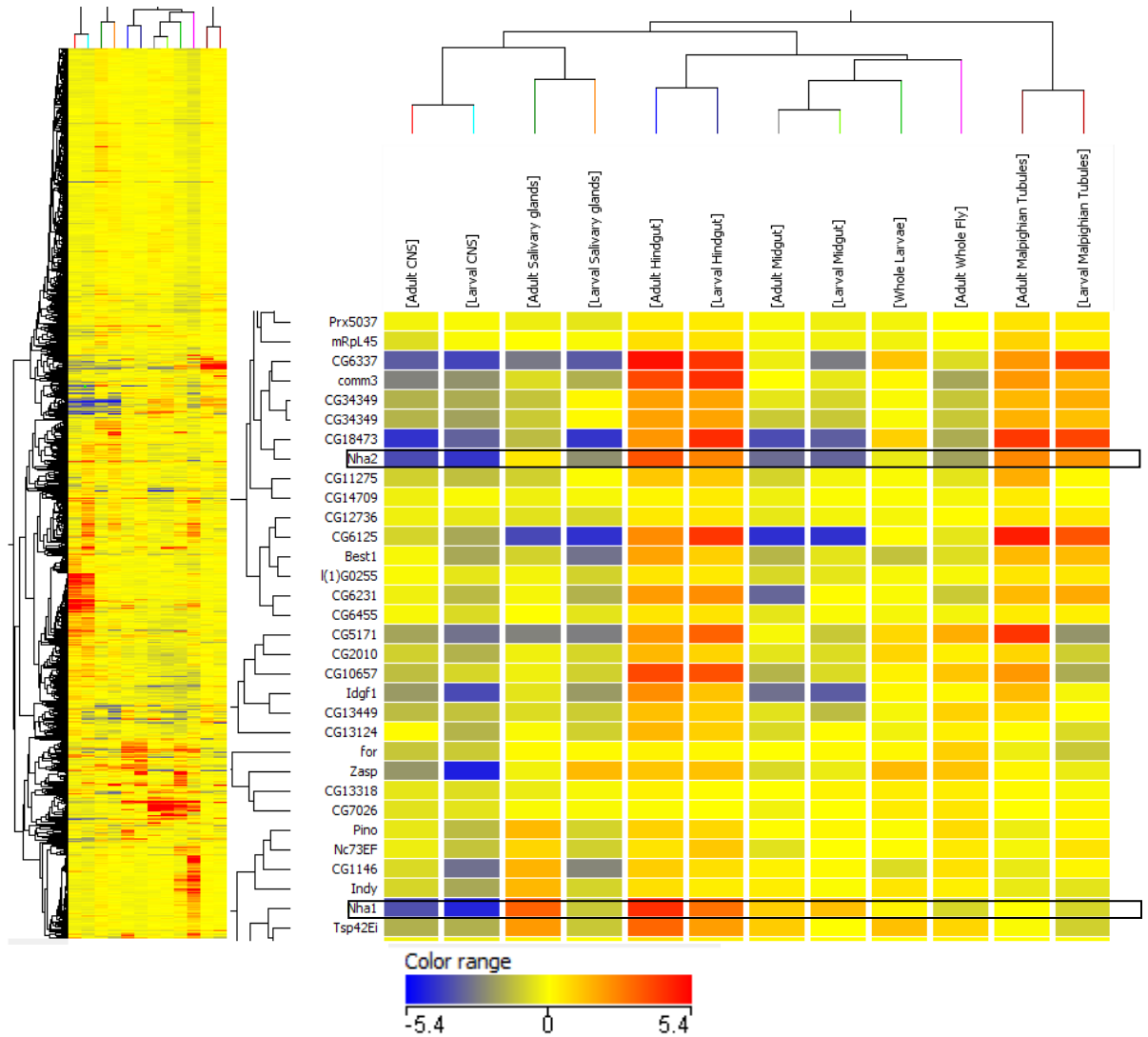


**Figure 4-2 Hierarchical clustering of epithelial transcriptomes.**

The vertical heatmap (left) represents the total (1880) number of probesets (that represent 18500 transcripts). (right) An area of the heat map was taken to show the arrangement of genes (horizontal) and the tissues (vertical) on the basis of their transcriptomic similarities. The colour range (bottom) indicates the log-transformed intensity of gene expression from high (red) to low (blue). The epithelial (but not neuronal) tissue enriched apically localised  $\text{Na}^+/\text{H}^+$  antiporters (*Nha1* & *Nha2*) show faithful co-clustering (shown in the black horizontal boxes).

Hierarchical clustering (HC) of transcriptomes was performed in order to understand the global gene expression similarities across the epithelia and translate the similarity into tissue-tissue functional relationships on an intuitive heatmap diagram. This kind of clustering demands the datasets to their highest quality and consistency (Bjorklund et al., 2006; Eisen et al., 1998; Ling et al., 2009). The quality was tested in two-independent ways including Affymetrix experimental hybridisation controls and principal component analysis (PCA) statistical method, and found to be satisfactory (Chapter 2: Materials and Methods). The clustering arranged the transcriptomes both vertically (conditions-tissues) and horizontally (entities-genes) (Figure 4-2) on the basis of their global similarity of expression.

Interestingly, the most closely related transcriptomes were the pairs of cognate adult and larval tissue transcriptomes which cluster under one branch although they undergo extensive remodelling during metamorphosis. However, this was consistent with the number of related genes that were differentially expressed in each tissue over their respective whole organism. This analysis also confirmed the validity of the method and the quality of the datasets.

The hierarchical tree was branched into two. The first branch includes the tubules, and the other branch includes the rest of the transcriptomes. The rest of the transcriptomes were split into two branches: one including the CNS and salivary glands; and the other including the guts and the whole animals. From this data, the most unique transcriptomes belong to both larval and the adult tubules as they were placed in a single branch from the rest of the transcriptomes. The guts and the whole animals were the immediate neighbours of the tubules. The gut transcriptomes were the closest and in one branch along with the whole animal transcriptomes. Next to guts and whole animals were the salivary glands and CNS which branched into one.

### **4.2.2 Epithelial signatures**

The adult- and larval- specific signature for each individual epithelium was obtained by finding genes that were only enriched in either stage over their respective adult whole fly or whole larvae transcriptome.

For each epithelium, the larval and adult signatures were compared against each other to find the common and unique signature genes between two stages. Among the 5-fold or more enriched genes, there are hundreds that show a unique and common expression pattern within each epithelium of larval and adult stages (Figure 4-3).

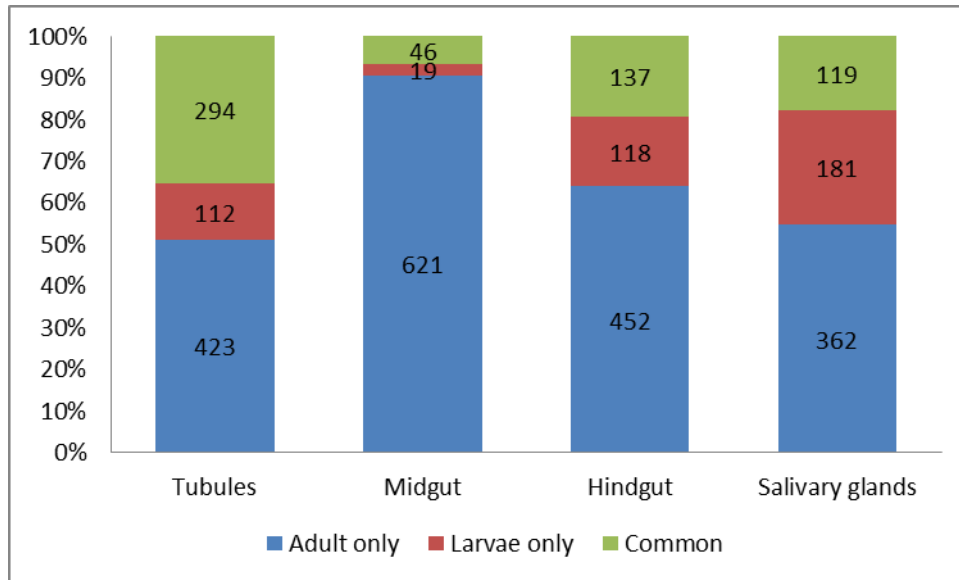


**Figure 4-3** Number of genes enriched (at least 5-fold) in larvae, adult or in both epithelia (FDR $\leq$ 0.05).

Larval and adult epithelia were compared against their respective whole animals to obtain the fold changes. The number of larval- and adult-specific enriched genes was obtained along with the commonly enriched in both. This analysis shows how many of the genes confined to a particular developmental stage, in addition to commonalities between two developmental stages.

A list of the 50 most enriched unique and common probesets (genes) for adult, larval transcriptomes were obtained to see if they describe their manifestation. The novel GO: transport genes were then analysed with Online Mendelian Inheritance in Man (OMIM) to identify any human disease phenotypes that match the cognate fly tissues (Borate and Baxevanis, 2009).

#### 4.2.2.1 Salivary glands

The top 50 adult (but not larval) salivary gland enriched probesets represent 16 known, 20 and 10 novel genes with and without GO terms respectively including 3 unannotated probesets (Table 4-1A). The known genes include *5-HT2*, *DNasell*, *Drip*, *ine*, *Buffy*, *yellow-d*, *Nep5*, *GS*, *Fsh*, *trol*, *Ir*, *pio*, *NLaz*, *wbl*, *5-HT7* and *stumps*.

Not surprisingly, *serotonin (5-hydroxytryptamine or 5-HT) receptor 2 and 7 (5-HT2 & 7)* are highly abundant in the adult salivary glands, although they have been shown to be expressed in the brain and modulating the aspects of circadian and aggressive behaviours (Johnson et al., 2009; Nichols, 2007). It is well known that two separate 5-HT receptors in blowfly salivary glands mediate secretion through two independent signaling mechanisms; constituting the key second messengers cAMP and  $\text{Ca}^{2+}$  (Berridge, 2005).

The *Drip* is consistently expressed across the epithelia, and abundant in the adult salivary glands, to probably facilitate the secretory functions of salivary glands.

The yellow-d belongs to the family of yellow proteins that show high similarity to the family of major royal jelly proteins produced by bees, which are discussed below. The *Buffy* is the *Drosophila* ortholog of human  $\text{BCL}^{-2}$ , an anti-apoptotic and cell cycle suppressor that was shown to act downstream of *Rpr*, *Grim*, *Hid* to block caspase-dependent cell death (Quinn et al., 2003). As the expression of *Rpr* and *hid* plays a crucial role in the ecdysone mediated cell death during metamorphosis, the apoptosis mediated by these genes need to be probably suppressed by the high expression of *Buffy* during the adult stages. Interestingly, the *ine* was shown to encode a neurotransmitter; its expression is very high in the adult salivary glands. Accordingly, an increased neuronal excitability phenotype is seen in *ine* mutants (Huang and Stern, 2002). However, it has also been implicated in the regulation of osmotic balance of the fly by potentially contributing to the osmolyte concentrations in Malpighian tubules and hindgut (Huang et al., 2002; Huang and Stern, 2002). However, it is highly abundant in the salivary glands indicating the probable functions of salivary glands in the osmotic balance of the fly.

The novel GO: Transport genes include *CG7589*, *CG15094* and *CG6836*. The *CG7589* shows high expression in the salivary glands, in addition to its expression in the tubules. It has an OMIM entry: gamma-aminobutyric acid receptor, gamma-2 (GABRG2G), a member of the GABA-A receptor gene family of pentameric ligand-gated ion channels which is associated with childhood epilepsy.

The *CG15094* was identified as a gene that potentially encode  $\text{Na}^+$  and  $\text{PO}_4^{3-}$  transporter by GO: biological process, and related to a known  $\text{Na}^+$ -dependent inorganic phosphate cotransporter (*NaPi-T*), which shows tubule-specific expression. Thus the OMIM entry directs it, like NaPi-T, to human SLC17A8, a  $\text{Na}^+/\text{PO}_4^{3-}$  cotransporter or vesicular glutamate transporter (VGLUT3) and conspicuously identified as a gene that is involved in deafness.

**Table 4-1 The top 50 genes enriched in salivary glands.**

(A) Adult Enrichment		(B) Larval Enrichment		(C) Common Enrichment		
Gene Symbol	FCA	Gene Symbol	FCA	Gene Symbol	FCA (asg/awf)	FCA (lfsg/wlf)
CG31202	244	CG32073	48	sens	160	65
CG32984	185	Muc68Ca	47	CG34290	129	47
CG32198	174	Pip	44	Sox21b	100	15
5-HT2	127	Pip	42	sage	84	21
CG14934	117	GRHRII	38	CG18581	77	48
CG7589	107	CG12506	38	nvY	75	23
CG12310	101	CG32071	37	LysP	66	12
CG15515	98	CG9737	36	eyg	65	16
CG6074	63	Y	36	l(3)82Fd	65	11
DNasell	55	sesB	36	CG8708	63	41
Drip	50	Eig71Ea	36	CecC	57	50
CG18088	49	CG14850	35	CG30371	53	17
CG14880	45	CG15741	35	fkh	43	15
ine	42	Pip	28	CG13461	36	34
CG13946	41	CG2217	27	CG30411	36	12
CG17121	39	CG15530	27	1634865_at	34	14
CG5630	39	CG13694	26	toe	32	19
Buffy	37	CG6763	26	CG15890	30	10
CG31516	36	CG17134	22	net	29	17
yellow-d	33	CG31809	21	CG13950	26	30
CG5630	32	PH4alphaSG1	21	sage	25	16
Nep5	29	CG31810	20	CG14118	25	12
CG7408	29	CG4334	20	GalNAc-T2	24	11
GS	27	CG5402	20	GalNAc-T2	24	15
CG15094	26	CG32074	20	PH4alphaSG2	22	18
CG8668	26	CG34105	20	Tie	20	12
CG15385	25	CG34279	19	p24-1	19	15
1640606_x_at	24	CG12715	18	Gmap	18	11
Fsh	24	CG17362	18	FucTA	16	30
CG33099	23	CG33256	17	CG10918	15	14
CG9098	22	Pip	17	CG13947	15	30
CG8483	22	hoe2	16	CG14252	14	13
trol	22	CG17362	16	CG30104	10	11
1633370_s_at	22	CG14852	16	CG6225	10	14
lr	22	CG13445	16	CG33169	10	10
CG31036	22	Br	15	CG30394	8	12
CG31431	22	CG12508	15	cry	8	29
CG6836	21	1637802_at	15	CG15743	8	15
pio	21	Eig71Eb	15	Hsp70Bbb/c/a	8	14
CG3655	21	CG13170	14	CG34276	8	48
NLaz	21	l(1)G0222	14	pgant5	5	10
CG6675	21	CG17283	13	D	83	6
CG4839	21	CG10830	13	Awh	80	7
wbl	21	Pip	12	CG13285	70	7
CG4267	21	CG15404	12	CG6688	56	8
5-HT7	20	CG15438	12	1624816_at	41	8
stumps	20	Pip	12	CG15822	38	8
CG7510	19	Cdc6	12	GlcAT-P	29	6
CG14356	19	CG31704	12	CG18507	29	10
1625316_s_at	19	1639017_at	12	CG18507	28	7

The top 50 larval (but not adult salivary gland) enriched probesets represent 12 known, 10 and 22 novel genes with and without GO terms respectively, including 2 unannotated probesets (Table 4-1B).

The known genes include *Muc68Ca*, *pip*, *GRHR11*, *y*, *sesB*, *Eig71Ea*, *PH4alphaSG1*, *hoe2*, *br*, *Eig71Eb*, *l(1)G0222* and *Cdc6*. The yellow(y) proteins are associated with normal pigmentation, and implicated in morphology and locomotion of the organism (Drapeau, 2001). Its closest counterparts found to be the major royal jelly proteins (MRJPs) in honeybees that comprise 12.5% of the mass, and 82-90% of the protein content largely constituting essential amino acids and thought to be important as nutrients (Schmitzova et al., 1998). The royal jelly facilitates the development of a queen bee from bee larvae. Although the biological functions still remain to be explored, recent findings suggest they may be important in the epigenetic control of the honeybee transcriptome (Foret et al., 2009). Interestingly, all known transcripts of the *pip* show specific enrichment in the larval salivary glands.

The novel GO: Transport genes include *CG4334*, *CG10830*, and *CG15438*. The *CG4334* encode a putative metal ion transporter. The *CG10830* has an OMIM entry: KCTD7, K<sup>+</sup> channel tetramerization domain-containing protein 7, implicated in progressive myoclonic epilepsy-3 in consanguineous Moroccan family members. The *CG15438* has an OMIM entry: *SLC17A5*, a gene associated with lysosomal sialic acid storage disorder (SSD). SSD is an autosomal recessive neurodegenerative disorder that may come in two forms including severe infantile form and slowly progressive adult form.

The larval salivary gland highly enriched genes encode secretory proteins (*sgs1*, 3, 4, 5, 7, 8), which are required in the pupal adhesion, and are required for larvae to moult into pupae. For example, the larval serum proteins are produced by the fatbody (Roberts et al., 1991; Wolfe et al., 1977).

The three subunits (alpha, beta and gamma) of larval serum proteins are encoded by 3 paralogous genes that may have been duplicated in evolution from a common ancestor (Brock and Roberts, 1980). These genes occupy the list of most highly enriched genes of the larval feeding salivary glands. However, the other larval tissues including tubules, midgut, and hindgut show predominant

expression of these genes which could be needed in large amounts during metamorphosis. Interestingly, the three null alleles of all three subunits together were shown to be dispensable for the organism survival (Roberts et al., 1991). Other *glue* genes, that encode newglue 1 and 2, required for pupal adhesion, were also enriched.

The top 50 commonly enriched probesets in both adult and larval salivary glands represent 22 known, 8 and 17 novel genes with and without GO terms respectively (Table 4-1C). The known genes include *sens*, *Sox21b*, *navy*, *LysP*, *eyg*, *l(3)82Fd*, *CecC*, *fkh*, *toe*, *net*, *sage*, *GalNAc-T2*, *PH4alphaSG2*, *Tie*, *P24-1*, *Gmap*, *FucTA*, *cry*, *Hsp70Bbb*, *pgant5*, *D*, *Awh* and *GlcAT-P*. Only one GO inferred novel transport gene, *CG30394*, was found to be encoding a putative amino acid transporter. But, the other predominant expression patterns include the transcription factors related to development, antimicrobial peptides related to innate immunity, and genes related to proteolysis.

The *forkhead (fkh)* is the closest homologue of human *FOXOA* transcription factor gene, and a well-known developmental gene required for correct development of the endoderm and ectoderm derived parts of the epithelia including guts, salivary glands, and tubules.

The ecdysone induced transcriptional regulation of programmed cell death is widely studied in *Drosophila* salivary glands, in that the *fkh* is down regulated when the cell death activators reaper and hid need to be optimally expressed for the ecdysone prepupal pulse to induce the destruction of the obsolete larval tissues (Baehrecke, 2005; Thummel, 2007).

In addition to cell death, *fkh* controls many interrelated transcriptional networks that regulate autophagy, phospholipid metabolism, hormone controlled signaling pathways, glucose and fatty acid metabolism (Liu and Lehmann, 2008a). The *fkh* target genes faithfully found in our analysis in the list of larval and adult commonly enriched genes which include *sage*, *senseless* encode transcription factors and *prolyl-4-hydroxylase*, *PH4asg2*, and are involved in the modification of secreted proteins. Developmentally, the cooperative control of *fkh* and *sage* directly regulates the expression of *PH4asg2* and *sage* and indirectly regulates the expression of *PH4asg1* to regulate tubule lumen size to eventually accelerate

the secretion (Abrams et al., 2006). The other fkh targets found in the larvae include *sgs*, and *ng* in our direct comparisons of adult against larval tissue transcriptome (Table 4-7).

The proteins that participate in O-Glycosylation, encoded by *GalNAc-T2* and *pgant5* were also enriched. These proteins transfer N-Acetylgalactosamine residue from UDP-GalNAc to the hydroxyl group of serine or threonine residues of the target proteins and are highly relevant to the secretory functions of the salivary glands. The *Eyg* (*eye gone*) and *twin of eyegone* (*toe*) show high specificity of expression in both larval and adult salivary glands, and the adult eye. They have been shown to be involved in the compound eye morphogenesis, but not known for any salivary gland-related functions. Malpighian Tubules

#### 4.2.2.2 Malpighian Tubules

The top 50 adult (but not larval) tubule enriched probesets represent 16 known, 16 and 16 novel genes with and without GO terms respectively; including 2 unannotated probesets (Table 4-2A). The known genes include *Hsp70Aa*, *Hsp70Bbb*, *alpha-Est6*, *Tsp42Eq*, *p38c*, *Jhl-26*, *PhKgamma*, *Hsp70Bc*, *Kua*, *Cyp6a2*, *mthl14*, *l(2)08717*, *Oscillin*, *fusl*, *Fmo-1*, and *comm3*.

The novel GO: Transport genes include *CG14694*, *CG10226*, *CG17664* and *CG7720*. The *CG14694* has an OMIM entry: SLC19A3, a member of micronutrient transporter family, that transport reduced folate and has been implicated in biotin-responsive basal ganglia disease. It was first diagnosed in patients with consanguineous parents with origins from Saudi, Syria and Yemen. The *CG10226* belongs to an ABC transporter, ABCA4 in humans, with an OMIM entry: age related macular degeneration.

The *CG17664* has an OMIM entry: AQP3, a water channel implicated in blood group GIL. The *CG7720* encodes a putative SLC family transporter, a sodium-iodide symporter in humans, with an OMIM entry: SLC5A5, implicated in congenital hypothyroidism. The human counterpart plays a key role in the plasma membranes of the lactating breast and other tissues in I<sup>-</sup> uptake, the first step in the biosynthesis of iodine-containing thyroid hormones (Dohan et al., 2007).

The top 50 larval (but not adult) Malpighian tubule enriched probesets represent 19 known, 16 and 12 novel genes with and without GO terms respectively; including 2 unannotated probesets (Table 4-2B). The known genes include *Btd*, *Jhe*, *Jhedup*, *rdgc*, *TwdlG*, *SelR*, *bw*, *csul*, *Or35a*, *cad*, *ome*, *Pvf1*, *AttD*, *l(3)82Fd*, *E23*, *BG642312*, *sprt*, *pyd* and *shn*.

The novel GO: transport genes include *CG10505*, *CG8850*, *CG7888*, *CG11897* and *CG6293*. The *CG10505* has an OMIM entry: PMP70, an ABC transporter associated peroxisomal disorder with Zellweger spectrum. The *CG6293* is included in the family that code permeases that may transport xanthine, uracil and vitamin C according to Pfam (Finn et al., 2010).

The top 50 commonly enriched probesets in both adult and larval tubules represent 9 known, 23 and 14 novel genes with and without GO terms respectively; including an additional unannotated probeset (Table 4-2C). Interestingly, *scarlet* which is highly enriched and only found in tubules, at both larval and adult stages, encodes a protein that participates in the eye pigment biosynthetic process indicating tubule's key role in this function.

*Gp150-like* is highly enriched and has a human ortholog: *aspirin* (*ASPN*) with OMIM entry associated with lumbar disc degeneration/osteoarthritis. *ASPN* belongs to a family of leucine-rich repeat proteins, and is an extracellular matrix component expressed abundantly in the articular cartilage of individuals with osteoarthritis, in the pathogenesis of the disorder (Kizawa et al., 2005). Why this is important in a simple invertebrate like a fly? The functionally distinct initial segment of the fly anterior tubule (Sozen et al., 1997) is a place for mineralised concretions (Wessing et al., 1992). *Gp150-like* found to be highly enriched in the initial segment of the tubule in our previous microarray study (unpublished). This broadens the horizon of an invertebrate tissue as a place to study a gene, important in human pathology, given its genetic and physiological amenability.

The *NaPi-T* is highly enriched in both stages and found to be highly specific to tubules. Other genes enriched include the *Oatp58Da* and *Oatp58Da* which have no human orthologs; *irk3* and *Sr-CIV*, encoding a protein product with a STAT binding consensi (Kwon et al., 2008), involved in defence response.

**Table 4-2 The top 50 genes enriched in Malpighian tubules.**

(A) Adult Enrichment		(B) Larval Enrichment		(C) Common Enrichment		
Gene Symbol	FCA	Gene Symbol	FCA	Gene Symbol	FCA(at vs awf)	FCA( lft vs wlf)
CG32024	59	CG13312	41	Sr-CIV	49	29
CG32843	57	Btd	34	CG33282	91	43
CG13313	49	Jhe	34	CG15408	68	27
CG17636	46	Jhedup	33	CG8837	85	25
CG32023	42	CG6475	30	CG3285	63	22
CG6602	42	CG3264	25	CG15406	32	20
CG14694	39	CG10505	20	CG18095	85	54
CG4484	34	CG8850	19	CG15279	35	22
CG7144	34	rdgC	18	lrk3	50	35
CG33012	29	CG14958	18	CG34043	53	40
CG9444	28	CG13516	18	Oatp58Da	57	47
CG10226	27	CG13836	18	Oatp58Db/gb	61	30
CG7992	27	CG32626	16	CG3270	45	21
CG10170	25	rdgC	15	NaPi-T	78	27
CG7881	23	CG17646	14	CG13905	75	35
CG13309	23	CG14949	13	CG32195	43	22
Hsp70Aa/b	23	CG14963	13	st	98	24
CG13656	22	CG3303	12	CG10006	45	30
CG17664	22	TwdlG	11	CG14606	62	40
CG9629	22	CG7888	11	CG3014	42	41
CG5431	22	CG15771	10	CG5361	58	25
Hsp70Bbb	22	SelR	10	CG6465	52	22
1638611_at	21	bw	10	Ugt86Dd	29	21
CG33258	20	1631349_s_at	10	CG14857	22	21
alpha-Est6	20	csul	10	CG17751	84	36
Tsp42Eq	20	Or35a	10	CG16727	94	21
p38c	20	cad	10	CG11659	150	45
CG5849	20	CG9062	9	CG5697	40	27
CG1315	20	CG14856	9	CG6733	26	20
Jhl-26	19	CG6225	9	CG17110	61	30
CG8079	19	1638280_at	9	CG31106	48	25
Phkgamma	18	ome	8	CG10553	24	20
Hsp70Bc	18	CG34198	8	CG31097	46	32
CG7720	18	Pvf1	8	CG31380	48	23
CG15706	18	AttD	8	CG42235	62	33
Kua	17	CG11897	8	CG42235	74	61
Cyp6a2	17	CG32234	8	CG42235	69	52
CG30411	17	CG4586	8	CG42235	60	23
CG31562	17	l(3)82Fd	8	CG42235	66	23
CG13604	17	E23	7	CG2187	33	28
mthl14	17	BG642312	7	CG11889	26	33
l(2)08717	17	CG6364	7	CG3690	62	33
CG6891	17	CG6293	7	CG2680	29	26
CG13827	17	sprt	7	CG15221	39	40
1639729_s_at	16	CG30375	7	CG8028	78	46
Oscillin	16	pyd	7	CG14195	31	21
CG42329	16	CG10301	7	CG18814	19	31
fusl	16	CG7431	7	1631526_s_at	19	23
Fmo-1	16	shn	7	Ugt35b	20	37
comm3	16	CG9328	7	Cyp6a8	31	20

*Sr-CIV* has been shown to be upregulated in *Nurf* mutants (that show inflammatory syndrome) in which NURF was implicated as a regulator of a large set of JAK/STAT target genes (Kwon et al., 2008). The tubule senses the bacteria and may constitute a cell-autonomous system of immunity (McGettigan et al., 2005). *Sr-CIV* has a putative concanavalin A-like lectin/glucanase domain.

The lectins and glucanases are found in all orders of life and show the common property of reversibly binding to specific complex carbohydrates. Some catalyse beta-glucans found in microorganisms (Hahn et al., 1995). This observation reinforces the idea that tubules may act as an independent system in potentiating innate immune responses to the pathogenic bacteria within their milieu.

Other genes that did not show up in the top list, but did in the 10-fold or over upregulated lists include the famous *xanthine dehydrogenase* (or *rosy*), *white*, *urate oxidase* (*uro*). In that, *rosy* and *white* are well characterised classical mutants. The localisation of *rosy* and *uro* have been established to be peroxisomal (Beard and Holtzman, 1987; Wallrath et al., 1990). Mutations in *rosy* and *white* cause eye colour phenotypes, thus are important in the associated pigment biosynthesis and transport processes (Beyenbach et al., 2010b).

The *rosy* gene encodes a bifunctional oxidoreductase that can act as a dehydrogenase or an oxidase depending on the substrate and acceptor availability (Parks and Granger, 1986; Stirpe and Della Corte, 1969). It catalyses the conversion of hypoxanthine to xanthine, and further to uric acid (Beard and Holtzman, 1987; Reaume et al., 1989). Most interestingly, the *Drosophila rosy* mutants recapitulate the human inborn error of metabolism, xanthinuria type I, caused by mutations in the human homolog of *rosy* (Beyenbach et al., 2010b). In conjunction, the studies using sedimentation gradient centrifugation, established that *rosy*-localised peroxisomal size, shape, and centrifugal behaviour are similar to peroxisomes of vertebrates (Beard and Holtzman, 1987; Parks and Granger, 1986).

*Uro* encodes a functional urate oxidase that converts uric acid to 5-hydroxyisourate which eventually is converted to allantoin. In humans and many primates uric acid is the end product of the catabolism of purines because they have a non-functional gene (Wu et al., 1989).

The peroxisomal localisation of *rosy* is interesting which could regulate the downstream effectors of the peroxisomal resident enzymes in the purine degradation pathway.

For example, by the end of embryogenesis, distal tubule cells transport the organic solutes of urate (urates) into the lumen, where they precipitate as uric acid crystals but not until they hatch they are able to clear it by fluid transport process (Beyenbach et al., 2010a). As insects go through successive developmental stages from larvae to adult, the excretory load increases on the organism. For this task, Malpighian tubules have to rapidly adapt, as they are largely established during embryogenesis unlike other epithelial tissues (Beyenbach et al., 2010a; Skaer, 1993). Nevertheless, peroxisomes in the tubules play essential roles in the transport and excretory mechanisms of tubules, at both adult and larval stages.

#### 4.2.2.3 Midgut

The top 50 probesets in the adult (but not larval) represent 8 known, 23 and 16 genes with and without GO terms respectively (Table 4-3A). The known genes include *lectin-24A*, *pcl*, *Vha100-4*, *ninaD*, *Lvpl*, *Cry*, *Ugt86Dc* and *CG3841 (nmo)*. The two genes that encode *nmo*, a protein that participates in the planar cell polarity, are *CG7892* and *CG3841*. Interestingly *CG7892* shows ubiquitous expression, while the *CG3841* is specifically expressed in the midgut and shows some expression in testis.

The novel GO: Transport genes include *CG17930*, *CG6901*, *CG17929*, *CG33514*, *CG9981*, *CG9903*, *CG31636* and *CG33514*. According to the Interpro protein signature database (Hunter et al., 2009), both the protein products of *CG17930* and *CG6901* are classified into the general substrate transporter family, which may transport sugars according to the Pfam (Finn et al., 2010). The Affymetrix® chip has two independent probesets for detecting *CG33514*, and they detect similar tissue-specific expression patterns. The Interpro suggests that the putative *CG33514* protein product has several cellular retinaldehyde-binding and alpha-tocopherol domains. The cellular retinaldehyde-binding domains function in the phospholipid metabolism and transport. The alpha-tocopherol domain shows stereoselectivity and binds to  $\alpha$ -Tocopherol, which is a form of vitamin E.

The CG9981 is classified as GO: phospholipid transporter which has an OMIM entry: autosomal recessive deafness, associated with *P*-type ATPase, the plasma membrane  $\text{Ca}^{2+}$ -transporting ATPase (PMCA): ATP2B2. The CG9903 is a GO: sodium transporter. The Pfam suggests that it may belong to  $\text{Na}^+$ /bile acid co-transporters that function in the liver in humans in the uptake of bile acids from portal blood plasma. In another family member ARC3 from *Saccharomyces cerevisiae*, CG9903 was identified as a putative transmembrane protein, involved in the resistance to arsenic compounds. The CG31636 is related to OMIM entry: ataxia with isolated vitamin E deficiency that is explained in the later sections.

Other genes enriched include the ones that participate in proteolysis, carbohydrate, and lipid metabolic process. Only 19 probesets are enriched at least 5-fold or higher in larval (but not adult) that represent 5 known 5 and 7 novel genes with and without GO terms respectively; including two additional unannotated probesets (Table 4-3B).

Only 46 probesets enriched at least 5-fold in both adult and larvae representing 17 known, 12 and 16 novel genes with and without GO terms respectively; including two additional unannotated probesets (Table 4-3C). The novel GO: Transport genes include CG32054, CG32053 and CG7912.

Table 4-3 The top 50 genes enriched in midgut.

(A) Adult Enrichment		(B) Larvae Enrichment		(C) Common Enrichment		
Gene Symbol	FCA	Gene Symbol	FCA	Gene Symbol	FCA (amg vs awf)	FCA (lfmg vs wlf)
CG15263	137	CG7248	22	CG10659	55	7
CG31446	70	1629230_at	16	CG6277	44	5
CG34040	69	CG12951	11	NPC1b	33	5
CG5770	55	mirr	10	Ugt86Dh	31	5
CG34040	50	Yp1	9	Muc68E	31	11
CG34316	42	1638967_at	7	CG32054	29	9
CG17930	42	CG18606	7	1635270_at	27	5
CG6901	38	CG5541	7	CG33346	26	7
CG42335	33	CG7589	6	Cyp309a1	24	5
CG3739	30	CG14204	6	CG31720	23	5
lectin-24A	30	grn	5	exex	22	11
CG3934	29	Epac	5	CG13658	21	6
Pcl	29	CG4991	5	CG15170	20	7
CG9465	29	CG9896	5	Try29F	20	7
Vha100-4	28	CG18628	5	CG7381	19	5
CG7025	27	nimC3	5	Tk	18	5
CG5724	27	CG15816	5	Myo28B1	18	7
CG16997	27	CG33272	5	Myo28B1	18	6
ninaD	26	CG7720	5	CG8690	17	8
CG17929	26			CG16965	17	7
CG31148	26			CG31259	16	6
CG16732	26			CG12194	16	6
CG14500	26			CG17167	16	7
CG8093	26			Amyrel	16	10
CG18748	26			CG18635	16	5
LvpL	26			CG30360	15	8
CG34005	26			CG11318	15	7
CG30272	25			CG9555	15	8
CG1946	25			CG32053	15	8
CG15533	25			sens-2	13	6
CG33514	24			1638487_at	12	6
CG34236	24			CG18744	12	5
CG34005	24			Takl1	12	5
CG2772	24			lab	11	7
CG9981	24			CG14219	11	8
CG18577	24			Cyp12d1-p	10	9
Cry	23			CG7912	10	6
Ugt86Dc	23			CG12780	10	6
CG32483	22			CG32843	10	6
CG9903	22			CG4363	10	6
CG8693	22			Cyp6a14	9	7
CG31636	22			CG33337	9	22
CG9826	22			Cyp9f3Psi	9	6
CG33514	22			CG42348	9	6
CG12766	22			LvpH	6	6
CG11909	21			CG7408	5	6
Nmo	21					
CG15423	21					
CG18480	21					
CG11149	21					

#### 4.2.2.4 Hindgut

The top 50 probesets in the adult (but not larval) hindgut represent 4 known, 18 and 24 novel genes with and without any GO terms respectively; including one additional unannotated probeset (Table 4-4A). The known genes include *Cpr62Ba* (*Cuticular protein related*), *yellow-b*, *NepYr*, and *TwdIT*.

The novel GO: Transport genes include *CG42269*, *CG10026*, *CG3823*, *CG7888*, and *CG33970*. The *CG42269* is only expressed in the hindgut; according to OMIM, it is a *Drosophila* homolog of human *SLC22A12* which encodes URAT1, a urate-anion exchanger, associated with renal hypouricemia. The URAT1 shows luminal plasma membrane localisation in the proximal tubule epithelium of the human kidney (Enomoto et al., 2002). Thus, *CG42269* may be a probable fly candidate in the adult hindgut luminal reabsorption of the urate, to counter excessive excretion. Both the *CG10026* and *CG3823* are highly abundant in hindgut; other tissues show similar enrichment including larval fatbody (functionally analogous to human liver) and crop. They have a single OMIM entry, the tocopherol transfer protein alpha (TTPA) implicated in ataxia with isolated vitamin E deficiency. The northern blot analysis of several human tissues revealed that it is expressed only in the liver (Arita et al., 1995). Although there is a mouse model for TTPA (Terasawa et al., 2000), and a genome wide study comparing the gene expression in heart tissue of TTPA null mice with that of wild-type mice (Vasu et al., 2007), the *Drosophila* homologs' adult hindgut specific expression pattern suggest hindgut's role in the reabsorption of the vitamin E. The rest of the two genes including *CG7888* and *CG33970* are inferred to be involved in amino acid transmembrane transport and transport respectively. It is interesting to note from the above observations with respect to hindgut's role in the reabsorption and homeostasis of useful metabolic compounds.

**Table 4-4 The top 50 genes enriched in hindgut.**

(A) Adult Enrichment		(B) Larval Enrichment		(C) Common Enrichment		
Gene Symbol	FCA	Gene Symbol	FCA	Gene Symbol	FCA(ahg vs awf)	FC(lfng vs wlf)
CG9993	171	CG7906	63	CG1143	103	14
CG34462	88	CG9021	54	CG13177	100	21
CG17999	79	CG15615	33	CG15870	86	33
CG32234	68	CG2157	31	Cyp49a1	80	21
CG34109	67	CG9269	27	CG4459	76	28
CG34109	63	Aret	26	CG3604	76	15
CG6867	59	CG9702	25	CG14949	75	15
CG42269	47	Cpr49Ae	24	CG32564	73	12
CG4726	43	CG15394	20	CG7365	71	28
1639350_at	40	Ggamma30A	20	byn	70	28
Cpr62Ba	39	Esp	19	Cyp301a1	59	20
CG3332	37	CG15212	19	CG13215	53	17
CG13618	36	CG15890	17	comm3	52	19
CG5639	34	CG13748	17	CG31530	51	55
CG32234	32	CG13028	17	Fsh	48	25
yellow-b	32	CG14516	17	Ahcy89E	48	11
CG9427	32	Osi6	17	Pkg21D	44	16
NepYr	31	Aret	17	CG4623	44	15
CG7422	31	CG8303	15	CG14872	39	25
CG18417	30	Ork1	15	CG8008	36	11
TwdlT	29	Retn	14	CG31176	32	19
CG31810	29	CG13082	14	ine	31	13
CG4660	28	Rpr	14	swi2	31	19
CG11550	28	SP71	14	1629538_s_at	31	17
CG40486	28	CG15213	13	CG5404	30	21
CG32850	27	CG14826	13	CG31100	30	15
CG12990	27	CG9196	13	CG14275	29	23
CG12995	26	CG15213	12	lrk2	29	15
CG6074	26	CG9747	12	CS-2	25	11
CG32234	26	Tup	12	fkh	25	10
CG30047	25	Doc2	12	Rh50	24	18
CG32284	24	CG13313	11	CG4462	23	12
CG31809	24	CG7802	11	CG12826	22	16
CG10200	24	CG15201	11	CG6836	22	17
CG34109	23	CG13228	10	CG12655	21	14
CG14830	23	CG11147	10	1638195_at	21	34
CG10026	23	CG5002	10	CG13616	19	11
CG15088	22	Shn	10	CG32397	18	15
CG15822	21	Pip	10	CG16820	18	15
CG3823	21	Cpr49Ag	9	Cyp4aa1	17	20
CG7888	21	CG5910	9	1630614_s_at	16	15
CG13024	20	CG32645	8	CG18473	15	11
CG33012	20	l(2)08717	8	CG31900	13	12
CG32850	20	CG30387	8	CG33143	13	14
CG17190	20	Tadr	8	CG5070	13	26
CG42246	20	Tadr	8	CG10702	11	19
CG5928	20	CG14720	8	RluA-1	10	23
CG2650	19	CG13217	8	CG31676	10	17
CG33970	18	AdoR	8	D	10	16
CG14253	18	CG30334	8	otp	9	11

The top 50 probesets in the larval (but not adult) hindgut represents 16 known, 8 and 22 novel genes with and without any GO terms (Table 4-4B). The known genes include *aret*, *Cpr49Ae*, *Ggamma30A*, *Esp*, *Osi6*, *Ork1*, *retn*, *rpr*, *SP71*, *tup*, *Doc2*, *shn*, *pip*, *Cpr49Ag*, *l(2)08717*, *tadr* and *AdoR*. The GO inferred novel transport genes include *CG9702*, *CG11147* and *CG5002*. All the three novel transport genes have OMIM entries.

The *CG9702* and *CG5002* belong to human SLC transporter, *SLC26A4*; *CG11147* belongs to the ABC family transporter, *ABCC11*.

The top 50 enriched genes in both adult and larval hindgut represent 16 known, 11 and 20 novel genes with and without GO terms; including an additional 3 unannotated probesets (Table 4-4C). The known genes include *Cyp49a1*, *byn*, *comm3*, *Fsh*, *Ahcy89E*, *Pkg21D*, *ine*, *swi2*, *Irk2*, *CS-2*, *fkh*, *Rh50*, *Cyp4aa1*, *RluA1*, *D*, and *otp*. The *byn* is expressed in the hindgut proliferation zone (HPZ) where the stem cells are able to self-renew and produce epithelial cells to replace the aged cells for the proper function (Takashima et al., 2008).

#### 4.2.2.5 Functional compartmentalisation of the epithelia

At least 5-fold enriched gene lists for each epithelium were used to classify the function according to GO terms. The most significantly enriched ( $P \leq 0.001$ ) ontology terms were sorted by their adjusted *P*-value, the lowest being the most significant and first in the list (Table 4-5). This analysis was only shown for adult epithelia as larval epithelia showed similar functional compartmentalisation. The most significantly enriched GO terms in the salivary glands include Golgi and vesicle mediated processes. These terms reiterate the secretory function of the salivary glands. The tubule enriched GO terms include active transmembrane transporter activity, membrane transport, anion and cation transporter activity and oxidoreductase activity. The mitochondria play a pivotal role in the ATP-dependent processes. Accordingly, they are abundant in the apical microvilli of the tubule, where the epithelial V-ATPases drives fluid transport.

The midgut enriched GO terms include catalytic activity, peptidase and protease activity hydrolase and lipase activity, thus suggesting midgut in the nutrient metabolism. The hindgut enriched GO terms are mostly similar to tubule GO terms and they include active and secondary active transmembrane transporter activity and metal ion transport. This data therefore support the general functions of the tubule and hindgut in the osmoregulatory and excretory functions. In addition, this analysis shows the places to study the functions of a novel gene.

**Table 4-5 GO functional classification of epithelial signatures. The significantly (FDR≤0.001) enriched GO terms are arranged according to their *P*-value, the lowest being the most significant. For each tissue, besides the GO term, % count, percentage number of genes present in the analysis is shown.**

Salivary glands		Malpighian tubules		Midgut		Hindgut	
GO Term	% Count	GO Term	% Count	GO Term	% Count	GO Term	% Count
RCAF complex	15.23	transmembrane transporter activity	22.88	catalytic activity	88.71	secondary active transmembrane transporter activity	8.43
chromatin remodeling complex	15.23	secondary active transmembrane transporter activity	10.03	hydrolase activity	54.84	membrane	78.65
Golgi apparatus	18.54	transmembrane transport	22.88	serine-type peptidase activity	16.13	membrane part	54.49
polytene chromosome	17.22	transporter activity	27.27	serine hydrolase activity	16.13	transporter activity	23.6
Golgi apparatus part	13.25	active transmembrane transporter activity	12.85	peptidase activity	25.48	active transmembrane transporter activity	8.43
chromatin assembly	16.56	substrate-specific transmembrane transporter activity	14.42	proteolysis	26.45	transmembrane transporter activity	10.67
nucleosome	15.23	substrate-specific transporter activity	14.42	peptidase activity, acting on L-amino acid peptides	20	transmembrane transport	10.67
nucleosome assembly	15.23	ion transmembrane transporter activity	12.54	serine-type endopeptidase activity	14.19	intrinsic to membrane	54.49
chromatin assembly or disassembly	16.56	ion transmembrane transport	12.54	monooxygenase activity	8.06	monooxygenase activity	10.11
protein-DNA complex	15.23	monooxygenase activity	9.4	metabolic process	93.23	integral to membrane	53.93
DNA packaging	16.56	metal ion transmembrane transporter activity	5.33	heme binding	8.71	substrate-specific transmembrane transporter activity	8.43
protein-DNA complex assembly	15.23	ion transport	17.55	tetrapyrrole binding	8.71	ion transmembrane transporter activity	7.87
protein-DNA complex subunit organization	15.23	anion transmembrane transporter activity	7.21	hydrolase activity, hydrolyzing O-glycosyl compounds	5.48	cation transmembrane transporter activity	7.87
nucleosome organization	15.23	anion transport	7.21	electron carrier activity	10.65	ion transmembrane transport	7.87
DNA conformation change	16.56	microsome	7.52	microsome	6.45	microsome	8.99
cytoplasmic membrane-bounded vesicle	6.62	vesicular fraction	7.52	vesicular fraction	6.45	vesicular fraction	8.99
Golgi membrane	10.6	electron carrier activity	11.91	hydrolase activity, acting on glycosyl bonds	7.1	metal ion transport	7.3
chromatin	16.56	solute:cation symporter activity	3.76	triglyceride lipase activity	4.19	membrane fraction	9.55
membrane-bounded vesicle	6.62	membrane	54.55	endopeptidase activity	14.52	substrate-specific transporter activity	8.43
Golgi vesicle transport	2.65	oxidation reduction	22.88	glucuronosyltransferase activity	3.87	metal ion transmembrane transporter activity	3.93

### 4.2.3 Adult-specific functions

To obtain common signatures of adult-specific functions of the epithelial tissues, the epithelial transcriptomes were compared against the adult whole fly. An ‘epithelial signature’ for adult and larval epithelia separately and combined for both was obtained. The number of commonly enriched genes across adult, larval and both epithelia includes 309 and 327 and 106 respectively (Figure 4-4). Out of 106 genes that show similar expression pattern across the epithelia, 66 were novel and the other 40 were known genes. The list of known genes is represented in Table 4-6.

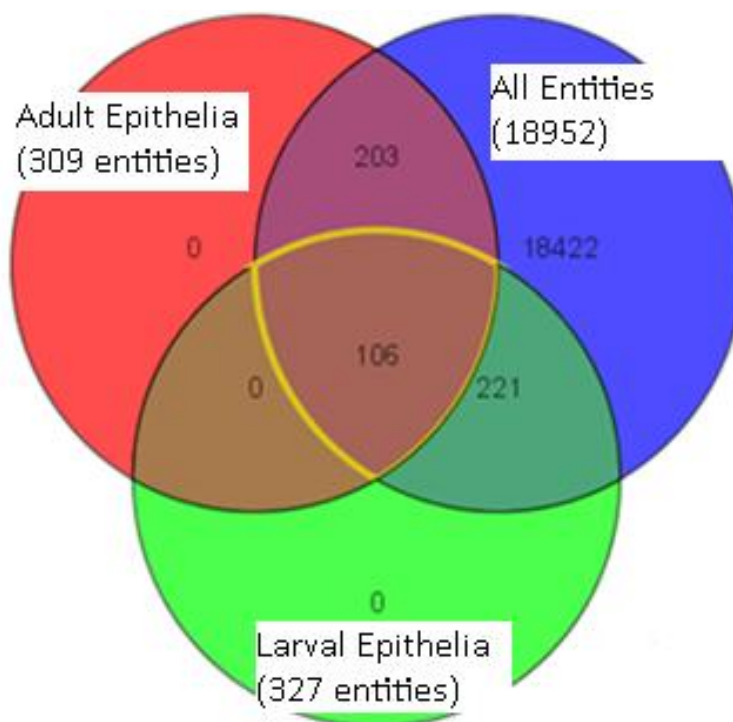


**Figure 4-4** The commonly enriched genes in both adult and larval epithelia in the adult context. An enriched list for each epithelium was obtained by comparing them against the whole fly. Then at least 2-fold enriched genes were used to find the common genes among the epithelia. First a signature for both larval and adult epithelia was obtained separately, and then a final epithelial signature for both was obtained.

A quick glance at the commonly enriched genes across the epithelia shows the famous epithelial genes encoding epithelial transcription factors (bowl); a water channel (Drip); an epithelial hormone receptor (Hr39), a potassium channel (KCNQ) and equally, all other genes, that have been implicated in epithelial tissue development or function.

**Table 4-6 The known genes that are consistently enriched (at least 2-fold) across epithelia. FDR≤0.05.**

Gene Symbol	Transcript ID	Fold change over adult whole fly							
		AHG	AMG	ASG	AMT	LFHG	LFMG	LFSG	LFMT
Bowl	CG10021-RB	7.06	3.23	14.84	10.8	5.5	5.57	10.92	11.49
bru-2	CG31761-RC	5.9	3.05	5.57	8.76	8.25	2.93	2.91	6.98
Cdep	CG31536-RA	3.69	4.86	6.04	4.87	4.89	4.35	4.01	5.87
CHKov1	CG10618-RA	3.71	3.92	18.42	3.67	5.13	5.15	7.53	3.01
Cyp12e1	CG14680-RA	2.78	4.43	2.82	5.28	5.47	9.08	10.91	12.12
Cyp12e1	CG14680-RA	4.43	4.88	2.83	5.07	6.36	8.89	12.68	20.28
Cyp9c1	CG3616-RA	7.29	3.99	3.76	8.52	16.9	9.12	7.07	10.13
Drip	CG9023-RA	5.57	3.79	63.1	8.19	14.55	3.67	5.98	10.03
Eap	CG32099-RA	2	2.29	2.09	6.72	3.01	2.11	4.32	5.57
Edem2	CG5682-RA	2.34	6.05	2.79	2.07	3.38	3.78	6.91	3.14
G-sa60A	CG2835-RC	3.15	2.13	3.31	3.7	4.52	2.27	2.92	3.24
Hr39	CG8676-RB	4.75	3.68	10.28	9.89	8.27	7.46	7.47	12.98
Jim	CG11352-RC	3.54	2.75	2.35	7.03	5.07	2.79	6.81	4.06
KCNQ	CG33135-RA	7.59	12.35	2.11	10.95	40.65	6.65	2.64	9.18
Kr-h1	CG18783-RA	4.27	2.53	7.86	7.66	2.12	2.08	5.11	2.29
Kst	CG12008-RA	3.83	6.21	2.3	2.67	4.17	4.33	2.19	4.63
l(1)G0168	CG33206-RA	3.56	2.4	20.46	3.45	4.83	4.02	17.58	6.2
Lola	RH31485	6.94	3.33	5.93	8.67	5.21	2.25	6.71	3.95
Lqf	CG8532-RB	2.28	2.14	2.06	5.86	6.34	4.85	3.01	10.03
Mitf	CG40476-RA	3.98	3.04	5.26	2.81	4.73	3.07	6.73	2.82
Mkk4	CG9738-RA	2.22	2.36	2.26	3.04	2.77	3.02	3.88	3.08
MsP-300	CG31916-RA	4.51	4	2.89	2.99	5.85	7.44	5.34	4.74
mthl3	CG6530-RA	3.58	3.13	2.25	11.25	41.15	17.97	12.66	56.7
mthl4	CG6536-RB	5.61	3.54	3.7	15.62	7.85	4.76	24.77	8.28
mthl4	CG6536-RA	4.79	4.63	2.79	6.42	4.54	4.45	16.94	8.27
Nhe1	CG12178-RA	3.05	2.41	10.53	5.97	2.78	2.91	14.04	4.11
Ome	CG32145-RA	5.54	8.87	8.6	4.18	5.72	7.19	6.21	4.58
p24-2	CG33105-RA	2.02	3.99	10.77	2.05	2.46	3.72	6.6	4.51
Pvr	CG8222-RA	3.74	3.42	13.09	5.78	3.22	2.52	4.94	2.65
Rab6	CG6601-RA	2.77	3.31	4.5	2.17	3.64	3.19	14.64	4.28
Rhp	CG8497-RA	2.44	5.76	3.64	7.71	8.76	5.96	5.35	6.02
Scrib	CG5462-RC	4.34	7.82	5.05	6.27	5.48	9.92	4.26	15.32
Scrib	CG5462-RC	3.37	4.88	3.06	5.9	3.95	6.01	3.34	9.94
Smox	CG2262-RA	3.1	2.38	2.29	12.77	3.92	4.63	2.51	4.76
Snoo	CG7093-RA	3.11	2.75	2.8	5.33	3.98	3.1	5.4	4.92
Su(dx)	CG4244-RD	2.65	4.93	2.14	6.7	3.26	7.84	2.8	4.32
Syb	CG12210-RB	3.88	4.06	2.56	2.48	3.09	4.09	3.01	4.47
Traf-like	CG4394-RC	4.3	14.78	2.89	14.07	6.73	20.61	3	26.33
Troll	CG7981-RB	6.01	3.69	23.66	5.9	4.21	7.51	3.88	5.88
unc-115	CG31332-RC	4.47	3.94	4.9	2.99	4.54	3.62	4.52	3.19

#### 4.2.4 Direct comparison: adult tissue vs. larval tissue

The direct comparison of adult against larval tissue yields the developmental specificity of the gene expression. Adult- and larval-specific enrichments for top 20 genes are presented in Table 4-7. This analysis was performed to obtain larval tissue specific expression over the adult tissue and vice versa. However, this comparison does not show whether the gene that was highly enriched in larval tissue is specific for that tissue. A quick glance at the table shows that adult performs predominantly metabolic functions such as carbohydrate and fatty acid metabolism. Larval tissues abundantly express glue and larval storage proteins that have the roles in pupal adhesion, nutrition and metamorphosis.

These include glue proteins, larval storage proteins, mucins and salivary gland secretion proteins. For example, in insects, larval storage proteins form hexameric complexes and used as storage sites for amino acids for the adult organ development.

**Table 4-7 Direct comparison of adult vs larval epithelial tissue.**

The top 20 genes that show high enrichment are presented in the table for adult and larvae separately over their respective larval or adult tissues. Gene symbol and absolute fold changes (over adult or larval tissue) are shown. FDR≤0.05.

	Hindgut		Midgut		Malpighian Tubules		Salivary glands	
	Gene Symbol	FC	Gene Symbol	FC	Gene Symbol	FC	Gene Symbol	FC
Adult	CG10096 /// CG	696	CG5107	640	CG33258	601	CG33109	1616
	CG12990	435	CG34324	396	CG13309	546	Est-6	932
	nrv3	353	Muc68D	323	CG32024	299	NLaz	698
	CG33258	309	CG14645 /// Rp	309	Tps1	297	CG14934	472
	CG13618	280	CG3906	250	Hex-C	230	CG16826	439
	Yp3	239	CG12374	229	CG32444 /// Ds	159	CG32984	432
	Yp2	227	CG17192	200	cry	150	CG1678	225
	Yp1	191	CG34040	188	CG13313	103	sgl	175
	CG32850	102	CG11878	179	CG5171	91	CG31202	172
	MtnC	96	CG31300	154	CG6602	78	CG11043	158
	cry	94	CG15263	151	CG12493	60	CG6074	156
	CG14661	90	CG8834	144	CG4404	59	CG6327	132
	CG34109-RB	86	CG7542	131	lrk2	55	DNaseII	121
	CG34109-RB	78	CG14125	127	NLaz	50	CG3655	115
	CG7781	75	CG15199	122	kar	46	CG15515	98
	CG3290	74	CG33173	122	Cyp6a17	44	Timp	98
	Obp18a	70	Cht8	111	Cyp6g1	43	CG9396	94
	CG4404	70	CG10477	101	CG3290	41	MtnA	74
	CG34462	70	CG11669	100	CG32023	41	CG7768	74
	CG3823	69	lectin-37Db	88	CG3597	40	Tsp42Eg	72
Larval	CG7299	650	Muc96D	915	CG13312	206	CG7587	1031
	Lsp1gamma	555	Muc96D	597	CG10505 /// Dr	192	ng1	981
	Lsp1beta	554	CG17826	512	Lsp1gamma	192	Sgs3	976
	CG11018 /// Lcp	525	CG34282	493	Lsp1beta	151	Muc68Ca	850
	CG6044 /// Lcp	396	CG5084	375	CG3264	142	Sgs1	839
	Lsp1alpha	389	CG7290	370	Jhe	124	Muc68Ca	792
	CG4367	386	CG31789	314	Lsp1alpha	110	CG12715	707
	CG9021	291	CG6947 /// Dmi	292	CG14949	78	CG17362 /// Cc	668
	Lcp65Ab1 /// Lc	288	obst-J	283	AttD	59	Sgs8	657
	CG9702	226	CG4367	266	Obp99b	57	Sgs7	616
	Lsp2	221	CG14302	260	Lsp2	57	ng1 /// ng2	590
	CG9269	211	CG10154	258	Btd	48	Sgs4-RB	574
	Lcp65Ab2	193	CG33128	201	regucalcin	46	Lsp1gamma	549
	Cpr49Ag	149	CG14300	183	CG6475	45	CG14265-RB	520
	Lcp3	132	CG8664 /// sesE	163	CG8850	43	Pig1-RB	498
	CG17738	131	Muc26B	148	CG15820	42		488
	CG32249	118	CG4362	137	CG3292	42	CG31698	479
	Lcp65Aa	107	CG8629	136	CG10912	37	Eig71Ee	473
	Obp99b	106	CG7715	134	CG11491-RF	34	CG15404	464
	CG11491-RF	104	obst-G	129	Jhedup	33	CG13460	462

### 4.2.5 Ingenuity pathway analysis (IPA)

Using ortholog/paralog mapping in ingenuity pathway analysis knowledgebase (IPA-KB) that holds vertebrate functional information, all genes enriched, at least 2-fold in *Drosophila* epithelial tissues were mapped to their vertebrate counterparts (Materials and Methods). A total of 3241 unique genes from the epithelial signatures, mapped to IPA knowledgebase in which 2092 were eligible for network analysis. The mapped genes (Figure 4-5) were analysed for their potential vertebrate functions/diseases, canonical pathways and molecular network functional classes. Then the functional classes were compared amongst the epithelia to find similarities and differences. The results are described in the order of their significant enrichment in their potential functions (biological and toxicological), canonical pathways and molecular networks.

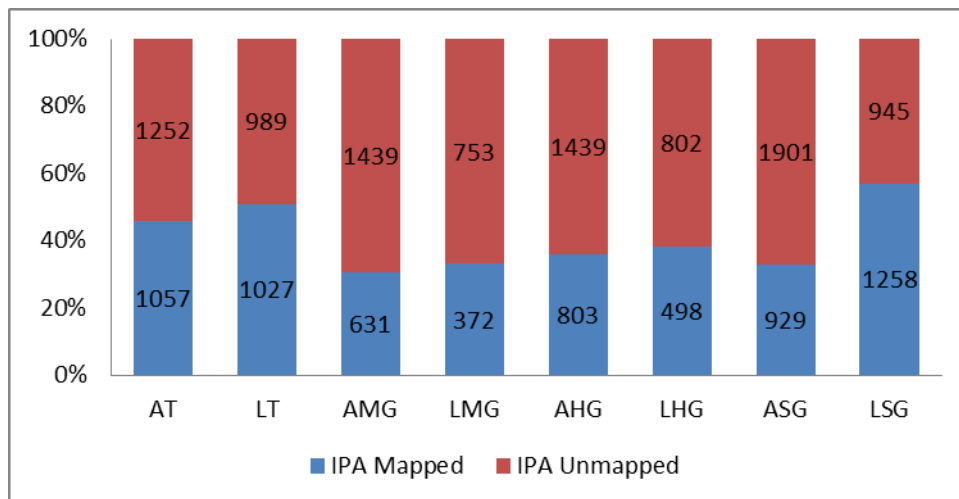


**Figure 4-5 Mammalian ortholog/paralog mapping of *Drosophila* epithelial signatures.** The genes at least 2-fold ( $FDR \leq 0.05$ ) upregulated in each epithelial tissue with respect to their adult or larval whole organism were used to map to vertebrate orthologs (including paralogs) using IPA. The percentage of mapped vs unmapped is presented for each epithelium. Abbreviations: AT (adult tubule), LT (larval tubule), AMG (adult midgut), LMG (larval midgut), AHG (adult hindgut), LHG (larval hindgut), ASG (adult salivary glands) and LSG (larval salivary glands).

#### 4.2.5.1 Biological functions

A wide range of vertebrate biological functional classes were enriched in *Drosophila* epithelia ranging from protein degradation to animal behaviour. The differential enrichment of functional classes among the epithelia was interesting (Figure 4-6).

For example, biological functions including lipid metabolism (Figure 4-6A), small molecule biochemistry (Figure 4-6B), post-translational modifications (Figure 4-6C) and cancer (Figure 4-6E) were almost enriched in all the epithelia for both adult and larvae. However, these functions show more significant enrichment in one tissue over the other. For example, lipid metabolism and small molecule biochemistry functions were more significantly enriched in guts than any tissue (Figure 4-6A). In the same way, post-translational modification functions were more significant in salivary glands and larval tubules than others (Figure 4-6C). Salivary glands do not show significant enrichment for biological functions related to renal system and urological development and function (Figure 4-6D), but they do show enrichment for protein folding function (Figure 4-6F). The cancer related functions are more significantly enriched in hindgut (Figure 4-6E).

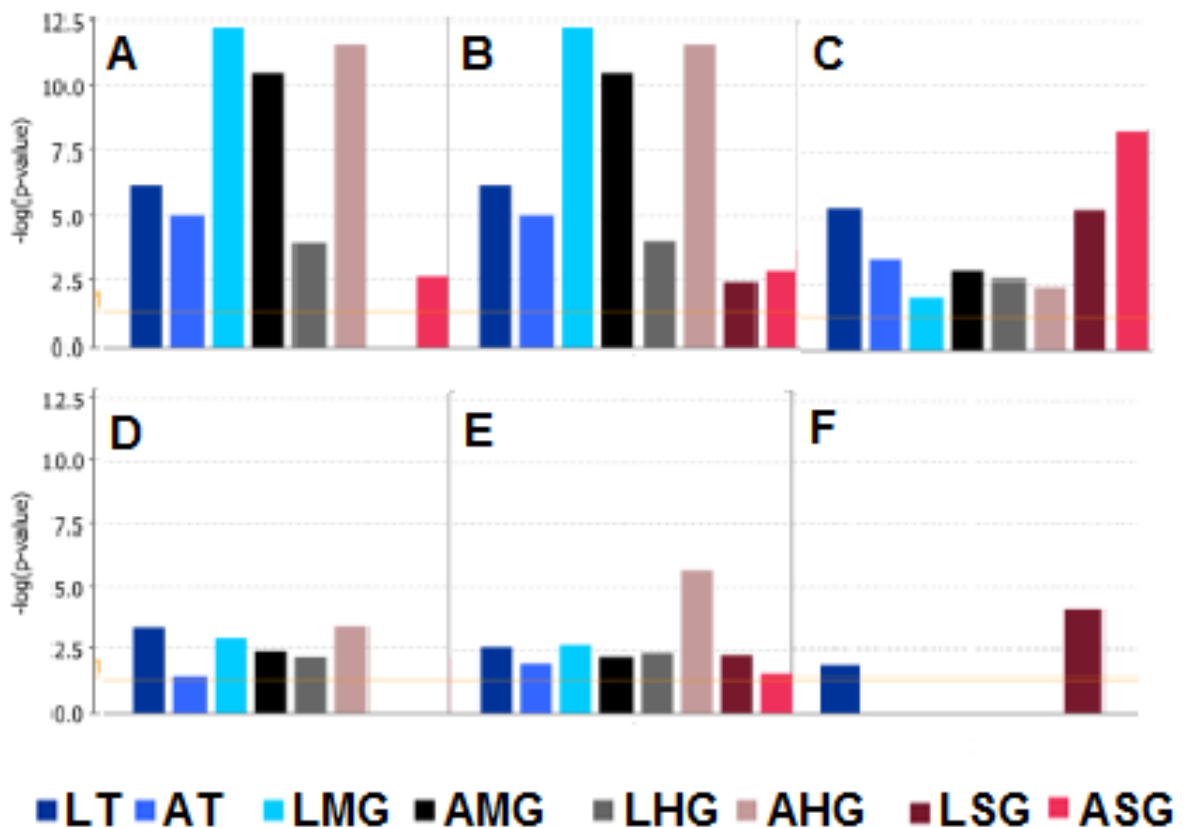


**Figure 4-6** Mammalian biological functions enriched in *Drosophila* epithelia. At least 2-fold enriched genes in each epithelium for both larvae and adult were analysed for their potential vertebrate biological functions using the IPA. Significantly enriched biological functions (above the threshold) include lipid metabolism (A), small molecule biochemistry (B), post-translational modification (C), renal system and urological system development and function (D), cancer (E) and protein folding (F). Biological functions including A, B, C and E are significantly enriched in all the epithelia except that the lipid metabolism functions are not enriched in larval salivary glands. Renal and urological system development and functions (D) enriched in all the epithelia except in salivary glands. Protein folding functions are significantly enriched in larval salivary glands and larval tubules (F). Abbreviations: L = larvae; A = adult; T = tubule; MG = midgut; HG = hindgut; SG = salivary glands.

#### 4.2.5.2 Toxicology functions

The signature genes were scored against known mammalian toxicology related functions. This analysis showed which of the *Drosophila* epithelial tissues could be the most analogous in function to human tissues. The toxicology functions enriched in the epithelia include liver, cardiac and kidney and related toxicology functions. This analysis shows how the *Drosophila* epithelia are functionally analogous to the mammalian tissues. In addition, the analysis indicates the potential overlap in tissue functions. The most significantly enriched toxicology functions in all the tissues include cardiac arteriopathy (Figure 4-7A), cardiac hypertrophy (Figure 4-7B), renal nephritis (Figure 4-7C), liver cholestasis (Figure 4-7D), liver cirrhosis (Figure 4-7E), and liver damage (Figure 4-7F). Strikingly, all these functions are predominantly shared by different tissues. Moreover, enrichment of functions of cardiac- liver- and renal-related in the tissues other than their human counterpart suggests that there may be potential overlap in these functions. It additionally suggests that there is a lack of functional data in the IPA database. However, some functions are exclusive to some tissues. For example, cardiac arteriopathy functions are not enriched in larval midgut and larval salivary glands (Figure 4-7A). Interestingly, hindgut shows significant enrichment for most of the functions (Figure 4-7). Functions related to liver cholestasis (Figure 4-7D) are the most significant in the larval midgut. In the same way, liver damage related functions are the most significant in adult tubules (Figure 4-7F).

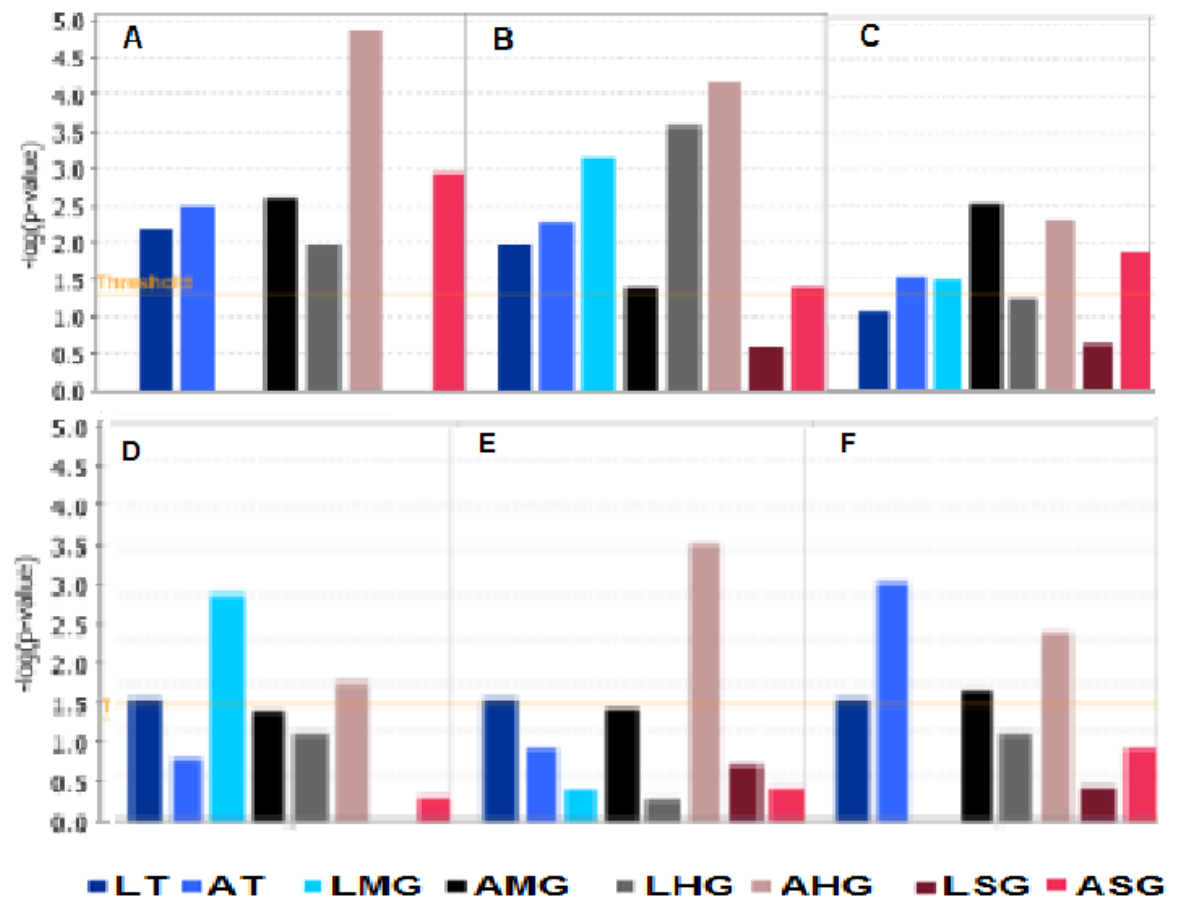


**Figure 4-7 Mammalian toxicology functions enriched in *Drosophila* epithelia.** At least 2-fold enriched genes in each epithelium for both larvae and adult were analysed for their potential vertebrate toxicology functions using the IPA. Significantly enriched functions include (above the threshold) cardiac arteriopathy (A), cardiac hypertrophy (B), renal nephritis (C), liver cholestasis (D), liver cirrhosis (E) and liver damage (F).

### 4.2.5.3 Canonical pathways

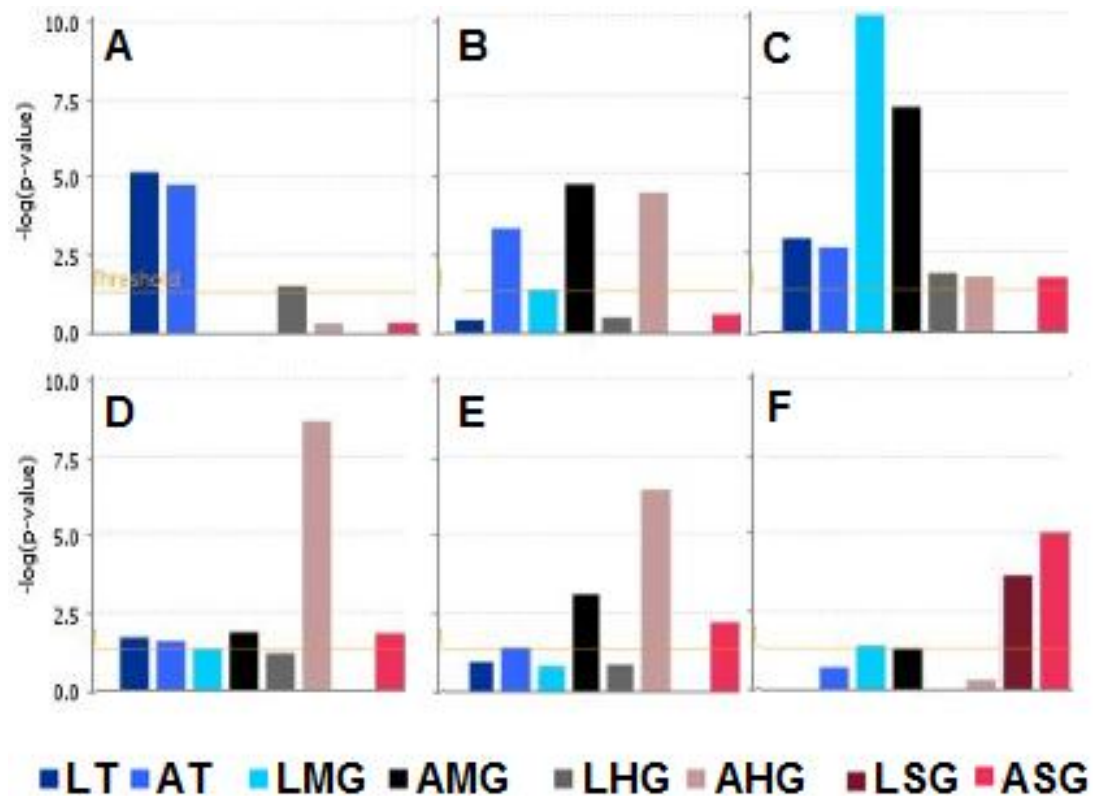


**Figure 4-8 Mammalian canonical pathways enriched in *Drosophila* epithelia.** At least 2-fold enriched genes in each epithelium were analysed for their potential vertebrate canonical pathways using the IPA. Significant pathways (above the threshold) enriched in each epithelia include valine, leucine and isoleucine degradation (A), metabolism of xenobiotics by cytochrome P450 (B), sphingolipid metabolism (C), colorectal cancer metastasis signaling (D), human embryonic stem cell pluripotency (E) and N-Glycan biosynthesis (F). They are respectively enriched in tubules, gut, midgut, hindgut, hindgut and salivary glands. However, some pathways have overlapping enrichments in different tissues, for example, metabolism of xenobiotics by cytochrome P450 (B) and sphingolipid metabolism (C) are enriched both in tubules and midgut.

The significantly enriched canonical pathways show interesting distribution among the epithelia (Figure 4-8). For example, valine, leucine and isoleucine degradation were enriched in tubules with the most significance (Figure 4-8A). All these amino acids are essential and branched chained that produce NADH and FADH<sub>2</sub> for the probable energy demands of the tubule. All the adult epithelia were more significantly enriched for xenobiotic metabolism excluding salivary glands (Figure 4-8B). The sphingolipid metabolism pathway was enriched in adult and larval midgut most significantly (Figure 4-8C). Colorectal cancer metabolism signaling was enriched in the adult hindgut most significantly (Figure 4-8D). The human embryonic stem cell pluripotency was enriched in both adult mid and hindgut (Figure 4-8E). The N-Glycan biosynthesis was enriched in the salivary glands most significantly (Figure 4-8F).

#### 4.2.5.4 Molecular networks

Network analysis was performed to enrich potential biological networks in the epithelia and their (overlapping) epithelial interactions as a group in a global network (Figure 4-9).

Genes are called 'network eligible' only if they have at least one interaction with any other molecule in the IPA (Chapter 2). There were about 94 networks enriched in all the tissues (the top 5 were shown in Table 4-8) with the total number of genes mapping to these networks reaching to 2092 as mentioned earlier. All the networks obtained were presented as an interaction map to show how intricately they interact with each other.

The comparative analysis of the networks yielded important functional insights into these epithelia to their vertebrate cognate tissue functions.

When the top networks were overlaid with their associated functions, at least one interesting network was found for each tissue in terms of their conserved function. For example, the network that is involved in the protein trafficking function was significantly enriched in salivary glands but not in others (Figure 4-10).

Interestingly, the potential biological functions that these molecules implicated include protein (and their fragments) transport, infection of cervical cancer cell lines, cell stage of cervical cancer cell lines and arrest in metaphase of cervical cancer cell lines.

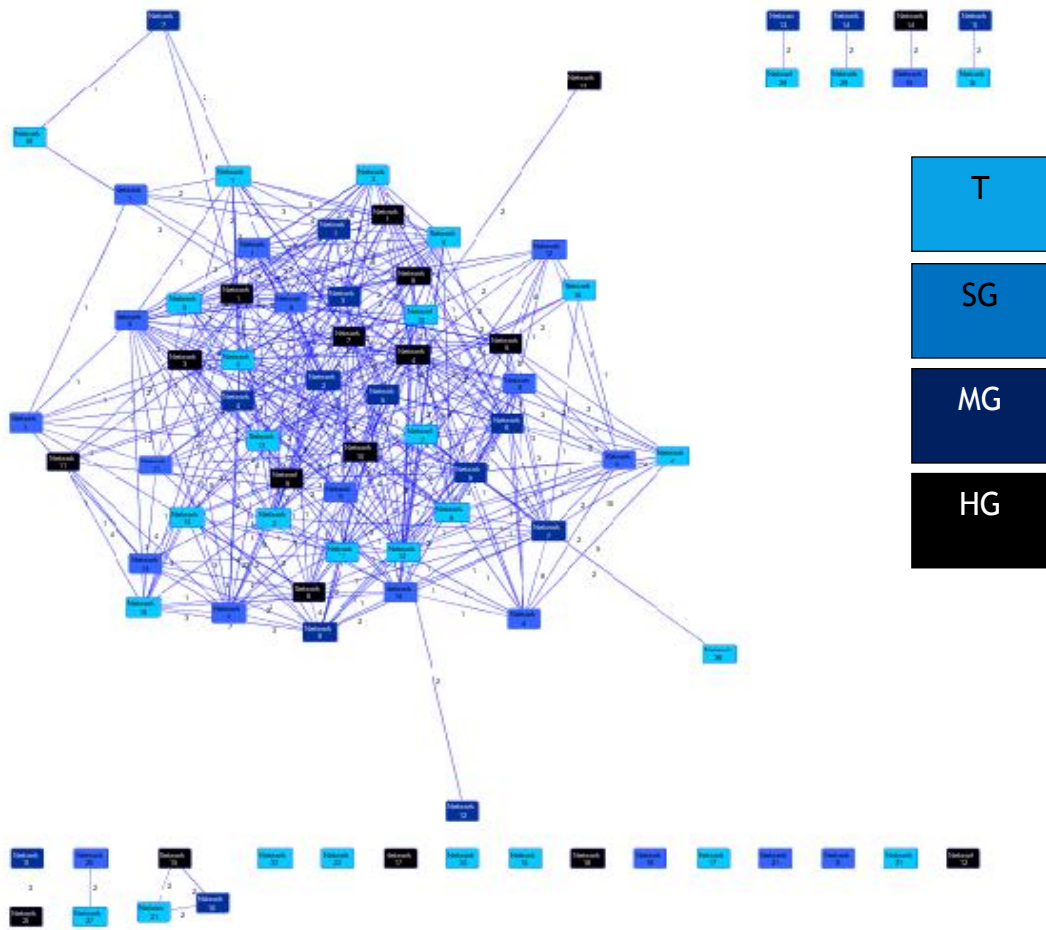


**Figure 4-9 Network analysis of epithelial enriched genes.**

All the genes that were eligible for network analysis in IPA are shown here. Networks are constructed for each tissue individually (colour coded) and are then put together to show how they interact with each other and how many molecules they have in common in their enriched lists. The genes that form separate networks are shown as 'orphan' networks. An example of a network is shown in the below Figure.

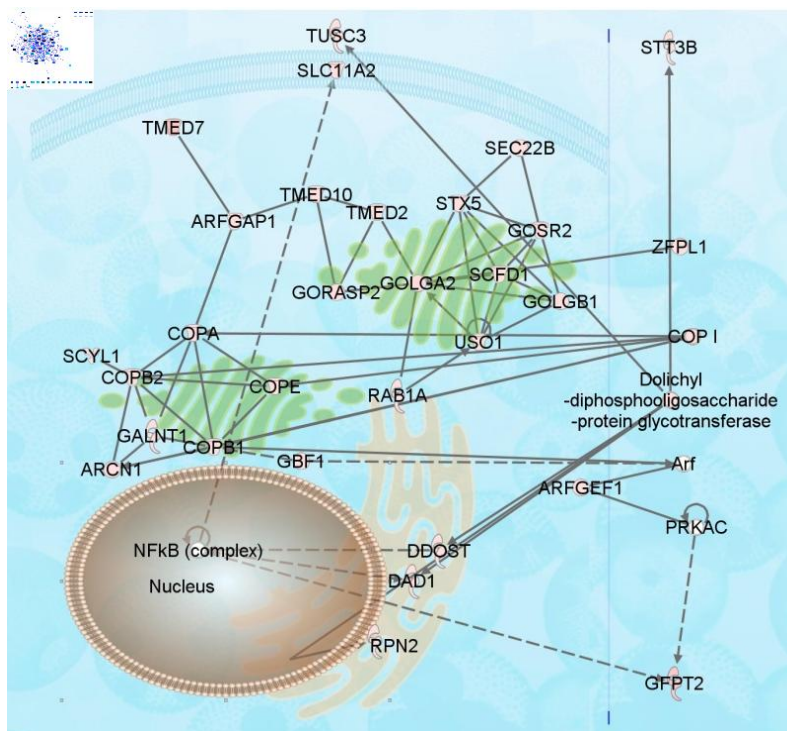


**Figure 4-10 Network analysis of salivary gland enriched, protein trafficking function (pulled from the inset).** The significantly enriched protein trafficking function related genes are presented here in terms of their cellular localisation. Known biological interactions (direct, arrowhead lines; indirect, straight lines) are shown. The genes with unknown localisations are placed right to the vertical line.

**Table 4-8 Top 5 IPA networks for each epithelium.**

The epithelial signature genes were enriched for vertebrate networks. Then they were sorted on the basis of their highest significance for comparative understanding of tissue-specific functions.

		ID-Associated Network Functions-Score			
		Malpighian Tubules	Midgut	Hindgut	Salivary glands
Adult	1 Infectious Disease, Cellular Assembly and Organization, Lipid Metabolism 32	1 Cellular Growth and Proliferation, Cellular Development, Tissue Morphology 34	1 Endocrine System Development and Function, Small Molecule Biochemistry, Lipid Metabolism 32	1 Cardiac Hypertrophy, Cardiovascular Disease, Developmental Disorder 37	
	2 Developmental Disorder, Cell Death, Lipid Metabolism 29	2 Cell Death, Cell-To-Cell Signaling and Interaction, Cell Morphology 25	2 Cell Death, Hematological System Development and Function, Tissue Morphology 31	2 Cellular Assembly and Organization, Cell Death, Cancer 31	
	3 Cellular Movement, Cancer, Cell Morphology 27	3 Cellular Movement, Drug Metabolism, Endocrine System Development and Function 20	3 Cellular Movement, Cell Death, Cellular Development 27	3 Reproductive System Development and Function, Cellular Development, Cellular Growth and Proliferation 29	
	4 Cell Morphology, Cellular Function and Maintenance, Molecular Transport 27	4 Gene Expression, Lipid Metabolism, Molecular Transport 17	4 Cell Morphology, Cellular Movement, Cellular Assembly and Organization 25	4 Cell Signaling, Molecular Transport, Nucleic Acid Metabolism 25	
	5 Cell Death, Lipid Metabolism, Small Molecule Biochemistry 22	Cancer, Renal and Urological Disease, Cell Cycle 17	5 Genetic Disorder, Metabolic Disease, Cellular Assembly and Organization 23	5 Infectious Disease, Cell Death, Cell-To-Cell Signaling and Interaction 25	
Larvae	1 Cancer, Gastrointestinal Disease, Cell Death 37	1 Cellular Movement, Cellular Growth and Proliferation, Gene Expression 38	1 Cell-To-Cell Signaling and Interaction, Cellular Assembly and Organization, Tissue Development 38	1 Cellular Assembly and Organization, Cellular Function and Maintenance, Cell Morphology 37	
	2 Cellular Assembly and Organization, Endocrine System Development and Function,	2 Lipid Metabolism, Small Molecule Biochemistry, Drug Metabolism 26	2 Cellular Movement, Cell Death, Drug Metabolism 33	2 DNA Replication, Recombination, and Repair, Gene Expression, Cellular Assembly and Organization	
	3 Lipid Metabolism, Small Molecule Biochemistry, Cell Morphology 29	3 Molecular Transport, Lipid Metabolism, Small Molecule Biochemistry 19	3 Cell Death, Cellular Growth and Proliferation, Cellular Development 28	3 Gene Expression, RNA Post-Transcriptional Modification, Cell Signaling 35	
	4 Cell Cycle, Cellular Growth and Proliferation, Endocrine System Development and Function 26	4 Cancer, Cell Death, Gene Expression 17	4 Cell Death, Cancer, Neurological Disease 17	4 Gene Expression, Cell Death, Cellular Development 33	
	5 Gene Expression, Cellular Growth and Proliferation, Cell Death 19	5 Cellular Assembly and Organization, Cell Death, Cellular Growth and Proliferation 15	5 Nutritional Disease, Metabolic Disease, Renal and Urological Disease 14	5 Cell Morphology, Cellular Growth and Proliferation, Connective Tissue Development and Function 25	

### 4.3 Discussion

This study investigated epithelial tissues in more detail. As the tissue-specific transcriptomes of the FlyAtlas provide quality datasets (Chintapalli et al., 2007), a comparative analysis of the epithelial transcriptomes was thought to provide insight into similarities and differences in epithelial function. Furthermore, this kind of analysis is useful to generate testable hypothesis, to fill the phenotype gap, and to learn potential functions of the epithelia from each other. The primary PCA analysis of all the FlyAtlas transcriptomes showed less variation of gene expression among the epithelia comparatively with the neuronal and reproductive tissues (Figure 2-4). This clearly suggests that there is a distinction between epithelial tissues and other tissues.

To find the commonality in the epithelia, first, gene expression signatures were obtained for each epithelium for further analysis. For each epithelium, there were hundreds of thousands of genes that showed high specificity of expression or high enrichment (Figure 4-1), and a large fraction of these have no functions (novel genes shown in Section 4.2.2). The gap between the number of genes that are uncharacterized and the number of phenotypes that are available is large which is called the phenotype gap (Dow, 2003; Dow and Davies, 2003). This suggests that a large number of novel genes need to be characterized to fill this gap and try to elaborate our understanding of the genomes. This should be the primary goal of the functional genomics which would be highly achievable, when the genes are studied where they predominantly are expressed, but not where they are first studied (Chintapalli et al., 2007). To this end, epithelial tissues shows the way, as the conservation of function from humans to flies seem to be convincingly high enough to pursue studying functions of novel *Drosophila* genes, where a human disease homologue is present like that analysed here using the OMIM database (Section 4.2.2).

A hierarchical clustering tree showed interesting tissue relationships (Figure 4-2). The larval and adult transcriptomes of each epithelia branched in the same node confirming their identity and the method. The *Drosophila* gut develops as a simple epithelia surrounded by visceral mesoderm (Lengyel, 2002). Although, the origin of the midgut is separate from other ectodermal originated epithelia or primary epithelia, the midgut transcriptome clustered in the middle of the hindgut and the whole fly transcriptome. This may indicate that the transcriptomes may be largely specified by their environmental interaction of particular epithelia.

The comparative analysis of the top 50 most enriched unique and common genes between two developmental stages of an epithelium, show the differing functional demands of different life stages (Section 4.2.2 & 4.2.4). The commonly found genes between larvae and adult epithelia always showed at least two-fold higher enrichment in the adult (for example, compare 2nd column with 3rd of Table 4-1C). A possible explanation for this is that they may not be as much needed in larvae than the adult. The other explanation could be the whole transcriptome of the larvae might be mostly coming from the epithelial tissues.

Obsolete tissues formed through successive developmental stages undergo moderate to extensive remodelling at pupal stages to form adult epithelium. The gene expression changes are huge between larvae and adult epithelia. A high number of genes expressed (at least 5-fold upregulated) show adult-specific enrichment (Figure 4-3).

Developmental origins of epithelial tissues have similarities and differences. They are also specialised in function according to their external and internal milieu. Every epithelium shows a unique gene expression signature markedly due to their morphological specification during development and functional interaction with their internal and external milieu. The epithelial tissues play crucial roles in the organismal homeostasis, to stably maintain the internal environment despite external perturbations. They transport fluid at remarkable rates, secrete proteins and metabolise organic compounds, and protect the animal against external environment. Thus, all these functions are represented in the GO functional compartmentalisation analysis of the epithelia (Table 4-5). The metabolic homeostasis (sugar and lipid) is achieved by the concerted action of epithelial tissues by their variety of functions including transport, secretion, absorption, digestion, and excretion. The conservation of the regulatory mechanisms involved in metabolic homeostasis has been gaining momentum from insights provided by model organisms such as *Drosophila*, in particular (Leopold and Perrimon, 2007). This analysis reinforces the conservation at different levels.

How far do the transcriptomes of both larval and adult tubules tell us about their differences for example, in terms of organismal excretory load? As insects go through successive developmental stages from embryonic to larval to adult, the excretory load increases on the organism. For this task, tubules have to rapidly adapt, as they are largely established during embryogenesis unlike other epithelial tissues (Beyenbach et al., 2010a; Skaer, 1993). This is not only reflected in the gene ontologies for both larvae and adult (Table 4-5), those have predominantly similar terms and also the number of commonly enriched genes exceeding the average to 35% (Figure 4-3).

Insect epithelia are energised by an apical vacuolar (V)-type ATPase (V-ATPase), a multisubunit ATP pump, which consists of a membrane bound  $V_0$  and peripheral  $V_1$  complex (Wieczorek et al., 2009; Wieczorek et al., 1999). This partners with an apical alkali metal antiporter ( $K^+$  or  $Na^+/nH^+$ ) for balancing the loss of protons (Wieczorek et al., 1991). There are at least 33 genes that encode presently known V-ATPase subunits including the accessory proteins in which 13 have been proposed to show epithelial functions (Allan et al., 2005). The molecular identity of the antiporters that partner V-ATPases is now revealed for *Drosophila* and *Anopheles* species (Day et al., 2008; Rheault et al., 2007). This analysis did not find many V-ATPases in the top epithelial lists because they show high abundance across most of the tissues. The genes encoding *Nha1* and *Nha2* were found to be abundant in the tubule, hindgut and salivary glands but not in the neuronal tissues (Chintapalli et al., 2007). Interestingly, hierarchical clustering showed coregulation of *NHAs* with two probable,  $Ca^{2+}$ -activated  $Cl^-$  channel genes namely *Best1* and *Best2* (Figure 4-2).

There are seven known antimicrobial peptides (AMPs) in *Drosophila* which play crucial roles in protecting and defending the organism against pathogenic microbial flora (Imler and Bulet, 2005). It was previously shown that some of these peptides were tissue specifically regulated in response to the local and systemic infections (Levashina et al., 1998; Tzou et al., 2000). Epithelial tissues show distinct specificities of AMP gene expression.

For example, while *cecropin C* is well abundant in both larval and adult salivary glands (Table 4-1C), *attacin D* is only enriched in the larval tubule (Table 4-1A). Obtaining a common signature between adult-specific functions across the epithelia from larvae to adult showed some interesting candidates (Figure 4-4 and Table 4-6). The direct comparisons of adult vs. larval epithelia showed the stage-specificity of expression (Table 4-7).

The striking functional parallels between some of the vertebrate and invertebrate epithelial tissues have been obtained by several decades of hard work (Greenspan and Dierick, 2004).

The origins of epithelial tissue development have been described to be different from vertebrates to invertebrates; for example, the hindgut epithelium arises from endoderm in vertebrates and ectoderm in insects (Compos-Ortega and Hartenstein, 1997; Wolpert, 1998; Sulston, 1988).

However, the significance of the germ layer distinction still remains elusive. For example, the evidence for conservation of function from *Drosophila* hindgut to human hindgut could be demonstrated by comparing their analogous functions. IPA analysis of *Drosophila* epithelial enriched genes in the vertebrate disease and function context showed that there are many genes, including novel ones that have human disease orthologs, and are expressed in analogous tissues of the fly (Section 4.2.5). Approximately 30-60% of the genes that show at least 2-fold upregulation in the *Drosophila* epithelia were mapped to IPA database (Figure 4-5).

### **4.3.1 Limitations of the IPA**

The ortholog/paralog mapping in IPA depends on the information in Homologene. All the duplicate identifiers (in this case, Affymetrix identifiers, which may identify different transcripts of a single gene) are mapped to a single molecule (gene) in IPA, it is envisaged that the analysis is limited to gene level functional analysis rather than at the transcript level. IPA calculation of significance of network/functional analysis depends on the information present in its knowledgebase.

In the salivary glands and tubules, 2/74 and 4/74 'nucleotide sugars metabolism' canonical pathway molecules were enriched respectively, so is the *P*-value calculated, so that 4/74 molecules (in tubules) but not 2/74 molecules (in salivary glands) pass the *P*-value filter to be called as significantly enriched canonical pathway in that tissue. This is because the IPA supports all the 4/74 molecules to be significant in that canonical pathway.

If a pathway is not significantly enriched in all of the tissues, that group of genes were either not there in *Drosophila* or they are not conserved. However, one single key gene in a tissue will show its related pathway to be significantly enriched in that tissue.

A gene might be present in several networks with varying  $P$ -value and if we filter the molecule with their expression enrichment and on the basis of their  $P$ -value significance, it could narrow down the list of to potentially significant functions, diseases, and canonical pathways. If a tissue specifically enriched gene is categorised into a pathway with less significance ( $P$ -value), it either indicates that it is not essential or it needs further characterisation.

## 4.4 Conclusion

Tissue-specific transcriptomic enrichment data adds value to systems biology's well needed extensive genome annotation. There is about 50% of the annotated genome that is differentially expressed across the epithelia over the adult fly. While the developmental functions of most of the known genes are well studied, there is a lot of scope for studying adult-specific functions, as at least 70% of the genes are still novel or not functionally explored. Every epithelial tissue could be in its own right a model test bed to study the genes that are abundant in that tissue. All the epithelia have distinct functional similarities to perform specialised functions while retaining a 'gene expression signature'. From GO functional enrichment point of view, one could propose for each organelle of the cell in question to study, there is a convenient tissue to use as a model test bed in *Drosophila*. By identifying the epithelial enriched genes associated with human disease, phenotypes may help design the targeted drug screening in such a simple organism for identifying the lead compounds for human disease intervention and cure.

## 5. Microarray analysis of positional asymmetry of renal tubules in *Drosophila*

### Summary

In humans and other animals, the internal organs are positioned asymmetrically in the body cavity, and disruption of this body plan can be fatal in humans. The mechanisms by which internal asymmetry are established are presently the subject of intense study; however, the functional significance of internal asymmetry (outside the brain) is largely unexplored. Is internal asymmetry functionally significant, or merely an expedient way of packing organs into a cavity?

Like humans, *Drosophila* shows internal asymmetry, with the gut thrown into stereotyped folds. There is also renal asymmetry, with the rightmost pair of renal (Malpighian) tubules always ramifying anteriorly, and the leftmost pair always sitting posteriorly in the body cavity accordingly, transcriptomes of anterior-directed (right-side) and posterior-directed (left-side) Malpighian (renal) tubules were compared in both adult male and female *Drosophila*.

Although genes encoding the basic functions of the tubules (transport, signalling) were uniformly expressed, some functions (like innate immunity) showed positional or gender differences in emphasis; others, like  $\text{Ca}^{2+}$  handling or the generation of potentially toxic ammonia, were reserved for just the right-side or left-side tubules, respectively. These findings correlated with the distinct locations of each tubule pair within the body cavity. Well known developmental genes (like *dorsocross*, *dachshund* and *doublesex*) were showed continuing, patterned expression in adult tubules, implying that somatic tissues maintain both left-right and gender identities throughout life. Accordingly, the physical asymmetry of the tubules in the body cavity is directly adaptive. Now that the detailed machinery underlying internal asymmetry is starting to be delineated, our work invites the investigation, not just of tissues in isolation, but in the context of their unique physical locations and milieux.

## 5.1 Introduction

The vertebrate body plan is internally asymmetric (Burn and Hill, 2009; Levin and Palmer, 2007; Lopez-Gracia and Ros, 2007), and although complete *situs inversus* is benign in humans, partial disruption of this asymmetric organization (for example in herotaxy) can be lethal (Kartagener and Stucki, 1962; Sharma et al., 2008; Sutherland and Ware, 2009). Although separated by 450 M year of divergent evolution, many insect body plans show similar internal asymmetry; for example, the alimentary canal of the classical developmental model *Drosophila* starts development symmetrically, but is then thrown into highly stereotyped folds within the body cavity.

Just as human kidneys sit slightly differently in the abdomen, so the *Drosophila* Malpighian (renal) tubules show marked asymmetry; the two tubule primordia initially sit dorsoventrally at the midgut/hindgut boundary, then a rotation of the developing alimentary canal sets the dorsal tubules on the right side, and the ventral tubules on the left side, of the body (Coutelis et al., 2008) (Figure 5-1). Remarkably the right-side tubules always elongate anteriorly within the body cavity into the thorax, while the left-hand tubules always grow posteriorly (Beyenbach et al., 2010a). There is a clear advantage to this distribution, as it ensures that the tubules ramify throughout the body cavity (haemocoel). Thus the haemolymph, although circulating only sluggishly, is nonetheless regulated efficiently. However, the tubules also display morphological differences. The right-hand tubules contain conspicuous distal initial and transitional segments.

Although no such segments are visible in the left-hand tubules, genetic markers that label initial and transitional domains in the anterior tubules also label smaller and otherwise morphologically cryptic domains in the posterior tubule (Sozen et al., 1997). Unusually, the *Drosophila* Malpighian tubule is capable of providing both developmental and functional readouts (Beyenbach et al., 2010b), as its transport and signalling physiology has proved highly amenable to study (Dow and Davies, 2003). Although the cells of the initial domain are thin and do not display prominent structural adaptations for ion transport (like abundant mitochondria or deep microvilli), this region is capable of excreting  $\text{Ca}^{2+}$  at extremely high rates (Dube et al., 2000a).

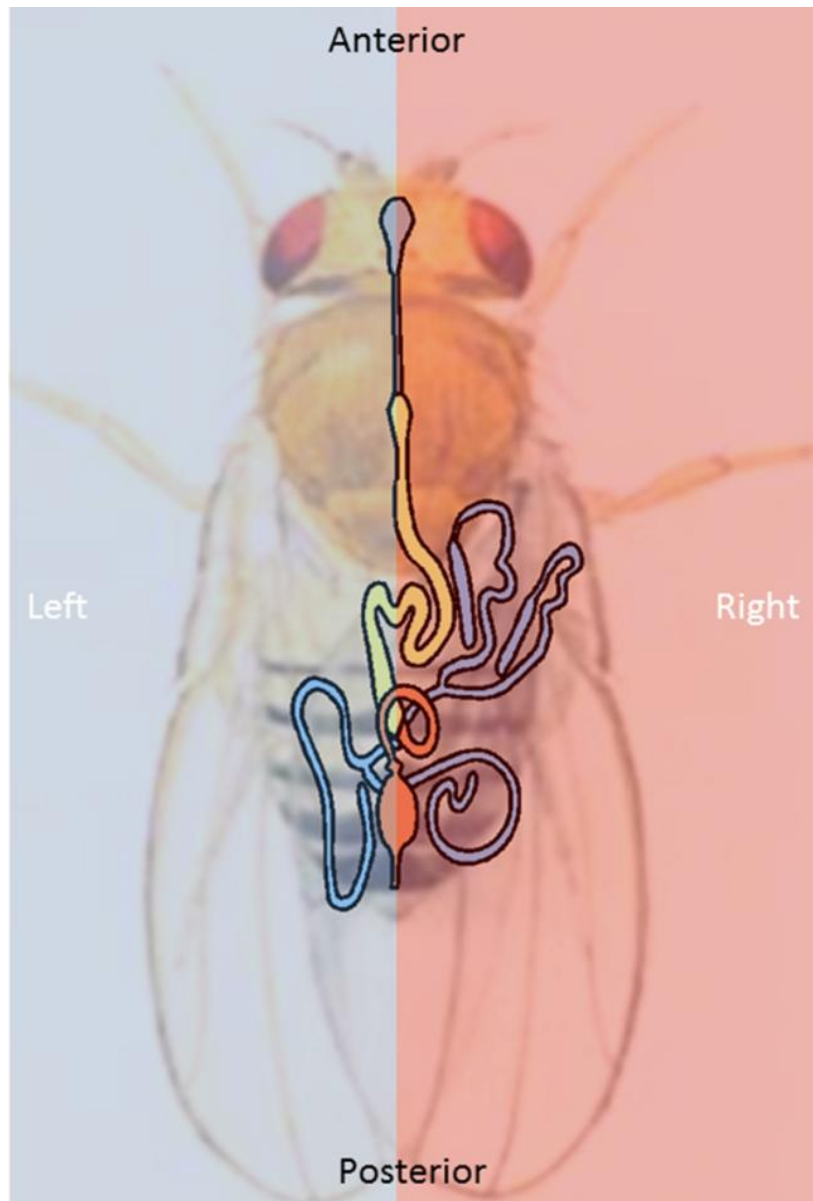


**Figure 5-1 Internal asymmetry in *Drosophila*.**

The alimentary canal is divided into ectodermal foregut (grey), endodermal midgut (yellow) and ectodermal hindgut (orange). The midgut and hindgut are thrown into tightly defined loops and folds, the most obvious consequence being that the two pairs of Malpighian (renal) tubules (blue) are oppositely directed. The right pair (with conspicuous dilated initial segment) is always directed anteriorly and wraps around the midgut; whereas the left pair are directed posteriorly and associate with the hindgut.

There is thus already some evidence of functional asymmetry in this simple kidney, and this is reinforced by asymmetric gene expression: the homothorax / dorsotonal transcription factor is expressed exclusively in the initial segment of the right-hand tubules (Wang et al., 2004). One approach to address this and other possible asymmetries in the tubule is to compare the transcriptomes of right- and left-hand tubules; so in this study a comprehensive analysis was performed, using Affymetrix version 2 chips on left- and right-hand tubules.

The results showed previously unsuspected lateral or sex-specific asymmetry in expression in a diverse set of genes, including those involved in positional specification in the embryo, and others involved in signalling. The data thus allow a reappraisal of functional sequelae of positional asymmetry in somatic tissues in higher organisms.

## 5.2 Results

### 5.2.1 Left vs. right: genes upregulated in right-side tubules suggest an interplay with the gut

As the posterior tubule appears morphologically similar to the anterior (right) tubule, but with a reduced initial segment (Sozen et al., 1997), the left tubule transcriptome was thought to be broadly a subset of the right tubule. Indeed, of 88 genes significantly changed (at FDR<0.05), 74 genes were significantly upregulated in right tubules, compared with only 14 in left tubules (Table 5-1).

**Table 5-1 Genes with significant expression differences between right (anterior) and left (posterior) tubules.**

Gene Symbol	Gene Title	P-value(Tissue)	Fold-Change(A vs. P)
CG14963	CG14963	1.93E-19	1940.88
CG16762	CG16762	1.71E-10	239.659
Best2	Bestrophin 2	1.40E-10	63.5515
Doc1	Dorsocross	5.03E-12	52.3512
CG6225	CG6225	2.84E-08	18.503
Doc3	Dorsocross3	3.78E-12	16.6997
NijA	ninjurin A	2.74E-10	15.2286
Ag5r	antigen 5-related	1.05E-05	12.4774
CG13748	CG13748	1.44E-09	10.6488
CG10587	CG10587	2.84E-08	6.21122
CG5194	CG5194	1.05E-06	5.23835
CG3074	CG3074	1.05E-07	5.08742
CG31248	CG31248	3.74E-09	5.0542
Ptp10D	Protein tyrosine phosphatase 10D	4.03E-09	4.72262
CG16743	CG16743	1.57E-08	4.60355
CG12602	CG12602	2.03E-09	4.40782
CG18746	CG18746	2.75E-06	4.26911
CAH1	Carbonic anhydrase 1	1.23E-06	4.25813
debcl	deborg	3.66E-09	4.16467
CG7634	CG7634	3.42E-07	4.04019
dac	Dachshund	1.83E-05	3.95692
Ace	acetylcholine esterase	1.10E-08	3.51503
out	outsiders	7.10E-05	3.43072
pgant8	polypeptide GalNAc transferase 8	1.89E-08	3.42025
CG34454	---	1.48E-05	3.34883
hth	dorsotonals	3.30E-08	3.26943
Btk29A	Btk family kinase at 29A	5.30E-07	3.14005
betaggt-1	type I Geranylgeranyl Transferase	1.30E-06	3.06347
Ddc	Dopa decarboxylase	4.01E-06	3.03603

CG1146	CG1146	7.29E-07	2.73723
CG42314	CG42314	1.86E-07	2.69998
CG6954	CG6954	1.04E-06	2.69589
lh	<i>putative lh-channel</i>	1.63E-06	2.6158
sdt	CG12657	5.00E-09	2.61408
CG6688	CG6688	8.18E-06	2.5747
CG8837	CG8837	7.52E-07	2.4715
CG18507	CG18507	1.06E-06	2.29762
CG18095	<i>gp150-like</i>	2.80E-05	2.23849
CG13189	CG13189	4.33E-07	2.23458
CG9717	CG9717	2.33E-08	2.21586
ko	<i>knockout</i>	5.96E-05	2.18748
Rhp	<i>Rhopilin</i>	8.45E-07	2.13755
CG18507	CG18507	1.65E-05	2.09275
CG8547	CG8547	1.94E-06	2.08754
CG30116	CG30116	1.42E-05	1.88332
CG42542	---	1.77E-06	1.80539
stumps	<i>heartbroken</i>	6.33E-05	1.80312
CG5867	CG5867	1.02E-07	1.79515
CG15209	CG15209	2.38E-06	1.78683
CG18812	CG18812	3.62E-06	1.77495
CG2976	CG2976	1.73E-07	1.75695
Lmpt	<i>Limpet</i>	0.000186	1.74574
CG18249	CG18249	3.70E-05	1.71547
CG1674	CG1674	5.93E-05	1.6942
CG13067	CG13067	1.33E-05	1.68701
CG7724	CG7724	2.67E-05	1.68625
CG31284	<i>water witch</i>	5.84E-06	1.6782
CG8012	CG8012	9.51E-05	1.67114
GstE10	<i>Glutathione S transferase E10</i>	2.33E-05	1.65665
CG17111	CG17111	0.000112	1.65491
CG7992	CG7992	4.56E-08	1.65211
danr	<i>Distal antenna related</i>	0.000108	1.6388
capaR	<i>capa receptor</i>	1.16E-05	1.6228
CG5630	CG5630	1.85E-05	1.61542
Ahcy89E	<i>AdoHcyase-like</i>	0.000138	1.58219
CG11852	CG11852	7.90E-05	1.57078
Nep2	<i>Nepriylsin 2</i>	8.19E-06	1.55144
wun	<i>wunen</i>	1.82E-05	1.52748
Irk3	<i>Inwardly rectifying potassium channel 3</i>	0.000135	1.47707
Hmgcr	<i>columbus</i>	2.25E-06	1.40475
CG14767	CG14767	9.32E-05	1.38802
Muc11A	<i>Mucin 11A</i>	6.61E-10	1.28682
CG8230	CG8230	0.000142	1.24257
CG34284	---	0.00015	-1.20485
su(Hw)	<i>suppressor of hairy-wing</i>	0.000161	-1.2369
multiple hits	---	9.52E-05	-1.25591
fat2	<i>fat-like</i>	1.28E-07	-1.48107
bab2	<i>bric-a-brac</i>	0.00017	-1.5376
CG15353	CG15353	0.000182	-1.86275
bowl	<i>bowel</i>	8.66E-07	-1.93196
CG33281	CG33281	1.52E-07	-2.43081
CG33281	CG33281	3.50E-07	-2.72487
CG11779	CG11779	0.000132	-3.32843
nemy	<i>no extended memory</i>	2.01E-05	-3.75797
alpha-Est6	<i>Esterase-6</i>	3.89E-08	-3.83112
CG3376	CG3376	5.09E-07	-7.59369
CG14957	CG14957	9.18E-07	-9.03153

The results implicate the right-side tubules in specific defence and  $\text{Ca}^{2+}$  handling roles. *CG14963* is 1940x upregulated in right (anterior) tubules, and the FlyAtlas reports that expression of this gene is utterly specific to the tubule. What function could be performed entirely by just two out of 4 tubules? *CG14963* encodes a protein containing an insect allergen related repeat, associated with nitrile-specific detoxification.

To discourage herbivores, some plants (notably brassicas) have developed a glucosinolate-myrosinase system as a chemical defence mechanism, and consequently insects, like caterpillars of the small white butterfly (*Pieris rapae*), have adapted to produce a detoxifying molecule, nitrile-specifier protein (NSP) (Wheat et al., 2007). BLASTP searches reveal proteins closely similar to *CG14963* are found throughout the Diptera, but that the Dipteran branch is rather diverged from the Lepidopteran branch. The implication is that *CG14963* is part of a Dipteran adaptation to dietary challenge. Why then is this gene confined to, and expressed at high level in, the right-hand tubules (Table 5-1)?

The key observation is that the right-hand tubules ramify anteriorly to surround the midgut, whereas the left-hand tubules are confined to the posterior abdomen, where they surround the hindgut. The tubules are major tissues of detoxification (Yang et al., 2007); so if a toxic compound were released by digestion, and passed through the highly permeable midgut, it would thus be a task for primarily the anterior tubules to neutralize the compound. Conversely, the left tubules might be expected to be enriched for genes involved in detoxifying compounds leaching from the hindgut; this will be demonstrated later.

A similar defensive role is implied for *CG16762*, another gene strongly (240x) up-regulated in right-hand tubules (Table 5-1), and with tubule-restricted expression. BLASTP searching reveals similarity to TsetseEP, a mucin implicated in tsetse susceptibility to trypanosome attack. As all BLASTP hits are confined to the Schizophora, the gene family may represent a highly specific adaptive radiation within this subset of the Diptera, to defend against microbial attack.

Although *Drosophilids* are not susceptible to trypanosome attack, dog heartworm (*Dirofilaria immitis*) is an intracellular parasite of the Malpighian tubules of culicid mosquitos; so there may be a general requirement for the tubule to defend against luminal pathogens.

By contrast, the left-side tubules, which wrap around the hindgut, show 3.8x enrichment for the probeset 1634658\_a\_at ([www.flyatlas.org](http://www.flyatlas.org)), which corresponds to *CG42708*, a mitochondrial glutaminase (Iliadi et al., 2008). FlyAtlas reports that this gene is particularly highly expressed in the tubules and hindgut. Glutaminase generates ammonia stoichometrically in the generation of glutamate from glutamine, and is found in kidney and liver in mammals: in kidney, the resulting ammonium ion can be used to rescue bicarbonate in the collecting duct (Marquez et al., 2006). Although abundantly produced in freshwater insects (where it can effectively diffuse away to harmless levels), ammonia is generally held to be a toxic and undesirable metabolite in terrestrial insects (ChapmanRF, 1982). Our data suggest that this reaction is concentrated in tissues in the back end of *Drosophila*, thus compartmentalizing it away from other potentially sensitive tissues. To confirm the spatial segregation of glutaminase activity, glutamine:glutamate ratio was assayed in acutely-dissected head, thorax and abdomen in adult flies, showing that the ratio is lowest in the abdomen (Figure 5-2).

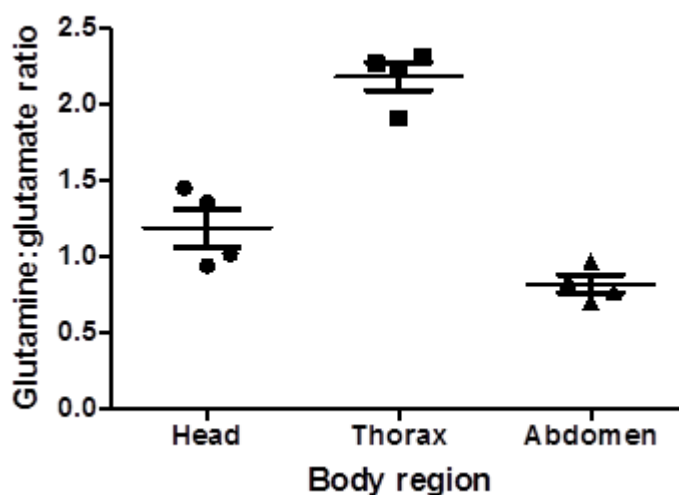


**Figure 5-2 Ammonia is high at the back end of the fly.** As an indicator of ammonia, glutamine and glutamate ratio was measured using LC-MS coupled to a high sensitive detector called Orbitrap.

*Best2* encodes (of four *Drosophila* bestrophins) the most closely related to human bestrophin 1, a  $\text{Ca}^{2+}$ - and/or volume-activated  $\text{Cl}^-$  channel of retinal pigmented epithelial cells, which is mutated in Best's macular dystrophy (Caldwell et al., 1999; Marmorstein et al., 2000). However, Bestrophins play wider roles: they are implicated in epithelial-to-mesenchymal transitions in human kidney (Aldehni et al., 2009), and in olfactory transduction (Pifferi et al., 2006). In *Drosophila*, *Best1* also mediates a  $\text{Ca}^{2+}$ - and/or volume-activated chloride current (Chien and Hartzell, 2007).

FlyAtlas reports that, although expressed in eye, *Best2* is abundant in epithelia; in adult tubule, it is 64x enriched in right-hand tubules (Table 5-1). From this observation, bestrophins became the candidate genes to unravel their potential functions using *Drosophila* as a model organism (Chapters 6, 7 & 8).

Given that there are real functional differences between left- and right-side tubules, and that these are underpinned by significant transcriptional differences, it is interesting to start to identify the transcriptional programme involved in specifying asymmetry. The three Dorsocross transcription factors are found in a cluster on chromosome 3L. These T-box, p53-like, brachyury transcription factors were originally implicated in heart formation (Hatton-Ellis et al., 2007)] at the dorsal midline, under control of decapentaplegic and wingless. They are possibly the products of recent gene duplication, because they have similar embryonic expression profiles, and are partially redundant. Post-embryonically, however, FlyAtlas (Chintapalli et al., 2007) reveals differences in expression.

*Doc1* is expressed mainly in tubule, hindgut and testis; *doc2* is confined to the hindgut, and *doc3* to tubule, hindgut and heart. Our data are consistent with reported embryonic expression in only the anterior tubules (Reim and Frasch, 2005); overexpression of *Doc* genes in the embryonic hindgut results in failure of the posterior tubules to develop, leaving only the anterior pair (Hatton-Ellis et al., 2007).

Although *Doc* genes are implicated in the very earliest stages of tubule specification, these data show that they continue to be expressed in the same spatially restricted pattern (*Doc1* is 52x, and *Doc3* is 17x, enriched in anterior rather than posterior tubule) through larval and into adult life, suggesting that the anterior/posterior distinction remains functionally significant throughout life, and that continued expression of *Doc* genes (or dorsocross transcriptional network) likely maintains that identity.

Other transcription factors enriched in right-side tubules are *dachshund* (4.0x), the *ski proto-oncogene* homologue important in development of the legs and eyes, but not previously implicated in tubule function; and *homothorax* / *dorsotonals* (3.3x), also important in eye development. By contrast, *bric-a-brac* (1.5x), *bowl* (1.9x) and *suppressor of hairy wing* (1.2x) are all significantly enriched in the left-side (posterior) tubules (Table 5-1).

### **5.2.2 A mechanism for asymmetric $Ca^{2+}$ handling**

The only known functional asymmetry in tubule function is the anterior-specific storage excretion of  $Ca^{2+}$  as phosphate-rich mineral concretions in the enlarged initial segments of the right-side tubules (Dube et al., 2000a). Based on results implicating *SPoCk*, the secretory pathway  $Ca^{2+}/Mn^{2+}$  ATPase, and *Best2* (Shown in the following chapters) in  $Ca^{2+}$  handling in tubule initial segment, it is possible to build a model for spherites formation in the tubule. Interestingly, the right-side tubule transcriptome is enriched for genes implicated in  $Ca^{2+}$  and phosphate transport, and for peroxisomal biogenesis, allowing a conceptual model for spherite generation to be built a model that was functionally tested (Chapter 8 and Figure 8-16). Calcium could be admitted to the specialized peroxisome by entry through a trp-like plasma membrane channel, together with a peroxisomal isoform of *SPoCk*; phosphate is provided by the  $Na^+$ /phosphate cotransporter, *NaPi-T*; the membrane is polarized by a specialized V-ATPase (with protons provided by a highly enriched isoform of carbonic anhydrase), and charge balance provided by the *Best2* chloride channel. Calcium is stabilized in the peroxisome by *calexcitin*, a specialized  $Ca^{2+}$ -binding protein originally identified in sarcoplasmic reticulum. There is also scope for regulation of the pathway, because of high enrichment of calmodulin and a calmodulin-responsive transcriptional activator.

### 5.3 Discussion

The key outputs of this work are: detailed transcriptomic datasets that outline the scope and extent of differences between male and female, and left and right insect Malpighian tubules; interesting novel hypothesis on the spatial and gender compartmentalization of different processes; and preliminary experimental data that suggest that some of these transcriptomic differences really do have physiological significance. For the first time, a transporting epithelium has been profiled for expression according to both its gender and its disposition within the body.

The results show that all tubules are not equivalent; although they perform the same key functions (the generation of urine, detoxification and excretion of waste material) they also perform some tasks (like innate immune defence) with different emphases; and some tasks, (like  $\text{Ca}^{2+}$  homeostasis) are remarkably dimorphic in their transcriptional repertoire. The neuroendocrine control of tubules, though substantially the same for all, also shows subtle distinctions. Importantly, it appears that the same transcription factors which determine positional identity and gender in the early embryo persist into adulthood, implying that identity of the tubules remains important, and that these transcription factors must be considered to be important for more than early development.

This work demonstrates relevance of the morphological asymmetry in terms of functional optimization of complex tissues in the whole organism, specifically putting transport processes near the organs that generate their substrates, and with both local and central control of output. The final model is that the basic fluid transport and homeostatic functions of the tubule are common to left and right tubules; but functional sequelae result from the proximity of the right-side tubules with the highly permeable midgut, and the left-side tubules with the excretory and concentrative power of the hindgut. Both dietary toxins and overabundant solutes (like  $\text{Ca}^{2+}$ ) must be sequestered rapidly by the tubules before they impact on the whole insect. Local signalling by neuroendocrine cells embedded along the length of the midgut (Veenstra, 2009) could complement central signals, by relaying information about the gut contents directly to the tubules.

The compartmentalization of ammonia handling to the hindgut and closely-coupled left-side tubules would equally protect the insect against toxic levels of an essential metabolite. We and others have previously argued that the high number of anonymous (undocumented) genes with highly tissue-specific expression patterns found in FlyAtlas (Chintapalli et al., 2007) suggests that researchers need to become more interested in specific tissues within the organism, in order to functionally characterize the whole genome. This principle is demonstrated further here; although we have previously-identified novel tubule-specific genes (Wang et al., 2004), the present dataset shows that the principle further extends to sidedness and to gender, offering fascinating insights as to likely novel functions.

The power of *Drosophila* genetics will allow a detailed examination of the interactions between tissues in their natural physical layout within the whole organism, and so allow an understanding of gene functions in an organotypic, organismal context. In an insect, this level of understanding is of great benefit to developing insights that might lead to novel control methods; but it further suggests that there may be asymmetry to be uncovered in other epithelia in the future.

## 6. Functional studies on *Drosophila* bestrophins

### Summary

Mutations in *Best1*, encoding bestrophin 1, cause autosomal dominant Best disease, a disease associated with vitelliform macular degeneration. In the diagnostic EOG, patients show a diminished light peak, which was thought to be caused by the altered basolateral  $\text{Cl}^-$  conductance of the RPE cells. The disease leads to the accumulation of lipofuscin in retinal pigment epithelial cells (RPE), and fluid- and debris-filled retinal detachments, probably leading to the degeneration of the macula of the eye. Bestrophins have been predominantly thought to be  $\text{Ca}^{2+}$ -activated  $\text{Cl}^-$  channels due to the pathological diagnostic features and subsequent biophysical characterisation. However, this hypothesis has not completely explained the variety of diseases that different mutations in bestrophins cause. The *in vitro* studies using cell culture systems and *Xenopus levis* oocytes failed to single out bestrophins as CaCCs, because of the native interfering currents of these models. Furthermore, a mouse knockout model neither showed any retinal pathology nor displayed any alteration in  $\text{Ca}^{2+}$ -activated  $\text{Cl}^-$  current. However, nobody has ever used *Drosophila* as a model organism to elucidate bestrophin function. *Drosophila*, with its powerful arsenal of post-genomic techniques and its wealth of genetic mutants, could provide real insight into organismal level functions of these proteins. The *Drosophila* genome encodes all four human homologues (*Best1*, *Best2*, *Best3* and *Best4*) and therefore is suitable to study functions in an integrative physiology context. The gene expression patterns were investigated using FlyAtlas. This analysis suggested that *Best1* is neuronal and epithelial expressed while *Best2* is predominantly expressed in the epithelial tissues including the eyes. However, *Best3* and *Best4* showed high enrichment in the testes indicating specialised roles. The reverse genetic approach was employed using the GAL4/UAS system to ablate the expression of four bestrophins individually and assess the viability of the flies, at all developmental stages. This analysis revealed that *Best2* and *Best3* are essential for fly viability, while *Best1* and *Best4* are dispensable. The analysis of localisations using bestrophin YFP fusions suggested that they show diverse localisations. The localisations for *Best1* and *Best2* were confirmed to be apical plasma membranes and peroxisomes, respectively.

Best3 and Best4 showed intracellular localisations that may represent endolysosomal vesicles and endoplasmic reticulum, although these have not been confirmed. The salt survival analysis confirmed that *Best1* is an essential gene in the regulation of salt; as the knockdowns and deletions showed reduced survival on high salt diets than their controls. In contrast, the flies with reduced levels of *Best2* expression showed increased resistance to high salt diet indicating that it may not be a CaCC.

## **6.1 Bestrophins as candidate CaCCs**

### ***6.1.1 Identification in human disease***

The importance of bestrophins came from the fact that they manifest in Best disease in the human eye. The first bestrophin was identified and named as VMD2 in 1998 as the mutations within this human gene result in vitelliform macular dystrophy (degeneration) (VMD) (Figure 6-1) (Marquardt et al., 1998; Petrukhin et al., 1998). It is also called Best vitelliform macular dystrophy (BVMD) or Best disease as it was named after a German ophthalmologist, Friedrich Best, who published the first genetic pedigree analysing this disorder in 1905. The macular dystrophy is an eye disease that can potentially lead to progressive vision loss. In BMD patients, the degeneration was proposed to be caused by the sub-retinal (macular) deposition of egg yolk-like (vitelliform) lipoprotein called lipofuscin. However, it is characterised by a depressed light peak in the diagnostic electrooculogram (EOG) in all stages of disease progression, including in phenotypically normal carriers (Pinckers et al., 1996).

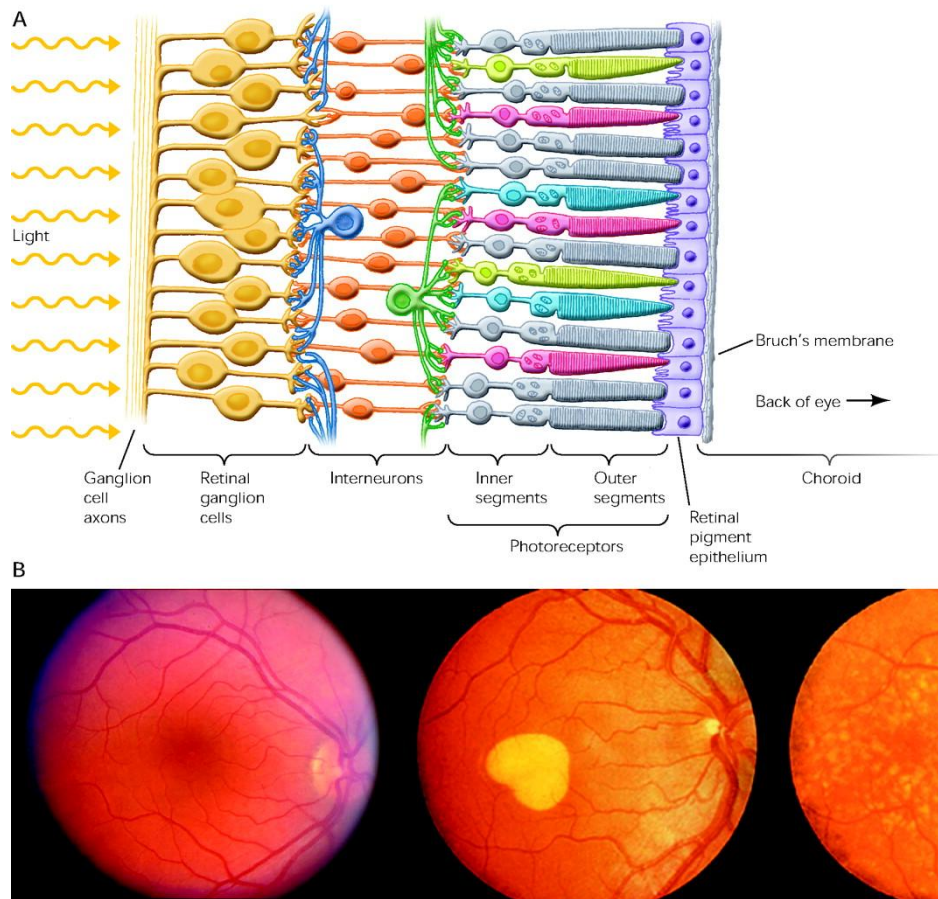


**Figure 6-1 Human retina in health and disease.**

**(A) Retinal organisation from ganglion cell axons to the retinal pigment epithelium (RPE) in the back of the photoreceptors. (B) The ophthalmoscopic images of retinas. The yellowish spot on the right of each retina is the optic nerve. Normal retina, Best vitelliform macular dystrophy (vitelliform stage), and age-related macular degeneration are shown from left to right. Taken from (Hartzell et al., 2005b)**

The pathophysiological contributions of several bestrophin mutations lead to different kinds of macular degeneration including BVMD (Marquardt et al., 1998; Petrukhin et al., 1998), adult-onset vitelliform dystrophy (Kramer et al., 2000), and autosomal dominant vitreoretinopathy (Yardley et al., 2004). In addition, *Canine* multifocal disease models were also presented by (Guziewicz et al., 2007). These findings have been further supported by Best1 localisation to the basolateral plasma membrane of retinal pigment epithelia (RPE) (Guziewicz et al., 2007; Marmorstein et al., 2000).

Best disease is rare in the general population, probably because it is caused by genetic factors unlike the age-related macular degeneration (AMD) that is caused by both environmental and genetic factors (Hartzell et al., 2005b). However, it shares some important phenotypic features with AMD, the leading

cause of visual deterioration in the elderly population of the developed countries. In the UK alone 250,000 people have been registered as visually impaired and almost the same number are affected by it to a lesser degree (according to [www.maculardisease.org](http://www.maculardisease.org), accessed on 1st February, 2012).

### **6.1.2 Structural aspects**

With the exception to other CaCCs, bestrophins have been well characterised in terms of their biophysical properties and their molecular structural aspects. Current topological predictions based on *in silico* and *in vitro* structural studies suggest that bestrophins may have 4-6 distinct transmembrane alpha-helices, and a large C-terminal cytoplasmic region (Figure 6-2). First structure-function analysis of bestrophins by Tsunenari et al. (2003) suggested four out of six TMDs (TMD1, -2, -4 and -6) traverse the membrane, and TMD3 forms a cytoplasmic side hydrophobic loop, while TMD5 forms a re-entrant loop (Figure 6-2A). In addition, they proposed the cytosolic face of both N- and C-termini of the protein.

More recent studies in dog pancreas ER microsomes, led to an alternative topology for predicted TMDs (Milenkovic et al., 2007b) (Figure 6-2B). Using Lep H1 membrane targeting domain, hBest1 TMDs were targeted to ER microsomal membranes as single entities, and as combinations. These studies suggested that TMD1, -2, -4, -6 were capable of being incorporated into the membrane as singular entities, in that, only TMD1, -2, -5 and -6 can traverse the membrane. Furthermore, the same study provided additional data suggesting the integration of hBest1 into plasma membrane may depend on some of the critical amino acid residues that cluster near predicted TMDs.

However, the first model was argued as more favourable in terms of the experimental parameters in addition to contradicting facts in the second model (Hartzell et al., 2008). The above studies have been mainly employed hBest1, in that all the TMDs span the first 350 amino acids of the N-terminus of the protein. Importantly, the N-terminus region is highly conserved across species, thus these studies may show a general insight into the TMD topology across Bestrophin family of proteins.

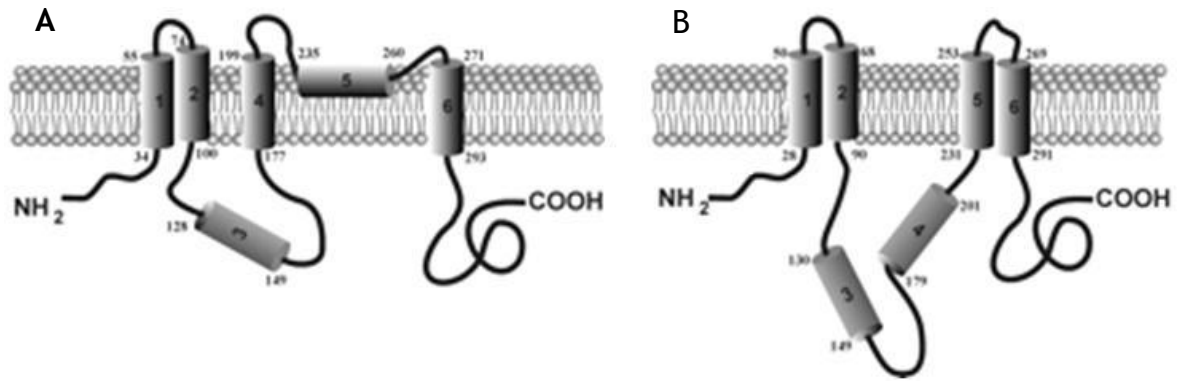


**Figure 6-2 Transmembrane topology of hBest1.**

(A) According to Tsunenari et al., (2003) model, four (1, 2, 4 and 6) out of 6 TMDs traverse the plasmamembrane, and the rest of the 2 TMDs (3 and 5) form a hydrophobic cytosolic loop and a re-entrant loop respectively. (B) According to Milenkovic et al., 2007 model, 4 TMDs (1, 2, 5 and 6) traverse the plasma membrane and the other two TMDs (3 and 4) form a relative hydrophobic loop. However, both models proposed N- and C- termini endup in cytosolic side (modified from Milenkovic et al., 2007).

Immunoprecipitation studies suggested that bestrophins may exist as tetramers or pentamers in a heterologous expression system (Sun et al., 2002). Homo-oligomerisation was predominantly seen when hBest1 with myc- and Rim3F4-tags were cotransfected, than when they were cotransfected in combination with *Drosophila* or *C. elegans Best1*. However, these conclusions were not supported by another study by (Stanton et al., 2006). These authors performed hydrodynamic studies on porcine Best1 (pBest1) that was extracted from porcine RPE cells using 1% Triton X-100 containing buffer. Using sedimentation calculations, they concluded that pBest1 may exist as a dimer.

In support of this, when they heterologously expressed the pBest1 in HEK cells, a significant fraction of the protein was found as aggregates with the same experiments as above. This aggregation of overexpressed protein, led these authors to rule out a tetrameric or pentameric stoichiometry for Best1.

Nonetheless, both studies showed that bestrophins may form oligomers. These observations are in consistent with the fact that the mutant versions of bestrophins can alter channel gating, even if they were oligomerised with a wildtype bestrophin.

### 6.1.3 $\text{Cl}^-$ channel function of bestrophins

In BVMD patients, reduced light peak in the electrooculogram (EOG) was thought to be caused by defects in epithelial ion transport. Electrophysiological studies in different species including chickens, cats and geckos revealed that the light peak may be caused by  $\text{Cl}^-$  conductance in the RPE basolateral membranes (Chien et al., 2006; Gallemore, 1997). The BVMD causing bestrophins presents a distinct family of proteins. The initial proposal of a  $\text{Cl}^-$  channel function of bestrophins was also based on the functional roles of RPE cells where Best1 was found in the basolateral membranes of these epithelial cells (Sun et al., 2002). The RPE cells play a vital role in retinal structure and function. They absorb, lactate, and lipofuscin, transport fluid, and maintain the volume and composition of the sub-retinal space (Kenyon et al., 1994; Kunzelmann et al., 2007).

Upon the activation of photoreceptors by light, the apical membranes of RPE cells that hyperpolarize and give rise to the c-wave component of the EOG. Further, the hyperpolarization causes the activation of  $\text{Cl}^-$  channels in the basolateral membrane leading to depolarization of the membrane. This depolarization causes the characteristic light peak in the EOG which was believed to be caused by  $\text{Cl}^-$  current ( $I_{\text{ClCa}}$ ), which is diminished in the BVMD disease patient.

The first convincing evidence for a  $\text{Cl}^-$  channel function of bestrophins came from studies on human, *Drosophila* and *Caenorhabditis elegans* proteins (Sun et al., 2002). The  $\text{Cl}^-$  currents were activated upon heterologous expression of various bestrophins in HEK cells. These  $\text{Cl}^-$  currents were thought to be the representatives of bestrophin expression as different bestrophins showed current-voltage differences and activation by  $\text{Ca}^{2+}$  (Tsunenari et al., 2003). The hBest1 elicited currents showed small amount of outward rectification and time dependency. In addition, the currents were dependent on intracellular  $\text{Ca}^{2+}$ , as they were almost abolished at nominally zero free- $\text{Ca}^{2+}$  buffered with  $\text{Ca}^{2+}$ -chelator EGTA. This observation led to the hypothesis that bestrophins may be activated by intracellular  $\text{Ca}^{2+}$ .

Other evidence suggests the Cl<sup>-</sup> function of bestrophins came from the site directed mutagenesis studies where the gating, selectivity and pharmacology of these channels was altered with the mutagenesis of key protein residues. These studies convincingly showed the probable Cl<sup>-</sup> channel function of bestrophin channels (Qu et al., 2006; Qu et al., 2004; Qu and Hartzell, 2004). For example, the mutation at position 93 in mBest2 results in significant channel gating, in that the mutant channel, upon hyperpolarization, activates the currents that show time dependency and inward rectification. In addition, the rectification has been shown to be modulated by mutating an electroneutral amino acid, phenylalanine, at position 80 with either a positively charged arginine or negatively charged glutamate (Qu and Hartzell, 2004).

#### **6.1.4 Bestrophins as CaCCs**

Since the discovery of mutations in Best1, responsible for the Best disease, there has been extensive amount of data suggesting bestrophins as the components of CaCCs (Hartzell et al., 2008). At the same time, another hypothesis evolved implicating the bestrophins as Ca<sup>2+</sup> channel regulators (Marmorstein et al., 2009), and is separately discussed in Chapter 7.

So far, hBest1 (Barro Soria et al., 2009; Tsunenari et al., 2003), hBest4, mBest2 (Pifferi et al., 2006; Qu et al., 2004) and xBest2 (Qu et al., 2003) have been implicated in the Ca<sup>2+</sup>-activated Cl<sup>-</sup> conduction with an estimated K<sub>d</sub> of ~200 nM of Ca<sup>2+</sup>. This may suggest like for other CaCCs, bestrophins act upon intracellular elevations of Ca<sup>2+</sup> concentrations.

Furthermore, bestrophins have biophysical properties similar to those of endogenous CaCCs in terms of their direct activation by physiological elevations of intracellular Ca<sup>2+</sup> with an anion permeability sequence. These have been demonstrated conclusively using mutant versions of wildtype bestrophins that alter anion permeability and the knockdown of *Best1* causes reduced I<sub>ClCa</sub> (Chien et al., 2006; Hartzell et al., 2008; Qu et al., 2004).

However, the mechanisms of action of Ca<sup>2+</sup> is so far not clear as there are no direct Ca<sup>2+</sup> binding sites found in bestrophins in *in silico* analysis. However, several hypotheses have been put forward from the experimental observations.

For example, in hBest4, a high density of acidic amino acid residues are found that exhibits similarity to the  $\text{Ca}^{2+}$  bowl of BK  $\text{K}^+$  channels and proposed to be possible  $\text{Ca}^{2+}$  binding sites (Tsunenari et al., 2006). However, increased activation of endogenous *Drosophila* bestrophins and hBest1 in excised membrane patches in the whole cells upon ATP stimulation may suggest a complicated mechanism.

Other mechanisms that regulate bestrophin function may exist including cAMP, cGMP-dependent phosphorylation via nitric oxide (NO) in calu-3 cells (Duta et al., 2006; Duta et al., 2004) or regulation via direct interaction with protein phosphatase 2A (Marmorstein et al., 2002). Furthermore, protein-protein interaction through proline-rich amino acids or autoinhibitory domain found in bestrophins at the C-termini in different bestrophins have been proposed to regulate bestrophin  $\text{Cl}^-$  channel function (Hartzell et al., 2008).

### **6.1.5 Physiological functions of bestrophins**

The direct activation of  $\text{Cl}^-$  channel function of bestrophins by  $\text{Ca}^{2+}$  with an anion selectivity sequence has shown strong evidence for their potential function as CaCCs (Hartzell et al., 2005a; Kunzelmann et al., 2007). In particular, the data from the point mutations of hBest1 and mBest2 showing similar biophysical properties with classical CaCCs in terms of their rectification, voltage dependence and kinetics, further suggested CaCC function (Hartzell et al., 2008). In intact S2 cells, Best1 has been shown to be regulated by changes in cellular osmolarity, independently of  $\text{Ca}^{2+}$  (Chien and Hartzell, 2007). Thus, Chien and Hartzell (2007) proposed Best1 as a type of volume-regulated anion channel (VRAC) involved in the control of cell volume. They convincingly showed that volume-activated  $\text{Cl}^-$  currents exist in S2 cells, and these currents can be abolished by RNAi. Furthermore, the RNAi effects can be rescued by overexpression of *Best1*. Moreover, an impaired ability in regulation of cell volume was seen in response to hypoosmotic solutions when *Best1* expression was reduced using RNAi. These have been supported by the amplitude of the Best1 current and the ability of the cells to undergo RVD. These regulatory mechanisms suggest for at least Best1, that it may be dually regulated by  $\text{Ca}^{2+}$  and cell volume.

The *hBest1* is expressed in the RPE, the epithelia that line the photoreceptor outer segments. The retinal homeostasis is controlled by RPE, by regulating the composition of the fluid surrounding the photoreceptor outer segments, provide nutrients for regeneration of the visual pigment, the retinoid and involved in phagocytosis of shed photoreceptor discs (Strauss, 2005). Bestrophins may possibly involve in any of these functions. However, like the CFTR knockout mouse model, the bestrophin knockout mouse model does not phenocopy the human eye disease and neither does it show any gross visual deficit or retinal pathology (Marmorstein and Marmorstein, 2007).

mBest2 was proposed as a candidate coding for CaCC currents in the olfactory sensory neurons (OSNs) through the GPCR signaling and influx of  $\text{Ca}^{2+}$  via CNG channels using *in vivo* expression studies and *in vitro* biophysical characterisation in HEK cells (Pifferi et al., 2006). This activation has been proposed to amplify the response, causing the largest fraction of the olfactory receptor potential. However, the same authors published more findings refuting their prior hypothesis. In their second round of experiments, they used the knockout mouse, lacking *Best2*, and compared them with wildtype. They found no significant differences in their olfactory physiologies both in intact epithelium and isolated OSNs (Pifferi et al., 2009). This clearly excludes the possibility of mBest2 coding for  $I_{\text{ClCa}}$  in mouse OSNs.

As discussed earlier, many epithelia exhibit clear  $I_{\text{ClCa}}$ , implicating CaCCs in the epithelia as detrimental for function. However, detailed characterisation of molecular components of epithelial CaCCs has not been published. Gene expression reports suggest *mBest1* and *hBest1* are expressed in the salivary glands, in parallel to their expression in various cell types (Barro Soria et al., 2009; Kunzelmann et al., 2007).

### **6.1.6 *Drosophila bestrophins***

The data available on *Drosophila* bestrophins are very scarce, except that Criss Hartzell's group showed *Drosophila* bestrophins as single entities that may mediate  $I_{\text{ClCa}}$  (Chien et al., 2006). However, there is a serious lack of integrative physiological approach in previous studies that attempted to study the functions of bestrophins *in vitro*. This is where *Drosophila* is useful.

Furthermore, the studies relied on *in vitro* cell culture system may not recapitulate the physiological context of a protein in question. In addition, there are no specific  $\text{Cl}^-$  channel blockers available in order to clearly implicate bestrophins as single entities responsible for  $I_{\text{ClCa}}$ , and thus to reveal their functional significance *in vivo*. The overlapping pharmacology of all extant  $\text{Cl}^-$  channels with other channels such as  $\text{K}^+$  channels may not be useful in these studies to clear the ambiguity in function (Greenwood and Leblanc, 2007).

The focus of this thesis has been on the four bestrophin genes that are known to be expressed in the fly. Given its genetic physiological amenability, *Drosophila* was thought to provide insight into organismal functions of these proteins.

Using a reverse genetics approach, in combination with *Drosophila* physiological tools such as fluid secretion assays along with neuropeptide  $\text{Ca}^{2+}$  agonists (such as capa and Drosokinin), had been thought to provide clues into bestrophin function as the candidate CaCCs. The tubules of *Drosophila melanogaster* are functional homologues of human kidney, containing around 150 cells, could be potential models to study  $\text{Ca}^{2+}$ -mediated  $\text{Cl}^-$  conduction and  $\text{Cl}^-$  transport processes. The major functions of these include purification of the haemolymph (blood) of waste materials, excretion and adjustment of primary urine, thus playing a major role in physiological homeostasis. It has been shown that stellate cells are major sites of  $\text{Cl}^-$  conduction and that they express maxi  $\text{Cl}^-$  channels, like tweety (O'Donnell et al., 1998). The efflux of  $\text{Cl}^-$  can be stimulated by peptide hormone Drosokinin, which acts through its cognate G-protein coupled receptor signaling mechanism, that elevates intracellular  $\text{Ca}^{2+}$ , specifically in stellate cells (Radford et al., 2002; Terhzaz et al., 1999a).

As there is a serious gap between *in vitro* (and biophysical studies) and organismal functions of these channel proteins, it was envisaged that *Drosophila melanogaster* would be a potential model to investigate the roles *in vivo*.

## 6.2 Results

### 6.2.1 *Bestrophins in Drosophila melanogaster*

Bestrophins have been found to be widely conserved across the species (Hartzell et al., 2008). *Drosophila* genome encodes four bestrophins, Best1-4. All four show high sequence similarity at the N-terminus with variable C-termini (Figure 3A). In addition, Best1, Best2 and Best3, 4 show more sequence similarity to each other. The ensemble hydropathy analysis suggests that these proteins have 2-5 putative TMDs, in that Best2 has the least number and Best1-PA, Best1-PB, Best1-PC, Best3 and Best4 have 4, 5, 5, 5 and 5 TMDs respectively ([www.ensembl.org](http://www.ensembl.org)). However, the Expasy server predicts 4 TMDs in all isoforms of Best1, 2 TMDs for Best2 (like the ensemble prediction), 3 TMDs for both Best3 and Best4 ([www.Expasy.org](http://www.Expasy.org)).

### 6.2.2 *Gene expression*

Bestrophins are highly conserved across species from vertebrates to invertebrates (Hartzell et al., 2008). The FlyAtlas data show interesting tissue-wide expression patterns (Table 6-1). *Best1* & *Best2* are expressed in the tubules suggesting the suitability of tubules for functional studies using reverse genetics. In addition, both *bestrophins* are expressed in most of the adult tissues. However, *Best3* and *Best4* are specific to testis.

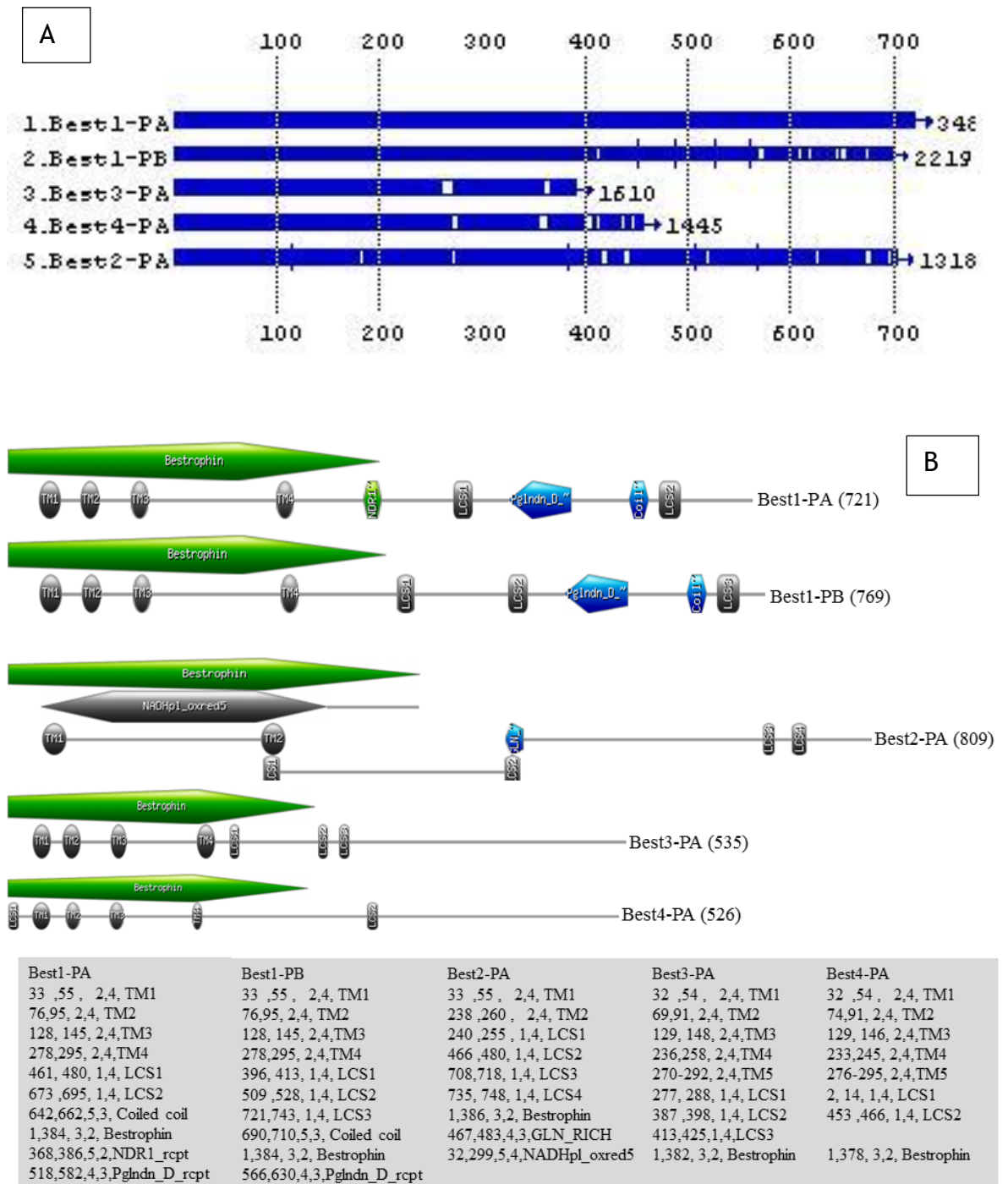


**Figure 6-3 Protein sequence alignment and putative protein sequence features of *Drosophila* bestrophins.**

**(A)** Bestrophin protein sequence alignment using CLUSTALW alignment. **(B)** The protein features were obtained from Expasy protein server (Gasteiger et al., 2003). All four bestrophins are shown including the two isoforms of Best1. They all show a highly conserved bestrophin domain (green). The putative transmembrane domains are shaded in black; each shows 2-4 TMs. Other interesting domains predicted include prostaglandin D receptor (Pglndn\_D\_rcpt) in Best1 and NADH plastoquinone oxidoreductase domain in Best2. Interestingly none of them show the  $Ca^{2+}$  binding EF hand domains.

**Table 6-1 Microarray gene expression data for all four bestrophins in various tissues of *Drosophila melanogaster*.**

The data were obtained from the FlyAtlas (20<sup>th</sup> January, 2012). The gene expression (mRNA signal) and its enrichment is shown for each tissue. The standard error is omitted for clarity purposes as it is mostly less than 5% of the mRNA signal. The mRNA signal is colour coded from red to blue and the colour range indicates high to low abundance respectively.

Tissue	Best1		Best2		Best3		Best4	
	mRNA Signal	Enrichment						
Brain	144	0.9	7	0	2	0.1	2	0.2
Head	158	1	220	1.2	1	0.1	3	0.3
Eye	60	0.3	139	0.7	2	0.1	0	0
VNC	270	1.7	8	0	4	0.2	4	0.4
Salivary gland	133	0.8	487	2.5	6	0.3	11	0.9
Crop	551	3.4	412	2.2	2	0.1	4	0.4
Midgut	79	0.5	32	0.2	9	0.5	7	0.7
Tubule	551	3.4	127	0.7	6	0.3	4	0.4
Hindgut	644	3.9	442	2.3	5	0.3	6	0.5
Heart	148	0.9	16	0	2	0.1	3	0.3
Fat body	90	0.5	17	0	6	0.3	10	0.9
Ovary	428	2.6	183	1	2	0.1	4	0.4
Testis	25	0.2	114	0.6	134	6.7	128	11
Male accessory glands	274	1.7	1962	10	5	0.3	9	0.9
Virgin spermatheca	153	0.9	937	4.9	7	0.3	8	0.7
Mated spermatheca	179	1.1	1196	6.2	10	0.5	7	0.6
Adult carcass	95	0.6	136	0.7	7	0.4	10	1
Larval CNS	65	0.4	21	0.1	2	0.1	5	0.4
Larval Salivary gland	26	0.1	196	1	2	0.1	5	0.4
Larval midgut	155	0.9	9	0	12	0.6	12	1
Larval tubule	300	1.8	96	0.5	1	0.1	6	0.5
Larval hindgut	405	2.4	541	2.8	3	0.1	7	0.7
Larval fat body	23	0.1	3	0	18	0.9	23	2.1
Larval trachea	150	0.9	139	0.7	3	0.1	4	0.3
Larval carcass	82	0.5	210	1.1	2	0.1	6	0.5
S2 cells (growing)	435	2.6	0	0	2	0.1	42	3.7
Whole fly	163		191		19		11	

### Experimental Plan

From the above genomic and expression analysis, the following experimental plan was designed to investigate organismal functions of bestrophins.

- 1 Cloning of all 4 bestrophins of *Drosophila* for *in vitro* (S2 cells) and *in vivo* (fruit flies) functional analysis.
- 2 Transfection of S2 cells with YFP fusions of bestrophins constructs for fluorescent localisation within the cell. This would distinguish plasma membrane from endosomal (e.g., peroxisomes, mitochondria, ER, Golgi and others) localisation.
- 3 Validation of overexpressor and RNAi fly lines using qPCR, by crossing them with several GAL4 drivers (tubule principal cell, stellate cell tubule specific etc.). This shows if the mRNA levels are affected in the overexpressor and RNAi flies driven using ubiquitous GAL4 lines. The 'cell-specific knockdown' validations show which cells the bestrophins are expressed. For example in tubules, the anionic and cationic pathways are delineated into cell type-specific in that the stellate cells show anion conductance and the principal cells show cation conductance.
- 4 Assessment of the phenotypic characters (including survival, structural, morphological defects) of bestrophins using the transgenic fly lines. The observation of structural and morphological characters would show if the bestrophins play any developmental and morphological defects. Similarly, assessing the impact of high salt diet on *bestrophin* knockdowns and overexpressor would indicate their possible role in salt homeostasis.
- 5 *In vivo* localisations of YFP tagged bestrophins using different GAL4 drivers to see the cellular location of these proteins in different tissues of the fly and in specific cells of an individual tissue (tubule principal cell, stellate cells etc.).
- 6 Assaying fluid secretion rates of Malpighian tubules to see whether knockdown or overexpression causes any impairment.

This would show whether the proposed  $\text{Ca}^{2+}$ -activated  $\text{Cl}^-$  theory or the modulators of other  $\text{Ca}^{2+}$  channels stands to this phenotypic screening using tubules.

- 7 Assaying  $[\text{Ca}^{2+}]_i$  to see whether bestrophins modulates  $\text{Ca}^{2+}$  levels utilising transgenic recombinant  $\text{Ca}^{2+}$  reporter, aequorin. This would possibly link if bestrophins modulate  $\text{Ca}^{2+}$  signaling.
- 8 Immunoblotting of the protein extracts and immunolocalisation using the antibodies raised against bestrophins. This would validate if the antibodies specifically recognise bestrophins in various tissues they show mRNA abundance.

The results are presented first for Best1 & Best2 and then Best3 & Best4 as their comparative similarities and differences. This was because the coregulation of bestrophins across different tissues in the fruit fly, in that *Best1* & *Best2* show high coregulation (across the epithelial tissues) and *Best3* & *Best4* show the coregulation in testes (Table 6-1).

### **6.2.3 *Best1* & *Best2* are differentially expressed in Malpighian tubules**

Tubules show distinct functional domains. Tubule-specific microarrays in the FlyAtlas showed sex- and segment-specific differential expression of several genes, in that, *Best1* was found more in the females, both in anterior and posterior tubules with 2.2-fold (*t*-test;  $P=0.0273$ ) and 2.5 (*t*-test;  $P=0.0004$ ) respectively (Figure 6-4) and *Best2* was found more in the anterior tubules (30-40-fold,  $P=0.0005$ ) (Figure 6-5). Comparatively, *Best2* is more abundant in the head than the *Best1* (Figure 6-6). In the next chapter, *Best2* was confirmed to be specifically enriched in the eyes than anywhere else in the head (Figure 7-5)

The gender-specific, physiological demands may cause the differential expression of *Best1*. But, the differential expression of *Best2* was confirmed to be caused by the functionally distinct large initial segment, only found in the anterior tubules.

A qPCR was set up to investigate if *Best2* was differentially expressed in the initial segment and the rest of the segment of the anterior tubule by cutting them separate. This revealed *Best2* expression only in the initial segment but not in the rest of the anterior segment. These results were also confirmed by an *in situ* hybridization using anti-sense mRNA for *Best2* and found that it was only expressed in the initial segments (Figure 7-4).

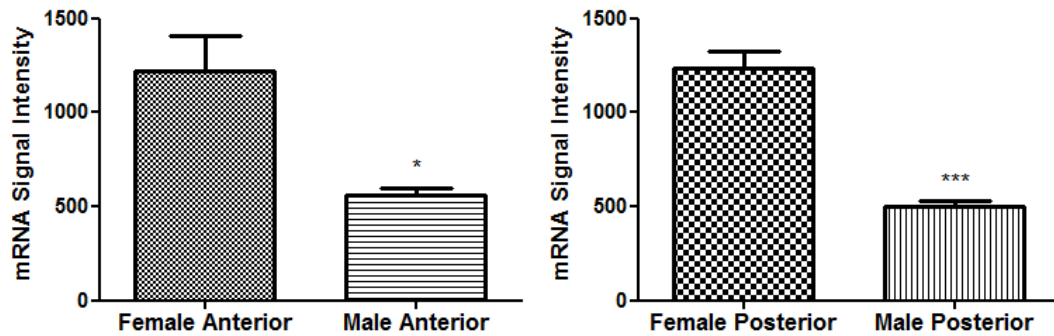


**Figure 6-4** *Best1* is more abundant in female than male tubules. Normalised Affymetrix mRNA signal intensities were plotted on Y for males and female tubules; separately for anterior and posterior. In both anterior and posterior female tubules, *Best1* was enriched 2.2-fold (*t*-test;  $P=0.0273$ ) and 2.5 (*t*-test;  $P=0.0004$ ) respectively, than their male counterparts.

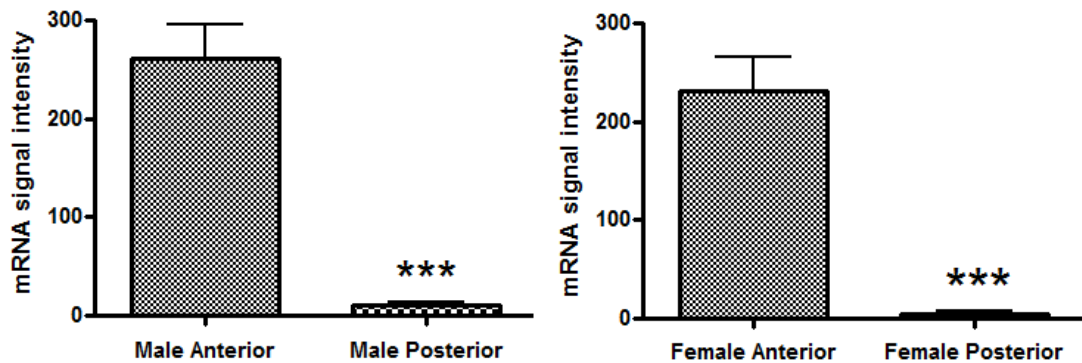


**Figure 6-5** *Best2* is highly enriched in both male and female anterior tubules than their posterior counterparts. Normalised Affymetrix mRNA signal intensities were plotted on Y for anterior and posterior tubules; separately for male and female. The differential expression was found to be statistically significant (*t*-test;  $P\leq 0.001$ ).

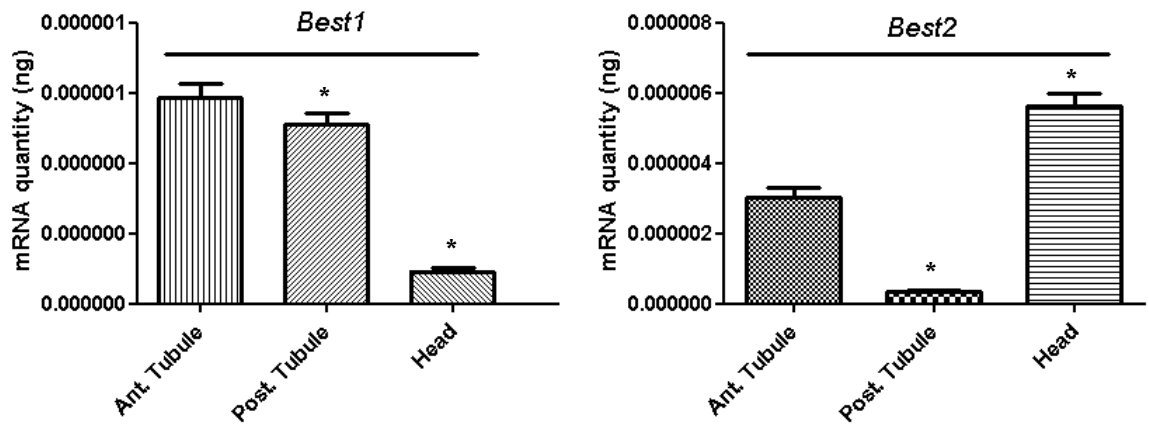


**Figure 6-6** The absolute quantification of *Best1* & *Best2* mRNA expression, in the tubules and heads, using qPCR. (left panel) *Best1* was found significantly higher in the tubules than the head. *Best2* shows anterior tubule abundance and significantly higher expression in heads than the anterior tubules (*t*-test,  $P \leq 0.05$ ).

#### **6.2.4 *Best1* & *Best2* show differential localisation both *in vitro* and *in vivo***

To study the subcellular localisations of bestrophins, both *in vitro* and *in vivo*, several YFP and V5 translational fusion constructs were engineered (Figure 6-7). *Best1* has one transcript annotated by Flybase in the beginning of the project, and at the later stages, another isoform was added. Accordingly, *Best1-RA* and *Best1-RB* were fused with YFP and V5 epitope tags respectively, for colocalisation purposes. *Best2* had one annotated transcript that was fused with YFP, and then separately with the V5.

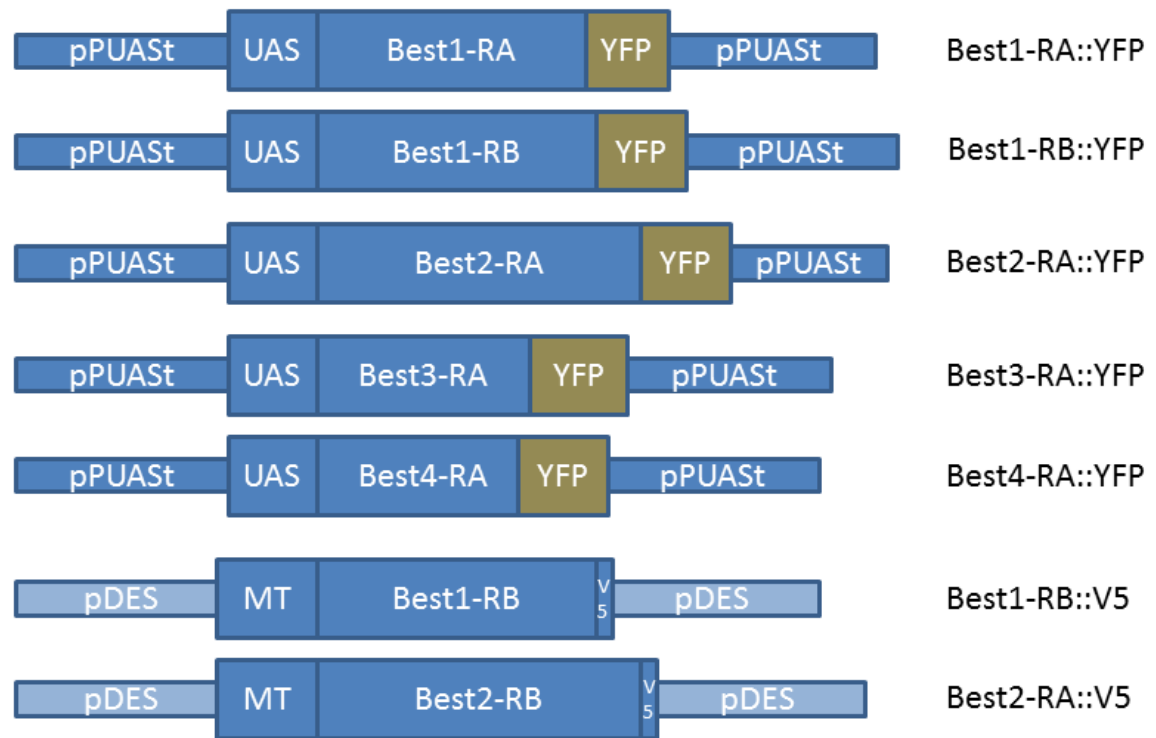


**Figure 6-7 Bestrophin translational fusion constructs.**

Several variants of bestrophin (YFP or V5) fusion constructs were generated for localisation of bestrophins in *Drosophila* S2 cells (pDES constructs) *in vitro*, and in tissues (pPUASt constructs) *in vivo*.

#### 6.2.4.1 *In vitro* localisation

*Best1-RA::YFP* and *Best1-RB::V5* were transiently transfected into S2 cells. Using immunocytochemical localisation *Best1-RB-V5* was detected using  $\alpha$ -V5 antibody (as the other transcript was fused with the YFP for localisation). Both the isoforms found in the plasma membranes of the S2 cells and showed colocalisation, as if they form dimers or multimers (Figure 6-8). In addition, a significant fraction of these fusion proteins is found intracellular.

*Best2* has one annotated transcript; accordingly it was cloned into pPUASt for localisation studies in S2 cells. The S2 cells were transiently transfected with the pPUASt-*Best2::YFP* along with a DES-GAL4 construct (that induces the expression upon CuSO<sub>4</sub> addition). The fluorescent imaging of the transfected cells revealed *Best2* localisation in the vesicular-like structures, like the ones that were observed for the peroxisomal localised SPOCk-C in previous findings (Southall et al., 2006). Unlike *Best1*, *Best2* did not show any plasma membrane localisation (compare Figure 6-8 with Figure 6-9). To confirm if *Best2* colocalises with the SPOCk-C, *Best2::YFP* transfected S2 cells were stained with  $\alpha$ -SPOCk-C antibody.

Indeed, Best2 colocalised with SPoCk-C, indicating Best2 probable localisation in peroxisomes (Figure 6-9).

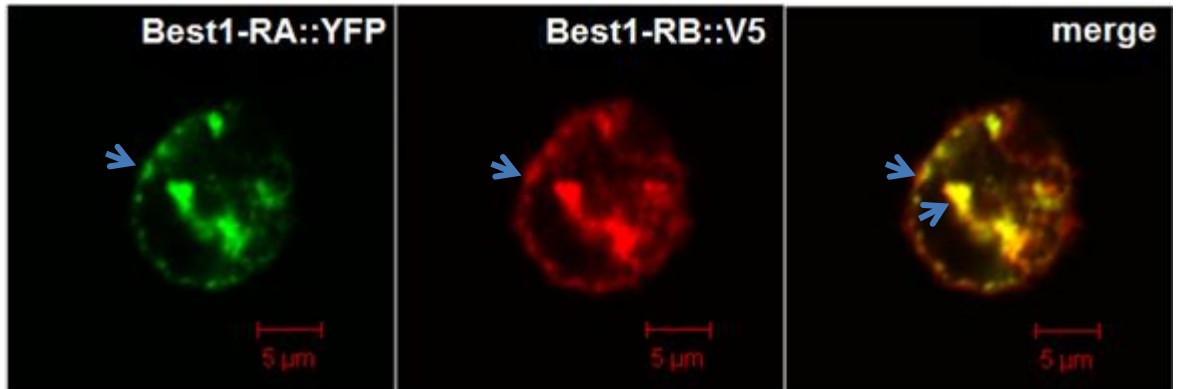


**Figure 6-8 Best1 localisation in S2 cells.**

The two isoforms of Best1 (RA & RB) translationally fused to YFP and V5 epitope tag respectively. They were constructed into the DES system and cotransfected into S2 cells. The expression was induced using  $\text{CuSO}_4$ , as the DES systems has  $\text{CuSO}_4$ -responsive metallothionein promoter, and the fusion proteins were in frame with the promoter. After 72 h of induction of expression, cells were washed, and fluorescent immunocytochemical (ICC) localisation was performed using confocal microscopy. The isoform A was localised using YFP fluorescence, and the isoform B was localised using  $\alpha$ -V5 antibody staining using rhodamine conjugated secondary antibody. Both the isoforms show significant overlap in localisation in plasma membranes and in the intracellular space (arrow heads).

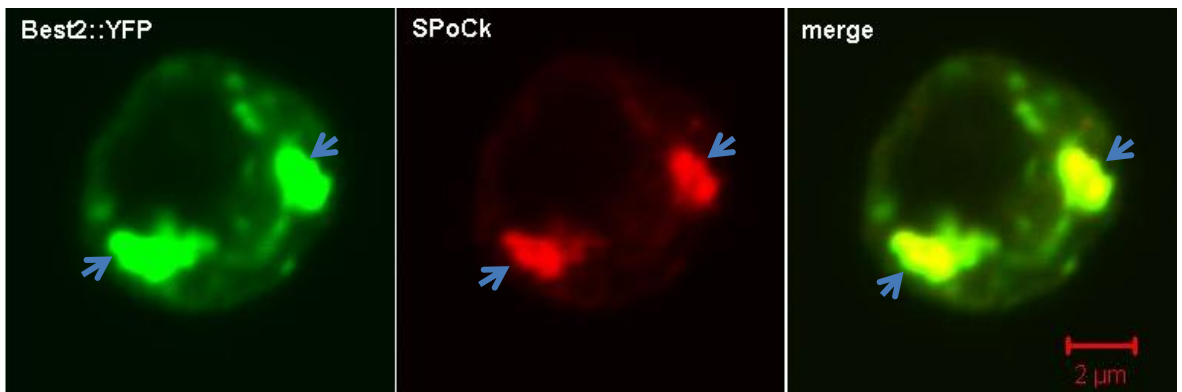


**Figure 6-9 Best2 colocalises with native peroxisomal SPoCk-C in S2 cells.**

*Best2-YFP* transfected S2 cells were stained with  $\alpha$ -SPoCk antibody (1:1000) that was published in Southall et al., (2006). An  $\alpha$ -mouse rhodamine antibody (1:500) was used as the secondary antibody and imaged using a confocal microscope system. The colocalisation is shown in the 'merge' picture.

#### 6.2.4.2 *In vivo* localisation

The transgenic animals harbouring UAS fused *Best1* & *Best2* YFP fusion constructs (Figure 6-7) were first induced using GAL4/UAS system *in vivo* for protein localisations. In order to do that, stable fly lines containing *hs-GAL4*; UAS-Bestrophin-(YFP) homozygous on second and third chromosomes respectively were generated. Then these flies were heat shocked for 1 h, starting from their 4<sup>th</sup> day of emergence, from their pupal cases, for another 3 times, once a day.

After the heat shock induction of transgenes, various tissues were dissected and the YFP fluorescence patterns were visualised under a confocal microscope. Initial observations suggested Best1-YFP & Best2-YFP localised to apical plasma membrane (Figure 6-10A) and vesicular structures in the tubules (Figure 6-11A) respectively. The Best1-YFP apical localisation was confirmed by staining the tubules with Phalloidin (rhodamine-conjugated) that stains F-actin filaments of the apical microvilli, where both were found colocalised (Figure 6-10B). The vesicular pattern seen for Best2-YFP was comparatively similar to the previously found SPoCk-C tubule peroxisomal pattern (Figure 6-11B). Thus, the Best2-YFP tubules were stained with  $\alpha$ -SPoCk-C antibody and found that both Best2-YFP and SPoCk-C colocalise (Figure 6-11C).

To further confirm Best2-YFP localisation to peroxisomes *in vivo*, the stable flies were crossed to the flies harbouring peroxisomal-targeted aequorin (Aequorin<sub>perox</sub>). These flies were heat shock induced for the expression of the transgenes. Then, tubules were dissected out and immunostained using a rabbit  $\alpha$ -Aequorin antibody as the primary and  $\alpha$ -rabbit Texas-Red as the secondary antibodies. These were then stained with a nuclear stain DAPI and visualised under a confocal microscope.

The Best2-YFP colocalised with the Aequorin<sub>perox</sub>, confirming its peroxisomal localisation in tubules, and in various tissues (Figure 6-12). However, only some peroxisomes that show Aequorin<sub>perox</sub>, only show Best2-YFP (Figure 6-12, shown using light arrow heads).

The Best2 peroxisomal localisation was also confirmed using an independent approach by Western blotting technique. For this, peroxisomes were purified from the flies expressing Best2-aequorin fusion protein (hs-GAL4; UAS-Best2-Aequorin). The rest of the fraction was also collected to see if the protein was localised elsewhere besides peroxisomes.

The two protein fractions were separated on a sodium dodecyl sulfate polyacrylamide gel by electrophoresis (SDS-PAGE), and immunoblotted onto Hybond™ ECL (Amersham UK) nitrocellulose membrane. The blotted protein was detected using rabbit  $\alpha$ -Aequorin antibody as the primary and  $\alpha$ -rabbit Cy5-labelled antibody as the secondary antibodies. Then, the fluorescence was imaged using a Typhoon variable mode imager (GE Healthcare UK). The antibody detected a band of ~110 kDa in the peroxisomal protein fraction but not in the rest of the fraction (Figure 6-13). This was of the right size for the Best2-aequorin fusion protein, further confirming peroxisomal localisation of Best2.

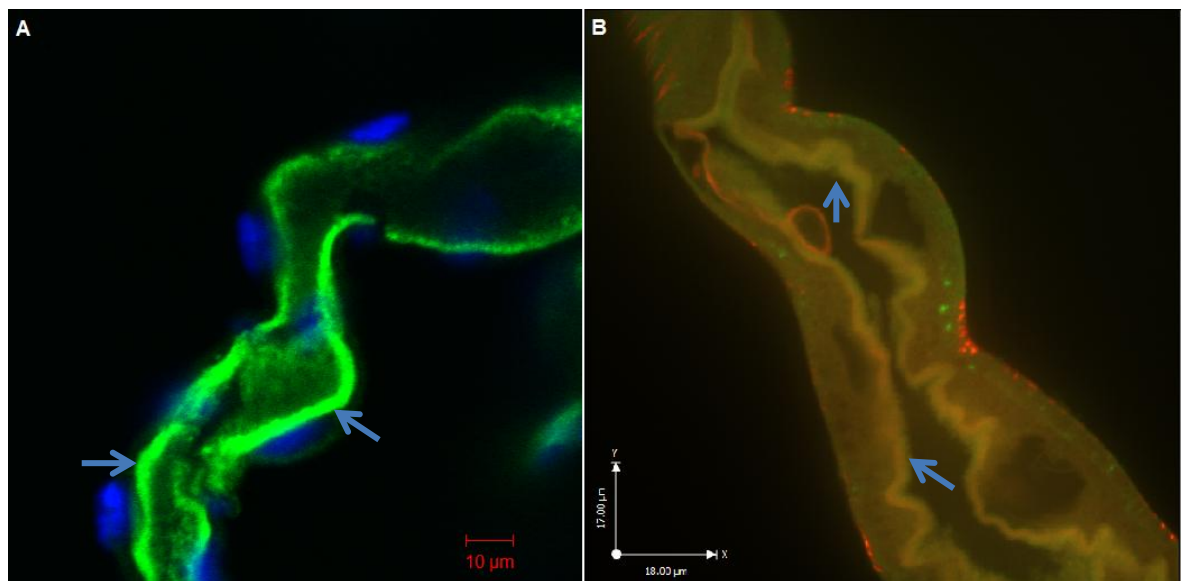


**Figure 6-10 Best1::YFP localises in the apical plasma membrane of the tubules.** UAS-Best1::YFP driven *in vivo* in the tubules using hs-GAL4 ubiquitously (A) and F-actin filaments were stained with phalloidin (B). The tubules were dissected out, formaldehyde fixed and stained with rhodamine conjugated phalloidin that binds with F-Actin filaments in the tubules. The nuclei were stained with DAPI and visualised under confocal microscope. The apical localisation is shown using arrow heads.

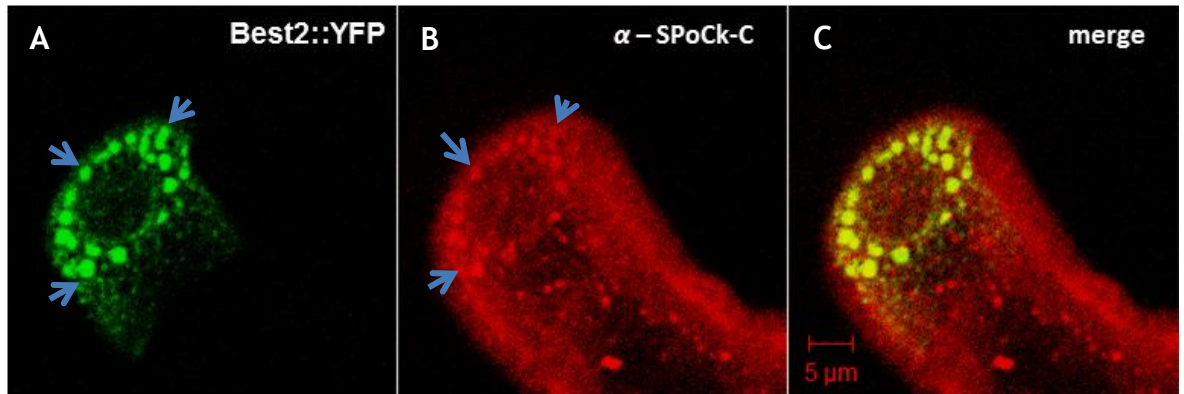


**Figure 6-11 Best2::YFP colocalises with peroxisomal SPoCk-C in tubules.** UAS-*Best2::YFP* was driven ubiquitously, *in vivo*, in the tubules using *hs-GAL4*, and stained with  $\alpha$ -SPoCk-C antibody (1:200). The representatives of peroxisomal location of the two proteins are shown using the arrow heads. The colocalisation is shown in the merge picture.

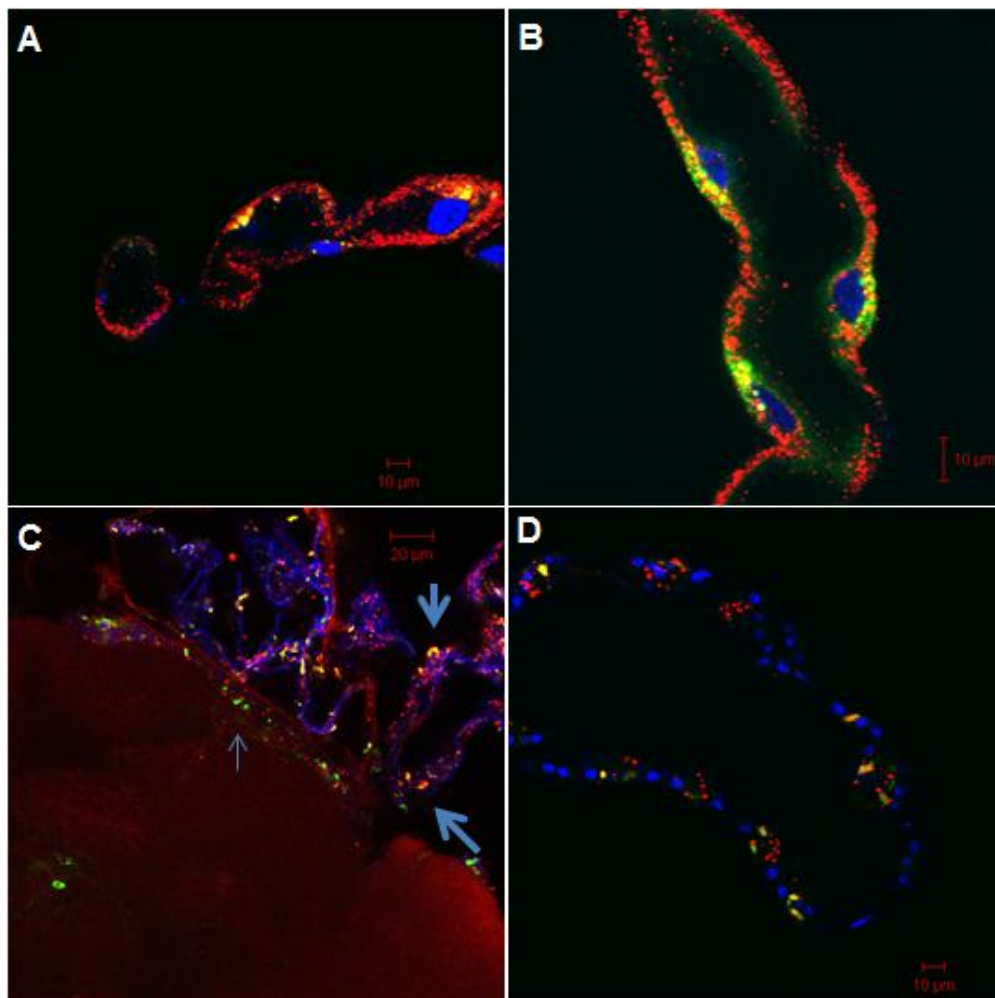


**Figure 6-12 Best2 is peroxisomal *in vivo*.** The colocalisation of Best2-YFP with Aequorin<sub>perox</sub> *in vivo* in various adult *Drosophila* tissues is shown. The tissues expressing *Best2-YFP* and Aequorin<sub>perox</sub> dissected out and formaldehyde fixed. They were then stained with rabbit  $\alpha$ -aequorin antibody as the primary and  $\alpha$ -rabbit alexa-fluor as the secondary antibodies. The tissues shown include tubules (A & B), trachea (C, thick arrow heads) and male accessory gland (D). Peroxisomal localisation of both Best2-YFP and Aequorin<sub>perox</sub> is shown using thick arrow heads. However, only some peroxisomes that show Aequorin<sub>perox</sub>, only show Best2-YFP (shown using light arrow heads).

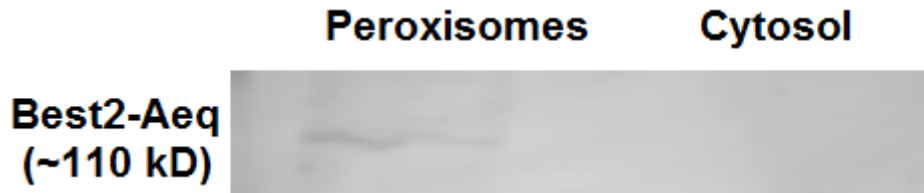


**Figure 6-13** Western blot of Best2-Aeq from the protein extracted from the purified peroxisomes.

Best2-Aeq was expressed in the whole flies using *hs-GAL4* and peroxisomes were purified from the rest of fraction. Then both protein fractions were run on a polyacrylamide gel by electrophoresis and blotted on to the nitrocellulose membrane. The protein fractions were probed using rabbit  $\alpha$ -aequorin as primary and  $\alpha$ -rabbit Cy5 as the secondary antibodies. The right sized fusion protein band of 110 kDa was observed.

### 6.2.5 Making of transgenic fly lines and their validation

Several transgenic RNAi fly lines for *Best1* & *Best2* were generated using the Gateway™ recombinant vector pRISE to clone the inverted double-stranded complementary RNA. The Gateway™ destination vector consists of a *P*-element for genomic integration by the help of a *P*-transposase, in *Drosophila* germline, to segregate into successive generations through recombination. Using white marker, the transformants were selected and made either homozygous or heterozygous (if they were homozygous lethal, they were stabilised over balancer chromosomes as heterozygous insertions). Then, the fly lines were validated using GAL4/UAS bipartite system by driving the transgene expression using a variety of cell- or tissue-specific GAL4s or using a ubiquitous GAL4 such as Act5C-GAL4 or *hs-GAL4*.

The RNAi fly lines were validated using a ubiquitous GAL4, either Act5C-GAL4 or *hs-GAL4* (where the induction of the transgene was lethal using Act5C-GAL4) was used. Using qPCR, the percentage of knockdown or overexpression was quantified to proceed to functional studies. The absolute percentage of knockdown for UAS-*Best1*-RNAi, driven by Act5C-GAL4, was 66% (*t*-test,  $P < 0.0001$ ) to its heterozygous parental control (Figure 6-14). A *Best1* deletion line along with a rescue line (kind gift from Dr. Edward Blumenthal, Marquette University, USA) (Tavsanli et al., 2001), were validated using qPCR for expression, and found to be a complete null (Figure 6-14).

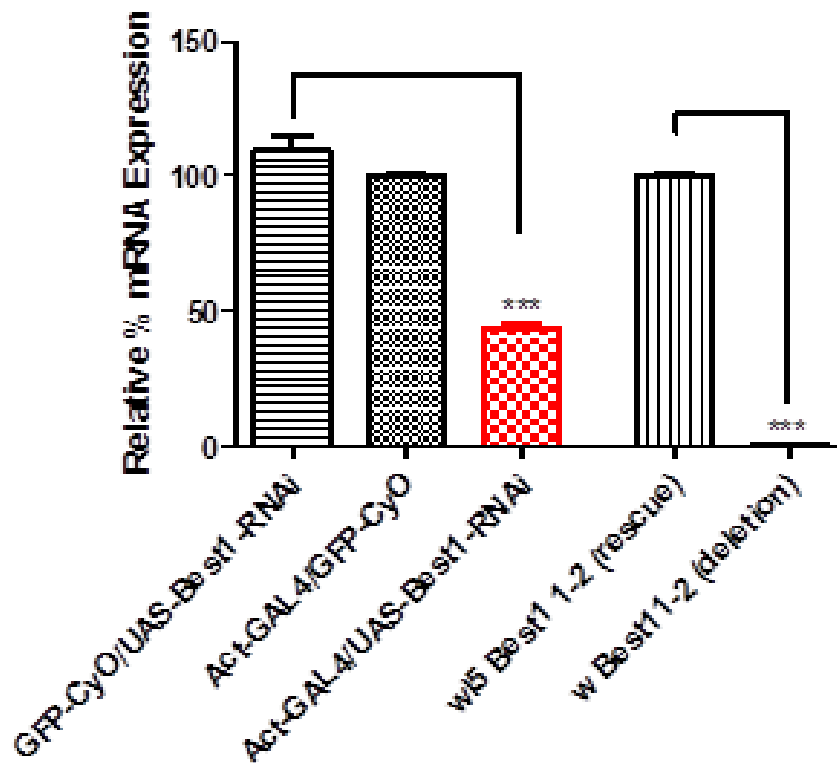


Figure 6-14 qPCR validation of *Best1-RNAi* and deletion flies.

RNAi for *Best1* was induced *in vivo* using GAL4/UAS system with a ubiquitous GAL4 driver, Act5C-GAL4. A qPCR was run, and expression was compared against the UAS-parental control. The *Best1* expression was reduced significantly in the RNAi induced flies than the controls (*t*-test,  $P < 0.0001$ ) with an absolute mean difference of 66%. The *Best1* deletion line was compared with the rescue line and found that the deletion line was a complete null (*t*-test,  $P < 0.0001$ ).

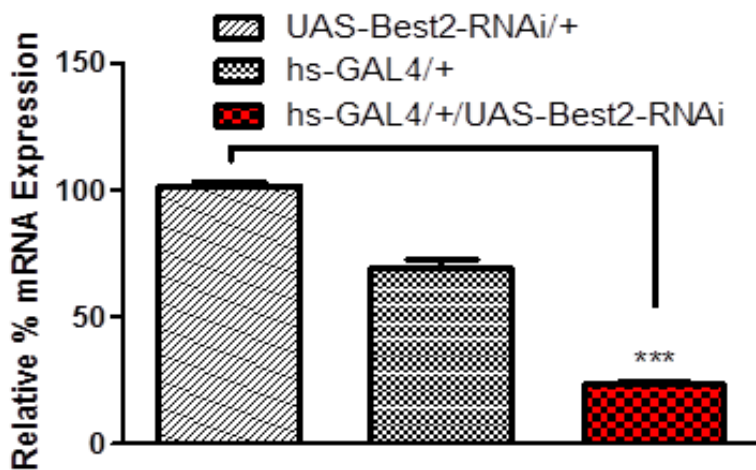


Figure 6-15 qPCR validation of *Best2-RNAi* knockdown.

The *Best2-RNAi* was driven conditionally in the adult flies using hs-GAL4. The RNAs were extracted and qPCR was performed. A significant knockdown of *Best2* expression was found in hs-GAL4>*Best2-RNAi* flies when compared to the heterozygous controls, with an absolute percentage mean difference of 78% (*t*-test,  $P < 0.0001$ ).

The UAS-*Best2-RNAi* was driven using hs-GAL4, as the Act5C-GAL4 showed lethality at the pupal stages of the fly development (Figure 7-3).

After the heat shock regimes, a qPCR was performed to validate the knockdown of gene expression. The percentage of knockdown was found to be 78% (*t*-test,  $P < 0.0001$ ) to its heterozygous parental control (Figure 6-15).

### 6.2.6 Salt and fluid regulation

Salt and fluid regulation is one of the important aspects of  $\text{Cl}^-$  channel function. Many of the epithelial  $\text{Cl}^-$  channels are involved in the transepithelial transport, fluid secretion, and cell volume regulation. *Best1* shows an interesting expression pattern across the major epithelial tissues as well as neuronal tissues (Table 6-1). However, *Best2* is the most abundant in the epithelial tissues, and in contrast with *Best1*, it is not significantly found in the neuronal tissues (Table 6-1). The epithelial abundance led to the investigation of survival analysis of RNAi and deletion flies on food containing elevated levels of salt and osmotic dietary conditions, to explore their potential functions in salt homeostasis. The high salt food regime consisted of normal food with an additional 4% NaCl. The high osmotic food regime consisted of normal food with the addition of 15% sorbitol.

#### 6.2.6.1 *Best1*

The transgenic flies used for *Best1*, including the flies, consisting of double stranded RNAs under the control of an upstream promoter element, UAS ( $w^+$ ;  $+/+$ ; UAS-*Best1*-RNAi) and the flies consisting the GAL4 transcription factor with an upstream enhancer element for Act5C (Act5C-GAL4), useful for ubiquitous expression of transgenes.

The transgenic animals of F1 generation, used for salt survival analysis, were contained in Act5C-GAL4 and UAS-*Best1*-RNAi, heterozygous on second and third chromosomes respectively ( $w^+$ ; Act5C-GAL4/ $+$ ; UAS-*Best1*-RNAi/ $+$ ). Essentially, the GAL4 induces RNAi ubiquitously all over the fly across the developmental stages. The F1 controls for these flies were their heterozygous CyO and UAS-*Best1*-RNAi on second and third chromosomes respectively ( $w^+$ ; CyO/ $+$ ; UAS-*Best1*-RNAi/ $+$ ). To control for the Actin-GAL4 insertion, an F1 progeny,  $w^+$ ; Act5C-GAL4/ $+$ ;  $+/+$  was also used.

In addition to GAL4/UAS system, a deletion mutant of *best1*, *w<sup>1</sup>; best11-2*, was also used, in which the entire gene has been removed by recombination along with a transgenic rescue line, *w<sup>1</sup>λ5; Best1 1-2*. These flies are viable and fertile and do not affect the photoreceptor cell integrity (Tavsanli et al., 2001).

Once the flies emerged from their pupal cases, they were collected as a batch of 20 flies in a vial and left for a day. Then they were separated as males and females into the food vials for another 3-4 d. At the age of 4-5 d, they were transferred into the food vials containing additional amounts (3% and 4%) of NaCl, and the number of dead flies was counted every 12-24 h. The same was repeated for the sorbitol survival assays with 15% sorbitol in the food for delineating the osmotic stress from the salt stress. The survival rates were plotted as percentage of survival on Y-axis over time on X-axis.

The ability of the flies to survive on a high NaCl diet was severely affected in the flies with reduced levels of *Best1* expression. The *Best1* knockdowns, both males and females, showed decreased survival rates than the control flies upon 4% NaCl feeding (Figure 6-16 M & F). However, the same survival phenotype was not seen with high sorbitol feeding, during the same time periods (Figure 6-16, dimmed lines).

Salt survival assays using *Best1* deletion flies confirmed the above findings using GAL4/UAS systems, where decreased survival was observed upon 4% NaCl feeding for the deletion flies comparatively with their genomic rescue flies (Figure 6-17). In contrast to their sensitivity to high salt, both the deletion and knockdown flies survived well on food containing 0.8M sorbitol over the same time periods (Figure 6-17, dimmed lines).

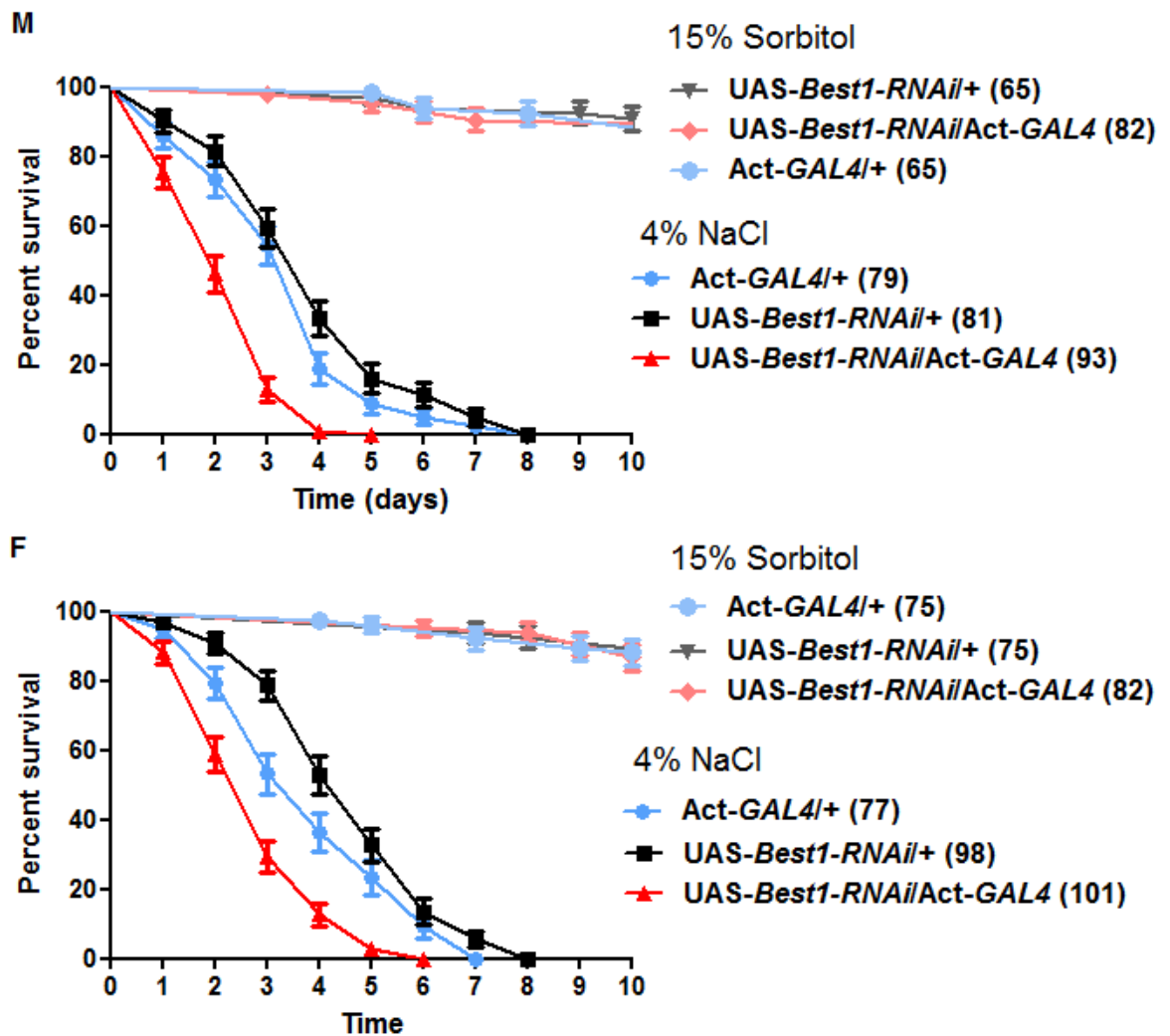


Figure 6-16 Salt sensitivity of *Best1-RNAi* knockdowns driven using *Act5C-GAL4*.

Once mated (males and females were kept in the same vial for 48 h) females were grown on normal food until the age of 3 days and then transferred on to the high salt (4% NaCl) or high osmotic (15% sorbitol) food regime. The survival counts were performed once a day. Survival curves for salt are shown in brighter colours, and the same for sorbitol are shown in dimmed colours. *Best1-RNAi* knockdown flies (red lines), both males (M) and females (F) showed marked decrease in ability to cope with high salt diet, than their controls (blue and black lines).

Median survival for males: Act-*GAL4*/+, 4 days; UAS-*Best1-RNAi*/+, 4 days; UAS-*Best1-RNAi*/Act-*GAL4*, 2 days. A Log-rank (Mantel-Cox) statistical algorithm was used to test the significance of difference between two survival curves; accordingly a *P*-value was obtained to denote the significance.  $P < 0.0001$  for comparisons of UAS-*Best1-RNAi*/Act-*GAL4* versus UAS-*Best1-RNAi*/+ and UAS-*Best1-RNAi*/Act-*GAL4* versus Act-*GAL4*/+. However, the same sensitivity was not observed on high sorbitol diet during the same time period.

Median survival for females: Act-*GAL4*/+, 4 days; UAS-*Best1-RNAi*/+, 5 days; UAS-*Best1-RNAi*/Act-*GAL4*, 3 days. A Log-rank (Mantel-Cox) statistical algorithm was used to test the significance of difference between two survival curves; accordingly a *P*-value was obtained to denote the significance.  $P < 0.0001$  for comparisons of UAS-*Best1-RNAi*/Act-*GAL4* versus UAS-*Best1-RNAi*/+ and UAS-*Best1-RNAi*/Act-*GAL4* versus Act-*GAL4*/+. However, the same sensitivity was not observed on high sorbitol diet during the same time period.

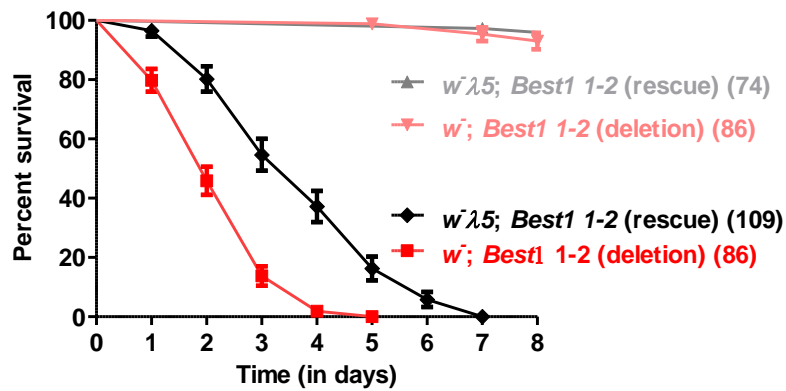


Figure 6-17 Salt sensitivity of *Best1* deletion.

Survival assays were performed similarly as in Figure 6-16, but by using *Best1*-deletion flies versus a genomic rescue flies. Data are only presented for male flies. This analysis also confirmed the role of *Best1* in the regulation of high salt concentrations. Median survival:  $w^{\lambda 5}; Best1\ 1-2$ , 4 days;  $w; Best1\ 1-2$ , 2 days. A Log-rank (Mantel-Cox) statistical algorithm was used to test the significance of difference between two survival curves ( $P < 0.0001$ ). However, the same sensitivity was not observed on high sorbitol diet during the same time period.

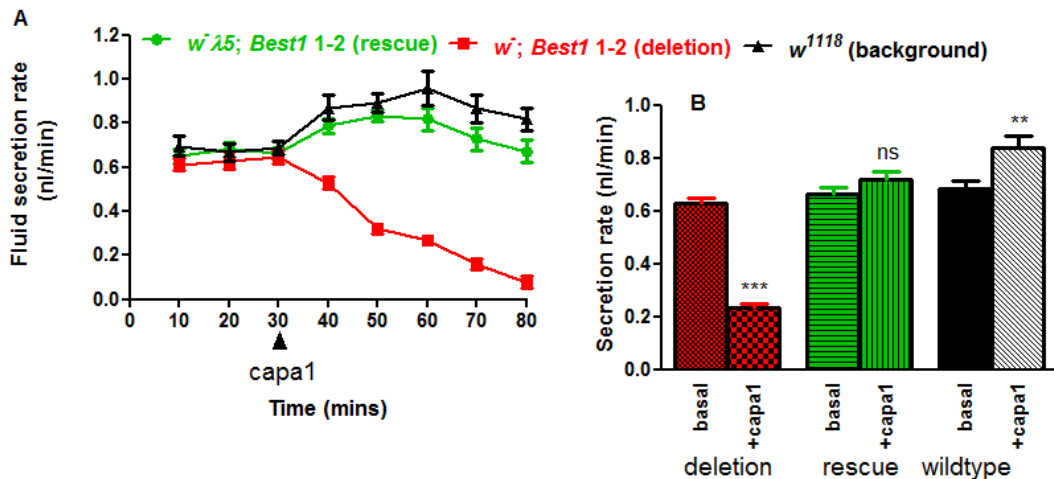


Figure 6-18 (A)  $Ca^{2+}$  agonist, capa1 inhibits fluid secretion in *Best1* deletion flies.

Tubule secretion assays were performed using modified Ramsay assay (Section 2.25). The  $Ca^{2+}$  agonist capa1 was added after 30 min of basal readings for every 10 min. An additional 50 min of secretion reading were taken for every 10 min. (B) The secretion rates were averaged as basal and capa1-stimulated and presented as a graph for statistical significance using a *t*-test, *P*-value. In deletions the capa1 inhibits secretion significantly from basals with a mean difference of  $0.396 \pm 0.026$  (*t*-test,  $P < 0.0001$ ) (red line), although it was not changed significantly in the rescue line (green line). The secretion went significantly up in the wildtype with a mean difference of  $-0.15 \pm 0.054$  (*t*-test,  $P < 0.05$ ) (black line).

Tubule secretion assays were successful with *Best1* deletion line, compared against its genomic rescue and a wildtype control. Although the basal (unstimulated) rate of fluid secretion was not significantly changed, the  $Ca^{2+}$  agonist, capa1 stimulated secretion was significantly inhibited in the deletion line when compared to the rescue and wildtype control (Figure 6-18).

This clearly demonstrates a potential role for Best1 in the stimulated  $\text{Ca}^{2+}$ -dependent secretion.

### 6.2.6.2 Best2

The transgenic flies used for *Best2* include the flies consisting of double stranded RNAs under the control of UAS ( $w^-; +/+; \text{UAS-}Best2\text{-RNAi}$ ), and the flies consisting the GAL4 transcription factor with an upstream heat-shock promoter (*hs-GAL4*), useful for conditional ubiquitous expression (unlike *Act5C-GAL4*) of transgenes, thus to mitigate the developmental lethality caused by the RNAi expression before adult emergence.

The above two flies were crossed and the F1 progeny ( $w^-; +/+; \text{UAS-}Best2\text{-RNAi}/hs\text{-GAL4}$ ) were assessed using salt survival analysis. The two parents of the F1 progeny were crossed into a wildtype background and used as heterozygous controls. These had the genotype  $w^-; +/+; hs\text{-GAL4}/+$  and  $w^-; +/+; \text{UAS-}Best2\text{-RNAi}/+$ . The F1 progeny were collected as a batch of 20 flies in a vial and left for two days. Then they were separated as males and females into the food vials for another 3-4 d, and heat shocked every day for 30 min at 37°C in an incubator. At the age of 4-5 d, the flies were transferred into the food vials containing additional amounts of NaCl (+4%), and the number of dead flies was counted every 12-24 h. The heat shocks were continued every 48 h until all the flies were counted dead. The survival rates were plotted as percentage of survival on Y-axis over time on X-axis.

Survival analysis was performed separately for males and females. In contrast to *Best1*, the *Best2* knockdowns (both males and females) showed increased survival rates than the control flies upon the salt feeding (Figure 6-19 M & F).

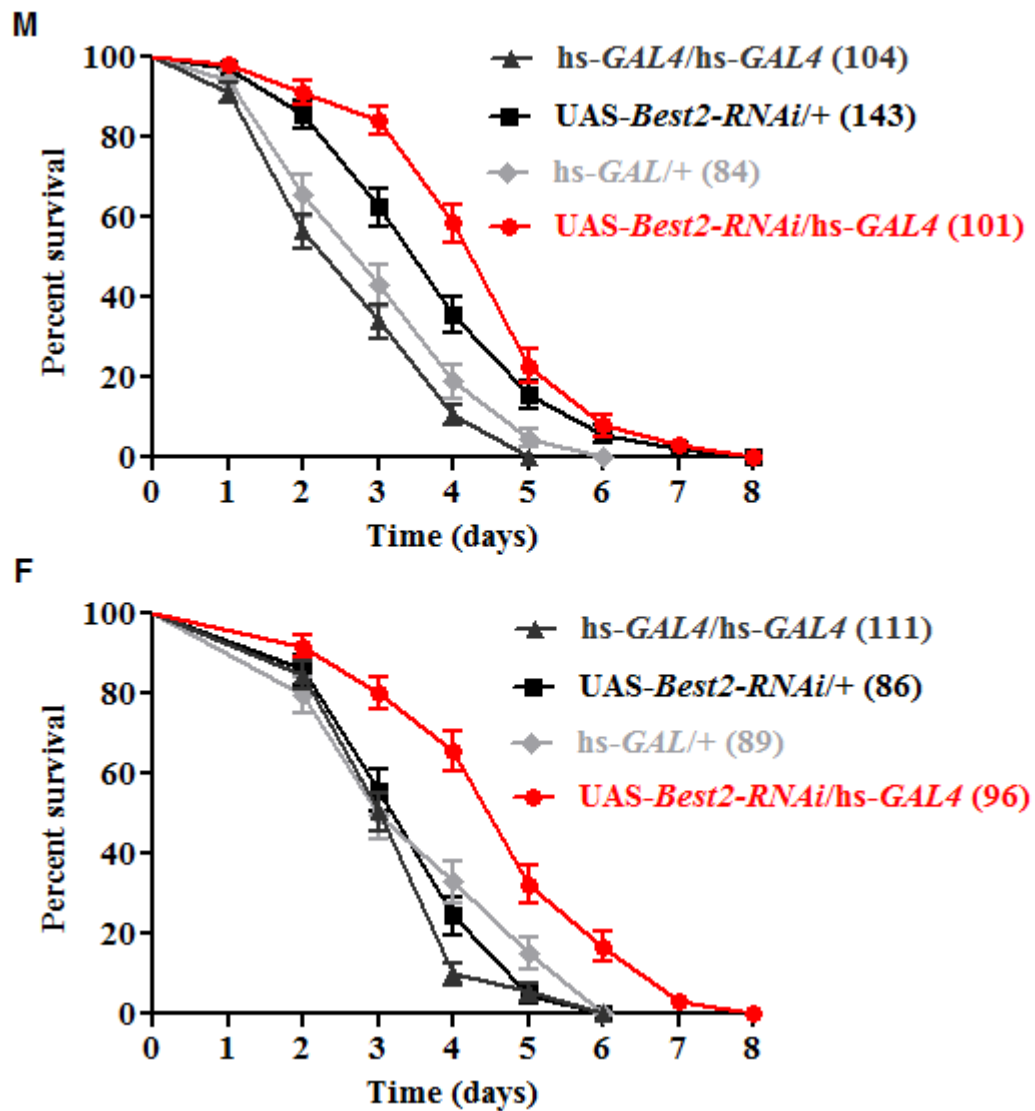


Figure 6-19 *Best2* knockdowns show increased salt resistance.

The protocol of salt survival was exactly followed like that of *Best1* assays on 4% NaCl food regimes. *Best2-RNAi* knockdown flies (red lines), both males (M) and females (F) showed marked increase in ability to cope with high salt diet, than their controls (black and hash colour lines).

Median survival for Males: *hs-GAL4/hs-GAL4*, 3 days; *UAS-Best2-RNAi/+*, 4 days, *hs-GAL4/+*, 3 days and *UAS-Best2-RNAi/hs-GAL4*, 5 days. A Log-rank Mantel-Cox statistical algorithm was used to test the significance of difference between RNAi versus control survival curves; accordingly a *P*-value was obtained to denote the significance.  $P < 0.0001$  for RNAi versus controls separately.

Median survival for Females: *hs-GAL4/hs-GAL4*, 4 days; *UAS-Best2-RNAi/+*, 4 days, *hs-GAL4/+*, 3 days and *UAS-Best2-RNAi/hs-GAL4*, 5 days. A Log-rank Mantel-Cox statistical algorithm was used to test the significance of difference between RNAi versus control survival curves; accordingly a *P*-value was obtained to denote the significance.  $P < 0.0001$  for RNAi versus controls separately.

### 6.2.7 *Best3* & *Best4* show high mRNA expression in the testis

*Best3* and *Best4* show an interesting genomic location in the fly because they are in close inverted repeat, suggesting recent gene duplication (Figure 6-20).

According to the FlyAtlas, they are specifically enriched in the testis.

Developmentally, *Best4* but not *Best3* is expressed between 8-14 h of embryonic development according to the highthroughput sequencing data of the FlyBase.

However, both show consistent regulation from third-instar larval stage.

When *Best3* and *Best4* were targeted using RNAi, *in vivo*, using GAL4/UAS system, with Act5C-GAL4 ubiquitous driver, RNAi for *Best3* but not *Best4* was lethal at pupal stages.

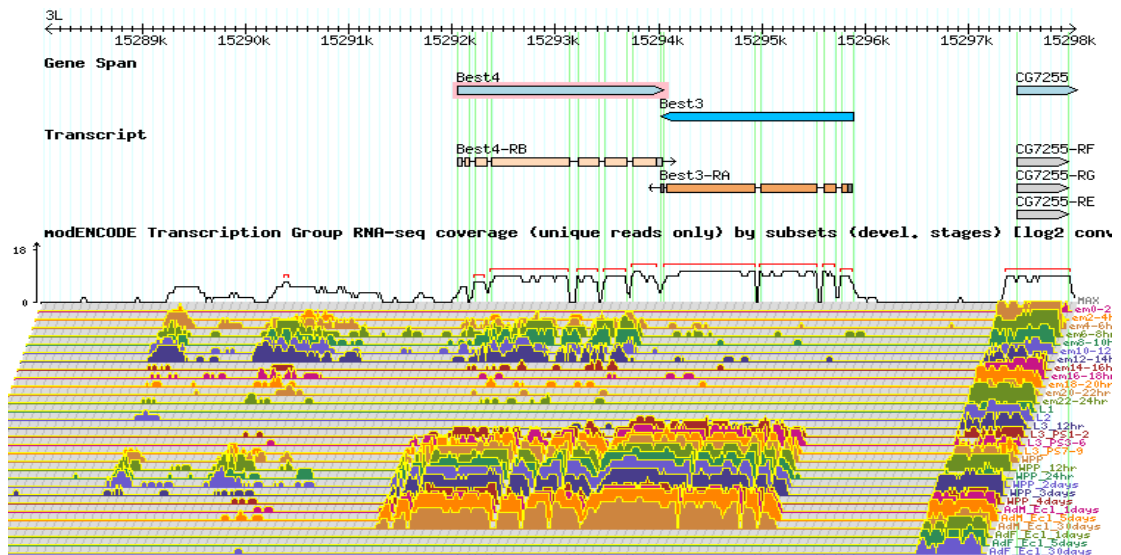


Figure 6-20 Genomic organisation of *Best3* & *Best4*.

*Best3* and *Best4* are transcribed from minus and plus strands of the 3L chromosome respectively (upper panel). Each has one annotated transcript and show differential expression between 8-14 h of embryonic development (lower panel). (Data obtained from Flybase.org on 12<sup>th</sup> Dec, 2011.)

### 6.2.8 *Best3* and *Best4* localisations

#### 6.2.8.1 *In vitro* localisation

The S2 cells were transiently transfected separately with *Best3::YFP* and *Best4::YFP* and induced for expression for 48 h. Then, they were washed with PBS and formaldehyde fixed. The nuclei were DAPI stained, and the cells were imaged using a confocal microscope system. Both fusion proteins showed distinct immunofluorescence patterns, in that, *Best3::YFP* may represent intracellular vesicles and *Best4::YFP* represents endoplasmic reticulum (ER) (Figure 6-21).

### 6.2.8.2 *In vivo* localisation

For the *in vivo* localisation, the Best3::YFP and Best4::YFP fusion constructs were expressed using the Act5C-GAL4 and found that the overexpression of Best3::YFP overexpression was semilethal as some escapers come out this cross and Best4::YFP overexpression was complete lethal. The lethality was at pupal stages. Furthermore, the escapers of Best3::YFP overexpression show morphologically defective testis (Figure 6-23). Then these were conditionally expressed using hs-GAL4, as explained in the previous section to avoid the lethality, and imaged for localisation *in vivo*. As the mRNA was detectably found only in the testis, the testes were imaged. Both bestrophins showed distinct intracellular localisations in that Best3::YFP seems to be localised to vesicular-like structures and Best4::YFP to ER, like the *in vitro* patterns in S2 cells (Figure 6-22).

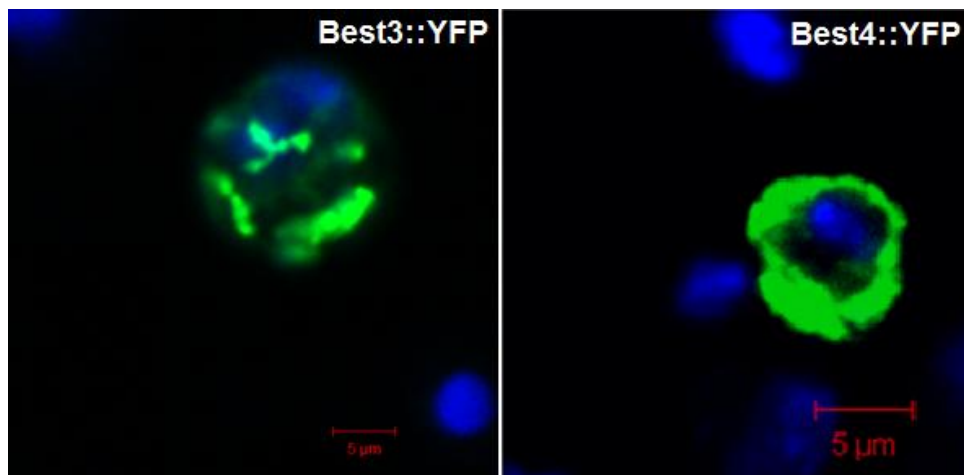


**Figure 6-21 Best3::YFP and Best4::YFP show distinct localisations in S2 cells.** The S2 cells were transfected with *Best3::YFP* and *Best4::YFP* and induced for expression for 48 h. The cells were then washed with PBS and formaldehyde fixed. The nuclei were stained using DAPI and visualised under a confocal microscope. The fluorescence patterns seems to be intracellular and not plasma membrane.

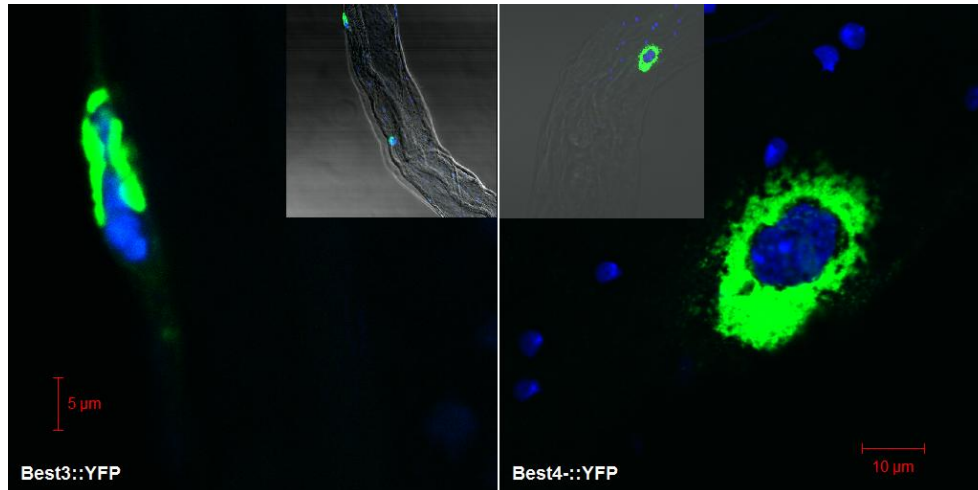


**Figure 6-22** Best3::YFP and Best4::YFP fluorescence was specifically found in the probable cyst cells of the testis *in vivo*.

*Best3-YFP* and *Best4-YFP* were expressed separately, using *hs-GAL4*, at the adult stages. The testes were dissected out and formaldehyde fixed and stained with a nuclear stain DAPI. A confocal microscope system was used to visualise the fluorescence. A magnified image from the inset (the probable cyst cell) is shown where the fluorescence was found. Although, both bestrophins were similarly localised to cyst cells of the adult testis, the intracellular localisation pattern seems to be different, in that, the Best3-YFP was localised to large vesicular-like structures and Best4-YFP was localised to ER-like network.

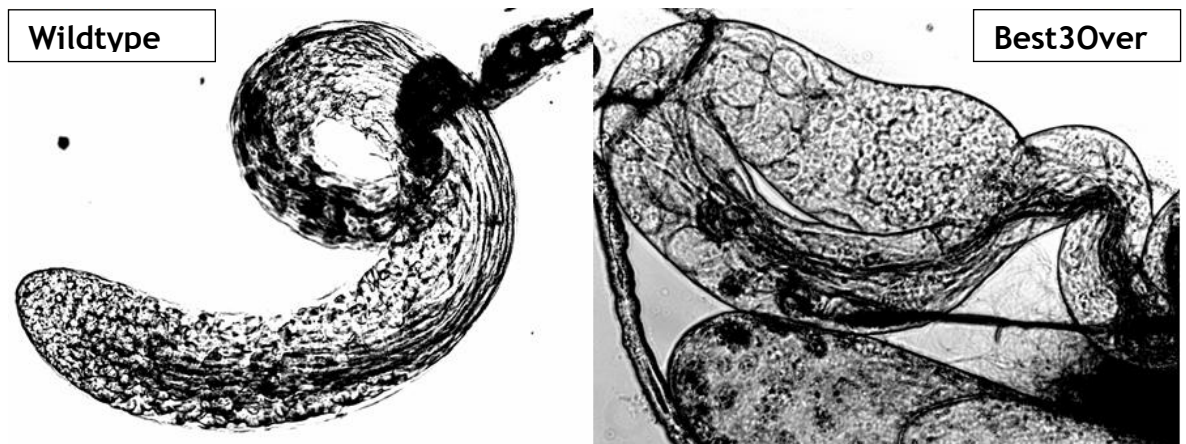


**Figure 6-23** Overexpression of *Best3* causes morphologically defective testis. The ubiquitous overexpression of *Best3* is semilethal and gives rise to few escaper flies. When the testes of the escapers were observed under a light microscope, they seemed morphologically defective.

## 6.3 Discussion

The reverse genetics approach, using a powerful model organism, where complementary approaches are possible, may help elucidate the functions of individual Cl<sup>-</sup> channels. To this end *Drosophila* is useful, with its powerful arsenal of post-genomic and physiological techniques to study organismal functions (Dow and Davies, 2003). In line with this theory, this study investigated organismal functions of bestrophins, and sets up a basis for further studies on bestrophin functions in general using *Drosophila* as a model organism.

*Drosophila* encodes all four of the homologs of human bestrophins. They show high sequence similarity at the N-terminus as revealed by the protein sequence alignment (Figure 6-3A). However, the C-terminus markedly differs between any two bestrophins. Interestingly, Best1 and 2 show putative Pglndn\_D\_rcpt and NADH plastoquinone oxidoreductase domain respectively (Figure 6-3B). The NADH oxidoreductase domain is only found in one other protein in the *Drosophila* euchromatic genome, called ND5. The ND5 complex participates in the mitochondrial electron transport chain. Interestingly, these domains have not been predicted for any other bestrophins except *Anopheles gambiae*.

The hydropathy analysis using two different programs suggested variable number of TMDs from 4 - 6. Interestingly, Best2 has only two predicted TMDs, atypical for an ion channel unless it complexes with any other subunits of a heteromultimer (Suzuki, 2006).

The expression patterns of the bestrophins have been investigated using FlyAtlas (Table 6-1). The *Best1* shows expression in the neuronal tissue in addition to the enrichment in the epithelial tissues. In contrast, *Best2* does not show detectable expression in the brain, although it is abundant in the eyes and other epithelial tissues (Table 6-1). The expression patterns of *Best1* and *Best2* were further confirmed by qPCR (Figures 6-4, 6-5 and 6-6). *Best3* and *Best4* were only found in the testis indicating specialised roles (Table 6-1).

Furthermore, *Best2* was highly enriched in the Ca<sup>2+</sup> storing anterior initial segment of the tubules compared to their posterior counterparts (Figure 6-5).

However, this distinction was not observed for *Best1*, although it showed female abundance (Figure 6-4). In contrast to *Best1* abundance in the neuronal tissue, *Best2* was highly enriched in the eyes (Table 6-1). In addition, *Best2* showed high abundance in the male accessory glands and spermatheca (Table 6-1). Both *bestrophins* were equally found in other epithelial tissues including salivary glands and hindgut indicating their potential roles in these tissues. The enrichment of *Best2* expression in the  $\text{Ca}^{2+}$  storing initial segment and the eyes suggest its potential epithelial roles, in that it may regulate  $\text{Ca}^{2+}$  transport or signaling. *Best1* does not seem to be an epithelial-specific gene, as it is also expressed in the neuronal tissue.

This study revealed for the first time *in vitro* and *in vivo* localisations for all four *Drosophila* bestrophins using bestrophin YFP fusion protein constructs. The localisations seem to differ markedly from one bestrophin to the other. Both the isoforms of *Best1* were predominantly found in the plasma membranes and showed significant intracellular trafficking *in vitro* (Figure 6-8). The *in vivo* localisation of *Best1* was interesting, in that, it was predominantly found in the apical plasma membranes of the tubules (Figure 6-10A). This was confirmed by the colocalisation of F-actin staining of phalloidin (Figure 6-10B). This localisation *in vivo* was in contrast to the hBest1 localisation as hBest1 was predominantly found in the basolateral membranes of RPE cells (Marmorstein et al., 2000). However, apico-basal polarisation of RPE cells is different from other epithelial tissues. For example the basolateral  $\text{Na}^+$ ,  $\text{K}^+$ , ATPase is polarised to apical membranes of the RPE (Strauss, 2005). In the tubules of *Drosophila*, an apical V-ATPase was thought to energise fluid secretion in the 'Wieczorek model' (Harvey and Wieczorek, 1997). However, a  $\text{Ca}^{2+}$ -activated  $\text{Cl}^-$  channel, such as *Best1* that is found in the apical membranes, was thought to explain secretion under stimulatory conditions upon which  $\text{Ca}^{2+}$  is elevated. To this end, the  $\text{Ca}^{2+}$  agonist *capa1* inhibited fluid secretion in the *Best1* deletion flies, in contrast to wildtype stimulatory action (Figure 6-18). This clearly demonstrates a role for *Best1* in  $\text{Ca}^{2+}$ -dependent apical secretion in the stimulatory conditions.

The intracellular trafficking of *Best1*, *in vitro*, may suggest mistargeting of overexpressed protein in the isolated cells as has been previously observed for bestrophin family members (Hartzell et al., 2008; Kunzelmann et al., 2007; Qu and Hartzell, 2004; Qu et al., 2003; Tsunenari et al., 2003).

However, some ClC channels have been found both in the plasma membranes and in the intracellular organelles (Jentsch et al., 2002).

In the airway epithelia, CFTR channels found to modulate the components of CaCCs channels at the apical plasma membranes. It also seems that CaCCs may compensate for the defective CFTR bicarbonate secretion (Zsembery et al., 2000). Interestingly, bestrophins have been shown to be highly permeable to  $\text{HCO}_3^-$  (Hartzell et al., 2008). These results suggest that CaCC activation could compensate for CFTR loss of function in cystic fibrosis, and that bestrophin may present an alternative target in cystic fibrosis. Thus, Best1 apical localisation may further provide evidence for an apical CaCC. Furthermore, in pancreatic acinal cells, cADPR and NAADP act through ryanodine receptors and elicit repetitive local  $\text{Ca}^{2+}$  spikes near apical membrane (Kunzelmann et al., 2007). This kind of mechanism may exist in the tubules that act to stimulates  $\text{Ca}^{2+}$ -activated  $\text{Cl}^-$  secretion given tubule apical membranes are packed with the mitochondria. The fluid secretion inhibition by the neuropeptide  $\text{Ca}^{2+}$  agonist capa1 (Figure 6-18) potentially reiterate such a mechanism in tubules for stimulatory apical secretion via the  $\text{Ca}^{2+}$ -activated  $\text{Cl}^-$  function of Best1. This finding coincides with the fact that several bestrophins including hBest1 are  $\text{Ca}^{2+}$ -activated with a  $K_d$  for  $\text{Ca}^{2+}$  between 150-200 nM (Hartzell et al., 2008). However, in the excised membranes patches endogenous *Drosophila* bestrophins seems to be activated by ATP, in addition to  $\text{Ca}^{2+}$  suggesting an interplay between ATP and  $\text{Ca}^{2+}$  that may regulate bestrophin CaCC function (Chien et al., 2006).

Best2, exclusively showed vesicular localisation *in vitro* (Figure 6-9), and *in vivo* (Figure 6-11) in various tissues (Figure 6-12). All the Best2-localised vesicles were confirmed to be peroxisomes. This localisation of Best2 is novel, and not reported for any other bestrophin. It is possible that, like ClCs, bestrophins may be important in the function of intracellular vesicles like peroxisomes. At least Best2 is such a candidate as it is highly found in the  $\text{Ca}^{2+}$  storing initial segment and colocalised with SPoCk-C (Figure 6-11). The SPoCk-C also coats the  $\text{Ca}^{2+}$  spherites that are highly abundant in the initial segment and into which  $\text{Ca}^{2+}$  is loaded (Southall et al., 2006).

For example, acidic stores like lysosomes and secretory granules act in concert with IP<sub>3</sub>-mediated ER and ryanodine receptor pathways where endocytosis plays key roles in the generation of repetitive local Ca<sup>2+</sup> spikes in the apical plasma membranes (Menteyne et al., 2006; Yamasaki et al., 2005).

Interestingly, accumulation of lipofuscin is the characteristic of Best disease, and in lysosomal storage diseases like neuronal ceroidlipofuscinosis (which leads to neurodegeneration). This led to the proposal that they may be involved in lysosomal function, as RPE cells are loaded with lysosomes, and these cells are involved in phagocytosis (Hartzell et al., 2008). Furthermore, the metabolic contributions of different organelles, in this case, for the proper function of photoreceptors, in different species may have emerged according to evolutionary pressures. As such, the localisation of Best2 may potentially be important for proper photoreceptor function in *Drosophila*, although no gross visual phenotypes were seen in the flies with reduced levels of expression of any of the bestrophins. The testes-specific Best3 and Best4 found to be intracellular both *in vitro* and *in vivo* and may represent vesicular and ER localisation respectively. These localisations themselves are fascinating in terms of the potential functional diversity of bestrophins.

The epithelial expression of *Best1* and *Best2* in *Drosophila* has given power to investigate their potential epithelial functions, for example in salt regulation. The salt sensitivity of flies with reduced or no expression of *Best1* suggest that it is an essential gene for regulating organismal excessive salt concentrations (Figure 6-16 & 6-17). However, when *Best1* was specifically reduced using a neuronal-specific GAL4, this phenotype was not seen indicating Best1 salt regulatory function via epithelial tissues (not shown). Furthermore, high sorbitol feeding (that induces osmotic stress) of the RNAi or deletion flies, did not affect the survival, within the similar time interval as observed upon NaCl feeding (Figure 16-16 & 16-17, dimmed lines). This suggests that NaCl feeding specifically induced the sensitivity but not the osmotic disturbance.

In contrast to *Best1*, *Best2* gene expression reduction did not affect the survival of the flies negatively, but rather it had a positive impact.

However, as one would expect, the dysfunction in an epithelial-specifically expressed  $\text{Cl}^-$  channel should make the flies more prone to high salt concentrations leading to the salt toxicity, and therefore a reduction in survival, as observed for *Best1*. Given the *Best2* expression in the  $\text{Ca}^{2+}$  storing initial segment of the tubules and eyes, it may allow one to draw a hypothesis that it may not be a  $\text{Cl}^-$  channel, rather a channel regulator and a better candidate in epithelial function as a whole. But, the whole point of studying bestrophins is that the dysfunction of human bestrophin causes retinal degeneration. However, a previous *Drosophila Best1* deletion model suggested *Best1* to be non-essential gene for fly viability and photoreceptor integrity (Tavsanli et al., 2001). The same study was extended as part of this thesis using *Best1* and *Best2* knockdowns separately or combined as double-knockdowns. This confirmed the previous observations that *Best1* was non-essential for the fly viability, but *Best2* in contrast is an essential gene at pupal development of the fly (Figure 7-3). Furthermore, both *Best1* and *Best2* knockdowns separately or combined did not show any gross morphological defects.

The most relevant model of human Best disease, 'bestrophin knockout mouse', did not phenocopy the human eye disease, and neither did it show any gross visual defect or retinal pathology (Marmorstein and Marmorstein, 2007). These observations suggest that bestrophins in different species may have different functional partners that may determine the overall function of the photoreceptors. The knockout mouse model of CFTR, did not show any disease pathology like human airway lung disease of CF patients (Guilbault et al., 2007). In this case, the  $\text{Cl}^-$  secretion was thought to be compensated by  $\text{Ca}^{2+}$ -activated  $\text{Cl}^-$  secretion. Thus, there may be a potential diversity in the functions of bestrophins, in that the compensatory mechanisms might rescue the dysfunction of bestrophins in these organisms. However, modelling the compensatory mechanisms might provide useful understanding of functions of these proteins in the model organisms.

The pH of the cellular compartments must be tightly regulated for the biological reactions to take place, and these must possess transporters in a complex bioenergetic framework. This may include a set of known  $\text{Na}^+$ ,  $\text{K}^+$  ATPases, V-ATPases,  $\text{Cl}^-$  channels,  $\text{K}^+$ ,  $\text{Na}^+/\text{H}^+$  exchangers.

In the endomembranes of endolysosomal pathway, however,  $\text{Cl}^-$  concentration has recently thought to be an important determinant of the vesicular function. Previously,  $\text{Cl}^-/\text{H}^+$  exchange rather the classical  $\text{Cl}^-$  channel function was thought to counteract the proton influx into the endosomes and lysosome mediated by V-ATPases (Scheel et al., 2005). However, mutants of ClC-5 and ClC-7 that uncouple  $\text{H}^+$  exchange and convert these exchangers to channels seem not to affect the pH of endosomes or lysosomes respectively. However, uncoupling mutants still show the pathological conditions like the knockouts of the same exchangers (Novarino et al., 2010; Weinert et al., 2010). These important findings led to the hypothesis that  $\text{Cl}^-$  concentrations might play essential roles in the function of the endomembranes. Previously, the allosteric effect of  $\text{Cl}^-$  was observed for intracellular ClCs (Davis-Kaplan et al., 1998). The localisation of Best2 to peroxisomes is the first ever identification of a probable channel to these organelles; although, it is not localised in all peroxisomes in various tissues (Figure 6-12). Given the importance of peroxisomes to the metabolic homeostasis, a  $\text{Cl}^-$  channel function of Best2 may show some insight into the function of peroxisomes. Furthermore, peroxisomes are the sites of  $\beta$ -oxidation of fatty acids second only to mitochondria. An interplay between  $\text{Cl}^-$  channels and fatty acids, at least in colonic epithelium, seems to exist. For example, the pharmacological agent, lubiprostone (Amitiza™), a functional fatty acid is used as the selective  $\text{Cl}^-$  channel activator which increases fluid secretion in chronic idiopathic constipation in adults.

It is also apparent that peroxisomes act as buffers of intracellular  $\text{Ca}^{2+}$  elevations, and may act as stores (Chapter 8) (Drago et al., 2008b; Lasorsa et al., 2008; Raychaudhury et al., 2006). Best2 colocalisation with SPoCk-C may indicate its potential role in the regulation of intracellular  $\text{Ca}^{2+}$  concentrations.

$\text{Ca}^{2+}$ -activated  $\text{Cl}^-$  channels are involved in epithelial salt transport and in regulation of several different physiological processes (Jentsch et al., 2002). The Malpighian tubules and hindgut of *Drosophila*, comprise the insect excretory systems, thus are important osmoregulatory organs. The tubules are the fastest known fluid secreting epithelium (Dow et al., 1994b; Maddrell, 1991).

Fluid secretion into the Malpighian tubule lumen is driven by an apical proton pump coupled to both apical and basolateral  $\text{Cl}^-$  conductances (O'Donnell et al., 1998).

The neuropeptide diuretic agents such as leucokinin and tyramine stimulate fluid secretion via opening a CaCC conductance in the stellate cells (Blumenthal, 2003; O'Donnell et al., 1998; Terhzaz et al., 1999a). In contrast, capa neuropeptide acts on principal cells, elevates intracellular  $\text{Ca}^{2+}$  leading to the increased fluid secretion (Rosay et al., 1997). Thus, the elevated  $\text{Ca}^{2+}$  levels may act on an apical CaCC, potentially Best1, leading to the increases in fluid secretion.

Luminal positive voltage gradients generated by V-ATPases of endomembranes of vertebrates and apical plasma membranes of insects seems to be counteracted by ClC exchangers and NHA(E) exchangers/antiporters respectively through  $\text{Cl}^-/\text{H}^+$  or  $\text{Na}^+$  or  $\text{K}^+/\text{H}^+$  exchange. This is because of the concentration gradients of  $\text{Cl}^-$  and  $\text{K}^+$  or  $\text{Na}^+$  exists in the cellular milieu. For example,  $\text{K}^+$  gradients are generated in the insect midgut goblet cells to counteract V-ATPase generated  $\text{H}^+$  luminal concentrations (Dow, 1989; Wieczorek et al., 1986). Upon hypotonic stress conditions, signal cascades open  $\text{Cl}^-$  selective channels and allow passive  $\text{Cl}^-$  outflow to decrease the osmotic pressure.

However, under hypertonic conditions when haemolymph concentrations of the fly increase for example, primary regulatory mechanisms will be activated in the osmoregulatory organs like tubules and hindgut to counter high salt concentrations thereby to decrease the toxicity of ions to the cells (Naikkhwah and O'Donnell, 2012). Hypertonic conditions may activate transient influx of  $\text{Ca}^{2+}$  into the tubule cells that may lead to the activation of  $\text{Cl}^-$  channels. This increases  $\text{Ca}^{2+}$ -activated  $\text{Cl}^-$  secretion followed by water and  $\text{Na}^+$  ions excreted into the lumen for their eventual removal out of the body. It is highly possible that Best1 may mediate  $\text{Ca}^{2+}$ -activated  $\text{Cl}^-$  secretion, thereby contributes to the organismal ionic homeostasis. This idea is supported by the fact that the flies with reduced or no expression of *Best1* become salt sensitive (Figure 6-16 & 6-17).

High sorbitol feeding, in contrast to salt feeding, does not cause the *Best1* knockdowns or deletion flies to be sensitive indicating it might not be a candidate VRAC (Chien and Hartzell, 2007). Thus, the disruption of *Best1* expression does not cause flies to be osmosensitive, unlike disruption of the *inebriated* gene (Huang et al., 2002); rather the disruption causes sensitivity to the salt. These data clearly suggest a role for *Best1* in the salt regulation, as might be expected to result from defective  $\text{Cl}^-$  transport. Thus, at least, *Best1* may facilitate  $\text{Ca}^{2+}$ -activated  $\text{Cl}^-$  currents, or it may be a component of a  $\text{Cl}^-$  channel complex, and are likely to play a very important role in epithelial salt homeostasis.

The salt resistance phenotype of *Best2* (Figure 6-19) is further investigated in the next chapter (Chapter 7).

## 6.4 Conclusion

This is the first ever study investigating organismal functions of bestrophins using *Drosophila* as a model organism in an integrative physiology approach. The reverse genetics approach using GAL4/UAS system, proved useful to assess the contributions of bestrophins for whole organismal function. This approach revealed *Best2* and *Best3* as essential genes for the fly viability, while it further confirmed *Best1* as a nonessential gene for fly viability. Furthermore, the knockdown of *Best1* or *Best2* separately and combined did not show any gross morphological defects. *Best1* seems to be important in regulating ionic homeostasis, as it has been revealed by salt survival assays. Furthermore, fluid secretion study identified *Best1* as a potential CaCC. Interestingly, *Best2* knockdowns showed increased resistance to salt feeding, indicating that it might be a potential channel regulator. This notion was reinforced by the virtue of its expression in the  $\text{Ca}^{2+}$  storing tubule distal initial segment and in the eyes along with other epithelial tissues such as salivary glands, crop, and hindgut. This study also revealed localisations of bestrophins *in vitro* and *in vivo*. Only *Best1* and *Best2* are widely expressed across various tissues. In contrast, *Best3* and *Best4* showed testis-specific expression. These restrictive expression patterns may imply that bestrophins are diverged in function.

Finally, this work shows important functional insights into *Drosophila* bestrophins that may potentially contribute to the general understanding of these proteins. This study may also provide a basis for further studies, using *Drosophila* as a model organism.

## 7. Further studies on *Drosophila* bestrophin 2

### Summary

As discussed in the previous chapter, two theories have evolved over the years for explaining bestrophin function and its associated disease pathology. The first theory suggests bestrophins as  $\text{Ca}^{2+}$ -activated  $\text{Cl}^-$  channels and the second theory suggests bestrophins as regulators of  $\text{Ca}^{2+}$  channels and therefore  $\text{Ca}^{2+}$  signaling. The Marmorstein lab developed two mouse models of Best disease. The first model was a *Best1*<sup>-/-</sup> knockout (Marmorstein et al., 2006) and the second model was either a heterozygous or homozygous knock-in of BVMD causing *Best1* allele, *Best1*<sup>+ / W93C</sup> or *Best1*<sup>W93C / W93C</sup> (Zhang et al., 2010b). Using the first model, the authors showed increased  $[\text{Ca}^{2+}]_i$  response upon ATP stimulation in the RPE cells (that were derived from *Best1*<sup>-/-</sup> knockout mouse) than their wildtype *Best1*<sup>+ / +</sup> littermates. This suggested that Best1, rather than being a CaCC, acts to suppress  $\text{Ca}^{2+}$  signaling. The same study showed that voltage-dependent  $\text{Ca}^{2+}$  channels (VDCCs) may contribute to light peak (LP) generation in the EOG; thus suggesting a role for  $\text{Ca}^{2+}$  in the LP generation. These observations led to the further suggestion that the disease pathology associated with the LP may not be the determinant of the loss of vision in Best disease, but rather an unknown mechanism via Best1-mediated  $\text{Ca}^{2+}$  signaling could play a role. In contrast to the knockout model, the knock-in model showed decreased  $[\text{Ca}^{2+}]_i$  response upon ATP stimulation. Unlike the knockout mouse, the knock-in mouse showed altered LP luminance-response function, accumulation of lipofuscin in RPE cells, and the formation of fluid- and debris-filled retinal detachments that correlate with human BVMD disease pathology. From the results using the second mouse model, the authors further argued that BVMD must result from Best1 dysfunction but not from the deficiency.

From the following observations of the previous chapters, Best2 (among all four *Drosophila* bestrophins) was thought to be a potential regulator of  $\text{Ca}^{2+}$  signaling (second theory) or homeostasis.

1. *Best2* shows high abundance in the  $\text{Ca}^{2+}$  storing enlarged initial segment and shows only nominal expression in the rest of the tubules.
2. Similarly, it shows high abundance in the eyes, and shows very nominal expression in the neuronal tissues.
3. The flies with reduced levels of *Best2* expression show increased resistance to a high salt diet.
4. *Best2* like *Best1*, and unlike *Best3* and *Best4* shows high mRNA abundance in other epithelial tissues including salivary glands, hindgut, and crop.
5. Interestingly, *Best2* also shows high abundance in the male accessory glands of the adult flies and the spermatheca of females (virgins and mated).

All the above findings reiterated the fact that *Best2* may be a potential modulator of  $\text{Ca}^{2+}$  signaling rather than a simple  $\text{Cl}^-$  channel. It may play an antagonistic role like *mBest1* (Zhang et al., 2010b), probably by antagonising  $\text{Ca}^{2+}$  signaling components such as the L-type  $\text{Ca}^{2+}$  channels that have been found in the RPE cells and equally shown to be expressed in the kidneys of humans to flies (Hayashi et al., 2007; MacPherson et al., 2001).

This study further details the characterisation of *Best2* function. It presents evidence that *Best2* is an essential gene, by gene expression knockdown using GAL4/UAS system. The lethality can be rescued by expressing a wildtype *Best2* in the ubiquitous knockdown background. This study also identifies the genetic location of *Best2* expression using cell-specific enhancer-GAL4s, in the initial segment of the tubules. In line with the increased salt resistance of *Best2* knockdowns, further data were obtained under oxidative stress conditions (induced using 1% hydrogen peroxide ( $\text{H}_2\text{O}_2$ )). These data showed increased oxidative stress resistance of the knockdowns. Taken together, all the data suggest that *Best2* may not be a CaCC, rather it may be a regulator of  $\text{Ca}^{2+}$  channel function, and thereby of  $\text{Ca}^{2+}$  signaling.

In support of this hypothesis, *Best2* knockdowns showed increased stimulatory secondary  $\text{Ca}^{2+}$  responses upon neuropeptide agonist, *capa1* stimulation.

The *capa1*-mediated secondary responses have been thought to be caused upon the activation of plasma membrane  $\text{Ca}^{2+}$  channels like that are of TRPL and/or CNGs. These observations in turn suggest that *Best2* may suppress  $\text{Ca}^{2+}$  signaling, mediated by plasma membrane  $\text{Ca}^{2+}$  channels. Further, a comparative analysis of eye- and tubule-specific transcriptomes showed potential overlap of  $\text{Ca}^{2+}$  signaling components. The signaling components that overlapped were belonged to PLCB signaling including *norpA* that encodes PLCB. The *norpA* expression was assayed in *Best2* mutants under normal and upon salt feeding. This showed *norpA* expression upregulation in control fed *Best2* mutant flies than the similarly fed wildtype flies. Furthermore, the *norpA* expression levels relatively increased to even higher levels, in *Best2* mutants, upon salt feeding, when compared to their wildtype controls fed on similar food regimes.

## 7.1 What is the link between increased secondary $\text{Ca}^{2+}$ elevations in *Best2* mutants and salt resistance?

The transcription of human *Cyp11b* demonstrated to be sensitive to  $\text{Ca}^{2+}$  and CamKII, and clinically implicated in human renal salt wasting. The above comparative analysis in combination with medical subject headings (MeSH) interactions and Homophila (a database that identifies fly homologues of human disease) analysis identified a cytochrome P450, *Cyp6a23*, as a *Drosophila* homolog of human *Cyp11b*. The *Drosophila* counterpart, the *Cyp6a23* is highly abundant in the tubules, crop and midgut. Given that the knockdowns of *Best2* show increased salt resistance and stimulatory  $[\text{Ca}^{2+}]_{\text{cyto}}$ , the *Cyp6a23* was thought to go up in the mutants that were fed on normal and salt food diet regimes.

Therefore, *Cyp6a23* expression was measured using qPCR and found that it is significantly higher in the *Best2* mutants both fed on normal and salt food regimes than the wildtype flies fed on similar diet regimes.

From the above observations, the  $\text{Ca}^{2+}$ -regulated INAD complexes were also tested using qPCR to investigate *Best2*'s potential  $\text{Ca}^{2+}$  modulatory role in the eyes. This analysis further showed the expression deregulation of the components of INAD complex in the eye. Taken together, the data clearly implicate *Best2* as a suppressor of  $\text{Ca}^{2+}$  signaling.

## 7.2 Results

### 7.2.1 Further validations of *Best2* transgenics

In addition to previous validations of knockdowns using *hs-GAL4* ubiquitous driver, the knockdowns were further validated using cell-specific GAL4 drivers. This was particularly useful for delineating cell-specific functional roles of *Best2*. Previously, enhancer trap GAL4 analysis identified cell-specific expression patterns in the tubules (Sozen et al., 1997). The *C42-GAL4* has been shown to be expressed in the principal (and bar-shaped cells in the initial) of the tubules. Using the GAL4/UAS system, *Best2-RNAi* was induced the *C42-GAL4* driver and mRNA levels were compared using qPCR. This showed *C42-GAL4* efficacy in driving *Best2-RNAi*. The mean percentage difference of expression between the RNAi and the UAS control was  $94.21 \pm 9.6$  (Figure 7-1).

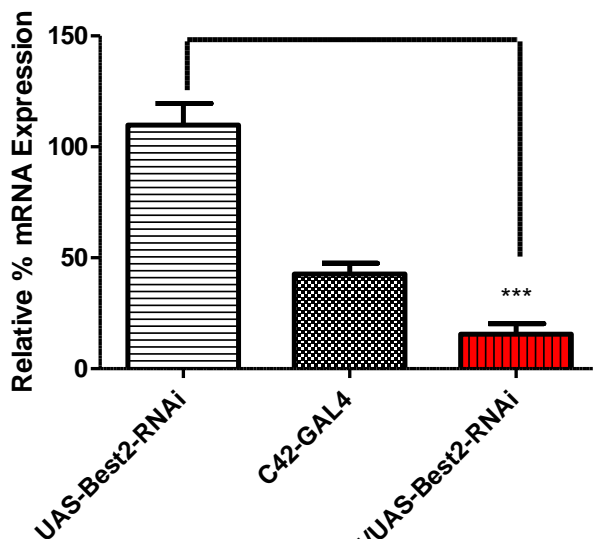


**Figure 7-1** Cell-specific knockdown of *Best2* expression. RNAi for *Best2* was driven using *C42-GAL4*. The anterior tubules were dissected and the total RNA was extracted. The cDNA was made and a qPCR was performed for the relative quantification of mRNA. The total mRNA was significantly reduced (*t*-test,  $P < 0.0001$ ) in *C42-GAL4* driven *UAS-Best2-RNAi* tubules, relative to their parental control, *UAS-Best2-RNAi*.

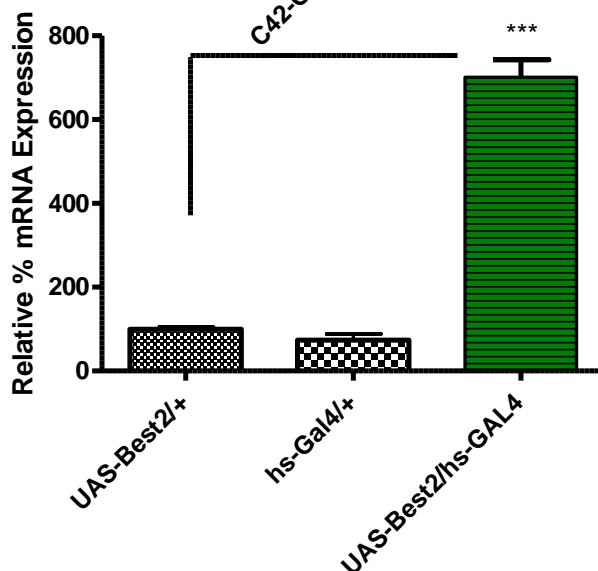


**Figure 7-2** qPCR validation of *Best2* overexpression flies. *Best2* was conditionally expressed in the adult using *hs-GAL4*. The total RNA was extracted from the whole flies and reverse transcribed to cDNA. A qPCR was performed for relative mRNA quantification. *Best2* mRNA was found significantly high in the overexpressors than the parental controls (*t*-test,  $P < 0.0001$ ).

### 7.2.2 *Best2* is an essential gene in *Drosophila*

The following analysis demonstrates that *Best2* is an essential gene in *Drosophila*. *Best2-RNAi* was driven ubiquitously using Act5C-*GAL4*/GFP-CyO, a ubiquitous *GAL4* driver heterozygous on second chromosome (balanced over GFP-CyO, a fluorescent and curly wing marker). Then, the progeny was followed over the developmental stages for lethality scoring to assess whether *Best2* is essential at any stage. The phenotypes scored were for fluorescent and non-fluorescent larvae.

The larval offspring that has the genotype of Act5C-*GAL4*/UAS-*Best2-RNAi*, is where RNAi is induced. This doesn't show any fluorescence. In contrast, the offspring with genotype: GFP-CyO/UAS-*Best2-RNAi*, is where RNAi is not driven as the Act5C-*GAL4* is absent and do show fluorescence. If the successful outcome of the developmental course can be followed, half and half percentage of flies with and without fluorescence should be observed.

The knockdowns showed lethality during third instar larvae until the pupal stages, as the percentage of non-fluorescent larvae observed was reduced during these stages, leading to complete lethality by the pupal stages (Figure 7-3, compare red with black bars). Thus, no adults were emerged from the pupal cases. In addition, the lethality was rescued by expressing a wildtype *Best2* transgene recombined into the lethal background by genetic recombination (Figure 7-3, compare green with white bars). This suggests that *Best2* is an essential gene during development. Interestingly, there were no phenotypic outcomes were observed with the ubiquitous knockdowns during the third-instar to pupal stages, although knockdowns did show an effect on the organismal survival. Furthermore, the C42-*GAL4* knockdown of *Best2* causes 25% lethality at 26 °C indicating its efficacy in reducing *Best2* expression (not shown). This result also validates the further characterisation using C42-*GAL4*.

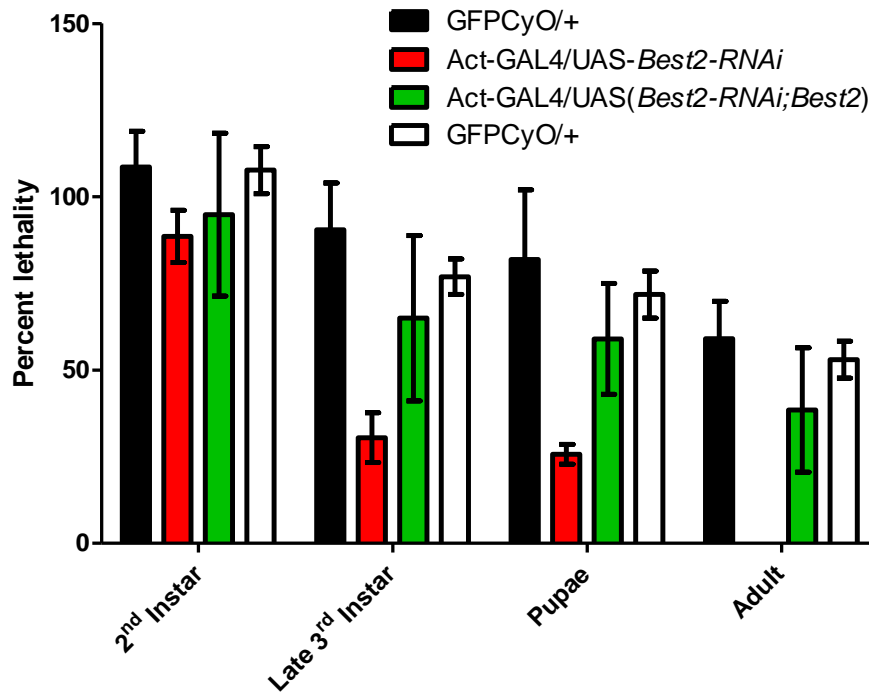


**Figure 7-3** *Best2* is an essential gene in *Drosophila*.

Using Act5C-GAL4 ubiquitous expression of *Best2*-RNAi, the lethality was followed over the developmental time course from 2<sup>nd</sup> instar larvae to the adult. The genetic cross consisted of crossing Act5C-GAL4/GFP-CyO to a UAS-*Best2*-RNAi/UAS-*Best2*-RNAi fly line. This should give rise (if the RNAi is not lethal) to 50% of Act5C-GAL4/UAS-*Best2*-RNAi (red bars) flies and 50% of GFP-CyO/UAS-*Best2*-RNAi flies (black bars). These two genotypes can be easily followed across developmental stages as the first genotype is non-fluorescent and the second genotype is fluorescent. When these genotypes were followed, the flies with the first genotype were gradually reduced to 'zero'; by the pupal stages suggesting that the *Best2* knockdown is lethal. Furthermore, introducing a wildtype *Best2* transgene (green bar, compare with non coloured bar), along with the RNAi transgene, rescues the developmental lethality.

### 7.2.2.1 *Best2* is confined to the Ca<sup>2+</sup> storing initial segment

In the anterior versus posterior microarray analysis, and the qPCR confirmation in the previous chapter (Chapter 6, Figure), *Best2* was found to be abundant in the anterior tubules (Chapter 5). In order to see if the expression was confined to the enlarged initial segment of the anterior tubules, a qPCR investigation was carried out. First, the wildtype anterior tubules were dissected and cut into two parts including the initial segment and the rest of the tubule (consisting upper, lower and main segments). This showed *Best2* mRNA expression only in the initial segment but not in the rest of the segment, with a percent mean difference  $90.79 \pm 4.2$  (*t*-test,  $P < 0.0001$ ) (Figure 7-4A). The residual expression found in the rest of the tubule may be related to background fluorescence.

Furthermore, these results were also confirmed by *in situ* hybridization using antisense mRNA probes (Figure 7-4B, compare with control sense probes, Figure 7-4C).

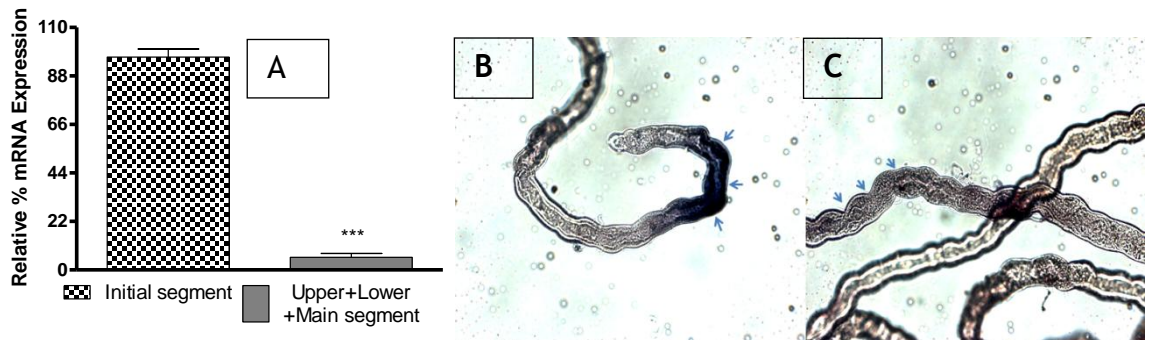


**Figure 7-4** *Best2* expression is confined to the  $\text{Ca}^{2+}$  storing anterior initial segment. (A) A qPCR probing *Best2* mRNA expression in the initial and the rest of the segments confirms *Best2* expression in the initial segment. An *in situ* mRNA hybridization of tubules probed with anti-sense (B) and sense (C) mRNA probes. A pronounced hybridization signal was found using anti-sense probes but not with sense probes, indicating *Best2* expression in only the initial segment (shown using arrowheads).

### 7.2.3 *Best2* is highly abundant in the eyes

The FlyAtlas microarray analysis revealed *Best2* abundance in the eyes (Table 6-1). *Best2* is enriched in the head than the whole fly with an absolute mean difference of 69% (*t*-test,  $P < 0.05$ ) (Figure 7-5). However, its expression was found to be more predominant in the eyes than the rest of the head, as its comparative expression with the whole fly was significantly higher than the heads with an absolute mean difference of 241% (*t*-test,  $P < 0.0001$ ) (Figure 7-5).

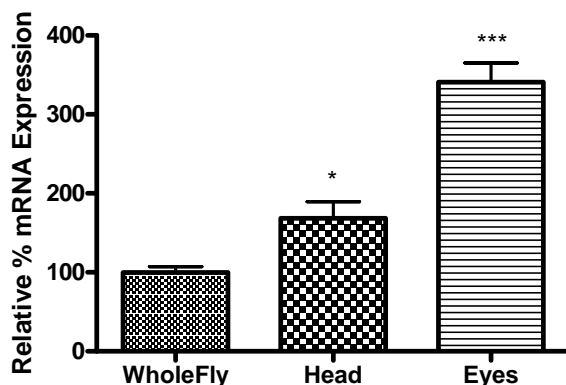


**Figure 7-5** *Best2* is highly abundant in the eyes.

A qPCR revealed *Best2* mRNA high abundance in the eyes than the heads and whole flies with the respective mean fold differences of  $68.53 \pm 22.29$  (*t*-test,  $P < 0.05$ ) and  $240.8 \pm 25.30$  (*t*-test,  $P < 0.0001$ ).

### **7.2.4 *Best2* mediates organismal oxidative stress responses**

In order to test if the salt stress resistance phenotype of *Best2* knockdowns recapitulates the oxidative stress resistance established for the genetic mutants of putative acyl-CoA oxidase (or enigma) in *Drosophila* (Mourikis et al., 2006), the knockdowns were subjected to oxidative stress induced with 1% H<sub>2</sub>O<sub>2</sub> feeding.

As the ubiquitous knockdown using *Act5C-GAL4* was lethal, *hs-GAL4* was used to conditionally express RNAi (knockdown) or wildtype *Best2* (overexpressor) at the adult stages. To control for genetic background mutations, first, all the flies were outcrossed using a wildtype ‘cantonised’ *white*, *w<sup>1118</sup>cs* strain as the RNAi and overexpressor constructs were germline transformed into *w<sup>1118</sup>*.

Then, *hs-GAL4/hs-GAL4* males were crossed to *UAS-Best2*, *UAS-Best2-RNAi* (1) and *UAS-Best2-RNAi* (2) virgin females, and *hs-GAL4/UAS-Best2*; *hs-GAL4/UAS-Best2-RNAi* (1); *hs-GAL4/UAS-Best2-RNAi* (2) males and females were selected from the progeny.

For the controls, *hs-GAL4/hs-GAL4* males or *UAS-Best2*, *UAS-Best2-RNAi* (1) or *UAS-Best2-RNAi* (2) virgin females were crossed to *w<sup>1118</sup>cs* and *UAS-Best2/+*, *hs-GAL4/+*, *UAS-Best2-RNAi* (1)/+ or *UAS-Best2-RNAi* (2)/+ males females were selected from the progeny.

All crosses were set up at 26°C and the flies were raised at standard density (20-30 flies per 7 ml tube), allowed to mate for 48 h after emerging (once mated) then sorted into 20 males and females into separate vials and raised for another 2 days before they were transferred on to diets (1% sucrose agar) with and without 1% H<sub>2</sub>O<sub>2</sub>. Vials were changed every 48 h and deaths per vial were scored until all flies were dead. The numbers of flies used in stress experiments were n = ~80-100. In line with the salt stress resistance phenotype, *Best2* knockdowns also showed increased resistance to oxidative stress, induced by H<sub>2</sub>O<sub>2</sub> feeding, while the overexpressors showed increased sensitivity to the same stress conditions.

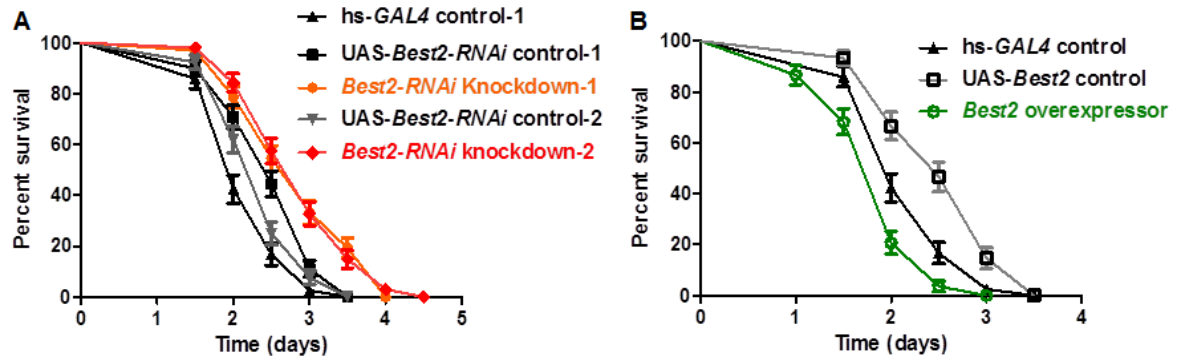


**Figure 7-6** *Best2* is antagonistic to survival on oxidative stress.

The *Best2* knockdowns show increased resistance (A) while the overexpressors show sensitivity to 1% H<sub>2</sub>O<sub>2</sub> diet feeding. Flies were fed on 1% sucrose agar media with 1% H<sub>2</sub>O<sub>2</sub> to induce oxidative stress or with water instead for the control. All the crosses were set up at 26°C and the flies were raised at standard density of 20-30 flies and once mated flies were separated as males and females and raised for another 2 days before they were transferred on to the diet regimes. Two independent crosses were set up for RNAi induction using two separate UAS-*Best2-RNAi*; one (1) obtained from the NIG-Japan stock centre and the other (2) was made in house to control for insertional effects. The deaths were counted every day until all the flies were dead, and plotted as percent survival on Y-axis against time on X-axis. The median survival (in days): hs-GAL4/+, 2 UAS-*Best2-RNAi* (1)/+, 2.5; hs-GAL4/UAS-*Best2-RNAi* (1), 3; UAS-*Best2-RNAi* (2)/+, 2.5; hs-GAL4/UAS-*Best2-RNAi* (2), 3; UAS-*Best2*/+, 2.5 and hs-GAL4/UAS-*Best2*, 2. The control curves were significantly different from the RNAi and overexpressors compared using log-rank (Mantel-Cox) tests, n = 80-120.

### 7.2.5 *Best2* regulates stimulated [Ca<sup>2+</sup>]

According to theory two to explain bestrophin function, bestrophins may regulate Ca<sup>2+</sup> channels probably via their large cytoplasmic C-terminus.

Consistent with this hypothesis, *Best2* shows an interesting expression pattern in the organs where Ca<sup>2+</sup> either plays a fundamental role in signaling or where it is sequestered (thereby contributing to the organismal homeostasis) such as the anterior tubule initial segments.

The salt and oxidative stress resistance phenotypes of *Best2* knockdowns in contrast to *Best1* further supported a role for *Best2* in regulating cellular signaling events mediated by Ca<sup>2+</sup>. The idea was that if *Best2* was only there to regulate salt, the salt phenotype of the knockdowns should have probably been like *Best1*.

In order to assess the hypothesis that bestrophins regulate voltage-dependent Ca<sup>2+</sup> channels (Marmorstein et al., 2006), tubules were used to obtain functional Ca<sup>2+</sup> readouts at a single-cell resolution.

This was achieved using genetic manipulation of *Best2* expression (by knocking down or overexpressing using GAL4/UAS systems) and targeted expression of recombinant cytosolic aequorins (Aequorin<sub>cyto</sub>) to measure Ca<sup>2+</sup>-dependent luminescence thus to measure [Ca<sup>2+</sup>] *in vivo*.

Because tubules have been best studied for Ca<sup>2+</sup> signaling at a single-cell resolution and *Best2* is expressed in the initial segments of the tubules, the tubule model was envisaged to be useful for *in vivo* functional Ca<sup>2+</sup> readouts to find if *Best2* impacts on Ca<sup>2+</sup> regulation. The functional Ca<sup>2+</sup> channels including transient receptor potential like (TRPL) and cyclic nucleotide gated (CNG) channels are found to be expressed in the tubules.

In the GAL4/UAS bipartite system, Aequorin<sub>cyto</sub> probes were expressed using C42-*GAL4*. The [Ca<sup>2+</sup>]<sub>cyto</sub> was measured in the intact anterior tubules of control flies and flies induced for *Best2-RNAi* or *Best2* over-expression as transheterozygotes with Aequorin<sub>cyto</sub> probes *in vivo*.

First, resting levels (without agonist stimulation) were measured for 2 min, and then the agonist (capa1) stimulated was measured. The capa1 shows characteristic biphasic [Ca<sup>2+</sup>]<sub>cyto</sub> response called primary and secondary responses. The primary and secondary responses were thought to be mediated by respective activation of PLC $\beta$  signaling then its coupling to the activation of plasma membrane Ca<sup>2+</sup> channels such as TRP family members including their closely related CNG channels.

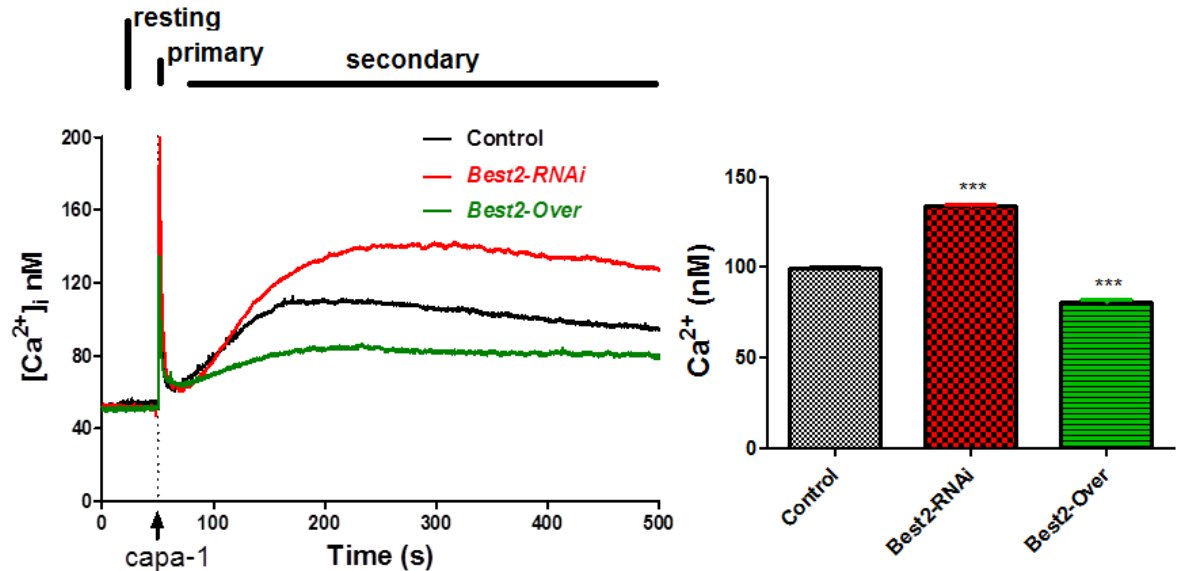


Figure 7-7 Best2 modulates secondary  $\text{Ca}^{2+}$  responses.

Calcium was measured in the anterior tubules of control flies and flies induced for *Best2-RNAi* or *Best2* overexpression using the cell-specific GAL4 driver C42-GAL4 in the transheterozygous background with *Aequorin<sub>cyto</sub>* probes allowing to measure  $[\text{Ca}^{2+}]_{\text{cyto}}$  *in vivo*. The resting levels (without an agonist) were measured for 2 minutes then the agonist (capa1) stimulated was measured. The capa1 shows the characteristic biphasic  $[\text{Ca}^{2+}]_{\text{cyto}}$  response called primary and secondary responses. The primary was characterised to be dependent on the PLC $\beta$  signaling and the secondary was thought to be mediated upon the activation of plasma membrane  $\text{Ca}^{2+}$  channels. The secondary  $[\text{Ca}^{2+}]_{\text{cyto}}$  responses were significantly different in both *Best2* knockdowns and overexpressors. The significance of difference in  $[\text{Ca}^{2+}]_{\text{cyto}}$  secondary response decay between control and RNAi or overexpressor background is shown in the bar graph (*t*-test,  $P < 0.0001$ ). The secondary  $\text{Ca}^{2+}$  decay can be characterised as the reduction in the  $[\text{Ca}^{2+}]$  in the cytosol over time.

The resting and primary  $[\text{Ca}^{2+}]_{\text{cyto}}$  levels were not significantly affected in both knockdowns and the overexpressors, while the secondary  $[\text{Ca}^{2+}]_{\text{cyto}}$  were significantly differed from the control (Figure 7-7). The significance of difference in  $[\text{Ca}^{2+}]_{\text{cyto}}$  secondary response 'decay' between control and RNAi or overexpressor background is shown in the bar graph (*t*-test,  $P < 0.0001$ ) (Figure 7-7). The secondary  $\text{Ca}^{2+}$  decay can be characterised as the reduction in  $[\text{Ca}^{2+}]_{\text{cyto}}$  in the cytosol over time. These results further suggest that Best2 suppresses  $\text{Ca}^{2+}$  signaling.

### 7.2.6 Characterisation of *Best2* mutants

I used hs-GAL4 as a ubiquitous GAL4 driver to induce *Best2-RNAi in vivo*, and performed salt and oxidative stress survival assays. However, this system needs several rounds of heat-shock that may potentially give rise to unwanted effects (Liu and Lehmann, 2008b). To further confirm the results of salt resistance of the hs-GAL4>*Best2-RNAi* knockdowns, an independent system was sought.

This led to a search in the *Drosophila* Bloomington stock centre for potential transposon insertions in the *Best2* gene that may either cause disruption of gene expression, function or both. This search identified two potential insertional mutants including *Best2*<sup>c04759</sup> and *Best2*<sup>c00039</sup> (Figure 7-8). These were then obtained and validated using qPCR analysis of gene expression. The qPCR confirmed reduced levels of expression in the mutants than the wildtype controls, though the reduction was not as significant as the RNAi knockdowns (Figure 7-11). The two mutant lines were tested if they show similar salt resistance phenotypes of the knockdowns. Consistently, both the mutants showed increased resistance to high salt food compared to the wildtype controls (Figure 7-9). Furthermore the salt eating behaviour of the mutant flies along with the wildtype flies was assessed and confirmed that all the flies were eating the food (Figure 7-10).

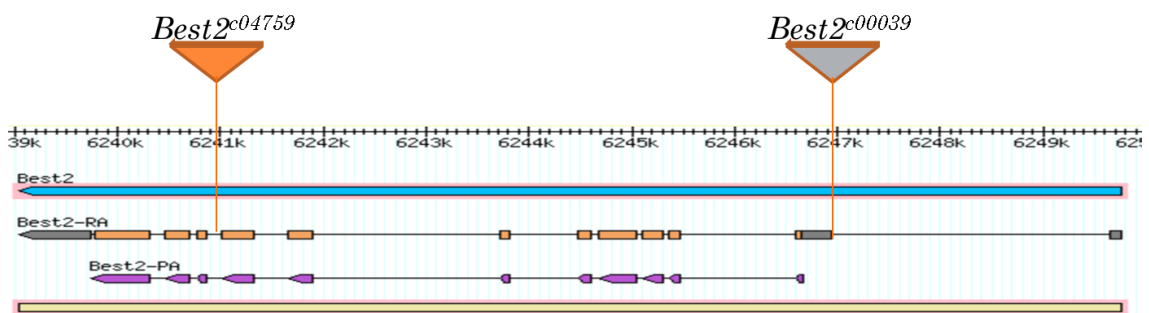


**Figure 7-8** The genomic location of transposon insertions of *Best2*. *Best2* is encoded by chromosome 3L of *Drosophila melanogaster*. It has a single annotated transcript with 11 exons. Two transposon insertional mutant stock available and the insertions are found one toward the 3' and the other towards 5' and within the UTR.

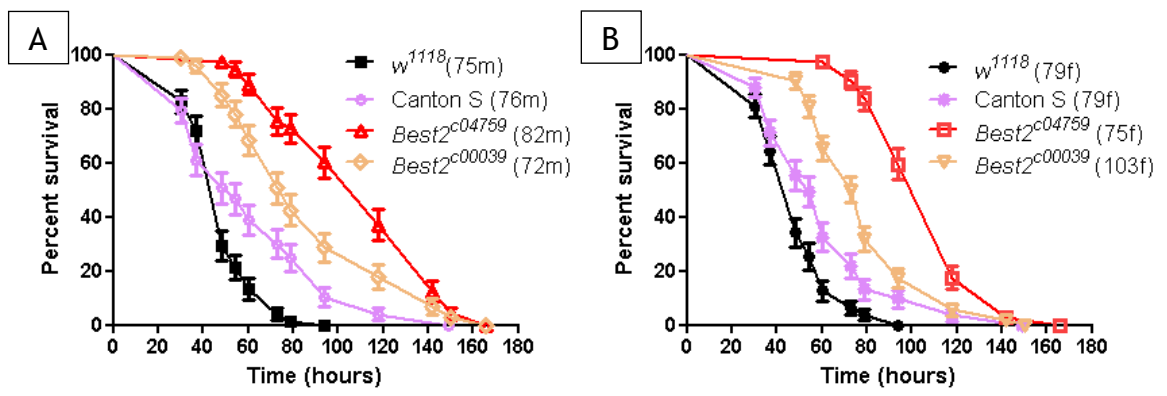


**Figure 7-9** *Best2* insertional mutants are salt resistant. Salt assays were performed as outline before on 4% NaCl food. All the assays were performed separately for males (A) and females (B). The data were obtained from four independent replicates; the total number of flies in all the replicates is shown in the brackets. Both the mutants of *Best2* show increased resistance over two wildtype controls including *w*<sup>1118</sup> and Canton S.

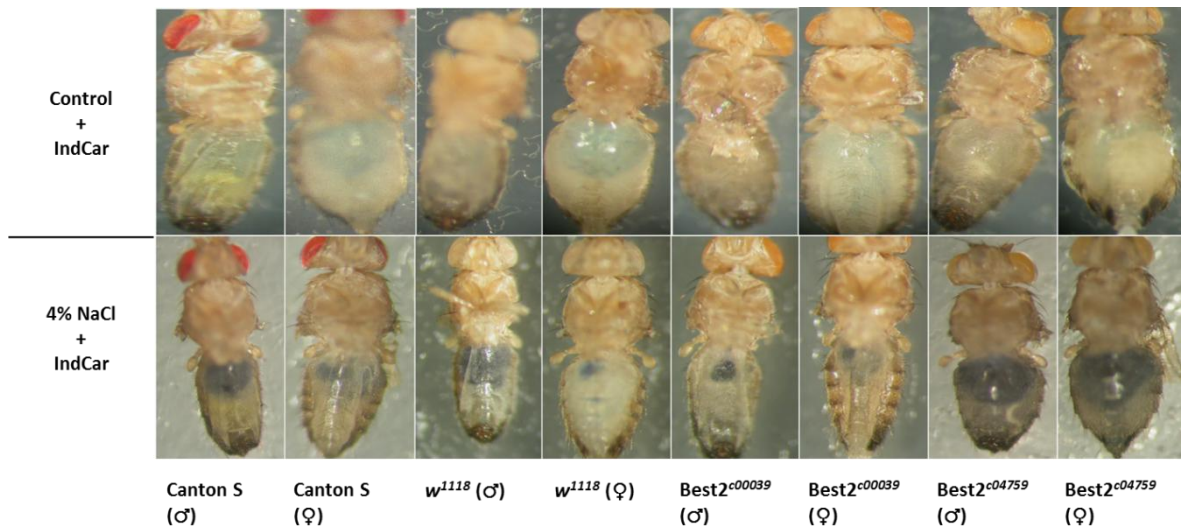


**Figure 7-10 Flies eat salt food.**

Fly eating behaviour was assayed using Indigo carmine dye. Similar experiments were performed elsewhere to show the satiety of the fly to high salt diet (Stergiopoulos et al., 2009). The indigo carmine (500 mg/ml) dye was added to the food and 20 flies were transferred to the normal and 4% NaCl containing food. After 24 h, their abdomens were observed for blue colour under a light microscope. All most all the flies including *Best2* mutants observed (control-fed, in the upper panel and salt-fed in the lower panel) showed blue colour indicating that they eat food (even with high amounts of salt). However, blue colour was more pronounced in the salt fed flies, as the colour depends on the pH. The Canton S flies are the wildtype and the  $w^{1118}$  are the wildtype with white mutation. The *Best2* mutants were generated in the isogenic  $w^{1118}$  background.

### **7.2.7 $Ca^{2+}$ -dependent gene expression is changed in *Best2* mutants under stress**

In many organisms from vertebrates to invertebrates, the amplitude and duration of intracellular  $Ca^{2+}$  elevations control diverse cell signaling mechanisms including differential activation of pro-inflammatory transcriptional regulators NF-kappaB, C-Jun N-terminal kinase (JNK) and NFAT (Dolmetsch et al., 1997). It has been established that the large transient  $[Ca^{2+}]_{cyto}$  rise activates the first two regulators while the low, sustained  $Ca^{2+}$  plateau activates NFAT.

In order to investigate a possible link between the salt stress resistance phenotypes and increased cytosolic  $Ca^{2+}$  elevations in the *Best2-RNAi* knockdowns and *Best2* insertional mutants, a comparative analysis of the transcriptomes of the eyes and the anterior tubules to understand similarities and differences in  $Ca^{2+}$  signaling. This was because *Best2* was found enriched in both of these tissues. The  $Ca^{2+}$  signaling components then were overlaid on to vertebrate signaling pathways using homology mapping and using Online Mendelian Inheritance in Man (OMIM).

A first look at the analysis revealed a surprising number of  $\text{Ca}^{2+}$  signaling components that were similarly expressed between tubules and eyes, in that *PLCB* signaling was one. Some of these components showed high conservations from flies to humans (Figure 1-5).

The *PLCB* pathway is a key component in the phototransduction pathway of *Drosophila*, because the null mutants of the PLC encoded by *norpA* do not respond to light excitation. In the photoreceptor cells, *PLCB* signaling mediates the activation of at least two classes of plasma membrane  $\text{Ca}^{2+}$  channels including TRP and TRPL. The most likely candidates that may trigger the  $\text{Ca}^{2+}$  efflux have been proposed to be the hydrolysis products of phosphatidyl inositol 4,5 bisphosphate ( $\text{PIP}_2$ ) including inositol triphosphate ( $\text{IP}_3$ ), diacylglycerol (DAG) or polyunsaturated fatty acids; each may elicit a unique cell signaling pathway (Berridge and Irvine, 1984; Hardie, 2007). However, it has been shown that  $\text{IP}_3\text{R}$  genetic mutants do not have an effect on phototransduction, in contrast to most other inositol mediated signaling systems (Acharya et al., 1997; Raghu et al., 2000).

In other systems, such as the midgut of the fly, *PLCB* signaling has been shown to be essential for normal host survival through ROS production by modulating dual oxidase (DUOX) activity (Ha et al., 2005; Milenkovic et al., 2007a). The activity of DUOX has also been shown to be  $\text{Ca}^{2+}$  dependent. It has been also shown in tubules that PLC-mediated signaling, through  $\text{IP}_3$ , is essential and coupled to  $\text{Ca}^{2+}$  elevations that were physiologically relevant in terms of fluid secretion (Pollock et al., 2003).

The expression of *norpA* that encodes *PLCB* was assayed using qPCR in both control and salt fed flies of wildtype and mutant flies. The control-fed and 'salt-fed' denotes normal food and 4% extra NaCl added food regimes respectively. The control-fed wildtype expression was compared against control-fed *Best2* mutant flies. In the same way, the salt-fed wildtype expression was compared against the salt-fed mutant flies. This analysis identifies the components that show upregulation in normal conditions that still remain upregulated in the salt-fed conditions.

The *norpA* expression was significantly upregulated in *Best2* mutants both in control-fed and salt-fed conditions over their respective controls fed on similar regimes (Figure 7-11). Furthermore, in the salt-fed mutants the expression was more pronounced than the control-fed conditions.

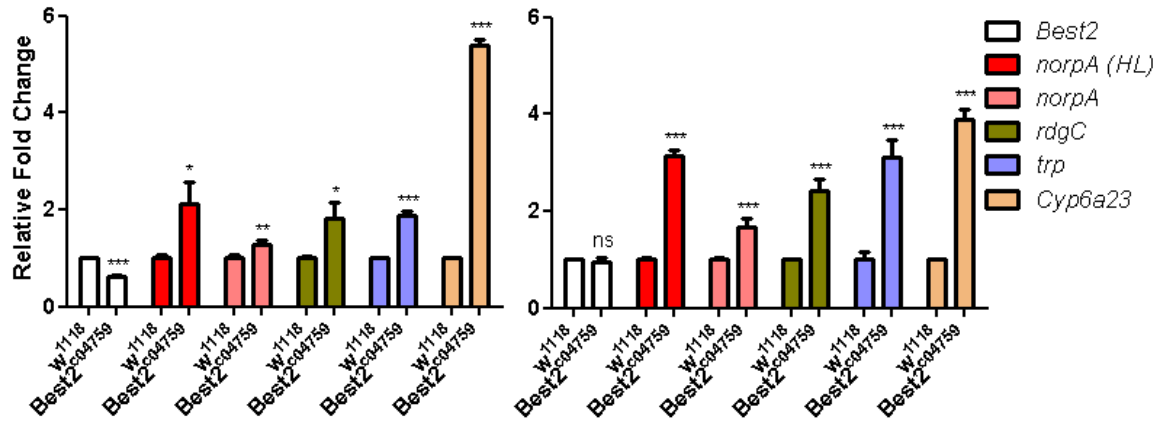


**Figure 7-11 Best2 regulates Ca<sup>2+</sup>-dependent transcription.**

A qPCR survey was carried out to assay some of the Ca<sup>2+</sup> signaling components, and Ca<sup>2+</sup>-dependent genes, in *Best2* insertional mutants versus wildtype flies, under control- (A) and salt-fed (B) conditions. The relative FC with respect to their controls are shown for each sample in the following table. The significance of FC mean difference is calculated using *t*-test, *P*<0.05.

**Table 7-1 The fold change (FC) mean differences and associated statistics of the data in Figure 13.**

genes	Statistics						
		<i>Best2</i>	<i>norpA</i> (HL)	<i>norpA</i>	<i>rdgC</i>	<i>trp</i>	<i>Cyp6a23</i>
Control-fed	<i>w</i> <sup>1118</sup>	1.005	1.02	1.02 ± 0.02	1.01 ± 0.01	1.01 ± 0.01	1.002
	<i>c</i> <sup>04759</sup>	0.6 ± 0.01	2.1 ± 0.3	1.3 ± 0.04	1.8 ± 0.2	1.87 ± 0.1	5.4 ± 0.1
	FC mean difference	0.4 ± 0.01	1.1 ± 0.3	0.25 ± 0.1	0.8 ± 0.2	0.87 ± 0.1	4.4 ± 0.1
	<i>t</i> -test ( <i>P</i> <0.05)	***	*	**	*	***	***
Salt-fed	<i>w</i> <sup>1118</sup>	1.003	1.01 ± 0.01	0.95	1.003	0.96	1.004
	<i>c</i> <sup>04759</sup>	0.96 ± 0.04	3.13 ± 0.1	1.7 ± 0.1	2.4 ± 0.1	3.1 ± 0.2	3.9 ± 0.1
	FC mean difference	0.05 ± 0.04	2.12 ± 0.1	0.73	1.4 ± 0.13	2.2 ± 0.2	2.9 ± 0.1
	<i>t</i> -test ( <i>P</i> <0.05)	ns	***	***	***	***	***

The INAD complex in the eye is extensively researched and an established route for phototransduction (Hardie and Raghu, 2001). This complex was proposed to be formed by a complex number of proteins that are attached to the PDZ domains of INAD with a short linker region. The whole complex then is stabilised by a multimeric membrane bound TRP channel.

The partnered proteins including TRP channels have been shown to be expressed in a defined number with appropriate stoichiometries proposed. The  $\text{Ca}^{2+}$  feedback loop is important to relay signal from the complex, and is probably a defining step in determining the stoichiometry of the complex via calmodulin.

The molecular mechanisms that regulate the  $\text{Ca}^{2+}$  feedback loop between the complex and cytosol remain unknown. Given bestrophins have been implicated in voltage-dependent  $\text{Ca}^{2+}$  channel modulation; it may link the feedback phenomenon. If Best2 regulates  $\text{Ca}^{2+}$  signaling, the mutants of the *Best2* was thought to impact on the INAD signaling complex. One possible way of testing this complex was to see if the tightly coexpressed INAD components change their expression in the *Best2* mutants at resting or at stress conditions.

Furthermore, the TRP channels including their closest members, CNGs have been implicated in many sensory systems including phototransduction, olfaction and taste, as well as in the perception of heat, touch, and pain by virtue of their expression and with further experimentation (Gillespie and Walker, 2001). The TRP channels have been equally shown to sense osmotic changes in the mechanotransduction in the sensory neurons (Gillespie and Walker, 2001).

The *trp* expression was assayed using qPCR and found its expression significantly upregulated in *Best2* mutants both in control-fed and salt-fed conditions over their respective controls fed on similar regimes (Figure 7-11). Furthermore, in the salt-fed mutants the expression was more pronounced than in the control-fed conditions.

In the same way, a  $\text{Ca}^{2+}$ /calmodulin-dependent *retinal degeneration C* (*rdgC*) was tested, and its expression found to be significantly higher in *Best2* mutants both in control-fed and salt-fed conditions over their respective controls fed on similar regimes (Figure 7-11). Furthermore, in the salt-fed mutants the expression was more pronounced than the control-fed conditions.

In order to test if  $\text{Ca}^{2+}$  plays a direct role in salt induced stress resistance, the expression of a cytochrome P450, *Cyp6a23* was measured, The *Cyp6a23* is a *Drosophila* homologue of mammalian *Cyp11b2* that has been implicated in salt wasting in human patients (Mitsuuchi et al., 1993; Williams et al., 2004).

Furthermore, in human adrenocortical cell lines, CAMK1 was found to augment Cyp11b2 promoter reporter expression, when the intracellular  $\text{Ca}^{2+}$  was elevated; thus indicating its  $\text{Ca}^{2+}$ -dependent gene expression regulation (Condon et al., 2002).

In *Drosophila*, *Cyp6a23* shows high mRNA abundance in tubules, crop and midgut. Using qPCR, this gene was found to be induced to 4- and 10-fold in the *Best2* mutants fed on normal and 4 % salt food respectively over their controls fed on similar diet regimes. This clearly demonstrates *Best2*'s potential role in regulating of intracellular  $[\text{Ca}^{2+}]$ . These changes in the  $[\text{Ca}^{2+}]$ , seems to be playing important roles when the organism encounters stress such as salt or oxidative stress.

### 7.3 Discussion

In this study, several important aspects of bestrophin regulation and function have been studied using a variety of genetic and physiological approaches. The studies using mutants were promising for explaining *Best2* function as a potential  $\text{Ca}^{2+}$  signalling modulator at the same time as a component in the  $\text{Ca}^{2+}$  homeostasis.

Further validations using cell-specific enhancer GAL4s suggested that *Best2* expression is confined to the  $\text{Ca}^{2+}$  storing initial segment (Figure 7-1). The overexpression line used in this was validated to be producing a high amount of mRNA when compared with its parental control (Figure 7-2). In the previous chapters, I found that the expression of *Best2-RNAi* using ubiquitous driver caused lethality. This lethality was investigated to determine the developmental stage where *Best2* expression was detrimental. This analysis confirmed the lethality between third instar larval stages and pupal stages (Figure 7-3). Furthermore, the lethality was rescued to show that it is due to the RNAi induction, but not because of the off-target effects. This was achieved by introducing a wildtype *Best2* transgene into the knockdown background. However, many metabolic genes seem to be essential at these developmental stages of *Drosophila*, and undergo rapid developmental transitions at these stages (Chung et al., 2009; Mourikis et al., 2006).

In the adult flies, *Best2* mRNA can be detected in various tissues (Table 6-1). It is predominantly expressed in the eyes (the analogous tissue of human disease), and nominally expressed in the neuronal tissue including brain and thoracoabdominal ganglion. These expression patterns were further validated using qPCR (Figure 7-5). Interestingly, *Best2* shows high abundance in the  $\text{Ca}^{2+}$  sequestering (and storing) distal initial segment of the tubules. This was also confirmed using qPCR probing *Best2* expression in the distal segment and in the rest of the segment separately (Figure 7-4A). Later this was confirmed using *in situ* hybridization (Figure 7-4 B & C).

Both tubules and eyes encounter oxidative stress at a regular basis, and the expression pattern of *Best2*, by virtue in these tissues, correlate with the proposed  $\text{Ca}^{2+}$  regulatory function of bestrophins. In the previous and current chapter, I found increased resistance of *Best2* knockdowns or mutants to the high salt diet. Previously, oxidative stress resistance of the genetic mutants of putative acyl-CoA oxidase (or enigma) has been established in *Drosophila* that were fed on paraquat (Mourikis et al., 2006). These flies also showed increased longevity. In addition, the ubiquitous overexpression of *dIP<sub>3</sub>K1* confers resistance to oxidative stress induced with  $\text{H}_2\text{O}_2$ , but not with paraquat (Monnier et al., 2002). The oxidative stress responses to different stressors may be mediated by different cell signaling pathways. The  $\text{IP}_3\text{K}$  family of proteins phosphorylate  $\text{IP}_3$  leading to the reduction of  $\text{IP}_3$  levels. This observation led to the proposal that  $\text{IP}_3\text{K}$ s act to possibly terminate the  $\text{IP}_3$ -mediated signaling cascade. However, the mechanisms of *dIP<sub>3</sub>K1* action have been suggested to be diverged from flies to humans, as the fly  $\text{IP}_3\text{K1}$  does not have a calmodulin-binding domain like its mammalian counterpart,  $\text{IP}_3\text{K-A}$ .

When the oxidative stress was induced by feeding the flies with  $\text{H}_2\text{O}_2$ , the *Best2* knockdowns showed increased ability to cope with the stress, while the overexpressors showed the reduced ability (Figure 7-6). This indicates that *Best2* with its potential  $\text{Ca}^{2+}$  regulatory function may mediate the stress responses, but probably downstream of  $\text{IP}_3$  signaling.

The tubule  $\text{Ca}^{2+}$  readouts in this study suggested that there was an increase in secondary  $[\text{Ca}^{2+}]_{\text{cyto}}$  in the knockdowns upon agonist, *capa1* stimulation (Figure 7-7).

This was consistent with the analysis of primary RPE cultures, derived from the mouse lacking *Best1* that revealed the antagonist role of Best1 in  $\text{Ca}^{2+}$  signaling (Neussert et al., 2010). This study showed increase in resting  $[\text{Ca}^{2+}]_{\text{cyto}}$ , as well as ATP-stimulated  $[\text{Ca}^{2+}]_{\text{cyto}}$  levels that were postulated to be downstream of PLC activation coupled to bafilomycin- and thapsigargin-sensitive store emptying (Neussert et al., 2010). However, the resting levels of  $[\text{Ca}^{2+}]_{\text{cyto}}$  were unchanged in the *Best2* knockdowns (Figure 7-7). Furthermore, overexpressing a wildtype *Best2* using GAL4/UAS system downgraded the *capa1* secondary stimulatory response, confirming the knockdown results, but without altering the resting  $\text{Ca}^{2+}$  levels. These results may not rule out the effect of knockdown or overexpressor on the resting  $\text{Ca}^{2+}$  levels as the quantitation may not be that sensitive to detect minute changes in the resting levels.

Taken together, these data suggest that the plasma membrane  $\text{Ca}^{2+}$  channels may be hyperactivated in *Best2* knockdowns and suppressed in overexpressors as the secondary  $[\text{Ca}^{2+}]_{\text{cyto}}$  decay was significantly reduced, thus leading to the elevated  $\text{Ca}^{2+}$  rises, for sustained periods of time, which was found opposite in the overexpressors. This was because the primary  $\text{Ca}^{2+}$  response upon *capa1* addition was not changed significantly in both the knockdowns and overexpressors as the primary response has been thought to be due to  $\text{IP}_3$ -stimulated transient efflux from the  $\text{Ca}^{2+}$  stores such as ER. The secondary *capa1* response has been thought to be due to the activation of plasma membrane  $\text{Ca}^{2+}$  channels.

Two additional *Best2* mutants have been validated to further support the findings from the GAL4/UAS system. These mutant flies have two independent transposon insertions in their genome in the *Best2* genomic locus; therefore they showed decreased expression levels and/or function. The decreased levels of expression of one of the mutants have been confirmed using qPCR (Figure 7-11). The mutant lines were assayed for salt resistance, as has been found for the knockdowns using GAL4/UAS system. Both the mutants showed increased resistance to high salt food (Figure 7-9). The satiety of the food was tested and confirmed that the flies eat salt food (Figure 7-10).

The insertional mutants were further used, to assay if the  $\text{Ca}^{2+}$ -dependent gene expression is affected, using qPCR and found that several interesting candidates were highly upregulated under control-fed and salt-fed conditions (Figure 7-11). The genes tested were obtained through a comparative analysis of transcriptomes of adult eyes and tubules which revealed many  $\text{Ca}^{2+}$  signaling components that showed similar expression patterns, and are highly conserved. Furthermore, Homogene and OMIM analysis revealed a surprising number of signaling components to be highly conserved between the fruit flies and vertebrates; the Homogene seeks evolutionary homology of proteins, and the OMIM analysis identifies fruit fly homologs of human genetic disorders.

Calcium signaling is a key component in visual transduction in the eyes (Hardie, 2007; Hardie and Raghu, 2001). The molecular mechanisms of visual transduction pathways are highly conserved from humans to flies. Calcium signaling plays divergent roles from visual to stress signaling, thus the spatiotemporal aspects of the signaling need to be tightly regulated. In that, the eyes occupy the primary position for both the events given their interaction with external environment. The events in these processes mediated by  $\text{Ca}^{2+}$  should therefore be tightly regulated.

Cytochrome P450 (CYPs) genes are widely found and well-studied in *Drosophila* (Chung et al., 2009). Some CYPs are developmentally important, and others do organismal detoxification functions. Overexpression of *Cyp6a23*, *Cyp6a2*, *Cyp6a8*, *Cyp6t3* and *Cyp6a19* has not been found to increase the survival of the flies on DDT, nitenpyram, dicyclanil and diazinon. However, the overexpression of *Cyp6g1* (DDT, nitenpyram and dicyclanil), *Cyp6g2* (nitenpyram and diazinon) and *Cyp12d1* (DDT and dicyclanil) caused the resistance to the insecticides shown in the brackets (Daborn et al., 2007). The human homolog of *Drosophila Cyp6a23* has been found to catalyse steroid metabolism. Infants with corticosterone methyl oxidase type I deficiency found to be caused by a defect in aldosterone synthesis and severe salt-wasting due to hyponatremia and hyperkalemia (Mitsuuchi et al., 1993). Interestingly, the *Cyp6a23* shows high abundance in the epithelia indicating its potential role in the epithelial function. The preliminary data using an RNAi directed against *Cyp6a23* suggested that it is potentially important in the regulation of salt (Appendix VII). In addition, this result further confirms the antagonistic role in the  $\text{Ca}^{2+}$  signaling.

However, peroxisomal localisation of Best2 is intriguing for the fact that this has been the first ever  $\text{Cl}^-$  channel that is found to localise to peroxisomes. The localisations of mBest1 in the mouse RPE cells were also interesting as it showed localisation to ER in addition to its basolateral plasma membrane localisation (Neussert et al., 2010).

Although, the localisation of Best2 needs further confirmations using an antibody, as the GFP protein fusion overexpressors may mistarget the proteins, the localisation can be true for the following reasons:

1. It is abundant in the  $\text{Ca}^{2+}$  storing initial segment consisting of around 30 cells out of ~150 in MT, in which (specialised) peroxisomes are thought to be abundant.
2. The Best2 fusion protein can be detected in the purified peroxisomes.
3. It is also abundant in the eyes where lysosomes are abundant, thus may represent lysosomal-related vesicles.

At least the vesicular pattern of the Best2 is interesting. Because the defective transport of endolysosomal vesicles cause devastating pathologies in humans. Moreover, Best disease is caused by accumulation of lipofuscin that is seen in other lysosomal storage diseases. For example, in Dent's disease, the defective acidification or  $\text{Cl}^-$  concentrations and defective membrane recycling seem to lead to excess renal excretion of  $\text{Ca}^{2+}$  and proteins perhaps through defective membrane recycling (Jentsch, 2007; Sun et al., 2002).

Interestingly, in line with the salt resistance phenotypes, *Best2* knockdowns also showed increased resistance to oxidative stress conditions (Figure 7-6). These results confirmed that Best2 may mediate the general  $\text{Ca}^{2+}$  signaling responses upon, for example, stress conditions that activate  $\text{Ca}^{2+}$ -mediated signal transduction pathways.

## 7.4 Conclusions

This study establishes Best2 as a regulator of Ca<sup>2+</sup> signaling in *Drosophila*. However, this finding has been previously shown for mBest2 knock-in mice where the dysfunction, not the deficiency, has been shown to suppress Ca<sup>2+</sup> signaling. However, this study, carried out as part of this chapter, clearly shows that the flies with reduced levels of *Best2* expression can cause an impact on Ca<sup>2+</sup> signaling along with the insertional mutants where the expression was not that severely affected. It seems that both the dysfunction and deficiency can cause the bestrophin phenotypes as it has been previously established, for example, for CFTR channels. Furthermore, the impact of Best2 on Ca<sup>2+</sup> signaling has been shown by the upregulation of several interesting Ca<sup>2+</sup>-dependent genes including *Cyp6a23*, and the components of INAD complex including a *trp* channel. These results clearly established tissue-specific roles of Best2. Finally, this study unravelled the existence of a potentially novel Ca<sup>2+</sup> signaling pathway mediated by Best2, which might help to elucidate similar mechanisms in higher order organisms to device therapeutic intervention in the disease.

## 8. Cell-specific peroxisome dynamics in the living organism

### Summary

Peroxisomes are ubiquitous and diverse organelles that perform key metabolic functions in almost every eukaryotic cell. They can house as many as 100 enzymes and perform a range of essential metabolic functions within the mammalian cell, from the  $\beta$ -oxidation of fatty acids to the degradation of  $\text{H}_2\text{O}_2$ . Defects in peroxisomal function can therefore result in a range of peroxisomal biogenesis disorders such as Zellweger spectrum syndrome (ZSS). Recently, peroxisomes have been shown to be dynamic regulators of cellular  $\text{Ca}^{2+}$  homeostasis and signalling *in vitro*.

This report provides an insight into *in vivo* mechanisms for peroxisomal  $\text{Ca}^{2+}$  buffering under resting and stimulatory conditions using *Drosophila*, and more specifically its renal system, the Malpighian tubules, a model tissue that provides a powerful array of genetic and genomic tools to study the regulation of both cytosolic and organellar  $\text{Ca}^{2+}$  signaling and transport mechanisms. In this study, targeted  $\text{Ca}^{2+}$ -dependent recombinant aequorin luminescent probes were used to generate distinct peroxisomal and cytosolic  $\text{Ca}^{2+}$  signatures ( $[\text{Ca}^{2+}]_{\text{perox}}$  &  $[\text{Ca}^{2+}]_{\text{cyto}}$ ). Therefore, the successful targeting of aequorin to the peroxisomes in an actively transporting live renal epithelium was achieved. The resting peroxisomal  $[\text{Ca}^{2+}]_{\text{perox}}$  concentrations were measured to be two-fold higher than the  $[\text{Ca}^{2+}]_{\text{cyto}}$ .

For agonist stimulated  $[\text{Ca}^{2+}]_{\text{perox}}$  response, a neuropeptide agonist (capa1) was used that shows characteristic biphasic  $[\text{Ca}^{2+}]_{\text{cyto}}$  response stemming from  $\text{IP}_3$ -induced ER  $\text{Ca}^{2+}$  efflux as primary, then leading to the activation of transient plasma membrane influx as secondary  $\text{Ca}^{2+}$  response. Peroxisomes did not buffer the rapid transients induced by  $\text{IP}_3$ -mediated  $[\text{Ca}^{2+}]_{\text{cyto}}$  efflux from the internal stores, although they did transiently uptake secondary  $[\text{Ca}^{2+}]_{\text{cyto}}$  increases upon the activation of plasma membrane  $\text{Ca}^{2+}$  channels. The external addition of cyclic guanosine monophosphate (cGMP), and zaprinast, a nonspecific PDE inhibitor that increases cGMP concentrations, separately induced  $[\text{Ca}^{2+}]_{\text{perox}}$  buffering response.

In agreement with this, induction of an RNAi transgene *in vivo* for *PDE1c*, that encodes a  $\text{Ca}^{2+}$ /calmodulin-dependent PDE, causes a non-characteristic primary and an enhanced secondary  $[\text{Ca}^{2+}]_{\text{perox}}$  response. A  $[\text{Ca}^{2+}]_{\text{perox}}$  signature for *Best2-RNAi* was also obtained that showed increased secondary responses when compared to the controls.

The  $[\text{Ca}^{2+}]_{\text{perox}}$  signatures were also validated by knocking down two *PEX* genes that encode peroxins, proteins required for normal peroxisomal protein assembly and formation. These *PEX* genes are specifically enriched in the tubules and are essential for proper renal-peroxisome formation. Finally, using an integrative systems approach, a model for peroxisomal  $\text{Ca}^{2+}$  sequestration and transport excretion mechanisms was obtained, that may be applied to relevant mammalian systems.

## 8.1 Novel roles of peroxisomes in Ca<sup>2+</sup> homeostasis

The ubiquitous intracellular messenger, Ca<sup>2+</sup> plays key roles in cellular and physiological processes including proliferation, differentiation, development and cell death (Berridge et al., 2000) to transepithelial transport, secretion (Berridge, 2005; Dow and Romero, 2010). Its roles in apoptosis and cell death are well documented (Berridge et al., 1998). For example the Ca<sup>2+</sup> concentrations in the ER regulates ceramide-induced apoptosis via TRP channels (Pinton et al., 2001; Wegierski et al., 2009).

Two recent reports suggest a role for peroxisomes in dynamic modulation of cell Ca<sup>2+</sup> homeostasis and signaling (Drago, Giacomello et al. 2008; Lasorsa, Pinton et al. 2008). These reports used two independent approaches to measure [Ca<sup>2+</sup>] in peroxisome lumen *in vitro*. The first report used GFP-based fluorescence resonance energy transfer (FRET) indicators (Dcpv) targeted to peroxisomes using KVK-SKL hexapeptide sequence. This approach was successful in obtaining [Ca<sup>2+</sup>]<sub>perox</sub> signatures at resting and upon agonist stimulation, and allowed to obtain [Ca<sup>2+</sup>]<sub>perox</sub> recordings one cell at a time, unlike aequorin approach that gives rise to [Ca<sup>2+</sup>]<sub>perox</sub> measurements for a group of cells. In GH3 cells, they demonstrated that in response to depolarization of the plasma membrane with the addition of KCl, peroxisomes buffer Ca<sup>2+</sup> with slow kinetics in parallel with [Ca<sup>2+</sup>]<sub>cyto</sub> rise. They concluded that [Ca<sup>2+</sup>]<sub>perox</sub> equilibrate with [Ca<sup>2+</sup>]<sub>cyto</sub> without needing any driving force like ATP and/or Na<sup>+</sup>/H<sup>+</sup> gradients. This was in consistent with previous findings (Jankowski et al., 2001); and their observation that the pH was indifferent between peroxisomes and cytosol even for example, under stimulatory conditions with Na<sup>+</sup> ionophore, monensin. However in these cells, Ca<sup>2+</sup> mobilisation from internal stores through TRH receptors via spontaneous action potential firing leading to the Ca<sup>2+</sup> influx through voltage-gated Ca<sup>2+</sup> channels, never resulted in an increase in [Ca<sup>2+</sup>]<sub>perox</sub>.

Under Ca<sup>2+</sup>-free conditions, no effect was seen in [Ca<sup>2+</sup>]<sub>perox</sub> by the addition of Ca<sup>2+</sup> ionophore, ionomycin, an unspecific Ca<sup>2+</sup> mobiliser from stores. Thus, peroxisomes seem to be insensitive to rapid transients as that are seen in GH3 cells by TRH (IP<sub>3</sub> production) or ionomycin.

However, they recognise for example, the  $\text{KCl}^-$ -dependent depolarization where  $[\text{Ca}^{2+}]_{\text{cyto}}$  reaches peak levels in 2 or more seconds, followed by a prolonged plateau level that lasts several seconds in cell systems.

The  $\text{Ca}^{2+}$  agonist, histamine mobilises  $\text{Ca}^{2+}$  in HeLa cells from internal stores through the production of  $\text{IP}_3$  which produces larger and relatively more prolonged  $[\text{Ca}^{2+}]_{\text{cyto}}$  elevations compared with GH3 cells. This was shown to result in more  $[\text{Ca}^{2+}]_{\text{perox}}$  buffering response to histamine in HeLa cells than the response in GH3 cells to TRH.

This finding was consistent with ionomycin induction of  $[\text{Ca}^{2+}]_{\text{perox}}$  response (100%) in HeLa cells than <5% in GH3 cells. Taken together, these data suggest larger and prolonged  $[\text{Ca}^{2+}]_{\text{cyto}}$  elevations cause peroxisomes to buffer  $\text{Ca}^{2+}$ . No significant heterogeneity in  $[\text{Ca}^{2+}]_{\text{perox}}$  was observed in the groups of peroxisomes, without ruling out the possibility that the peroxisomes for example, nearby the plasma membrane  $\text{Ca}^{2+}$  channels or ER may show differing  $[\text{Ca}^{2+}]_{\text{perox}}$  buffering response (Drago et al., 2008a). Peroxisomes show distinct buffering capacities from other organelles (Drago et al., 2008a; Lasorsa et al., 2008; Rizzuto and Pozzan, 2006). For example, unlike mitochondria,  $[\text{Ca}^{2+}]_{\text{perox}}$  increases, in response to agonists is much slower. The closest organelle to peroxisomes that partly recapitulate  $[\text{Ca}^{2+}]_{\text{perox}}$  buffering is the nucleus, although the peak values are 10 to 100-fold higher in the nucleus than peroxisomes.

The mechanistic insight obtained from the cell culture systems may not reflect the physiology of the whole animal. Thus, understanding peroxisomes' role in  $\text{Ca}^{2+}$  sequestration and homeostasis *in vivo* in an organotypic context could show real insight into physiological contributions of these organelles for organismal  $\text{Ca}^{2+}$  homeostasis. As the  $\text{Ca}^{2+}$  homeostasis by peroxisomes is a newly emerged concept, the *in vivo* mechanisms for  $[\text{Ca}^{2+}]_{\text{perox}}$  buffering is an exciting avenue to explore in multicellular organisms; plant  $[\text{Ca}^{2+}]_{\text{perox}}$  signatures have recently been obtained (Costa et al., 2010). The tubules of *Drosophila* fit the purpose in an animal, to explore the functions in an organotypic context as described in the following sections.

## **8.1.1 *Drosophila Malpighian (renal) tubules as an in vivo model to study peroxisome Ca<sup>2+</sup> homeostasis***

### **8.1.1.1 Morphology and functional domains**

Tubules are robust epithelial tissues that not only show distinct apico-basal polarity but also functional domains (Sozen et al., 1997). Each tubule is 2 mm long and 35 µm wide and are packed in an organised fashion in the body cavity, in that, one pair of tubules goes towards anterior and the other goes towards posterior, thus are called anterior and posterior tubules respectively. They constitute two major cell types including large principal cells and small stellate cells. In addition, the anterior tubules consist of a large initial segment, which was demonstrated to be functionally distinct from the rest of the tubule, that drives transepithelial Ca<sup>2+</sup> transport, from the haemolymph to the tubule lumen, in soluble form and at the same time, sequestering into spherites (also called as Type I concretions) and precipitating as calcium phosphate (Dube et al., 2000a; Dube et al., 2000b). Unlike the main segment, it does not seem to pump fluid at detectable rates (Dow et al., 1994b).

### **8.1.1.2 Tubule peroxisomes**

Tubules not only are the major organs for transepithelial transport and excretion, but also are responsible for metabolic and redox homeostasis. Tubule peroxisome abundance was previously shown using immunofluorescence microscopy (Southall et al., 2006). An isoform of secretory pathway Ca<sup>2+</sup>/Mn<sup>2+</sup> ATPase SPoCk-C was documented to be localised to the peroxisome-derived calcium phosphate spherites in the anterior initial segment. Genes related to peroxisomal catabolic processes such as H<sub>2</sub>O<sub>2</sub> degradation, very long chain fatty acid β-oxidation show high mRNA abundance in tubules in FlyAtlas (Table 8-1). These are including the famous catalase, *acyl CoA oxidase (Acox-57D-p)*, *urate oxidase (Uro)*, and *ry (xanthine dehydrogenase)*. Novel genes *CG11919* and *CG13827* annotated to be peroxisome biogenesis and fission factors respectively show high abundance of mRNA expression in tubules, suggesting the importance of peroxisome function. However, very little is known about these *Drosophila* genes.

The microarray profiling of gene expression in anterior versus posterior tubules provided a wealth of information that suggests a role for peroxisomes in the  $\text{Ca}^{2+}$  loading into the spherites, to store it in the insoluble calcium phosphate form (Chapter 5). This microarray revealed *Best2* expression at high levels in this part of the tubule and later it was found to be localised in the peroxisomes (Chapter 6). Thus, studying the function of peroxisomes using a genetically-tractable model tissue was hoped to provide real insight into the diversity of function of peroxisomes, from metabolism to transport.

**Table 8-1 Genes related to peroxisomes and their relative abundance in tubules.**  
**Genes that have peroxisomal targeting sequence (PTS) are coloured from red, brick red to green indicating PEX19, PTS1 and PTS2 signals, respectively. Abbreviations: GO, gene ontology; T, tubule; WF, whole fly; Pr, peroxisome; C, cytosol; M, mitochondria; L, lipid particle; PM, plasma membrane; Menv, mitochondrial envelope; Minner, mitochondrial inner membrane; PrM, peroxisome membrane; RNA sig, mRNA signal; FC, fold change tubule versus whole fly; Exp, expression in other tissues of the body.**

Gene Symbol	GO: Biological Process	GO: cell location	RNA sig.	FC	Exp
Uro	purine base metabolic process	Pr	6590	35	
CG11919	perox organization/(S)-2-hydroxy-acid oxidase /glycolate oxidase /FMN binding /nucleoside-triphosphatase	Pr	2653	22	
ry	determination of adult life span/compound eye pigmentation//xanthine dehydrogenase activity	Pr	770	18	F, S, EYE
CG13827	Carbo.Met.process/perox.fission//phosphotransferase activity, alcohol group as acceptor	PrM	1826	16	S, M, HG
CG14777		PrM	1941	10	S, G,U
Spat	glyoxylate catabolism/serine-pyruvate transaminase	Mm/Pr/L	1682	10	F, H, E
CG32103	transport //calcium ion binding	M/Pr	1170	7.2	U
CG7970	PMP22 type	Pr	2664	7	M, U
CG12338	Oxidation reduction	Pr	948	6	F, HU
Cat	response to oxidative stress/aging/Ca <sup>2+</sup> -dependent cell-cell adhesion	Pr/PM	4821	5	H, F, U
CG17597 / ScpX	phospholipid transport//acetyl-CoA C-acyltransferase	C/M/P/LP	1249	4	M, U
Acox57D-p	FA $\beta$ -oxidation // acyl-CoA dehydrogenase, acting on the CH-CH group of donors / FAD bin	Pr	621	4	Epi
CG4289	protein targeting to peroxisome	PrM	837	4	M,H,U
CG4663 (PEX13)	perox organization/protein import into perox matrix, docking	Pr	684	3.4	U
ScpX	phospholipid transport//SCPX-related thiolase	C/M/P/L	711	2.9	M,LF, U
CG9319	metabolic process	Pr	264	2.5	U
l(3)70Da (PEX1)	peroxisome organization//nucleotide binding / ATPase activity, (un) coupled	Pr	117	2.4	U
CG7601	oxidation reduction //binding	PrM	211	2.3	C, U
CG5325 (PEX19)	nervous system development //protein binding	Pr	640	2	C, U
CG7081 (PEX2)	peroxisome organization //protein binding/ zinc ion binding	PrM	219	2	H, Ep, F
CG3415	oxidation reduction	Pr	697	2	M, U
ide	Proteolysis	Pr	537	2	U, B
CG17544	FA $\beta$ -oxidation//acyl-CoA dehydrogenase	Pr	322	1.9	M, U
CG5009	prostaglandin metabolic process/ FA oxidation//acyl-CoA dehydrogenase activity	Pr	293	1.8	C, U
DhaP-at	glycerol-3-phosphate O-acyltransferase activity	M/Pr	162	1.8	C5, U
CG8315	peroxisome fission	Pr	302	1.7	C, U
CG8315	Peroxisome organisation (PEX11)	Pr	302	1.7	U
CG1662		PrM	207	1.4	U
CG1041	//carnitine O-acetyltransferase activity	M/Pr	173	1.3	S, AG
CG7864	Peroxisome organization (PEX10)		110	1	Epi
CG12428	HOMO: choline acetyl transferase	Pr	249	1	F, U
CG12703	//ATP binding cassette family D	Pr	315	0.6	U, F
CG13890	metabolic process	Pr	141	0.8	U
CG9527	FA $\beta$ -oxidation, phagocytosis//acyl-CoA DH, I	Pr	184	0.5	M
CG9577	metabolic process // HOMO: hydroxyl acyl CoA	Pr	228	0.7	C, F

### 8.1.2 Aequorin probes for $[Ca^{2+}]$ measurements *in vivo*

Aequorin is a  $Ca^{2+}$ -sensitive photoprotein, first isolated from the coelenterate, Jelly fish, *Aequoria victoria*. It is formed from apoaequorin, a 21 kDa polypeptide, and coelenterazine, a hydrophobic luminophore, bioluminescent as a complex in the natural system. To recapitulate the natural phenomena, first apoaequorin is expressed in a cell or a tissue, and then reconstituted to aequorin by incubating with coelenterazine to obtain its  $Ca^{2+}$ -dependent luminescence. The GAL4/UAS ectopic expression system, particularly, allows non-invasive and non-cytotoxic method to obtain  $[Ca^{2+}]_i$  reading *in vivo* (Rosay et al., 1997). The addition of ER targeting motifs to the C-terminus of the aequorin was shown to modify its stability and  $Ca^{2+}$ -dependent luminescence (Alvarez and Montero, 2002). However, peroxisome targeting motifs were demonstrated not to alter aequorin kinetics, and so such probes can be used for quantitative  $[Ca^{2+}]_{perox}$  measurements (Lasorsa et al., 2006). Lasorsa et al., (2006) calibrated the probes by perforating the cells with a mild-detergent digitonin which permeabilises cells by forming complexes with plasma membrane cholesterol. As the organellar cholesterol present at low levels, this method of permeabilisation was presumably chosen to control-perforate peroxisomes to calibrate the targeted aequorin probes with the addition of predefined concentrations of external  $Ca^{2+}$ . These calibrations confirmed the  $Ca^{2+}$ -dependent luminescence of targeted aequorins which was rather similar to the cytosolic wildtype aequorin probes.

In consistent with the previous report, under defined experimental conditions, pH was also not significantly different between cytosol and peroxisome lumen. However, peroxisomal pH in different cells and species was established to be slightly variable by different groups, in that it is slightly alkaline in mammalian fibroblasts (Dansen et al., 2000), or acidic (Lasorsa et al., 2004) or alkaline in yeast cells (van Roermund et al., 2004). Taken together these data suggest  $[Ca^{2+}]_{perox}$  measurements may be quantitatively compared against the cytosolic concentrations using the same back-integration algorithm (Lasorsa et al., 2008).

### ***8.1.3 Purpose of this study***

Upon the observations that suggested the tubules are enriched for peroxisomes and sequester, store and mobilise  $\text{Ca}^{2+}$  according to their metabolic needs, I decided to generate peroxisome-targeted aequorin probes to generate distinct  $\text{Ca}^{2+}$  signatures for tubule peroxisomes thereby to assess the impact of peroxisomal localised Best2.

## 8.2 Results

### 8.2.1 Renal peroxisomal targeting and validation of aequorin probes

Luminescent aequorin proteins are widely used for measuring intracellular  $\text{Ca}^{2+}$  quantitatively. Previously, aequorins have been successfully targeted to mitochondria, Golgi and peroxisomes to measure  $\text{Ca}^{2+}$  levels *in vivo* and *in vitro*. Recently, peroxisomal targeted probes (both luminescence- and FRET-based) have been characterised *in vitro* in multiple cell types for exploring peroxisome's role in cell  $\text{Ca}^{2+}$  homeostasis (Drago et al., 2008b; Lasorsa et al., 2008b). For the first time, in this study, aequorin probes were targeted to peroxisomes in a transporting renal epithelia, the tubules of *Drosophila melanogaster*, in a cell-specific manner to unravel peroxisome's role in  $\text{Ca}^{2+}$  homeostasis *in vivo*.

The targeting was achieved using a canonical peroxisomal targeting sequence tripeptide SKL (Ser-Lys-Leu) (Miura et al., 1992) to the C-terminus preceding KVK (Lys-Val-Lys), a positively charged tripeptide sequence (Figure 8-1). The KVK sequence has been shown to enhance the peroxisomal targeting according to the principles described by Neuberger et al. (Drago et al., 2008a; Neuberger et al., 2003a, b).

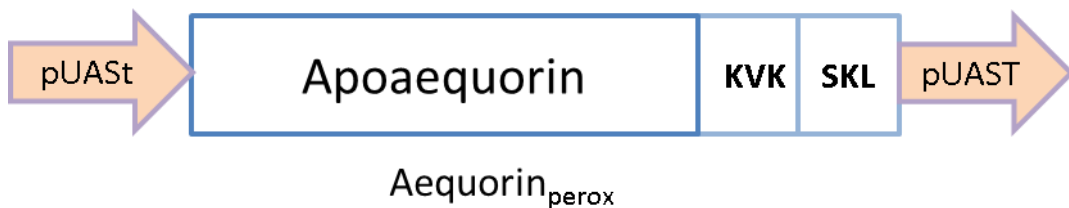


**Figure 8-1** Schema of the peroxisomal targeting construct.

An aequorin open reading frame (ORF) was C-terminally fused with KVK-SKL hexapeptide sequence before the stop codon and then cloned into a *Drosophila* germline transformation vector (pPUAST) for ectopic expression using GAL4/UAS system.

#### 8.2.1.1 Immunocytochemical localisation *in vitro*

Aequorin<sub>perox</sub> probes were first validated in *Drosophila* embryonic S2 cells, before they were sent for germline transformation to generate transgenic flies and *in vivo* characterisation in tubules.

The validations were carried out to test if the construct was functional and localised in the peroxisomes using immunocytochemical localisation (Figure 8-2); then to test if targeted aequorin gives a luminescence signal when reconstituted that is distinct from the Aequorin<sub>cyto</sub> using luminometry (Section 8.2.1.3).

For the immunocytochemical localisation, the germline transformation construct, pPUASt-Aequorin<sub>perox</sub> was also validated, before it was sent for microinjection. The S2 cells were transfected with the targeted construct along with a DES-GAL4 construct using lipofectamine reagent, a lipid based transfection reagent. DES (*Drosophila* expression system) vector allows the transgenes to be cloned downstream of a metallothionein promoter that can be inducible by CuSO<sub>4</sub>. After 12 h of transfection, the cells were induced for expression and incubated for another 48-72 h. They were then washed with phosphate buffer saline (PBS) and immunocytochemistry was performed using the methods described in Chapter 2: Materials and Methods. The peroxisomal localisation of Aequorin<sub>perox</sub> was confirmed with its colocalisation with the native peroxisomal catalase (Figure 8-2).

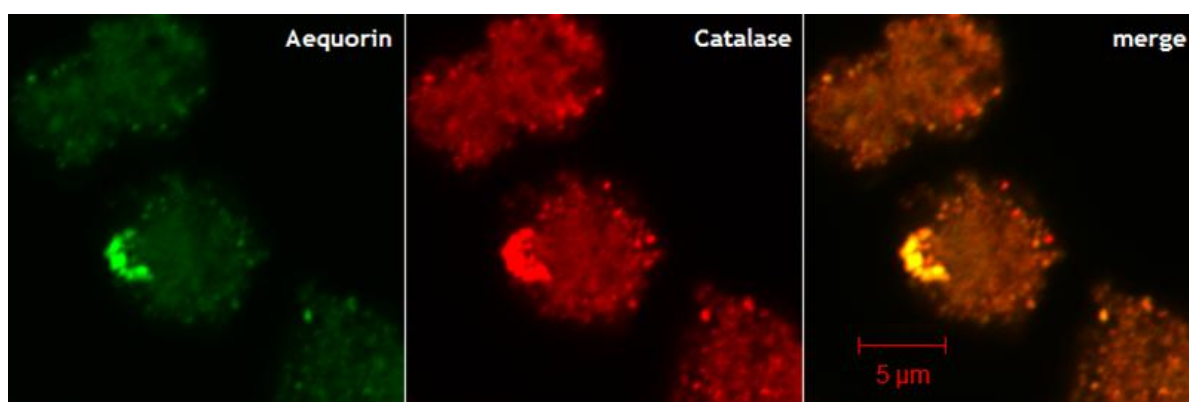


**Figure 8-2 Targeting of Aequorin<sub>perox</sub> and immunocytochemical localisation with native catalase in S2 cells.**

Cells heterologously expressing peroxisomal targeted aequorin were immunostained sequentially, first with mouse  $\alpha$ -catalase as the primary and  $\alpha$ -mouse Texas-Red conjugated IgG as the secondary antibodies; second with rabbit  $\alpha$ -aequorin as the primary and  $\alpha$ -rabbit FITC conjugated IgG as the secondary antibodies. Then DAPI was used to stain the nucleus. A confocal microscope system was used to image the fluorescence.

### 8.2.1.2 Immunocytochemical localisation *in vivo*

The pPUASt-Aequorin<sub>perox</sub> construct was germline transformed for making transgenic flies harbouring the transgene in the genome for GAL4/UAS ectopic expression system.

Out of 13 transformed fly lines obtained, 4 were validated and confirmed to be giving good luminescence values. Out of the four, one was selected for recombining into two different GAL4 harbouring flies separately for making stable flies constitutively expressing targeted aequorin regulated by cell-specific GAL4. These include C42-*GAL4*, and C710-*GAL4* that allow principal and stellate cell-specific expression of transgenes in tubules; both including the cells in the initial segment. Another GAL4 fly line, JAT20-*GAL4*, that drives transgene expression in the initial segment was also used for immunocytochemical localisation but not for  $[Ca^{2+}]_{\text{perox}}$  recordings as the luminescence readings were too low, probably due to its low strength in driving the transgenes.

The stable stocks then contained the constitutively expressing Aequorin<sub>perox</sub> under UAS regulation by the constitutive, cell-specifically expressing GAL4 transcription factor either under the control of C42 or C710 or JAT20-*GAL4* upstream promoter elements (C42-*GAL4*>Aequorin<sub>perox</sub> or C710-*GAL4*>Aequorin<sub>perox</sub> or JAT20-*GAL4*). Immunocytochemical localisations were performed on the tubules expressing targeted aequorins and confirmed their peroxisomal localisation using an antibody for native catalase (Figure 8-3A). The catalase antibody was tested on purified peroxisomes using Western blotting. Although, a right sized band (~57 kDa) for catalase appeared, other bands were also observed, showing the potential unspecific nature of the antibody (Appendix VIII). The peroxisomal targeting was confirmed using  $\alpha$ -aequorin antibody on immunoblotted protein purified from peroxisomes from the flies ectopically expressing the targeted aequorin which showed right band size of 21 kDa (Figure 8-3B).

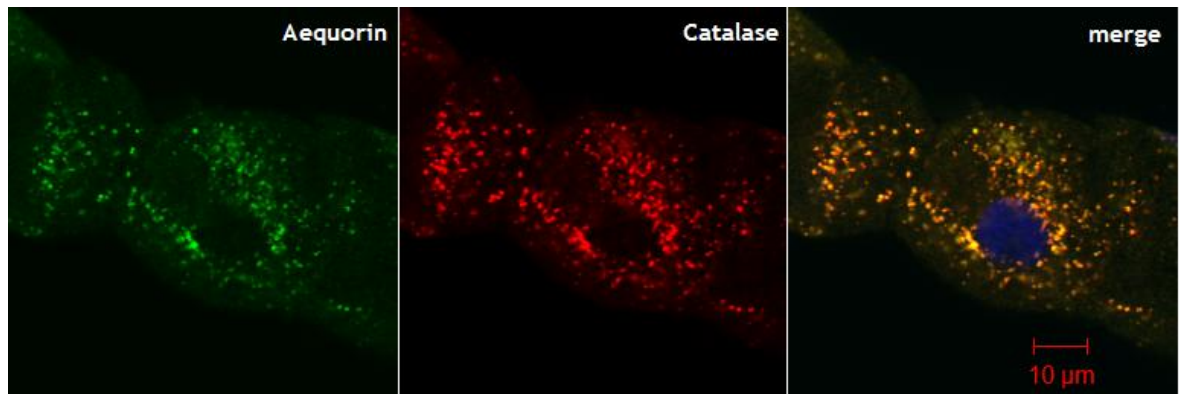
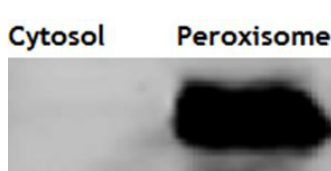
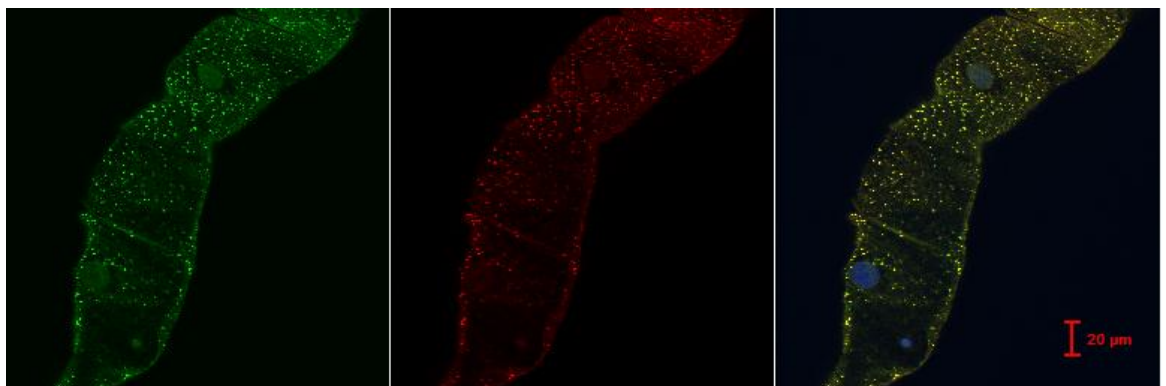


**Figure 8-3 Validation of Aequorin<sub>perox</sub> targeting *in vivo*.**

**(A)** Cell-specific targeting of Aequorin<sub>perox</sub> and immunocytochemical colocalisation with native catalase in tubules. The principal cell-specific GAL4 driver, C42-GAL4 was used to ectopically express the Aequorin<sub>perox</sub> in tubule, and then imaged for localisation. Tubules ectopically expressing peroxisomal-targeted aequorin were immunostained sequentially, first with mouse  $\alpha$ -catalase as the primary and  $\alpha$ -mouse Texas-Red conjugated IgG as the secondary; second with rabbit  $\alpha$ -aequorin as the primary and  $\alpha$ -rabbit FITC conjugated IgG as the secondary antibodies. Then the tubules were incubated with DAPI for 1 min to stain the nucleus (blue).



**(B)** Western blot of Aequorin<sub>perox</sub>. Protein from purified peroxisomes along with the rest of the cytosolic protein fraction as a negative control was used for blotting, and then probed using  $\alpha$ -aequorin (rabbit) as the primary and Cy5-labelled  $\alpha$ -rabbit antibody as the secondary. The blot was of expected size of 21 kD.



**(C)** Aequorin<sub>perox</sub> localisation in tubule anterior initial segment. The principal cell-specific GAL4 driver, C42-GAL4 was used to ectopically express the Aequorin<sub>perox</sub> in the whole tubule and then imaged for localisation.

### 8.2.1.3 [Ca<sup>2+</sup>]<sub>perox</sub> measurements in S2 cells

The targeted probes were validated in S2 cells and [Ca<sup>2+</sup>]<sub>perox</sub> signatures were obtained. As the aim of the project was to understand peroxisome Ca<sup>2+</sup> buffering mechanisms *in vivo*, the S2 cell [Ca<sup>2+</sup>]<sub>perox</sub> readouts were majorly used for probe validation purposes.

Both capa1 and Drosokinin neuropeptides have been studied *in vivo* in tubules and shown to elevate [Ca<sup>2+</sup>]<sub>cyto</sub> through IP<sub>3</sub>-dependent ER Ca<sup>2+</sup> release.

Combining the S2 cell system with the neuropeptides as  $\text{Ca}^{2+}$  agonist was a possibility to explore if peroxisomes play roles in  $[\text{Ca}^{2+}]$  buffering upon mobilisation from internal stores possibly leading to the activation and release from plasma membrane  $\text{Ca}^{2+}$  channels.

For this purpose, (along with germline transformation vector constructs) the targeted aequorins were constructed into *Drosophila* expression system (DES) vectors downstream of  $\text{CuSO}_4$ -responsive metallothioneine promoter for induction of expression in S2 cells for *in vitro*  $[\text{Ca}^{2+}]_{\text{perox}}$  measurements. The DES system reduces one additional plasmid cotransfection (thus reducing the transfection load) to induce the expression of the transgene, as pPUAST-transgene transfection needs another helper plasmid, DES-GAL4 for expression induction.

Therefore,  $[\text{Ca}^{2+}]_{\text{perox}}$  and  $[\text{Ca}^{2+}]_{\text{cyto}}$  traces were obtained in S2 cells and compared under control for resting levels, and in the presence of *capa1* and Drosokinin for stimulated levels (Figure 8-4). As the receptors for *capa1* and Drosokinin are only nominally expressed in S2 cells ([www.flyatlas.org](http://www.flyatlas.org)), the ORFs that encode these receptors (*capaR* and *LkR*) were separately transfected along with either cytosolic- or peroxisome-targeted aequorin ORFs and incubated for 1 h in Schneider's medium with 2.5 mM coelenterazine for reconstitution of apoaequorin to aequorin for  $\text{Ca}^{2+}$ -dependent luminescent measurements.

The resting and agonist (*capa1* and Drosokinin) stimulated  $[\text{Ca}^{2+}]$  levels were measured for cytosolic-(Figure 8-4 A & B, black line) and peroxisomal-(Figure 8-4 A & B, red line) targeted probes. The resting levels of  $[\text{Ca}^{2+}]_{\text{perox}}$  were 2-fold higher than the  $[\text{Ca}^{2+}]_{\text{cyto}}$  levels (Figure 8-4 i & ii). Upon stimulation, transient and more prolonged  $[\text{Ca}^{2+}]_{\text{perox}}$  (than the  $[\text{Ca}^{2+}]_{\text{cyto}}$ ) increase was observed, followed by a plateau (marked with star). After the plateau, the  $[\text{Ca}^{2+}]_{\text{perox}}$  levels gradually decreased but never falling off to the resting for a few minutes.

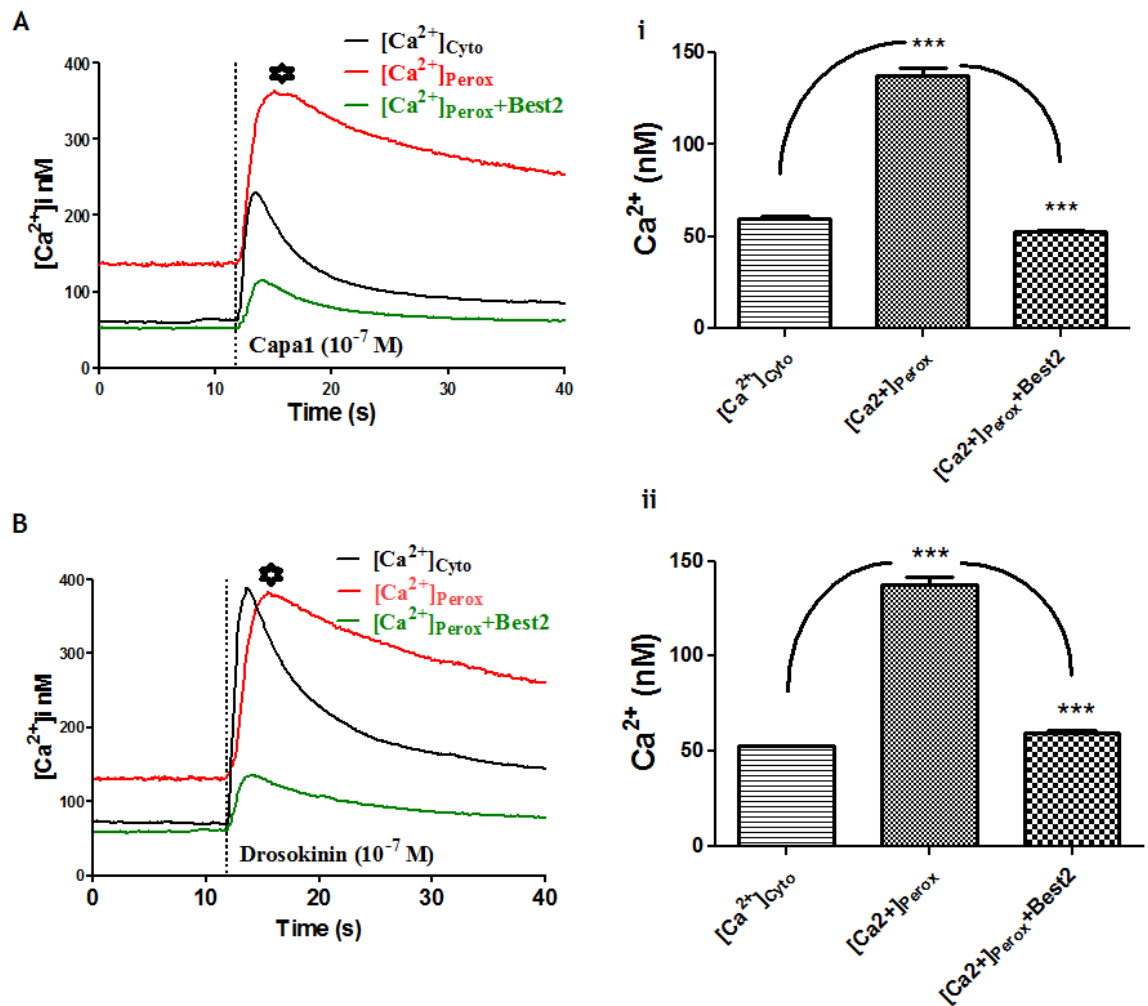


Figure 8-4  $[Ca^{2+}]$  measurements in S2 cells.

Calcium concentrations were measured in the cytosol (black line) and peroxisomes (red line) at resting and stimulated using luminometry. In a continuous readout, resting levels were measured first and then the stimulated levels either with capa1 (A) or Drosokinin (B). The differences in resting and stimulated are presented for statistical significance ( $t$ -test,  $P \leq 0.0001$ ) (i and ii). The plateau levels upon stimulation are shown using star marks in graphs A & B. The heterologous expression of *Best2* significantly reduced basal and stimulated  $[Ca^{2+}]_{perox}$  (green line).

In addition to the wildtype  $[Ca^{2+}]_{perox}$  readouts in S2 cells, another  $[Ca^{2+}]_{perox}$  readout was obtained after the overexpression of *Best2*. When the wildtype *Best2* was cotransfected, the  $[Ca^{2+}]_{perox}$  resting levels were decreased to  $[Ca^{2+}]_{cyto}$  and followed by a reduced stimulatory  $Ca^{2+}$  rise in peroxisomes upon capa1 and Drosokinin stimulation (Figure 8-4, green line).

#### 8.2.1.4 $[Ca^{2+}]_{perox}$ measurements in tubules

The  $[Ca^{2+}]_{perox}$  signatures were successfully obtained only for principal cells (including the cells in the initial segment) using C42-GAL4 >Aequorin<sub>perox</sub>.

In contrast, the signal from *C710-GAL4 >Aequorin<sub>perox</sub>* tubules was too low as it is only expressed in stellate cells (including the bar-shaped cells in the initial segment) which are relatively low in number (33/178 in anterior 22/133 in posterior tubules) (Sozen et al., 1997).

Firstly, *in vivo*  $[Ca^{2+}]_{perox}$  signatures at resting and stimulated (using  $Ca^{2+}$  mobilising neuropeptide agonist, *capa1*) were generated using live wildtype tubules. To investigate possible segment-specific peroxisomal  $Ca^{2+}$  buffering mechanisms,  $[Ca^{2+}]_{perox}$  signatures were generated separately for anterior (with and without initial segment), posterior tubules and just for initial segment of the anterior tubules without the rest of the segment (Figure 8-5). Then the  $[Ca^{2+}]_{perox}$  signatures were obtained in different genetic backgrounds, first to validate  $[Ca^{2+}]_{perox}$  signatures (Section 8.2.2) and to understand the mechanisms of  $[Ca^{2+}]_{perox}$  buffering (Section 8.2.3) in an intact epithelium.

To generate distinct  $[Ca^{2+}]_{perox}$  signatures, about 20, 20, 30 and 50 anterior, posterior, anterior without initial segment tubules and just initial segments were dissected respectively for each replicate in Schneider's medium. The hours of dissections (mornings, between 9 - 12 AM) were chosen to be similar so that the tubule diurnal cycles are maintained and reflected in all the replicated samples. Likewise, 15-30 replicates were generated for each sample. Tubules were cut-separated into two for initial segment and rest of the segment (without initial segment) samples.

Then the samples were incubated in Schneider's medium with 2.5  $\mu M$  coelenterazine for reconstitution for  $Ca^{2+}$ -dependent luminescence for 2 h. The  $[Ca^{2+}]_{perox}$  was measured using the standard procedures (Rosay et al., 1997). First resting levels were measured for 2 min and then the stimulated levels for another 16-20 min, reading the luminescence for every millisecond.

Consistent with the previous observations that the anterior initial segment plays a vital role in organismal  $Ca^{2+}$  homeostasis, and a place for peroxisomes, it gives prominent  $[Ca^{2+}]_{perox}$  buffering response in contrast to the posterior segment (compare Figure 8-5 A with D). The initial segment alone can show this response (Figure 8-5B) while the rest of the segment  $[Ca^{2+}]_{perox}$  response looks like posterior segment (Figure 8-5D).

The comparative analysis of  $[Ca^{2+}]_{cyto}$  and  $[Ca^{2+}]_{perox}$  signatures revealed that the peroxisomes buffer the transient secondary rises, but not the rapid transient primary rise upon *capa1* stimulation (Figure 8-6, left panel). The resting levels seem to be 2-fold higher in peroxisomes than the cytosol (Figure 8-6, right panel). Observing one  $[Ca^{2+}]_{perox}$  readout at a time revealed that the  $Ca^{2+}$  levels oscillate unlike  $[Ca^{2+}]_{cyto}$  (Figure 8-7). When cytosolic- and peroxisome-targeted probe was released into the high  $Ca^{2+}$  external media, they differ in the total luminescence, in that, the equilibration takes longer time for peroxisome-targeted probe than the cytosolic-targeted probe (Figure 8-8). Nevertheless, the data with the strong backup from the next section (Section 8.2.2) suggest the targeted aequorins exhibit similar  $Ca^{2+}$  response kinetics and indeed represent peroxisomal  $[Ca^{2+}]$  readings.

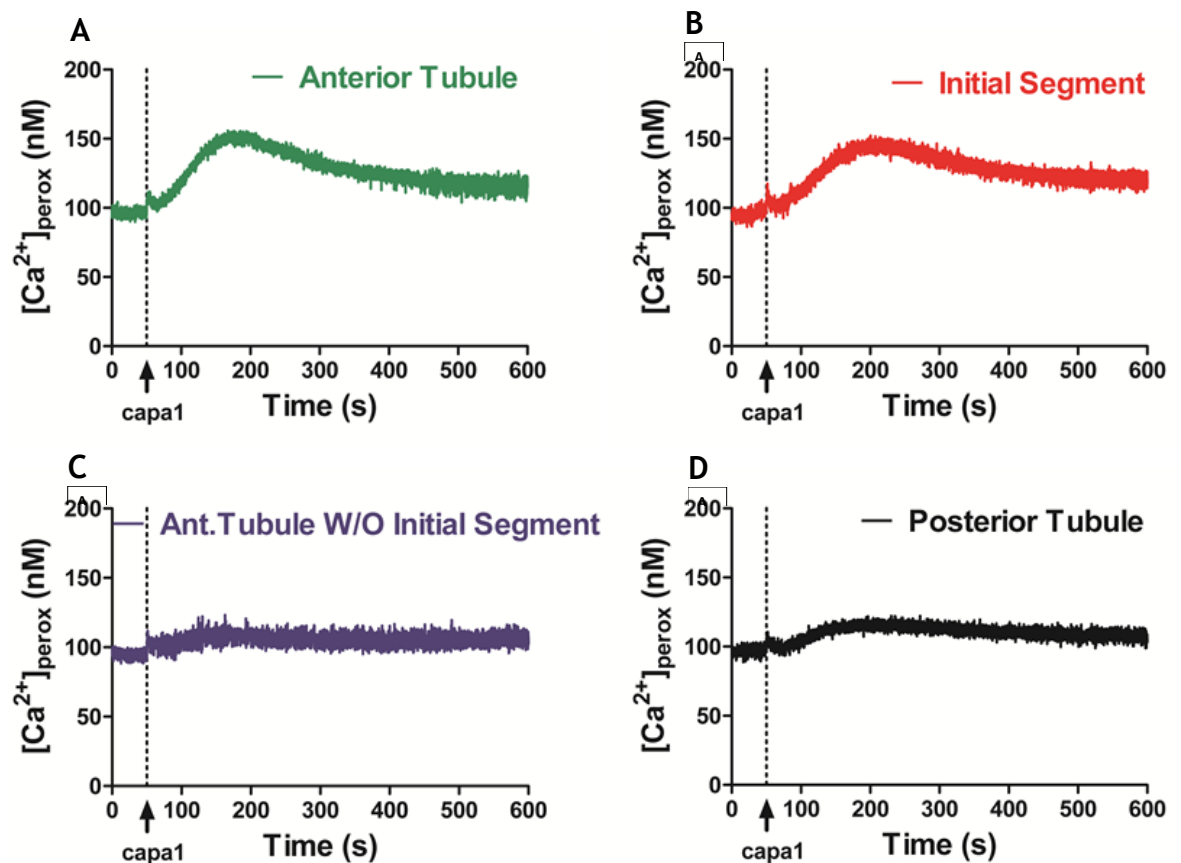


**Figure 8-5** Basal and stimulated  $[Ca^{2+}]_{perox}$  in tubules.

In a continuous readout, resting and stimulated (*capa1* at  $10^{-7}$  M)  $[Ca^{2+}]_{perox}$  (injected time point is shown using an arrow) were measured and presented in nanomolar concentrations on Y-axis against time over 10 min on X-axis.  $[Ca^{2+}]_{perox}$  were separately measured for anterior (with and without initial segment), posterior and just the initial segment without the rest of the segment.

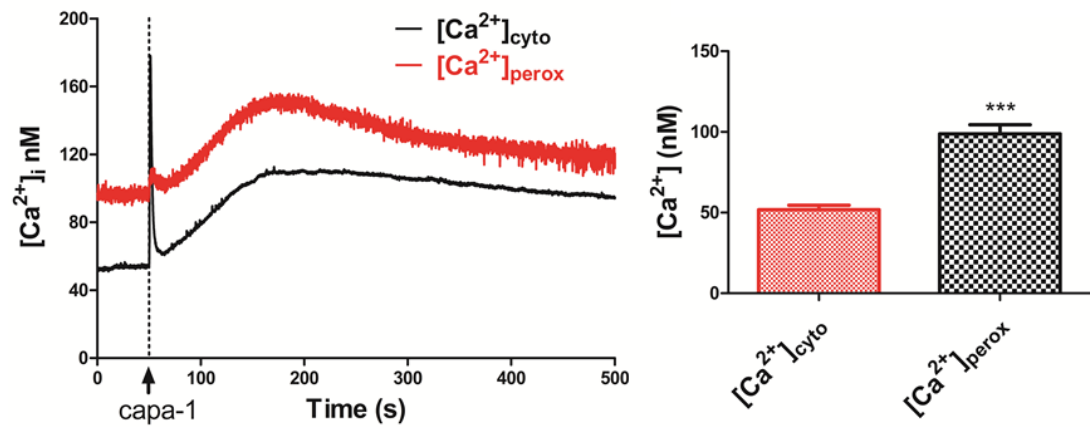


Figure 8-6 Comparison of quantitative  $[Ca^{2+}]_{cyto}$  and  $[Ca^{2+}]_{perox}$  measurements.  $[Ca^{2+}]_{cyto}$  was measured and presented along with  $[Ca^{2+}]_{perox}$ . The resting  $[Ca^{2+}]$  was found to be 2-fold higher in peroxisomes than the cytosol. The significance of difference ( $t$ -test;  $P \leq 0.0001$ ) is presented in the bar graph.

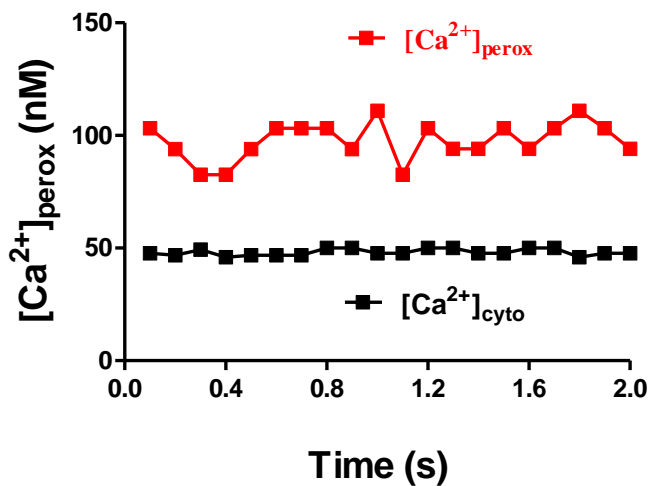


Figure 8-7 Typical resting  $[Ca^{2+}]_{cyto}$  and  $[Ca^{2+}]_{perox}$  measurements read every millisecond over 2 seconds. Peroxisomal  $Ca^{2+}$  seems to oscillate unlike the  $[Ca^{2+}]_{cyto}$ .

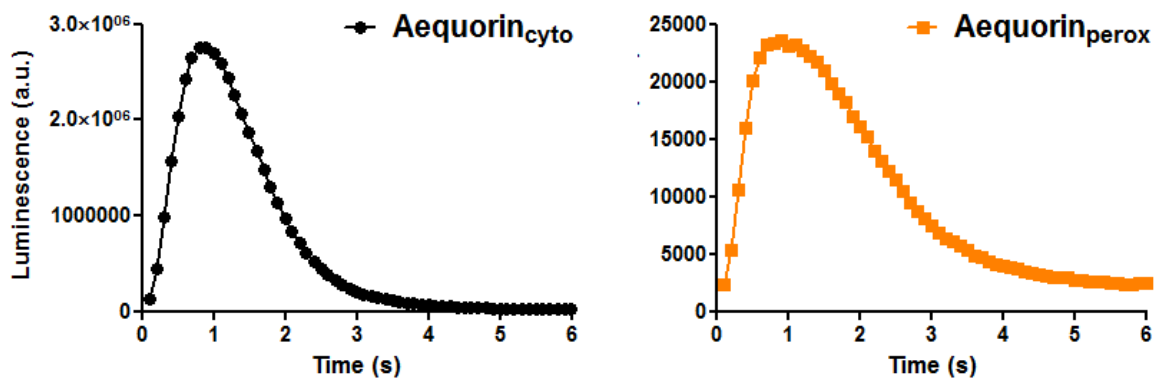


Figure 8-8 Equilibration of cytosolic and peroxisome targeted aequorin with the addition of Triton-X100 and high concentrations of  $Ca^{2+}$  containing solution.

### **8.2.2 Identification of novel peroxins CG11919 and CG13827 as the *Drosophila* orthologues of human PEX6 and PEX11**

Two questions became apparent after measuring tubule segment-specific  $[Ca^{2+}]_{\text{perox}}$  and comparing them with the  $[Ca^{2+}]_{\text{cyto}}$  measurements. These were including whether the targeting was altering  $Ca^{2+}$ -dependent luminescence of the aequorin, and if the quantitative comparisons can be made between cytosolic and peroxisomal  $[Ca^{2+}]$  measurements. A genetic intervention was devised to address these questions, and a search for peroxisome biogenesis factors that are abundant in tubules was launched in the FlyAtlas including the anterior and posterior tubule transcriptomes. This search led to the identification two *PEX* genes among the others that showed high abundance in the tubules and particularly in the anterior tubules where the peroxisomes are in high abundance (Figure 8-1). These include *CG13827* and *CG11919*, and were provocatively named as 'renal peroxins'.

Further comparative genomic approach and orthologue mapping identified these *PEX* genes as the *Drosophila* orthologues of human *PEX6* and *PEX11y*, respectively. The functions of the *PEX6* and *PEX11* gene families have been investigated previously in mammalian and yeast cells and implicated in the peroxisome biogenesis and fission respectively.

In humans there are three *PEX11* members including *PEX $\alpha$* , *PEX $\beta$*  and *PEX $\gamma$* , likewise *Drosophila* has three members including the one that belong to human *PEX $\beta$*  and the rest belong to *PEX $\gamma$*  (Figure 8-1).

The experimental plan was then setup to address if knocking down any of the two peroxins separately impairs the formation of peroxisomes. If the formation had been affected, it was hoped that the probes will be mistargeted possibly into the cytosol in *PEX6* knockdowns.

But, in the case of *PEX11* knockdowns, it was expected that peroxisomes could increase in size (or tubulated) and number as this gene has been implicated in the fission in mammalian and yeast cells (Li et al., 2002; Li and Gould, 2002).

The RNAi fly stocks were obtained for both genes from the VDRC stock centre (<http://stockcenter.vdrc.at/control/main>) to induce RNAi *in vivo* for their functional analysis. The immunocytochemical localisation of targeted aequorins in the RNAi backgrounds and then to obtain the  $[Ca^{2+}]_{\text{perox}}$  signatures for the same was carried out by cell-specifically ablating the expression of renal peroxins. The gene expression knockdown was induced separately for *CG11919* and *CG13827* using *C42-GAL4* driver, and confirmed using qPCR (Appendix IX and X). The knockdown of these genes did not cause developmental lethality either using *C42-GAL4* or *Act4C-GAL4*.

**Table 8-2 *PEX6* and *PEX11* gene expression across *Drosophila melanogaster* tissues (www.flyatlas.org).**

Affymetrix mRNA signals are presented for each gene against the tissues. *PEX11* family has three members in *Drosophila* that belong to  $\beta$  and  $\gamma$  genes of humans. The mRNA signal is predominant in tubules for both *CG11919* (*PEX6*) and *CG13827* (*PEX11 $\gamma$* ).

Tissue	<i>PEX6</i>	<i>PEX11</i>		
	<i>CG11919</i>	<i>CG8315/PEX11<math>\beta</math></i>	<i>CG13827/PEX11<math>\gamma</math></i>	<i>CG33474/PEX11<math>\gamma</math></i>
Brain	15 ± 2	98 ± 3	65 ± 2	2 ± 0
Head	376 ± 29	147 ± 2	81 ± 2	6 ± 1
Eye	154 ± 41	155 ± 4	53 ± 2	3 ± 1
Thoracoabd.ganglion	11 ± 1	125 ± 1	71 ± 4	3 ± 1
Salivary gland	4 ± 1	307 ± 4	783 ± 28	10 ± 2
Crop	7 ± 2	669 ± 25	523 ± 22	8 ± 2
Midgut	1 ± 0	401 ± 13	269 ± 1	8 ± 2
Tubule	2653 ± 159	302 ± 5	1826 ± 202	8 ± 1
Hindgut	58 ± 5	322 ± 8	327 ± 12	7 ± 1
Heart	172 ± 25	236 ± 11	106 ± 6	7 ± 0
Fat body	285 ± 59	182 ± 5	93 ± 10	23 ± 2
Ovary	0 ± 0	278 ± 3	96 ± 4	2 ± 0
Testis	4 ± 1	17 ± 2	29 ± 1	13 ± 1
Male acc. glands	3 ± 1	131 ± 7	124 ± 4	11 ± 1
Virgin spermatheca	1246 ± 66	131 ± 5	103 ± 2	40 ± 4
Mated spermatheca	483 ± 63	159 ± 14	94 ± 6	11 ± 1
Adult carcass	300 ± 19	171 ± 3	89 ± 6	13 ± 2
Larval CNS	1 ± 0	151 ± 7	67 ± 6	1 ± 1
Larval Salivary gland	6 ± 3	199 ± 18	742 ± 64	7 ± 1
Larval midgut	0 ± 0	233 ± 20	283 ± 16	19 ± 6
Larval tubule	1606 ± 89	186 ± 3	1432 ± 43	9 ± 1
Larval hindgut	25 ± 4	95 ± 2	224 ± 26	3 ± 1
Larval fat body	1390 ± 165	129 ± 9	129 ± 16	16 ± 2
Larval trachea	9 ± 10	230 ± 28	167 ± 15	4 ± 2
Larval carcass	3 ± 0	100 ± 4	262 ± 25	2 ± 0
S2 cells (growing)	2 ± 0	168 ± 6	38 ± 1	4 ± 1
Whole fly	120 ± 4	182 ± 3	116 ± 1	2 ± 0

### 8.2.2.1 Renal peroxins are functional in adult tubules

In order to test if the renal peroxins were functional in adult tubules, the stable fly lines *C42-GAL4>Aequorin<sub>perox</sub>* or *JAT20-GAL4>Aequorin<sub>perox</sub>* were separately crossed to either *UAS-CG13827-RNAi* or *UAS-CG11919-RNAi* fly lines to induce the RNAis and express *Aequorin<sub>perox</sub>* at the same time cell-specifically. This allowed the immunocytochemical localisation of *Aequorin<sub>perox</sub>* in wildtype and RNAi backgrounds (Section 8.2.2.1.1) then to obtain  $[Ca^{2+}]_{perox}$  signatures in the same (Section 8.2.2.1.2).

#### 8.2.2.1.1 *Cell-specific G11919 and CG13827 knockdown depletes peroxisomes and increases peroxisome abundance respectively in tubules*

The knockdown of *CG11919* using *C42-GAL4* depleted peroxisomes in a cell- and segment-specific manner in tubules. The *C42-GAL4* drives the knockdown in the principal cells of the main segment (including the cells in the initial segment). In these knockdown tubules, the *Aequorin<sub>perox</sub>* probe was mistargeted into the cytosol (Figure 8-9B) and also found to be trafficked possibly at cell-cell junctions in the initial, transitional, and main segment (Figure 8-10A, B & C). Interestingly, the depletion, thus mistargeting, was variable throughout the length of tubule, possibly due to the efficiency of knockdown and its metabolic state.

The knockdown of *CG13827* using *C42-GAL4* increased the abundance of peroxisomes, but not in the entire length of the tubule (Figure 8-9C). This effect was also seen using *JAT20-GAL4* which drives the knockdown (mildly) only in the initial segment where the aequorin was mistargeted to the cytoplasm (Figure 8-11).

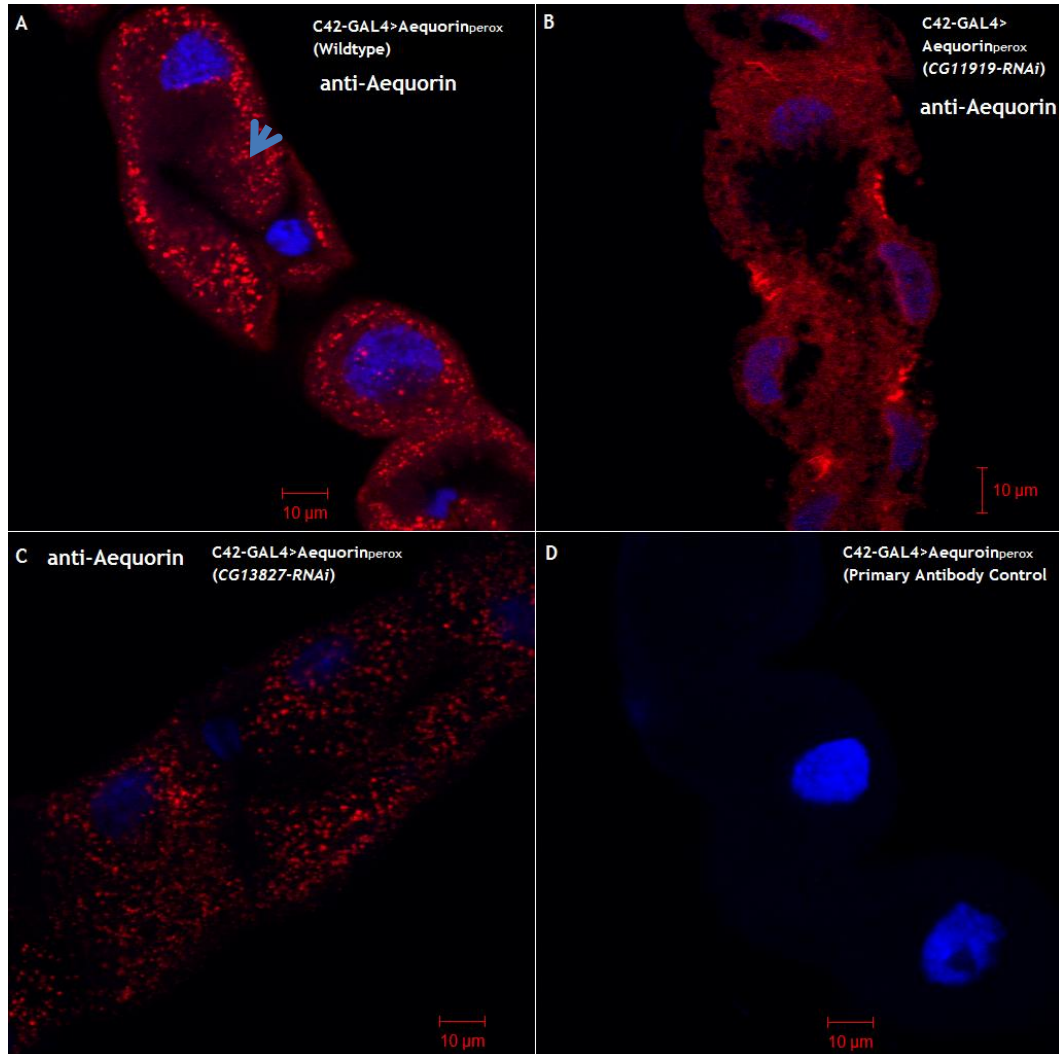


**Figure 8-9 Renal peroxins are functional.**

Cell-specific expression of Aequorin<sub>perox</sub> in tubules with different genetic backgrounds and immunostaining using rabbit anti-aequorin as the primary and anti-rabbit Texas-Red as the secondary antibodies. (A) Principal cells (with larger nucleus) but not stellate cells (star-shaped with small nucleus, arrowed) expressing the Aequorin<sub>perox</sub> in the wildtype. (B) Peroxisomes are depleted and Aequorin<sub>perox</sub> is diffused into the cytosol in *CG11919-RNAi* knockdowns. (C) The abundance of peroxisomes appears increased in *CG13827-RNAi* knockdowns. (D) Primary antibody controls.

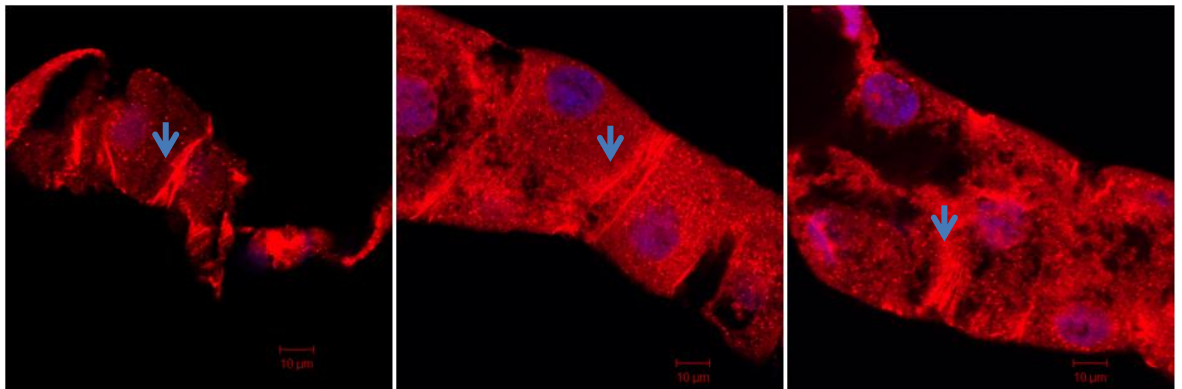


**Figure 8-10 Mistargeting of Aequorin<sub>perox</sub> in different parts of the tubules in C42-GAL4>CG11919-RNAi knockdowns.**

The initial, transitional and main segments are shown sequentially where the mistrafficking of Aequorin<sub>perox</sub> is shown using arrow heads.

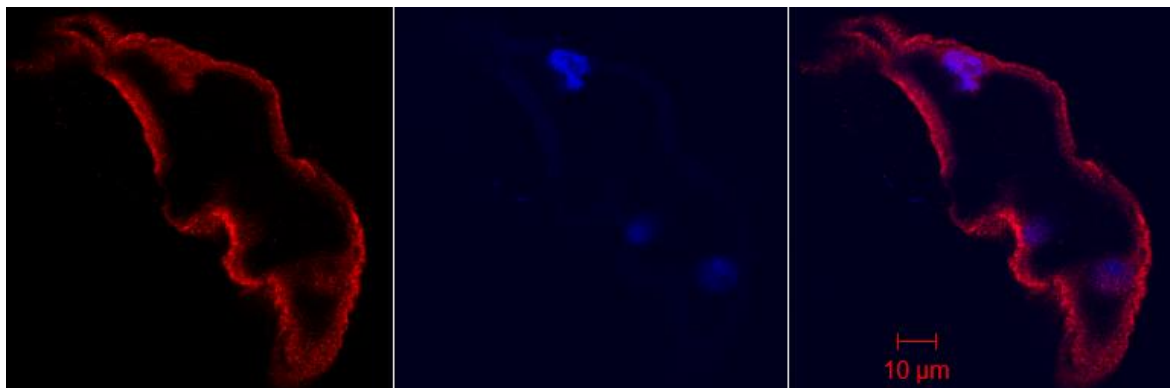


**Figure 8-11 Aequorin<sub>perox</sub> targeting in the initial segment of the *CG13827-RNAi* knockdown tubule.**

An initial segment GAL4 driver was used to ectopically drive the expression of both Aequorin<sub>perox</sub> and *CG13827-RNAi*; the Aequorin<sub>perox</sub> seen mistargeted into the cytosol.

### 8.2.2.1.2 Cell-specific renal peroxin knockdown deregulates $[Ca^{2+}]_{perox}$ buffering

Consistent with mistargeting of Aequorin<sub>perox</sub>, the resting and stimulated  $[Ca^{2+}]_{perox}$  rise was deregulated in both *CG11919-* and *CG13827-RNAi* knockdowns (Figure 8-12 A & B). The  $[Ca^{2+}]_{perox}$  measurements in *CG11919-RNAi* background reflected the mistargeting of the targeted probes. The resting levels of  $[Ca^{2+}]_{perox}$  were almost reduced to  $[Ca^{2+}]_{cyto}$  levels. In addition, the uncharacteristic stimulated rapid primary transients were seen like the ones that are found using Aequorin<sub>cyto</sub> in the wildtype background following sustained secondary rises. Therefore, it can be safely concluded that the kinetics of Aequorin<sub>perox</sub>, recapitulate the kinetics of the Aequorin<sub>cyto</sub> when they are diffused into the cytosol even with the additional targeting motifs at the Aequorin C-terminus. Then, these data suggest the targeted probe validity in quantitative  $[Ca^{2+}]_{perox}$  measurements and their suitability in comparisons with the  $[Ca^{2+}]_{cyto}$  measurements.

Not all the peroxisomes in the entire length of the tubule are affected by the *CG11919-RNAi* knockdown, probably due to differences in the percentage of knockdown in different parts of the tubule, and therefore the resting levels in this background were still high when compared to the wildtype cytosolic  $Ca^{2+}$  levels. This could be one of the reasons why the organism still copes with the reduced number of tubule peroxisomes.

While the increase in number of peroxisomes in *CG13827-RNAi* knockdown did not affect the resting levels, it did affect the *capa1* induced transient  $[Ca^{2+}]_{perox}$  uptake (Figure 8-12B).

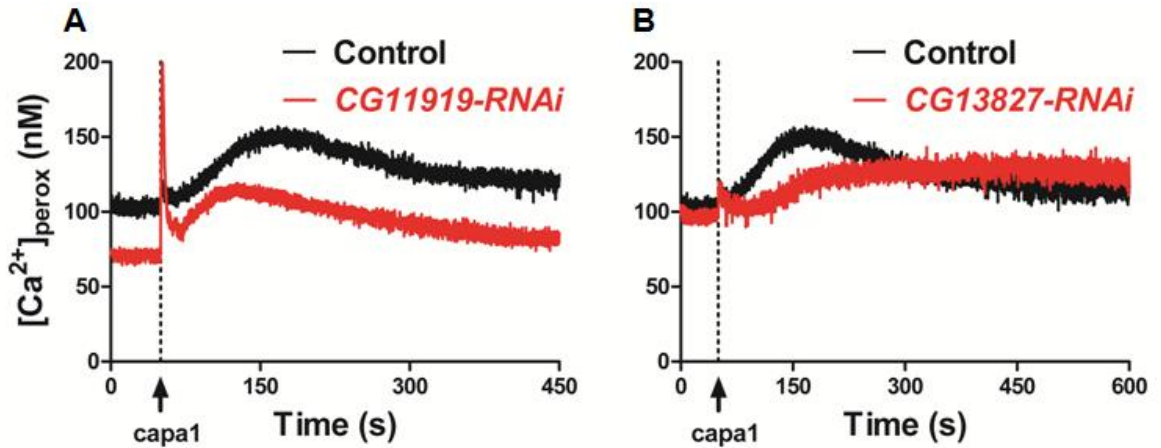


**Figure 8-12**  $[Ca^{2+}]_{perox}$  buffering is impaired in the *PEX* mutants.  $[Ca^{2+}]_{perox}$  signatures in the cell-specific knockdowns of *CG11919-RNAi* (A) and *CG13827-RNAi* (B) tubules. The resting and stimulated (*capa1*) were measured in the controls along with the knockdowns. The *CG11919-RNAi* impaired both resting and stimulated  $[Ca^{2+}]_{perox}$  measurements; while *CG13827-RNAi* knockdown impaired the stimulated  $[Ca^{2+}]_{perox}$ .

### 8.2.3 Identification of novel peroxisomal $Ca^{2+}$ sequestration and transport pathway in tubules

The neuropeptide *capa1* acts as an agonist and stimulates  $[Ca^{2+}]_{cyto}$  in tubules. The typical  $[Ca^{2+}]_{cyto}$  response to *capa1* constitutes two phases; a rapid transient primary and a sustained secondary rise. The primary response, possibly, is mediated by phospholipase C, *PLCB* (encoded by *norpA*) through  $IP_3$  ER  $Ca^{2+}$  store release. The secondary response is caused by the activation of plasma membrane  $Ca^{2+}$  channels. The probable candidates for the secondary influx are plasma membrane  $Ca^{2+}$  channels including TRPL and cyclic nucleotide gate channels (CNGs).

The CNGs were thought to be potential candidates that may be activated in response to *capa1* stimulation that increases cGMP production in tubules. From these observations, cGMP pathway was a candidate for stimulated transient  $Ca^{2+}$  uptake mechanisms into peroxisomes upon *capa1* stimulation. This was tested first using a genetic approach using RNAi fly resources directed against cGMP components, then by a pharmacological approach using cGMP pathway agonists and found to be a route for  $[Ca^{2+}]_{perox}$  entry.

### 8.2.3.1 cGMP regulates $[Ca^{2+}]_{\text{perox}}$ buffering

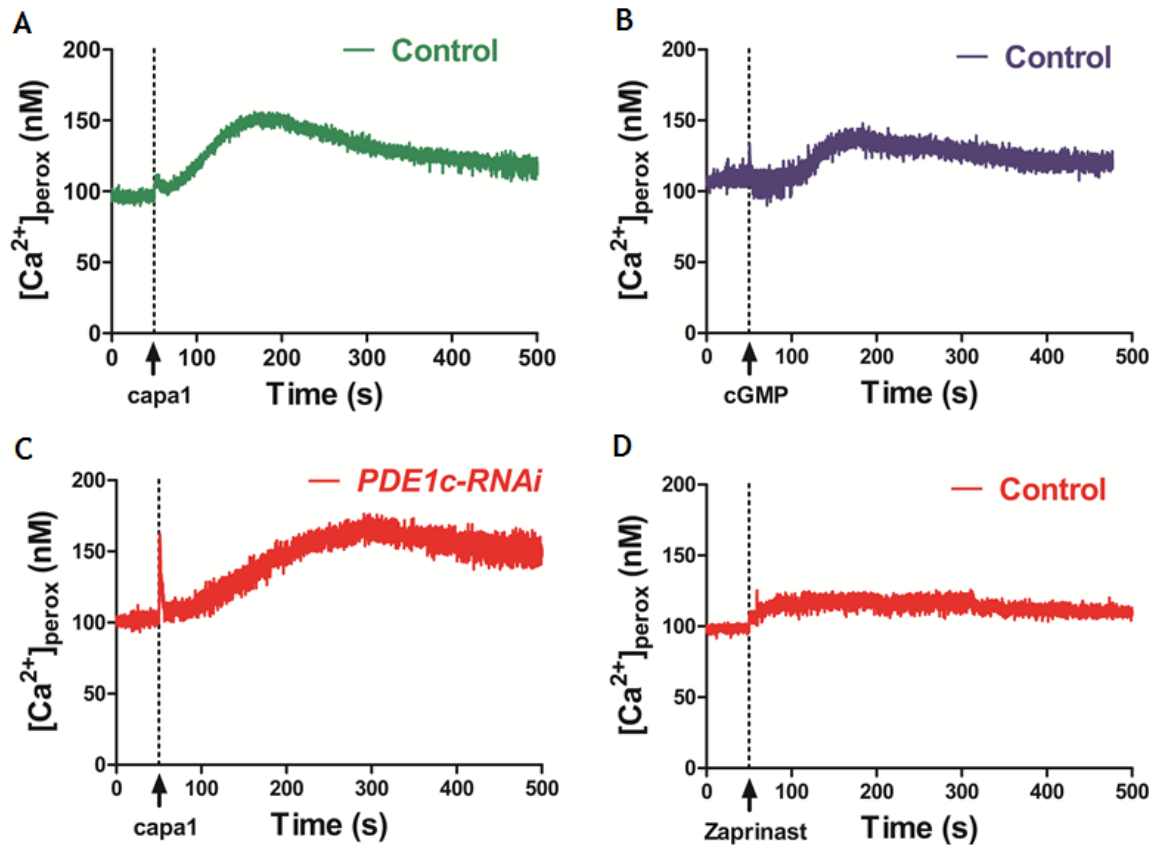


Figure 8-13 cGMP stimulates peroxisome  $Ca^{2+}$  uptake.

$[Ca^{2+}]_{\text{perox}}$  response to *capa1* in wildtype (A) and *PDE1c-RNAi* knockdowns (C) is shown. The response to external additions of cGMP ( $10^{-7}$  M), (B) and to a non-specific PDE inhibitor, zaprinast ( $10^{-6}$  M) (D) is also shown. The arrow heads with a dashed line indicates the time point where the respective peptide, cGMP or zaprinast was added.

#### 8.2.3.1.1 Peroxisomes buffer $Ca^{2+}$ in the course of sustained $[Ca^{2+}]_{\text{cyto}}$ elevations

The mechanism for rapid primary and sustained secondary  $Ca^{2+}$  transients upon *capa1* mobilisation was characterised to be mediated by  $IP_3$  induced store release, leading to the activation of plasma membrane  $Ca^{2+}$  channels producing transient  $Ca^{2+}$  influx respectively. Peroxisomes did not significantly respond to the rapid primary  $[Ca^{2+}]$  transients produced by *capa1*. However, they started buffering the slow transient secondary influx elicited by plasma membrane  $Ca^{2+}$  channels (Figure 8-13A) upon *capa1* stimulation.

### **8.2.3.1.2 Peroxisomes uptake $Ca^{2+}$ in response to external cGMP**

For a more direct evidence for a possible cGMP role in eliciting transient  $Ca^{2+}$  efflux into peroxisomes, several concentrations of cell-permeable cGMP (dibutyryl-cGMP) were added to tubules externally and  $[Ca^{2+}]_{\text{perox}}$  signatures were obtained. The optimal concentration for  $[Ca^{2+}]_{\text{perox}}$  response was found to be  $10^{-8}$  M (Figure 8-13B). This response was almost similar to the one produced by capa1 addition (compare Figure 8-13B with A).

### **8.2.3.1.3 Downregulation of *PDE1c*, a $Ca^{2+}$ /calmodulin-dependent PDE induces peroxisomal $Ca^{2+}$ uptake.**

The negative regulators of [cGMP] were the candidates to test if the modulation of cGMP levels affect  $[Ca^{2+}]_{\text{perox}}$  buffering at resting and in response to stimulation by capa1. A search was carried out in the FlyAtlas to find which PDEs were highly abundant in tubules and several PDEs were found including *PDE1c*. *PDE1c* belongs to the  $Ca^{2+}$ /calmodulin-dependent PDE1 family that acts in concert with  $Ca^{2+}$ . *PDE1c-RNAi* fly lines were obtained and  $[Ca^{2+}]_{\text{perox}}$  was measured in the cell-specific knockdown backgrounds for the *PDE1c*. The  $[Ca^{2+}]_{\text{perox}}$  response to capa1 was altered upon capa1 stimulation at both primary and secondary levels (Figure 8-13C). Normally, no significant primary buffering in response to capa1 by peroxisomes is observed (Figure 8-13A, see primary peak). However, *PDE1c* knockdown did give rise to an atypical primary  $[Ca^{2+}]_{\text{perox}}$  response with enhanced secondary rise for longer periods of time.

### **8.2.3.1.4 Zaprinast, a PDE inhibitor increases stimulated peroxisomal $Ca^{2+}$ uptake**

A pharmacological inhibitor of PDEs, zaprinast, has been shown to increase tubule cGMP levels at the apical regions of principal cells, suggesting a place for apically localised zaprinast-sensitive cG-PDE (Broderick et al., 2003). An experiment was designed to test whether zaprinast inhibition of tubule PDEs alone could elevate transient  $[Ca^{2+}]_{\text{perox}}$  buffering. Zaprinast was added to the tubules externally at varying concentrations and found to elicit  $[Ca^{2+}]_{\text{perox}}$  buffering at several different concentrations. It was found that zaprinast showed sustained  $[Ca^{2+}]_{\text{perox}}$  rise (Figure 8-13D).

### 8.2.3.1.5 *Best2* knockdown increases peroxisome $Ca^{2+}$ uptake

Increasing evidence suggests that bestrophins 1 & 2 may impact on  $Ca^{2+}$  channels (Marmorstein et al., 2006; Wu et al., 2007). The insights into purinergic activation of  $Cl^-$  current (by ATP and UTP) mediated by hBest1 was provided using HEK293 and clau-3 cells (Milenkovic et al., 2009). An ER localised isoform for hBest1 was found, and has been shown to interact with an ER- $Ca^{2+}$  sensor, stromal interacting molecule 1 (Stim1) in human airway epithelial cells (Barrosoria et al., 2010). Overexpressing *hBest1* augmented intracellular  $Ca^{2+}$  transients upon the stimulation of purinergic P2Y(2) receptors.

Interestingly, the *Drosophila* bestrophins, Best1 & Best2 localised to plasma membranes and peroxisomes in S2 cells, and various tissues of *Drosophila*, respectively (Figures 6-9, -11 & -12). The *in vitro* experiments using dissipating  $H^+$  and  $Na^+$  gradients in the cells strongly suggested a complex bioenergetic framework potentially including V-ATPase,  $Ca^{2+}/H^+$  and  $Ca^{2+}/Na^+$  activities accounting for  $Ca^{2+}$  buffering mechanisms in peroxisomes (Lasorsa et al., 2008). From these observations, I sought to identify if Best2 plays any role in  $[Ca^{2+}]_{\text{perox}}$  buffering using a genetic approach. Using GAL4/UAS system, *Best2-RNAi* was driven cell-specifically in the tubules and  $[Ca^{2+}]_{\text{perox}}$  was measured (Figure 8-14A). Although, the resting  $[Ca^{2+}]_{\text{perox}}$  levels were unchanged, the stimulated secondary maxima was significantly increased in the knockdowns (mean difference,  $32.6 \pm 6.8$  nM) (Figure 8-14B).

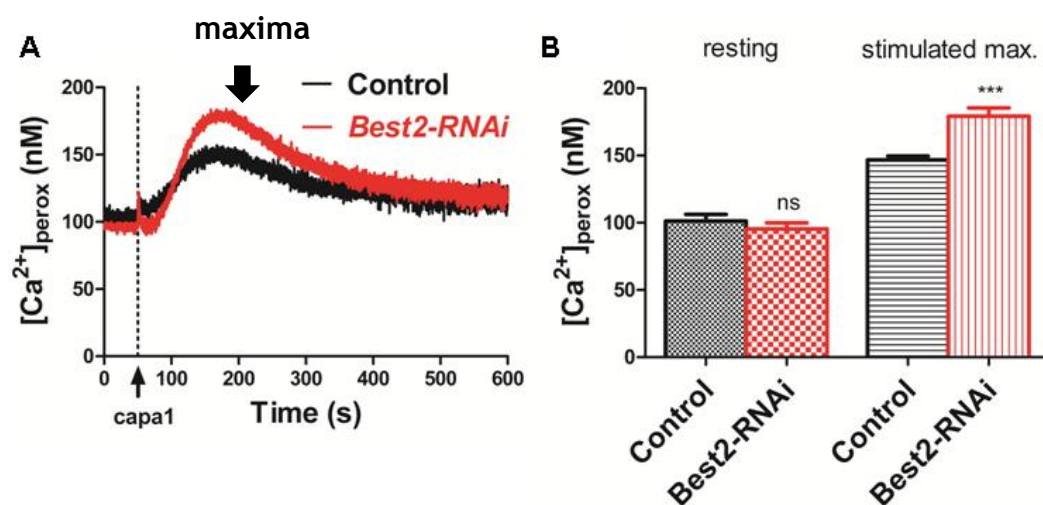


**Figure 8-14**  $[Ca^{2+}]_{\text{perox}}$  buffering in *Best2-RNAi* knockdowns is altered. (A)  $[Ca^{2+}]_{\text{perox}}$  response at resting and stimulated (capa1 at  $10^{-7}$  M) were plotted. (B) The resting levels were not changed significantly; the stimulated secondary transient rise was accelerated in *Best2-RNAi* tubules leading to the higher maxima than their control heterozygotes (*t*-test,  $P \leq 0.001$ ).

### 8.2.3.2 Spherite formation was affected in *CG13827-RNAi* knockdowns

The initial segment sequesters large amounts of  $\text{Ca}^{2+}$  into spherites (Dube et al., 2000a; Wessing, 1991), and these are peroxisomal in origin (Southall et al., 2006). The gene that encodes the peroxisome fission factor (*CG13827*) shows predominant expression in the anterior initial segment (Table 8-1, coloured). This was investigated for its potential impact on the spherite formation in the initial segment. The *CG13827-RNAi* was induced cell-specifically in tubules using C42-*GAL4* driver that induces RNAi in the initial segment. These tubules at adult stages were quickly dissected and immediately transferred on to a microscope slide for observation under light microscope. Interestingly, the spherites that are distinct from other concretions (in size they are larger) are less abundant in the *CG13827-RNAi* knockdowns than the wildtype (Figure 8-15A).

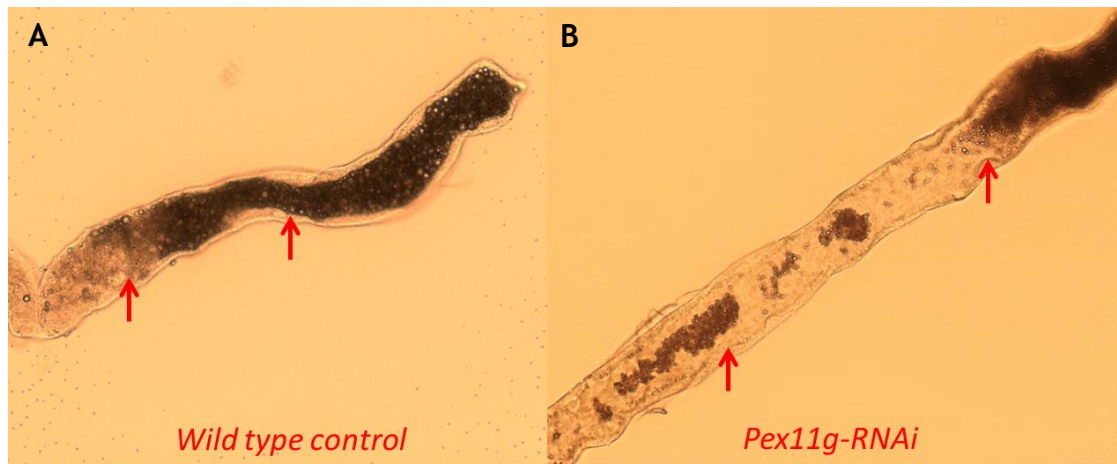


**Figure 8-15. Spherite formation was affected in *PEX* knockdowns.** The number of type I concretions (or calcium phosphate containing spherites) in *CG13827-RNAi* (or *PEX11g-RNAi*) are significantly reduced (indicated using arrow heads).

### 8.3 Discussion

Peroxisomes are single membrane bound organelles involved in a plethora of cellular metabolic functions thus contributing to cell survival & differentiation. For a long time, peroxisomes were thought to be acting as a permeability barrier, freely allowing the passage of only small molecules. However, evidence has been emerging against this idea, in the form of molecular identification of several peroxisomal membrane components that allow selective transport (Lasorsa et al., 2004; Palmieri et al., 2001; Rottensteiner and Theodoulou, 2006; Visser et al., 2007).

The recent characterisation of  $[Ca^{2+}]_{\text{perox}}$  buffering mechanisms *in vitro* argued a case for a probable peroxisomal membrane machinery for allowing  $Ca^{2+}$  into their lumen (Drago et al., 2008a; Lasorsa et al., 2008). Interestingly, they never seem to release  $Ca^{2+}$  into the cytoplasm like intracellular  $Ca^{2+}$  stores such as E(S)R, Golgi, mitochondria. But, rather they seem to sequester the slow transients of plasma membrane mediated  $Ca^{2+}$  influx raising the question of why peroxisomes need a complex bioenergetic framework as suggested by (Lasorsa et al., 2008).

In this study, the aequorin probes were successfully targeted to peroxisomes by a C-terminal KVK-SKL targeting sequence (Figure 8-1) *in vivo* in the renal transporting epithelia (Figure 8-3). The targeted protein was clearly trapped in the lumen, as demonstrated by its colocalisation with  $\alpha$ -catalase antibody (for the native peroxisomal catalase) (Figures 8-3 A & C). The peroxisomal localisation was also confirmed by Western blotting of protein from the purified peroxisomes from the whole flies expressing the targeted aequorin (Figure 8-3B).

The S2 cell  $[Ca^{2+}]_{\text{perox}}$  readouts were interesting (Figure 8-4). The S2 cells were originally derived from the primary cultures of late stage (20-24 h-old) embryos of *Drosophila melanogaster* (Schneider, 1972). Store operated calcium (SOC) channels are the characteristic of S2 cells, and these have been extensively characterised in this system (Yeromin et al., 2004). They are activated on the plasma membrane upon depletion of  $IP_3$ -sensitive ER  $Ca^{2+}$  stores and deactivated upon refilling (Yeromin et al., 2004). Comparatively, the basal  $[Ca^{2+}]_{\text{perox}}$  were higher than the  $[Ca^{2+}]_{\text{cyto}}$  in S2 cells.

Both *capa1* (Figure 8-4A) and *Drosokinin* (Figure 8-4B) elicited peroxisome  $\text{Ca}^{2+}$  uptake in concurrent with the cytosolic  $\text{Ca}^{2+}$  rises. Interestingly, peroxisomes showed little delayed response as the stimulated  $[\text{Ca}^{2+}]_{\text{perox}}$  reached their maximum after several seconds and stayed on for several seconds never reaching to near basal levels. This clearly indicates peroxisomes as the organelles that buffer  $\text{Ca}^{2+}$  potentially for excretion.

The tubule  $[\text{Ca}^{2+}]_{\text{perox}}$  readouts proved useful to understand the molecular mechanisms of  $\text{Ca}^{2+}$  transport via peroxisomes (Figure 8-5). Anterior tubules showed a more prominent peroxisomal  $\text{Ca}^{2+}$  buffering response when compared to posterior tubules (Figure 8-5, compare A with D). This was interesting because, each anterior tubule consists of an enlarged initial segment with around 30 specialised cells, in contrast to their posterior counterparts (Sozen et al., 1997). These segments in the anterior tubules alone store 25-30% of the total  $\text{Ca}^{2+}$  content of the whole animal (Dube et al., 2000b).  $\text{Ca}^{2+}$  in the initial segment is stored as the calcium phosphate in the spherites. From the X-ray microanalysis observations, the spherites were only seen in the cytosol and luminal side in the distal initial segment and proposed to transport  $\text{Ca}^{2+}$  and  $\text{Mg}^{2+}$  for their eventual excretion to save water (Wessing, 1991). Thus (specialised) peroxisomes may facilitate the loading of spherites with  $\text{Ca}^{2+}$  or the spherites are formed from the peroxisomes. Peroxisomes purified from bovine kidney and reconstituted into proteoliposomes suggest peroxisomal membranes constitute mechanisms for phosphate transport (Visser et al., 2005). The enrichment of NaPi-T transporter mRNA in the anterior tubules indicate the requirement of phosphate to precipitate  $\text{Ca}^{2+}$  possibly in the spherites.

Peroxisomes sense sustained  $\text{Ca}^{2+}$  changes due to the changes, for example, in the haemolymph, and buffer the extra cytosolic  $\text{Ca}^{2+}$  that appears in the initial segment cells. The resting levels measured were as high as 2-fold in peroxisomes under the given set of experimental conditions indicating their capacity to  $\text{Ca}^{2+}$  storage. Furthermore, they did not release  $\text{Ca}^{2+}$  upon agonist stimulation potentially to excrete as bulk. They buffer sustained secondary  $\text{Ca}^{2+}$  transients probably produced by the activation of plasma membrane  $\text{Ca}^{2+}$  channels. But they do not seem to buffer immediate  $\text{Ca}^{2+}$  transients produced by  $\text{IP}_3$ -induced ER  $\text{Ca}^{2+}$  efflux.

These findings are in consistent with the previous observations that upon hyperpolarization of plasma membranes, a slow transient peroxisomal  $\text{Ca}^{2+}$  increase was observed (Lasorsa et al., 2008).

The initial segment role in peroxisomal  $\text{Ca}^{2+}$  buffering became more apparent when a separate  $[\text{Ca}^{2+}]_{\text{perox}}$  readout was obtained for this segment.  $[\text{Ca}^{2+}]_{\text{perox}}$  signatures were obtained for anterior tubules that were cut-separated as initial and the rest of the segment. These unravelled a role for the initial segment in  $\text{Ca}^{2+}$  homeostasis in consistent with previous findings implicating this segment in  $\text{Ca}^{2+}$  sequestration and storage. The initial segment alone can give rise to agonist stimulated  $\text{Ca}^{2+}$  rise in peroxisomes (Figure 8-5B). In contrast, the rest of the segment failed to show this response (Figure 8-5C). Around 30 cells of the initial segment possibly regulate haemolymph  $\text{Ca}^{2+}$  concentrations, or the  $\text{Ca}^{2+}$  that is emanating from the gut through the plasma membrane  $\text{Ca}^{2+}$  channels that are in close contact with gut cells. Furthermore, the buffering of  $\text{Ca}^{2+}$  by peroxisomes by the tubules without initial segment exactly recapitulates the buffering by posterior segment peroxisomes (Figure 8-5, compare C with D). These results are in consistent with the microarray analysis of anterior versus posterior tubules, where a number of genes showed abundance in the anterior tubules than the posterior tubules (Table 5-1).

The posterior tubules have a very small initial segment. The microarray provides evidence that the posterior tubules may perform distinct functions other than the ones that are performed by the anterior tubules (Table 5-1). From the peroxisomal  $\text{Ca}^{2+}$  measurement, these tubules do not fully equip to buffer secondary plasma membrane transients in contrast to their anterior counterparts (Figure 8-5D).

### **8.1.1 Renal peroxins**

Many peroxisome biogenesis proteins have been identified, and some of their functions are well known (Nuttall et al., 2011; Purdue and Lazarow, 2001; Rucktaschel et al., 2011). Genetic complementation exists, in that the defects in one peroxins can be rescued by the other. Most of the peroxins show housekeeping functions and are expressed accordingly in all cells for the proper formation of peroxisomes.

However, some peroxins show substrate specificity and high abundance in the tissues (for example that metabolise lipids) investigated where the peroxisomes are high in number (van den Bosch et al., 1992; Wanders and Waterham, 2006). The peroxisome biogenesis disorders predominately manifest in the neuronal tissue along with liver and kidneys, though the reason for this is not known (Figure 1-6) (Steinberg et al., 1993).

In this study the two peroxins identified to be the *Drosophila* homologues of human *PEX6* and *PEX11*. Both peroxins found to be abundant in the renal tubules (Table 8-1). The ubiquitous knockdowns of these peroxins did not cause developmental lethality. Possibly, *PEX11y* function is redundant as there are 2 other related members that exist in *Drosophila* similar to their human counterparts (Table 8-1), or it may not be necessary. However, cell-specific conditional ablation revealed their functions in the adult renal tubules. The expression pattern of these genes in the tubules correlated with tubule initial segment peroxisome abundance.

The defects in *PEX6* function are the second most common causes of ZSS disorders in humans (Ebberink et al., 2010). *PEX6* participates in the recycling of *PEX5p* for the protein import into peroxisomes (Rucktaschel et al., 2011). Consistent with the significance of this protein in peroxisome biogenesis, the cell-specific knockdown of the *CG11919*, that is closest to the human *PEX6*, in tubules, led to a significant ablation of peroxisomes (Figure 8-9B, compare with A). This caused the diffusion of peroxisomal targeted probe into the cytoplasm (Figure 8-9B) and its mistrafficking to the cell-cell junctions (Figure 8-10). The peroxisomal  $\text{Ca}^{2+}$  response reflected these changes in peroxisomes, partially recapitulating the cytosolic  $\text{Ca}^{2+}$  response (Figure 8-12A). These observations clearly indicate a role for *PEX6* in the proper formation of peroxisomes in the renal tubules.

The *PEX11* family of proteins help bring the components required for the peroxisome division. The loss of *PEX11* function had a less severe effect on peroxisome abundance, while the overexpression had a marked affect where it promoted peroxisome division in mouse cells (Li and Gould, 2002). However, a peculiarity was shown for *PEX11y*, that its overexpression does not induce peroxisome proliferation in mammalian fibroblasts (Li et al., 2002).

Ablating the expression of *CG13827*, that is closest to the human *PEX11γ*, in tubules, showed an interesting phenotype. Knocking down using *C42-GAL4* increased peroxisome abundance in the main segment (Figure 8-9C, compare with A). This suggests that it has an essential role in tubule peroxisome proliferation. Consistent with the change in peroxisome abundance, the  $\text{Ca}^{2+}$  buffering by peroxisomes was altered in response to the agonist, *capa1* stimulation (Figure 8-12B).

These findings clearly demonstrate the functional significance of the renal peroxins in the tubules. In addition, they validate the peroxisomal  $\text{Ca}^{2+}$  signatures.

### **8.3.1 A mechanism for $[\text{Ca}^{2+}]_{\text{perox}}$ buffering and $\text{Ca}^{2+}$ spherites**

The *in vitro*  $[\text{Ca}^{2+}]_{\text{perox}}$  buffering mechanisms are laid out by two recent reports implicating these organelles in cell  $\text{Ca}^{2+}$  dynamics and homeostasis (Drago et al., 2008a; Lasorsa et al., 2008). Using a combination of different cell-types, pharmacology and  $\text{Ca}^{2+}$  agonists, these authors showed that peroxisomes buffer  $\text{Ca}^{2+}$  but never release it. Interestingly, peroxisomes only buffer sustained  $\text{Ca}^{2+}$  transients upon probably the activation of plasma membrane  $\text{Ca}^{2+}$  channels, but they do not seem to respond to the rapid transients. These observations strongly suggest a mechanism that needs to be activated in the peroxisomal membranes to facilitate the transient  $\text{Ca}^{2+}$  influx.

These observations along with the findings in this study suggest that the initial segment plays a major role in  $\text{Ca}^{2+}$  buffering via peroxisomes, possibly to sequester as spherites.  $\text{Ca}^{2+}$  cannot be metabolised like other second messenger molecules such as cAMP, cGMP, DAG and  $\text{IP}_3$ . The regulation of intracellular  $\text{Ca}^{2+}$  concentrations thus is an important phenomenon in the cell. In animals with open circulatory systems where the tissues are packed in the haemolymph,  $\text{Ca}^{2+}$  needs to be tightly regulated for the spatiotemporal aspects of its signaling component. The nearest correlate of peroxisomal function affecting the vesicular transport is lipid droplets, the vesicles that store fat in the form of triacylglycerides (TAGs).

For example, the defects in the peroxisomal  $\beta$ -oxidation of fatty acids lead (in some cases) to enlarged lipid droplets (Zhang et al., 2010a). These droplets are mobile depending upon the organism's metabolic needs. Although drawing parallels between unknown  $\text{Ca}^{2+}$  spherite formation and lipid droplets is quite vague, it is at least interesting to note the peroxisomal proper function in loading of the cargo into the vesicles.

The evidence in this report suggests a possible role for peroxisomal scission in generating  $\text{Ca}^{2+}$  phosphate spherites. The case then arises as to whether the peroxisomes undergo vesicular scission to become spherites for the eventual excretion. Peroxisomes undergo fission in that the fully formed peroxisome vesiculates and form new peroxisomes. The molecular components of scission may require  $\text{Ca}^{2+}$  and the loading of peroxisomes with  $\text{Ca}^{2+}$  probably initiates the peroxisome fission process to form the spherites to store, and upon the activation they might be mobilised. Taken together, a model for peroxisome  $\text{Ca}^{2+}$  handling in tubules can be built as shown in Figure 8-16.

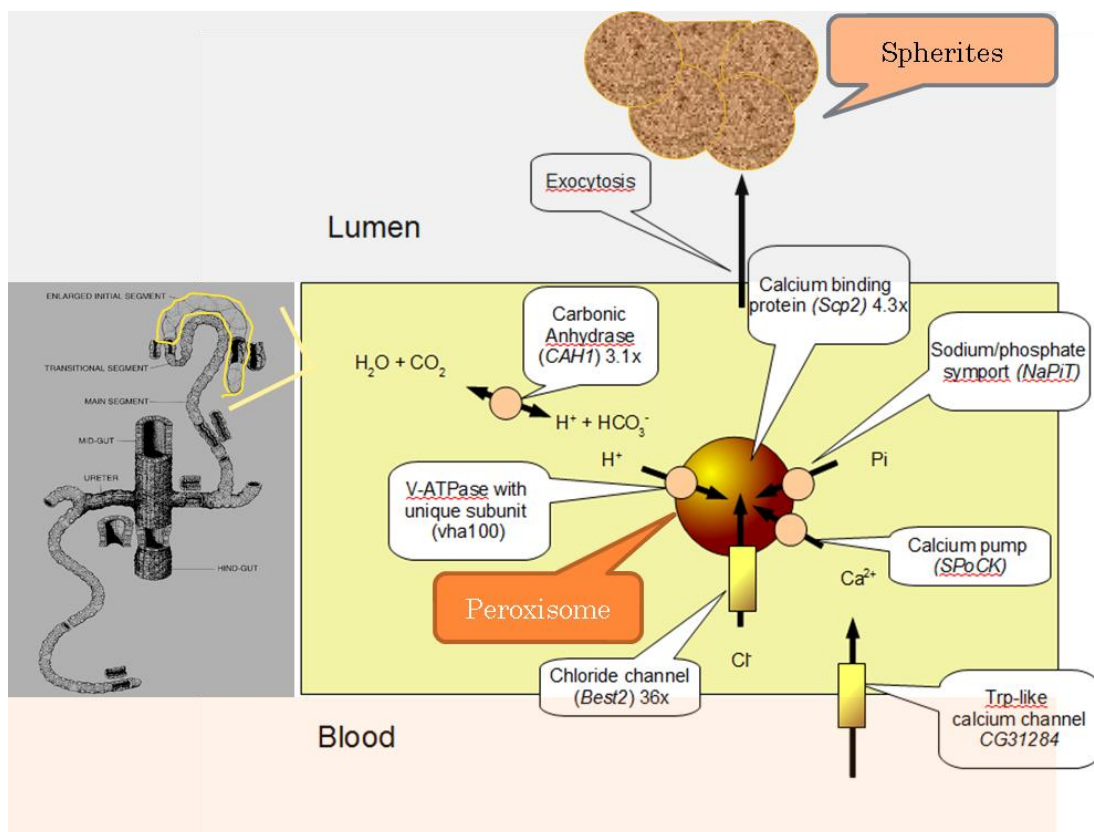


Figure 8-16. A model for peroxisomal  $\text{Ca}^{2+}$  sequestration and transport excretion.

Then the question arises when the peroxisomes buffer  $\text{Ca}^{2+}$ . From this investigation and others findings (Drago et al., 2008b; Lasorsa et al., 2008), it is apparent that peroxisomes transiently uptake  $\text{Ca}^{2+}$ , possibly stemming from the plasma membrane  $\text{Ca}^{2+}$  channels, for prolonged periods of time. This mechanism seems to be dependent on the second messengers such as cGMP that activate plasma membrane CNG channels. The neuropeptide agonist *capa1* mobilised  $\text{Ca}^{2+}$  into peroxisomes (Figure 8-6, red line). This response is markedly different from the cytosolic response (Figure 8-6, black line). The *capa1* action leads to the characteristic biphasic cytosolic  $\text{Ca}^{2+}$  response in tubules including primary (from ER) and secondary (from the activation of plasma membrane  $\text{Ca}^{2+}$  channels). Only, the secondary response was found for peroxisomes. But, the primary response can be obtained in the *CG11919-RNAi* knockdown background (Figure 8-12A). This suggests that peroxisomes only buffer prolonged  $\text{Ca}^{2+}$  transients upon the activation of plasma membrane  $\text{Ca}^{2+}$  channels such as CNGs. The *capa1* action elicits cGMP concentrations in the tubules that may gate CNG channels (Davies and Terhzaz, 2009). The addition of cGMP to the tubules elicits peroxisomal  $\text{Ca}^{2+}$  uptake which partially recapitulates *capa1* response (Figure 8-13B, compare with A). In addition, genetic and pharmacological reduction of PDE activity by an RNAi transgene directed against the *PDE1c* and a PDE inhibitor, Zaprinast respectively resulted in peroxisomal  $\text{Ca}^{2+}$  uptake (Figure 8-13 C & D). The *Best2-RNAi* knockdowns showed increased peroxisome  $\text{Ca}^{2+}$  buffering (Figure 8-14). The secondary cytosolic  $\text{Ca}^{2+}$  responses were significantly found increased in *Best2-RNAi* knockdowns as shown in the previous chapter (Figure 7-7). Thus the ablation of *Best2* expression seems to affect the stimulated  $\text{Ca}^{2+}$  levels in the tubules.

### **8.3.2 The significance of $\text{Ca}^{2+}$ in terms of peroxisome function**

Peroxisomal  $\text{Ca}^{2+}$  regulation, and its role in cell  $\text{Ca}^{2+}$  homeostasis, is a relatively new and exciting field given its potential implications in cell metabolism, redox homeostasis, and survival. It is well known that prolonged elevations in intracellular  $\text{Ca}^{2+}$  levels are deleterious to cells (Wegierski et al., 2009). In these circumstances,  $\text{Ca}^{2+}$  must be buffered for excretion. Peroxisomes probably contribute to this function whereby they buffer the sustained secondary  $\text{Ca}^{2+}$  transients elicited by plasma membrane channels into the cytoplasm and then store in the bulk insoluble pools for its eventual excretion.

The other potential questions that arise from this study and others include how many peroxisomal reactions is  $\text{Ca}^{2+}$  dependent? Previously, a  $\text{Ca}^{2+}$ /calmodulin-regulated catalase isoform has been localised in plant peroxisomes (Yang and Poovaiah, 2002). An increase in peroxisomal  $\text{Ca}^{2+}$  concentrations have been shown to increase  $\text{H}_2\text{O}_2$  scavenging activity via catalase (Costa et al., 2010). This establishes a route for a search of other peroxisomal functions for which  $\text{Ca}^{2+}$  is essential, in other systems. From animals to plants it is widely documented that reactive oxygen species (ROS), such as  $\text{H}_2\text{O}_2$  and superoxide ( $\text{O}_2^-$ ) are not only the by-products of redox homeostasis but essential as signal transduction components (Alvarez et al., 1998; Owusu-Ansah and Banerjee, 2009). These species are highly produced in peroxisomes, and their generation might suggest a role for peroxisomes in signal transduction processes. Furthermore, this study clearly demonstrated a role for anterior initial segment in buffering transient influx of  $\text{Ca}^{2+}$  into the cytoplasm. This is the characteristic functional attribute to this segment. Then, what does the rest of the tubule possibly do? The prominent example is the urate oxidase gene that participates in the conversion of uric acid to allantoin, which is only expressed in the main segment of the tubule. Other genes that are well-known in the oxidative stress resistance, such as *catalase* and *superoxide dismutase (SOD)*, probably are more prominent in the rest of the tubule.

## 8.4 Conclusion

Calcium homeostasis is a fundamental phenomenon required for organismal survival given its prominence in cellular signal transduction mechanisms. Equally, it is important in the formation of bones in vertebrate systems and their equivalents in other systems. The continuous  $\text{Ca}^{2+}$  diet supplement also needs to be regulated. Our understanding of the molecular machinery is rapidly increased over the years through the advancements in the genomic and post-genomic technologies. However, the systems approach for the functional analysis is rather lacking in a physiological perspective. *Drosophila*, more specifically its renal system, the tubules, provides a powerful array of genetic and physiological tools to study the regulation of both cytosolic and organellar  $\text{Ca}^{2+}$  signaling and transport mechanisms.

This study demonstrated the successful targeting of aequorin probes to peroxisomes in an actively transporting live renal epithelium to study *in vivo*  $[Ca^{2+}]_{\text{perox}}$  buffering mechanisms. The resting levels of  $[Ca^{2+}]_{\text{perox}}$  were found to be 2-fold higher than the  $[Ca^{2+}]_{\text{cyto}}$ . Peroxisomes act to buffer transient secondary  $Ca^{2+}$  efflux into the cytosol via plasma membrane  $Ca^{2+}$  channels like CNG channels that are activated in response to cGMP. External addition of cGMP induces  $Ca^{2+}$  uptake into peroxisomes in consistent with the uptake upon the pharmacological inhibition of PDEs with Zaprinast. Two independent genetic interventions through RNAis to peroxisome localised *Best2* and  $Ca^{2+}$ /calmodulin-dependent *PDE1c* mRNAs, although never resulted in significant resting  $[Ca^{2+}]_{\text{perox}}$  changes, they enhanced stimulated secondary maxima for the former and primary and secondary responses for the later. This reflects a possible triggering mechanism exist to buffer extraperoxisomal  $Ca^{2+}$  concentrations. Two *PEX* genes found to be highly abundant in the tubules and are confirmed to be essential for proper renal-peroxisome formation and proliferation. Finally, using an ‘integrative systems approach’, a model generated from microarray data was tested for its validity using fly renal system that may be applicable to mammalian renal  $Ca^{2+}$  sequestration and transport mechanisms.

## 9. General discussion and Future work

### 9.1 General discussion

Systems approach requires greater understanding of genomes. Model organisms are useful not only for generating systems level omics data sets but also are instrumental in integrating the datasets to allow to build predictive models (Joyce and Palsson, 2006). Omics data sets have been providing systems level annotation of nearly all components, broadly at three levels including components, interactions and functional states. Thus the omic annotation is a great step forward for the holistic understanding of systems, in the so called systems biology.

A case for *Drosophila* as a model organism is validated with its continuous usage to understand many biological questions. The advent of RNAi technology along with the GAL4/UAS binary systems to express transgenes *in vivo*, at a remarkable spatiotemporal resolution, has given further strength to this model organism to deploy reverse genetic approach to understand functions of genes. Comparative analysis of fully sequenced genomes identified a greater phenotype gap, the gap that is present between number genes to available phenotypes. The study carried out as part of this thesis is useful for further functional annotation of the genomes. The highlights of this study are presented by the order of chapters.

#### 9.1.1 FlyAtlas

The FlyAtlas pioneered the way to look at tissue-specific functions using transcriptomes.

1. FlyAtlas provides authoritative gene expression levels for multiple tissues of *Drosophila melanogaster* for both adult and larval tissues.
2. *Drosophila* tissues typically express around half of the computed transcriptome.
3. There are hundreds and thousands of genes that show tissue-specificity of expression.

4. The genes that have been classically studied in development for example, are expressed in surprising places. Thus arguing a case for tissue-specific studies of genes where they are highly abundant rather than where they are first found.

5. The genes that are expressed in tissues analogous to those involved in human disease provided further strength to *Drosophila* as a model organism to study human disease.

### **9.1.2 Epithelial transcriptomes**

The tissue-specific transcriptomes of the FlyAtlas provided quality data sets to understand epithelial function in detail. The comparative analysis of the epithelial tissues provided insight into their potential functions in addition to their conservation of function with their vertebrate counterparts.

1. Epithelial transcriptomes are highly organised and show similarity in expression from other transcriptomes such as reproductive and neuronal tissue transcriptomes which has been apparent in the PCA analysis.

2. The adult and larval transcriptomes of any single epithelium shows highest similarity to each other, thus fall as neighbours in the hierarchical tree.

3. In each epithelium, there are many novel genes that show high specificity of expression without any functional annotation. However, many of these show high similarity to human disease homologues thus allowing to guess their potential functions.

4. Enrichment of epithelial signature genes in vertebrate functions revealed their cognate functions to human tissues.

### **9.1.3 Renal asymmetry in *Drosophila***

The microarray analysis of tubule disposition or asymmetry in the body cavity revealed interesting insight into function.

1. Anterior tubules show high abundance for Ca<sup>2+</sup> handling genes.

2. Posterior tubules show abundance for genes involved in ammonia generation, for example.

#### **9.1.4 Functional studies on bestrophins and the identification of *Best2* as a modulator of $Ca^{2+}$ signaling and homeostasis**

$Cl^{-}$  channels have long been thought to be housekeeping in function in the regulation of cell volume and maintenance of the balance of electrical charge, unlike for example the  $Na^{+}$  and  $K^{+}$  channels that trigger nerve impulses. However, compelling evidence accumulated over the years suggesting  $Cl^{-}$  channels are equally important from neuronal signal propagation to salt regulation (Jentsch et al., 2002). The pharmacological approach to characterise  $Cl^{-}$  channel function has been hampered by the unspecific nature of the channel blockers (Greenwood and Leblanc, 2007). The low potency and broad specificity and tissue variability of these channel blockers made the studies more complex. Reverse genetic approach, using model organisms, where a wealth of genetic and physiological tools is available, argued as a most suitable approach to elucidate functions of a given gene (Dow, 2007; Dow and Davies, 2003).

Furthermore, comparative genomics (Ureta-Vidal et al., 2003) helped elucidate the molecular identity of the putative  $Cl^{-}$  channels in the fruit fly with the readily available gene expression data across multiple tissues (Chintapalli et al., 2007) that enable one to model the interaction of the  $Cl^{-}$  channels with other types of channels and transporters. This kind of an approach at systems level, permits advanced studies with prior knowledge of complex interplay of the ion transporter synergy in different compartments of the cell.

Using an integrative physiology approach, organismal functions of bestrophins were investigated in this study.

1. Firstly, a demonstration was made of cellular localisations for all *Drosophila* bestrophins. This showed the apical localisation of Best1-YFP, peroxisomal localisation of Best2-YFP, and intracellular localisations for Best3-YFP and Best4-YFP.
2. *Best1* and *Best4* are non-essential for fly viability; in contrast, *Best2* and *Best3* are essential for the same.

4. *Best1* is an essential gene for handling excessive salt load in the body.

5. *Best1* is a potential CaCC that function at the physiological elevations of intracellular  $\text{Ca}^{2+}$  concentrations.

4. *Best2* is a potential  $\text{Ca}^{2+}$  channel regulator, thus regulating  $\text{Ca}^{2+}$  signaling and homeostasis in the tissues it is highly abundant, the eyes and tubules respectively.

5. In addition, this study elucidates the molecular mechanisms of *Best2* function. The identification of  $\text{Ca}^{2+}$ -responsive, epithelial abundant, *Cyp6a23* upregulation in the *Best2* mutants, in addition to the identification of the upregulation of other  $\text{Ca}^{2+}$  signaling modules that are essential for the fly retina including the components of the INAD complex, gives a fascinating insight into *Best2* function. Furthermore, the upregulation of *retinal degeneration C (rdgC)* in the *Best2* mutants shows how the compensatory mechanisms are potentially deployed in the flies, possibly, to mitigate the effects of the dysfunction of *Best2*. This is in consistent with the fact that the knockdown of *Best2* does not cause any apparent morphological defect in the flies. This means a fly bestrophin model of human disease can be developed, potentially with a double knockdown of *Best2* and *rdgC*, for example. Nonetheless, these results may form a basis to search for similar mechanisms in vertebrate disease models thus to intervene therapeutically, for example to increase the expression of *rdgC* related genes in humans and mouse to delay or cure the degeneration in the eye.

### **9.1.5 Peroxisome dynamics in the living organism**

The potential peroxisomal localisation of *Best2* led to the investigation of peroxisomes in  $\text{Ca}^{2+}$  homeostasis and signaling. This study provided following insight into function of peroxisomes in terms of  $\text{Ca}^{2+}$  homeostasis and peroxisome function.

1. Aequorin probes are successfully targeted to peroxisomes in a live renal transporting epithelia

2. This study identified a novel peroxisomal  $\text{Ca}^{2+}$  sequestration and transport pathway.

3. This study also identified two novel renal peroxins that are essential for proper peroxisome biogenesis and proliferation in the renal tubules.

## 9.2 Future work

The Affymetrix GeneChips® have been used to generate FlyAtlas tissue-specific transcriptomes which interrogate gene expression for 18,880 annotated transcripts one at a time. The FlyAtlas data have been extremely useful for the research community. The usefulness can be seen from the citation report of the FlyAtlas that reached around 369 according to Google Scholar (accessed on January 29th, 2012).

The tissue-specific transcriptomic data has been extended using more advanced RNA-seq platform to generate digital readouts of every base-pair of expressed mRNA, without a bias towards annotated transcripts like the Affymetrix GeneChip®. This data needs to be further extended to other tissues, although it has been done elsewhere ([www.modencode.org](http://www.modencode.org)), the expertise at Glasgow is useful, to comparatively validate the results. As the systems biology requires highest quality datasets to build predictive biological models, this approach is useful. Furthermore, comparing the tissue-specific transcriptomes of *Drosophila* with the tissue-specific data sets of the vertebrate model organisms, for example, is useful to further validate the organotypic models of human disease in the fly.

This dissertation identifies bestrophins as multifunctional proteins by virtue of their expression, localisation and further functional characterisation in *Drosophila melanogaster*. However, the localisations need to be validated using appropriate antibodies.

Furthermore, the importance of functional characterisation of bestrophins comes from the fact that they are implicated in Best disease in the eye that causes retinal degeneration. Most of the diseases of the eye lead to various degeneration pathologies.

In this context, this thesis forms a basis for developing a *Drosophila* model for Best disease to understand the basis of disease for therapeutic intervention.

A microarray analysis of *Best2* mutants versus wildtype upon control- and salt-fed conditions may identify genes whose expression is changed in the *Best2* mutants so to build a model for the disease. This will also allow the investigation of interacting proteins that may modulate bestrophin function. In the *in silico* analysis Best2 protein showed a putative NADHpl oxidoreductase domain like the one that is found in mitochondrial ND5. It would be interesting to test if this domain is really functional as the interaction between ClC-3 and NADPH oxidase (nox), that generate  $O_2^-$  seems to exist within the cells (Lassegue.B., 2007).

## Appendices

### Appendix I: Fly food recipe

Fly food recipe (Mix the contents in 1 litre of H <sub>2</sub> O in the below order of preference.
10 g Tayo agar
1 tbsp Soya flour
15 g Sucrose
33 g Glucose
15 g Maize meal
10 g Wheat germ
30 g Treachle
35 g Yeast
Bring to boil, stirring constantly; simmer 10 min; allow to cool slightly to about 70 °C; leave for 20 min and then add:
10 ml Nipagin (of below formulation)
5 ml Propionic acid
[Nipagin = 25 g. Nipagin M (Tegosept M, p-hydroxybenzoic acid methyl ester) in 250 ml Ethanol]
Dispense:
Fly Vials = 8 ml
Fly Bottles = 70 ml

### Appendix II: Phosphate Buffer Saline (PBS)

Phosphate Buffer Saline (PBS) (in H <sub>2</sub> O)
137 mM NaCl
2.7 mM KCl
10 mM Na <sub>3</sub> PO <sub>4</sub>
2 mM KH <sub>2</sub> PO <sub>4</sub> , pH 7.4
Other solutions using PBS
For PBST: 0.25% TritonX-100 was added.
For PBSTw: 1% Tween20 was added.
For blocking buffer for westerns: 10% non-fat milk powder was added to PBSTw.
For blocking buffer for ICCs: 10% goat serum was added to PBST.

**Appendix III: *Drosophila* Schneider's media (www.invitrogen.com, (accessed on 26th August 2011))**

COMPONENTS	Molecular Weight	Concentration (mg/L)	mM
<b>Amino Acids</b>			
Glycine	75	250	3.33
L-Arginine	174	400	2.3
L-Aspartic acid	133	400	3.01
L-Cysteine	121	60	0.496
L-Cystine	240	100	0.417
L-Glutamic Acid	147	800	5.44
L-Glutamine	146	1800	12.33
L-Histidine	155	400	2.58
L-Isoleucine	131	150	1.15
L-Leucine	131	150	1.15
L-Lysine hydrochloride	183	1650	9.02
L-Methionine	149	800	5.37
L-Phenylalanine	165	150	0.909
L-Proline	115	1700	14.78
L-Serine	105	250	2.38
L-Threonine	119	350	2.94
L-Tryptophan	204	100	0.49
L-Tyrosine	181	500	2.76
L-Valine	117	300	2.56
beta-Alanine	89	500	5.62
<b>Inorganic Salts</b>			
Calcium Chloride (CaCl <sub>2</sub> -2H <sub>2</sub> O)	147	794	5.4
Magnesium Sulfate (MgSO <sub>4</sub> -7H <sub>2</sub> O)	246	3700	15.04
Potassium Chloride (KCl)	75	1600	21.33
Potassium Phosphate monobasic (KH <sub>2</sub> PO <sub>4</sub> )	136	450	3.31
Sodium Bicarbonate (NaHCO <sub>3</sub> )	84	400	4.76
Sodium Chloride (NaCl)	58	2100	36.21
Sodium Phosphate monobasic (NaH <sub>2</sub> PO <sub>4</sub> -2H <sub>2</sub> O)	156	1321	8.47
<b>Other Components</b>			
Alpha-Ketoglutaric acid	146	200	1.37
D-Glucose (Dextrose)	180	2000	11.11
Fumaric acid	116	100	0.862
Malic acid	134	100	0.746
Succinic acid	118	100	0.847
Trehalose	342	2000	5.85
Yeastolate		2000	-

**Appendix IV: *E. coli* growth media**

COMPONENTS	grams/litre
LB-broth	
Bacto-tryptone	10
Dried Yeast	5
NaCl	10
LB-agar	
Bacto-tryptone	10
Dried yeast	5
NaCl	10
Bacto-agar	15
SOC broth	
Bacto-tryptone	2 % (w/v)
Dried yeast	0.5 % (w/v)
NaCl	10 mM
KCl	2.5 mM
MgCl <sub>2</sub>	10 mM
MgSO <sub>4</sub>	10 mM
Glucose	20 mM

**Appendix V: Buffers for SDS-PAGE and Westerns**

From Sambrook and Russell, 2001
6 x SDS-PAGE Loading buffer
0.35 M Tris HCl, pH6.8
10.28 % (w/v) SDS
36 % v/v glycerol
5 % v/v b-mercaptoethanol
0.012 % w/v bromophenol blue
in 0.5 ml aliquots stored at -20 °C
Tris-Glycine Running Buffer (in 500 ml of H <sub>2</sub> O)
7.2 g Glycine
1.5 g Tris Base
6 ml 10% (w/v) SDS
Staining Solution
465 ml Brilliant blue R concentrate (Sigma)
535 ml H <sub>2</sub> O
Destaining Solution (in H <sub>2</sub> O)
10 % (v/v) Acetic Acid
45% (v/v) Methanol
Ponceau S Staining Solution (in 500 ml H <sub>2</sub> O)
1.5 g TCA
0.5 g Ponceau S stain
Transfer Buffer (in 1 litre of H <sub>2</sub> O)
20 % (v/v) Methanol
14.4 g Glycine
3 g Tris Base

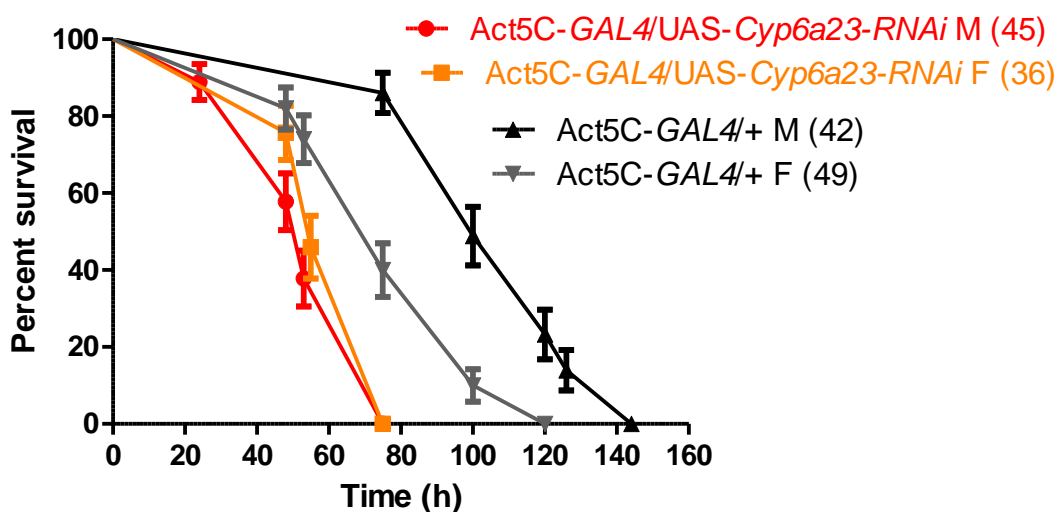
Resolving and Stacking gels for SDS-PAGE (from Sambrook and Russel, 2001)	
COMPONENTS	Vol. (ml)
Resolving gel 10%, volume for 2x 5 ml gels	
H <sub>2</sub> O	4
30 % acrylamide mix	3.3
1.5 M Tris (pH 8.8)	2.5
10 % (v/v) SDS	0.1
10 % (v/v) APS	0.1
TEMED	0.004
Stacking gel 5%, volume for 2x 1.5 ml	
H <sub>2</sub> O	2.1
30 % acrylamide mix	0.5
1.0 M Tris (pH 6.8)	0.38
10 % (v/v) SDS	0.03
10 % (v/v) APS	0.03
TEMED	0.003

### Appendix VI: Primers sequences and applications

Primer Name	Sequence (5' to 3')	Use
Best1-F	CAACAATGGACCGATGGCAAG	qPCR
Best1-R	TAGAGTTCCCGAAACGCTCACCAG	
Best2-F	TGGTCTTATTGGATACGACACGG	qPCR
Best2-R	AGGGATTGATTAGCACCTCGGC	
Best1-RA-F	CACCATGACAATTACGTACACAGGTGAAGT	Cloning overexpression
Best1-RAstop-R	TCAACTGCCGTTGATGGC	
Best1-RA-F1	CACCATGACAATTACGTACACAGGTGAAGT	Cloning overexpression C- fusion
Best1-RAnonstop-R	ACTGCCGTTGATGGCGTC	
Best1-RB-F	CACCAGTTTCACATTGGCGGTCCG	Cloning overexpression C- fusion
Best1-RBnonstop-R	TGGCATTTCATTTTTATTTAAGTCTTT	
Best2-RA-F	CACC ATGACTGTCTCGTATGCGGG	Cloning overexpression
Best2-RAstop-R	TCAGACGTACACCTCTCCGG	
Best2-RA-F	CACCATGACTGTCTCGTATGCGGG	Cloning overexpression C- fusion
Best2-RAnonstop-R	GACGTACACCTCTCCGGTCTT	
Best3-RA-F	CACC ATGACTGTCTCTTACACCGCTG	Cloning overexpression C- fusion
Best3-RAnonstop-R	TTTCTTAGATTTCGTCACCTGTCCTTATC	
Best4-RA-F	CACCATGACTGTGACCTATACCTCACGT	Cloning overexpression C- fusion
Best4-RAnonstop-R	ATCCTGCTTTTCCGCTTATTTG	
Aequorin-BglII-F	GC AGATCT ATGACAAGCAAACAATACTCA	Cloning Aequorin <sub>perox</sub>
Aequorin-KVK-SKL-XbaI-R	GC TCT AGA TTACAGCTTGGACTTCACCTTGGGGACAGCTCC ACC	

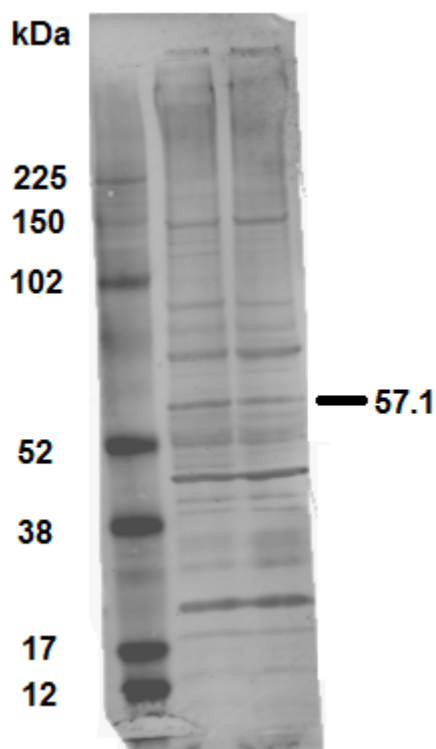
CG11919-F	TCGATCGAAGCCCTGCCGGA	qPCR
CG11919-R	AGACAGCCGGACGACCCACA	
CG13827-F	TTGTGGGGCGGCAAGCTGTC	qPCR
CG13827-R	TGGCTAAACACACTTTTCGAGTGCCG	
norpA (HL05775)-F	CGGAGAAGCGTTTACTACTGTGC	qPCR
norpA (HL05775)-R	GGCAAAGCGCAAAGTATTGGAG	
norpA-F	AGCAAGCAAAGATGTCGGCG	qPCR
norpA-R	TGGGCGAGTGTGTGTTTTTCG	
Cyp6a23-F	CACAACAACGAGTTTACCTACGAGG	qPCR
Cyp6a23-R	ATCACAACAGTGGTTCCTTGG	
trp-F	TCCAACCTCTACCAAATCATCTCG	qPCR
trp-R	TAATGCCGTAATCGTCCCGC	
rdgC-F	CACCAGGCACGGATAGTCAAAG	qPCR
rdgC-R	CCAGCAAGTCAATCGCAGTTTC	

**Appendix VII. *Cyp6a23* knockdowns show sensitivity to high salt feeding.** *Cyp6a23* gene expression was ablated using GAL4/UAS system using Act5C-GAL4 ubiquitous driver. Survival assays were performed according to the standard protocols. Median survivals for males: Act-GAL4/+, 100; Act-GAL4/UAS-*Cyp6a23*-RNAi, 53. Median survivals for females: Act-GAL4/+, 75; Act-GAL4/UAS-*Cyp6a23*-RNAi, 55. Log-rank (Mantel-Cox) Test,  $P < 0.0001$ .

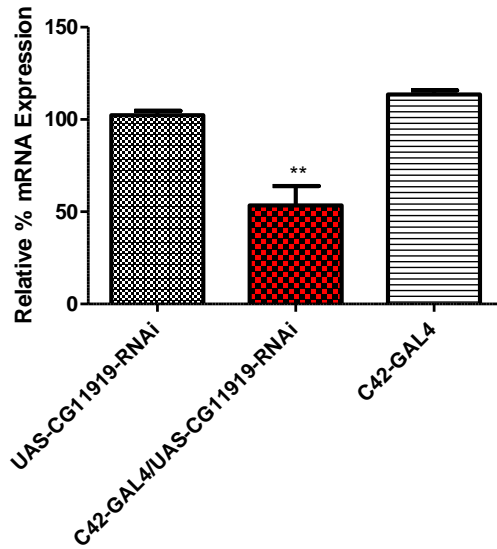


**Appendix VIII. Validation of the catalase antibody using Western blotting.**

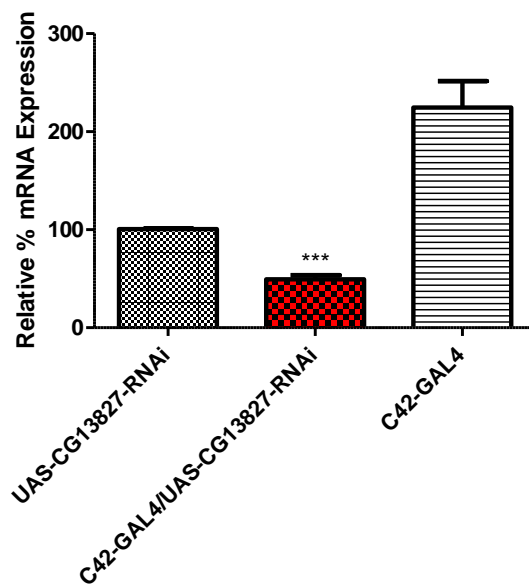
Protein extracts were obtained from purified peroxisomes of wildtype (A),  $w^{1118}$  and *Best2* mutants (B) and probed using mouse  $\alpha$ -catalase (Abcam, 1:100) antibody as the primary and  $\alpha$ -mouse Cy5 antibody (1:2000) as the secondary antibody were used to detect the catalase in purified peroxisomes. The blot was imaged using the Typhoon variable mode scanner (Amersham). The sample bands were compared against the proteins maker (ECLPlex fluorescent rainbow Marker). The antibody seems to be unspecific as it is detecting several proteins. However, there is band that may approximately of the right size (~57 kDa) for catalase.



Appendix IX. Validation of *CG11919-RNAi* using qPCR. The gene expression knockdown was validated in the *C42-GAL4* driven *CG11919-RNAi* tubules. The relative percentage of expression was calculated using UAS parental control as the baseline. The expression was significantly found reduced in the tubules driven for *CG11919-RNAi* with a mean fold difference of  $48.87 \pm 10.77$  (*t*-test,  $P < 0.05$ ,  $N = 4$ ).



Appendix X. Validation of *CG13827-RNAi* using qPCR. The gene expression knockdown was validated in the *C42-GAL4* driven *CG13827-RNAi* tubules. The relative percentage of expression was calculated using UAS parental control as the baseline. The expression was significantly found reduced in the tubules driven for *CG13827-RNAi* with a mean fold difference of  $51.21 \pm 4.228$  (*t*-test,  $P < 0.05$ ,  $N = 4$ ).



## References

- Abrams, E.W., Mihoulides, W.K., and Andrew, D.J. (2006). Fork head and Sage maintain a uniform and patent salivary gland lumen through regulation of two downstream target genes, PH4alphaSG1 and PH4alphaSG2. *Development* 133, 3517-3527.
- Acharya, J.K., Jalink, K., Hardy, R.W., Hartenstein, V., and Zuker, C.S. (1997). InsP3 receptor is essential for growth and differentiation but not for vision in *Drosophila*. *Neuron* 18, 881-887.
- Adams, J.U. (2008). Transcriptome: Connecting the Genome to Gene Function. *Nature Education* 1 (1).
- Adams, M.D., Celniker, S.E., Holt, R.A., Evans, C.A., Gocayne, J.D., Amanatides, P.G., Scherer, S.E., Li, P.W., Hoskins, R.A., Galle, R.F., *et al.* (2000). The genome sequence of *Drosophila melanogaster*. *Science* 287, 2185-2195.
- Adams, M.D., and Sekelsky, J.J. (2002). From sequence to phenotype: reverse genetics in *Drosophila melanogaster*. *Nat Rev Genet* 3, 189-198.
- Albeck, J.G., MacBeath, G., White, F.M., Sorger, P.K., Lauffenburger, D.A., and Gaudet, S. (2006). Collecting and organizing systematic sets of protein data. *Nat Rev Mol Cell Biol* 7, 803-812.
- Aldaz, S., Morata, G., and Azpiazu, N. (2003). The Pax-homeobox gene *eyegone* is involved in the subdivision of the thorax of *Drosophila*. *Development* 130, 4473-4482.
- Aldehni, F., Spitzner, M., Martins, J.R., Barro-Soria, R., Schreiber, R., and Kunzelmann, K. (2009). Bestrophin 1 promotes epithelial-to-mesenchymal transition of renal collecting duct cells. *J Am Soc Nephrol* 20, 1556-1564.
- Allan, A.K., Du, J., Davies, S.A., and Dow, J.A. (2005). Genome-wide survey of V-ATPase genes in *Drosophila* reveals a conserved renal phenotype for lethal alleles. *Physiol Genomics* 22, 128-138.
- Alvarez, J., and Montero, M. (2002). Measuring [Ca<sup>2+</sup>] in the endoplasmic reticulum with aequorin. *Cell Calcium* 32, 251-260.
- Alvarez, M.E., Pennell, R.I., Meijer, P.J., Ishikawa, A., Dixon, R.A., and Lamb, C. (1998). Reactive oxygen intermediates mediate a systemic signal network in the establishment of plant immunity. *Cell* 92, 773-784.
- Andrew, D.J., Henderson, K.D., and Sessaiah, P. (2000). Salivary gland development in *Drosophila melanogaster*. *Mech Dev* 92, 5-17.
- Andrews, J., Bouffard, G.G., Cheadle, C., Lu, J., Becker, K.G., and Oliver, B. (2000). Gene discovery using computational and microarray analysis of transcription in the *Drosophila melanogaster* testis. *Genome Res* 10, 2030-2043.
- Anraku, Y., Umemoto, N., Hirata, R., and Wada, Y. (1989). Structure and function of the yeast vacuolar membrane proton ATPase. *J Bioenerg Biomembr* 21, 589-603.

Arbeitman, M.N., Furlong, E.E., Imam, F., Johnson, E., Null, B.H., Baker, B.S., Krasnow, M.A., Scott, M.P., Davis, R.W., and White, K.P. (2002). Gene expression during the life cycle of *Drosophila melanogaster*. *Science* 297, 2270-2275.

Arita, M., Sato, Y., Miyata, A., Tanabe, T., Takahashi, E., Kayden, H.J., Arai, H., and Inoue, K. (1995). Human alpha-tocopherol transfer protein: cDNA cloning, expression and chromosomal localization. *Biochem J* 306 ( Pt 2), 437-443.

Arreola, J., Begenisich, T., Nehrke, K., Nguyen, H.V., Park, K., Richardson, L., Yang, B., Schutte, B.C., Lamb, F.S., and Melvin, J.E. (2002). Secretion and cell volume regulation by salivary acinar cells from mice lacking expression of the *Clcn3* Cl<sup>-</sup> channel gene. *J Physiol* 545, 207-216.

Ashburner, M. (1989). *Drosophila* (New York, Cold Spring Harbor Laboratory press).

Bader, C.R., Bertrand, D., and Schwartz, E.A. (1982). Voltage-activated and calcium-activated currents studied in solitary rod inner segments from the salamander retina. *J Physiol* 331, 253-284.

Baehrecke, E. (2005). Autophagy: dual roles in life and death? *Nat Rev Mol Cell Biol* 6, 505-510.

Baillie, G.S. (2009). Compartmentalized signalling: spatial regulation of cAMP by the action of compartmentalized phosphodiesterases. *FEBS J* 276, 1790-1799.

Bammler, T., Beyer, R.P., Bhattacharya, S., Boorman, G.A., Boyles, A., Bradford, B.U., Bumgarner, R.E., Bushel, P.R., Chaturvedi, K., Choi, D., *et al.* (2005). Standardizing global gene expression analysis between laboratories and across platforms. *Nat Methods* 2, 351-356.

Bargmann, C.I. (2001). High-throughput reverse genetics: RNAi screens in *Caenorhabditis elegans*. *Genome Biol* 2, REVIEWS1005.

Barish, M.E. (1983). A transient calcium-dependent chloride current in the immature *Xenopus* oocyte. *J Physiol* 342, 309-325.

Barro-Soria, R., Aldehni, F., Almaca, J., Witzgall, R., Schreiber, R., and Kunzelmann, K. (2010). ER-localized bestrophin 1 activates Ca<sup>2+</sup>-dependent ion channels TMEM16A and SK4 possibly by acting as a counterion channel. *Pflugers Arch* 459, 485-497.

Barro Soria, R., Spitzner, M., Schreiber, R., and Kunzelmann, K. (2009). Bestrophin-1 enables Ca<sup>2+</sup>-activated Cl<sup>-</sup> conductance in epithelia. *J Biol Chem* 284, 29405-29412.

Baumann, A., Frings, S., Godde, M., Seifert, R., and Kaupp, U.B. (1994). Primary structure and functional expression of a *Drosophila* cyclic nucleotide-gated channel present in eyes and antennae. *Embo J* 13, 5040-5050.

Baumgartner, M.R., Poll-The, B.T., Verhoeven, N.M., Jakobs, C., Espeel, M., Roels, F., Rabier, D., Levade, T., Rolland, M.O., Martinez, M., *et al.* (1998).

- Clinical approach to inherited peroxisomal disorders: a series of 27 patients. *Ann Neurol* 44, 720-730.
- Beard, M.E., and Holtzman, E. (1987). Peroxisomes in wild-type and rosy mutant *Drosophila melanogaster*. *Proc Natl Acad Sci U S A* 84, 7433-7437.
- Berridge, M.J. (2005). Unlocking the secrets of cell signaling. *Annu Rev Physiol* 67, 1-21.
- Berridge, M.J., Bootman, M.D., and Lipp, P. (1998). Calcium--a life and death signal. *Nature* 395, 645-648.
- Berridge, M.J., and Irvine, R.F. (1984). Inositol trisphosphate, a novel second messenger in cellular signal transduction. *Nature* 312, 315-321.
- Berridge, M.J., and Irvine, R.F. (1989). Inositol phosphates and cell signalling. *Nature* 341, 197-205.
- Berridge, M.J., Lipp, P., and Bootman, M.D. (2000). The versatility and universality of calcium signalling. *Nat Rev Mol Cell Biol* 1, 11-21.
- Bertalanffy, L.v. (1969). *General Systems Theory, Foundations, Development, Applications* (New York).
- Beyenbach, K.W., Skaer, H., and Dow, J.A. (2010a). The developmental, molecular, and transport biology of Malpighian tubules. *Annu Rev Entomol* 55, 351-374.
- Beyenbach, K.W., Skaer, H., and Dow, J.A. (2010b). The developmental, molecular, and transport biology of Malpighian tubules. *Annu Rev Entomol* 55, 351-374.
- Bier, E. (2005). *Drosophila*, the golden bug, emerges as a tool for human genetics. *Nat Rev Genet* 6, 9-23.
- Bjorklund, M., Taipale, M., Varjosalo, M., Saharinen, J., Lahdenpera, J., and Taipale, J. (2006). Identification of pathways regulating cell size and cell-cycle progression by RNAi. *Nature* 439, 1009-1013.
- Blumenthal, E.M. (2003). Regulation of chloride permeability by endogenously produced tyramine in the *Drosophila* Malpighian tubule. *Am J Physiol Cell Physiol* 284, C718-728.
- Bomont, P., Cavalier, L., Blondeau, F., Ben Hamida, C., Belal, S., Tazir, M., Demir, E., Topaloglu, H., Korinthenberg, R., Tuysuz, B., *et al.* (2000). The gene encoding gigaxonin, a new member of the cytoskeletal BTB/kelch repeat family, is mutated in giant axonal neuropathy. *Nat Genet* 26, 370-374.
- Borate, B., and Baxevanis, A.D. (2009). Searching Online Mendelian Inheritance in Man (OMIM) for information on genetic loci involved in human disease. *Curr Protoc Bioinformatics Chapter 1*, Unit 1 2.
- Brand, A.H., and Perrimon, N. (1993). Targeted gene expression as a means of altering cell fates and generating dominant phenotypes. *Development* 118, 401-415.

Brock, H.W., and Roberts, D.B. (1980). Comparison of the larval serum proteins of *Drosophila melanogaster* using one and two-dimensional peptide mapping. *Eur J Biochem* 106, 129-135.

Broderick, K.E., Kean, L., Dow, J.A., Pyne, N.J., and Davies, S.A. (2004). Ectopic expression of bovine type 5 phosphodiesterase confers a renal phenotype in *Drosophila*. *J Biol Chem* 279, 8159-8168.

Broderick, K.E., MacPherson, M.R., Regulski, M., Tully, T., Dow, J.A., and Davies, S.A. (2003). Interactions between epithelial nitric oxide signaling and phosphodiesterase activity in *Drosophila*. *Am J Physiol Cell Physiol* 285, C1207-1218.

Brown, S.D., and Peters, J. (1996). Combining mutagenesis and genomics in the mouse--closing the phenotype gap. *Trends Genet* 12, 433-435.

Bryant, S.H. (1969). Cable properties of external intercostal muscle fibres from myotonic and nonmyotonic goats. *J Physiol* 204, 539-550.

Bullard, D.C. (2001). Mind the phenotype gap. *Trends Mol Med* 7, 537-538.

Burn, S.F., and Hill, R.E. (2009). Left-right asymmetry in gut development: what happens next? *Bioessays* 31, 1026-1037.

Button, D., and Eidsath, A. (1996). Aequorin targeted to the endoplasmic reticulum reveals heterogeneity in luminal Ca<sup>++</sup> concentration and reports agonist- or IP<sub>3</sub>-induced release of Ca<sup>++</sup>. *Mol Biol Cell* 7, 419-434.

Byers, D., Davis, R.L., and Kiger, J.A., Jr. (1981). Defect in cyclic AMP phosphodiesterase due to the *dunce* mutation of learning in *Drosophila melanogaster*. *Nature* 289, 79-81.

Cabrero, P., Radford, J.C., Broderick, K.E., Costes, L., Veenstra, J.A., Spana, E.P., Davies, S.A., and Dow, J.A. (2002). The *Dh* gene of *Drosophila melanogaster* encodes a diuretic peptide that acts through cyclic AMP. *J Exp Biol* 205, 3799-3807.

Caldwell, G.M., Kakuk, L.E., Griesinger, I.B., Simpson, S.A., Nowak, N.J., Small, K.W., Maumenee, I.H., Rosenfeld, P.J., Sieving, P.A., Shows, T.B., *et al.* (1999). Bestrophin gene mutations in patients with Best vitelliform macular dystrophy. *Genomics* 58, 98-101.

Carles, A., Millon, R., Cromer, A., Ganguli, G., Lemaire, F., Young, J., Wasylyk, C., Muller, D., Schultz, I., Rabouel, Y., *et al.* (2006). Head and neck squamous cell carcinoma transcriptome analysis by comprehensive validated differential display. *Oncogene* 25, 1821-1831.

Carthew, R.W. (2003). *RNAi applications in Drosophila melanogaster*. (New York, Cold Spring Harbor Laboratory Press).

Carthew, R.W. (2005). Adhesion proteins and the control of cell shape. *Curr Opin Genet Dev* 15, 358-363.

Celniker, S.E., Wheeler, D.A., Kronmiller, B., Carlson, J.W., Halpern, A., Patel, S., Adams, M., Champe, M., Dugan, S.P., Frise, E., *et al.* (2002). Finishing a

whole-genome shotgun: release 3 of the *Drosophila melanogaster* euchromatic genome sequence. *Genome Biol* 3, RESEARCH0079.

Chang, C.C., South, S., Warren, D., Jones, J., Moser, A.B., Moser, H.W., and Gould, S.J. (1999). Metabolic control of peroxisome abundance. *J Cell Sci* 112 ( Pt 10), 1579-1590.

Chien, L.T., and Hartzell, H.C. (2007). *Drosophila* bestrophin-1 chloride current is dually regulated by calcium and cell volume. *J Gen Physiol* 130, 513-524.

Chien, L.T., Zhang, Z.R., and Hartzell, H.C. (2006). Single Cl<sup>-</sup> channels activated by Ca<sup>2+</sup> in *Drosophila* S2 cells are mediated by bestrophins. *J Gen Physiol* 128, 247-259.

Chien, S., Reiter, L.T., Bier, E., and Gribskov, M. (2002). Homophila: human disease gene cognates in *Drosophila*. *Nucleic Acids Res* 30, 149-151.

Chintapalli, S.T., Jing Wang, Mohammed Al Bratty, David G. Watson, Pawel Herzyk, Shireen A. Davies and Julian Dow (2012). Functional correlates of positional and gender-specific renal asymmetry in *Drosophila*. *PLoS One*.

Chintapalli, V., Wang, J., and Dow, J. (2007). Using FlyAtlas to identify better *Drosophila melanogaster* models of human disease. *Nat Genet* 39, 715-720.

Chong, L.a.L.B.R. (2002). Whole-istic Biology. *Science* 295, 1661.

Chung, H., Sztal, T., Pasricha, S., Sridhar, M., Batterham, P., and Daborn, P.J. (2009). Characterization of *Drosophila melanogaster* cytochrome P450 genes. *Proc Natl Acad Sci U S A* 106, 5731-5736.

Clark, A.G., Eisen, M.B., Smith, D.R., Bergman, C.M., Oliver, B., Markow, T.A., Kaufman, T.C., Kellis, M., Gelbart, W., Iyer, V.N., *et al.* (2007). Evolution of genes and genomes on the *Drosophila* phylogeny. *Nature* 450, 203-218.

Condon, J.C., Pezzi, V., Drummond, B.M., Yin, S., and Rainey, W.E. (2002). Calmodulin-dependent kinase I regulates adrenal cell expression of aldosterone synthase. *Endocrinology* 143, 3651-3657.

Costa, A., Drago, I., Behera, S., Zottini, M., Pizzo, P., Schroeder, J.I., Pozzan, T., and Lo Schiavo, F. (2010). H<sub>2</sub>O<sub>2</sub> in plant peroxisomes: an in vivo analysis uncovers a Ca(2+)-dependent scavenging system. *Plant J* 62, 760-772.

Coutelis, J.B., Petzoldt, A.G., Speder, P., Suzanne, M., and Noselli, S. (2008). Left-right asymmetry in *Drosophila*. *Semin Cell Dev Biol* 19, 252-262.

Cunningham, S.A., Awayda, M.S., Bubien, J.K., Ismailov, Il, Arrate, M.P., Berdiev, B.K., Benos, D.J., and Fuller, C.M. (1995). Cloning of an epithelial chloride channel from bovine trachea. *J Biol Chem* 270, 31016-31026.

Cuthbert, A.W. (2011). New horizons in the treatment of cystic fibrosis. *Br J Pharmacol* 163, 173-183.

Daborn, P.J., Lumb, C., Boey, A., Wong, W., Ffrench-Constant, R.H., and Batterham, P. (2007). Evaluating the insecticide resistance potential of eight

*Drosophila melanogaster* cytochrome P450 genes by transgenic over-expression. *Insect Biochem Mol Biol* 37, 512-519.

Dansen, T.B., Wirtz, K.W., Wanders, R.J., and Pap, E.H. (2000). Peroxisomes in human fibroblasts have a basic pH. *Nat Cell Biol* 2, 51-53.

Davies, S., and Terhzaz, S. (2009). Organellar calcium signalling mechanisms in *Drosophila* epithelial function. *J Exp Biol* 212, 387-400.

Davies, S.A. (2006). Signalling via cGMP: lessons from *Drosophila*. *Cell Signal* 18, 409-421.

Davies, S.A., Goodwin, S.F., Kelly, D.C., Wang, Z., Sozen, M.A., Kaiser, K., and Dow, J.A. (1996). Analysis and inactivation of *vha55*, the gene encoding the vacuolar ATPase B-subunit in *Drosophila melanogaster* reveals a larval lethal phenotype. *J Biol Chem* 271, 30677-30684.

Davies, S.A., Huesmann, G.R., Maddrell, S.H., O'Donnell, M.J., Skaer, N.J., Dow, J.A., and Tublitz, N.J. (1995). CAP2b, a cardioacceleratory peptide, is present in *Drosophila* and stimulates tubule fluid secretion via cGMP. *Am J Physiol* 269, R1321-1326.

Davis-Kaplan, S.R., Askwith, C.C., Bengtzen, A.C., Radisky, D., and Kaplan, J. (1998). Chloride is an allosteric effector of copper assembly for the yeast multicopper oxidase Fet3p: an unexpected role for intracellular chloride channels. *Proc Natl Acad Sci U S A* 95, 13641-13645.

Davis, R.L., and Kiger, J.A., Jr. (1981). Dunce mutants of *Drosophila melanogaster*: mutants defective in the cyclic AMP phosphodiesterase enzyme system. *J Cell Biol* 90, 101-107.

Day, J.P., Dow, J.A., Houslay, M.D., and Davies, S.A. (2005). Cyclic nucleotide phosphodiesterases in *Drosophila melanogaster*. *Biochem J* 388, 333-342.

Day, J.P., Wan, S., Allan, A.K., Kean, L., Davies, S.A., Gray, J.V., and Dow, J.A. (2008). Identification of two partners from the bacterial Kef exchanger family for the apical plasma membrane V-ATPase of Metazoa. *J Cell Sci* 121, 2612-2619.

Dent, C.E., and Philpot, G.R. (1954). Xanthinuria, an inborn error (or deviation) of metabolism. *Lancet* 266, 182-185.

Dohan, O., Portulano, C., Basquin, C., Reyna-Neyra, A., Amzel, L.M., and Carrasco, N. (2007). The Na<sup>+</sup>/I symporter (NIS) mediates electroneutral active transport of the environmental pollutant perchlorate. *Proc Natl Acad Sci U S A* 104, 20250-20255.

Dolmetsch, R.E., Lewis, R.S., Goodnow, C.C., and Healy, J.I. (1997). Differential activation of transcription factors induced by Ca<sup>2+</sup> response amplitude and duration. *Nature* 386, 855-858.

Dominguez, M., Ferres-Marco, D., Gutierrez-Avino, F.J., Speicher, S.A., and Beneyto, M. (2004). Growth and specification of the eye are controlled independently by *Eyegone* and *Eyeless* in *Drosophila melanogaster*. *Nat Genet* 36, 31-39.

- Dow, J.A. (2003). The *Drosophila* phenotype gap - and how to close it. *Brief Funct Genomic Proteomic* 2, 121-127.
- Dow, J.A. (2007). Integrative physiology, functional genomics and the phenotype gap: a guide for comparative physiologists. *J Exp Biol* 210, 1632-1640.
- Dow, J.A., and Davies, S.A. (2006). The Malpighian tubule: rapid insights from post-genomic biology. *J Insect Physiol* 52, 365-378.
- Dow, J.A., Maddrell, S.H., Davies, S.A., Skaer, N.J., and Kaiser, K. (1994a). A novel role for the nitric oxide-cGMP signaling pathway: the control of epithelial function in *Drosophila*. *Am J Physiol* 266, R1716-1719.
- Dow, J.A., Maddrell, S.H., Gortz, A., Skaer, N.J., Brogan, S., and Kaiser, K. (1994b). The malpighian tubules of *Drosophila melanogaster*: a novel phenotype for studies of fluid secretion and its control. *J Exp Biol* 197, 421-428.
- Dow, J.A., and Romero, M.F. (2010). *Drosophila* provides rapid modeling of renal development, function, and disease. *Am J Physiol Renal Physiol* 299, F1237-1244.
- Dow, J.A., P., J.M. (1989). Microelectrode evidence for the electrical isolation of goblet cell cavities in *Manduca sexta* middle midgut. *Journal of Experimental Biology*, 101-114.
- Dow, J.T., and Davies, S.A. (2003). Integrative physiology and functional genomics of epithelial function in a genetic model organism. *Physiol Rev* 83, 687-729.
- Drago, I., Giacomello, M., Pizzo, P., and Pozzan, T. (2008a). Calcium dynamics in the peroxisomal lumen of living cells. *J Biol Chem* 283, 14384-14390.
- Drago, I., Giacomello, M., Pizzo, P., and Pozzan, T. (2008b). Calcium dynamics in the peroxisomal lumen of living cells. *J Biol Chem* 283, 14384-14390.
- Drapeau, M.D. (2001). The Family of Yellow-Related *Drosophila melanogaster* Proteins. *Biochem Biophys Res Commun* 281, 611-613.
- Dube, K., McDonald, D.G., and O'Donnell, M.J. (2000a). Calcium transport by isolated anterior and posterior Malpighian tubules of *Drosophila melanogaster*: roles of sequestration and secretion. *J Insect Physiol* 46, 1449-1460.
- Dube, K.A., McDonald, D.G., and O'Donnell, M.J. (2000b). Calcium homeostasis in larval and adult *Drosophila melanogaster*. *Arch Insect Biochem Physiol* 44, 27-39.
- Dudai, Y., Jan, Y.N., Byers, D., Quinn, W.G., and Benzer, S. (1976). *dunce*, a mutant of *Drosophila* deficient in learning. *Proc Natl Acad Sci U S A* 73, 1684-1688.
- Duffy, J.B. (2002). GAL4 system in *Drosophila*: a fly geneticist's Swiss army knife. *Genesis* 34, 1-15.
- Duran, C., Thompson, C.H., Xiao, Q., and Hartzell, H.C. (2010). Chloride channels: often enigmatic, rarely predictable. *Annu Rev Physiol* 72, 95-121.

- Duta, V., Duta, F., Puttagunta, L., Befus, A.D., and Duszyk, M. (2006). Regulation of basolateral Cl(-) channels in airway epithelial cells: the role of nitric oxide. *J Membr Biol* 213, 165-174.
- Duta, V., Szkotak, A.J., Nahirney, D., and Duszyk, M. (2004). The role of bestrophin in airway epithelial ion transport. *FEBS Lett* 577, 551-554.
- Dutzler, R., Campbell, E.B., Cadene, M., Chait, B.T., and MacKinnon, R. (2002). X-ray structure of a ClC chloride channel at 3.0 Å reveals the molecular basis of anion selectivity. *Nature* 415, 287-294.
- Ebberink, M.S., Kofster, J., Wanders, R.J., and Waterham, H.R. (2010). Spectrum of PEX6 mutations in Zellweger syndrome spectrum patients. *Hum Mutat* 31, E1058-1070.
- Eisen, M.B., Spellman, P.T., Brown, P.O., and Botstein, D. (1998). Cluster analysis and display of genome-wide expression patterns. *Proc Natl Acad Sci U S A* 95, 14863-14868.
- Enomoto, A., Kimura, H., Chairoungdua, A., Shigeta, Y., Jutabha, P., Cha, S.H., Hosoyamada, M., Takeda, M., Sekine, T., Igarashi, T., *et al.* (2002). Molecular identification of a renal urate anion exchanger that regulates blood urate levels. *Nature* 417, 447-452.
- Erdmann, R., and Blobel, G. (1995). Giant peroxisomes in oleic acid-induced *Saccharomyces cerevisiae* lacking the peroxisomal membrane protein Pmp27p. *J Cell Biol* 128, 509-523.
- Espinosa, I., Lee, C.H., Kim, M.K., Rouse, B.T., Subramanian, S., Montgomery, K., Varma, S., Corless, C.L., Heinrich, M.C., Smith, K.S., *et al.* (2008). A novel monoclonal antibody against DOG1 is a sensitive and specific marker for gastrointestinal stromal tumors. *Am J Surg Pathol* 32, 210-218.
- Evans, J.M., Allan, A.K., Davies, S.A., and Dow, J.A. (2005). Sulphonylurea sensitivity and enriched expression implicate inward rectifier K<sup>+</sup> channels in *Drosophila melanogaster* renal function. *J Exp Biol* 208, 3771-3783.
- Finn, R.D., Mistry, J., Tate, J., Coggill, P., Heger, A., Pollington, J.E., Gavin, O.L., Gunasekaran, P., Ceric, G., Forslund, K., *et al.* (2010). The Pfam protein families database. *Nucleic Acids Res* 38, D211-222.
- Flicek, P., Amode, M.R., Barrell, D., Beal, K., Brent, S., Chen, Y., Clapham, P., Coates, G., Fairley, S., Fitzgerald, S., *et al.* (2011). Ensembl 2011. *Nucleic Acids Res* 39, D800-806.
- Foret, S., Kucharski, R., Pittelkow, Y., Lockett, G.A., and Maleszka, R. (2009). Epigenetic regulation of the honey bee transcriptome: unravelling the nature of methylated genes. *BMC Genomics* 10, 472.
- Friedrich, T., Breiderhoff, T., and Jentsch, T.J. (1999). Mutational analysis demonstrates that ClC-4 and ClC-5 directly mediate plasma membrane currents. *J Biol Chem* 274, 896-902.

- G.M. Coast, I.O., J.E. Phillips and D.A. Schooley (2002). Insect diuretic and antidiuretic hormones. *Adv Insect Physiol*, 279-409.
- Gallemore, R.P., Hughes, and S.S. Miller (1997). Retinal pigment epithelial transport mechanisms and their contributions to the electroretinogram. *Prog Retinal Eye Res* 509-566.
- Gandhi, R., Elble, R.C., Gruber, A.D., Schreur, K.D., Ji, H.L., Fuller, C.M., and Pauli, B.U. (1998). Molecular and functional characterization of a calcium-sensitive chloride channel from mouse lung. *J Biol Chem* 273, 32096-32101.
- Gasteiger, E., Gattiker, A., Hoogland, C., Ivanyi, I., Appel, R.D., and Bairoch, A. (2003). ExpASY: The proteomics server for in-depth protein knowledge and analysis. *Nucleic Acids Res* 31, 3784-3788.
- Ge, H., Walhout, A.J., and Vidal, M. (2003). Integrating 'omic' information: a bridge between genomics and systems biology. *Trends Genet* 19, 551-560.
- Giannakou, M.E., and Dow, J.A. (2001). Characterization of the *Drosophila melanogaster* alkali-metal/proton exchanger (NHE) gene family. *J Exp Biol* 204, 3703-3716.
- Gibson, M.C., and Perrimon, N. (2003). Apicobasal polarization: epithelial form and function. *Curr Opin Cell Biol* 15, 747-752.
- Giebultowicz, J.M., Stanewsky, R., Hall, J.C., and Hege, D.M. (2000). Transplanted *Drosophila* excretory tubules maintain circadian clock cycling out of phase with the host. *Curr Biol* 10, 107-110.
- Gillespie, P.G., and Walker, R.G. (2001). Molecular basis of mechanosensory transduction. *Nature* 413, 194-202.
- Glassman, E., and Mitchell, H.K. (1959). Mutants of *Drosophila Melanogaster* Deficient in Xanthine Dehydrogenase. *Genetics* 44, 153-162.
- Golic, K.G., and Golic, M.M. (1996). Engineering the *Drosophila* genome: chromosome rearrangements by design. *Genetics* 144, 1693-1711.
- Gould, S.J., Keller, G.A., Schneider, M., Howell, S.H., Garrard, L.J., Goodman, J.M., Distel, B., Tabak, H., and Subramani, S. (1990). Peroxisomal protein import is conserved between yeast, plants, insects and mammals. *EMBO J* 9, 85-90.
- Gradogna, A., Babini, E., Picollo, A., and Pusch, M. (2010). A regulatory calcium-binding site at the subunit interface of CLC-K kidney chloride channels. *J Gen Physiol* 136, 311-323.
- Graham, L.A., and Davies, P.L. (2002). The odorant-binding proteins of *Drosophila melanogaster*: annotation and characterization of a divergent gene family. *Gene* 292, 43-55.
- Greenspan, R.J., and Dierick, H.A. (2004). 'Am not I a fly like thee?' From genes in fruit flies to behavior in humans. *Hum Mol Genet* 13 Spec No 2, R267-273.

- Greenwood, I.A., and Leblanc, N. (2007). Overlapping pharmacology of Ca<sup>2+</sup>-activated Cl<sup>-</sup> and K<sup>+</sup> channels. *Trends Pharmacol Sci* 28, 1-5.
- Greenwood, I.A., Miller, L.J., Ohya, S., and Horowitz, B. (2002). The large conductance potassium channel beta-subunit can interact with and modulate the functional properties of a calcium-activated chloride channel, CLCA1. *J Biol Chem* 277, 22119-22122.
- Grubb, B.R., Vick, R.N., and Boucher, R.C. (1994). Hyperabsorption of Na<sup>+</sup> and raised Ca(2+)-mediated Cl<sup>-</sup> secretion in nasal epithelia of CF mice. *Am J Physiol* 266, C1478-1483.
- Gruber, A.D., Elble, R.C., Ji, H.L., Schreur, K.D., Fuller, C.M., and Pauli, B.U. (1998). Genomic cloning, molecular characterization, and functional analysis of human CLCA1, the first human member of the family of Ca<sup>2+</sup>-activated Cl<sup>-</sup> channel proteins. *Genomics* 54, 200-214.
- Guilbault, C., Saeed, Z., Downey, G.P., and Radzioch, D. (2007). Cystic fibrosis mouse models. *Am J Respir Cell Mol Biol* 36, 1-7.
- Guziewicz, K.E., Zangerl, B., Lindauer, S.J., Mullins, R.F., Sandmeyer, L.S., Grahn, B.H., Stone, E.M., Acland, G.M., and Aguirre, G.D. (2007). Bestrophin gene mutations cause canine multifocal retinopathy: a novel animal model for best disease. *Invest Ophthalmol Vis Sci* 48, 1959-1967.
- Ha, E.M., Oh, C.T., Bae, Y.S., and Lee, W.J. (2005). A direct role for dual oxidase in *Drosophila* gut immunity. *Science* 310, 847-850.
- Hahn, M., Pons, J., Planas, A., Querol, E., and Heinemann, U. (1995). Crystal structure of *Bacillus licheniformis* 1,3-1,4-beta-D-glucan 4-glucanohydrolase at 1.8 Å resolution. *FEBS Lett* 374, 221-224.
- Hardie, R.C. (2007). TRP channels and lipids: from *Drosophila* to mammalian physiology. *J Physiol* 578, 9-24.
- Hardie, R.C., and Raghu, P. (2001). Visual transduction in *Drosophila*. *Nature* 413, 186-193.
- Hartenstein, V. (1993). *Atlas of Drosophila Development* (Cold Spring Harbor Laboratory Press).
- Hartzell, C., Putzier, I., and Arreola, J. (2005a). Calcium-activated chloride channels. *Annu Rev Physiol* 67, 719-758.
- Hartzell, C., Qu, Z., Putzier, I., Artinian, L., Chien, L.T., and Cui, Y. (2005b). Looking chloride channels straight in the eye: bestrophins, lipofuscinosis, and retinal degeneration. *Physiology (Bethesda)* 20, 292-302.
- Hartzell, H.C., Qu, Z., Yu, K., Xiao, Q., and Chien, L.T. (2008). Molecular physiology of bestrophins: multifunctional membrane proteins linked to best disease and other retinopathies. *Physiol Rev* 88, 639-672.
- Hartzell, H.C., Yu, K., Xiao, Q., Chien, L.T., and Qu, Z. (2009). Anoctamin/TMEM16 family members are Ca<sup>2+</sup>-activated Cl<sup>-</sup> channels. *J Physiol* 587, 2127-2139.

Harvey, W.R., and Wieczorek, H. (1997). Animal plasma membrane energization by chemiosmotic H<sup>+</sup> V-ATPases. *J Exp Biol* 200, 203-216.

Hatton-Ellis, E., Ainsworth, C., Sushama, Y., Wan, S., VijayRaghavan, K., and Skaer, H. (2007). Genetic regulation of patterned tubular branching in *Drosophila*. *Proc Natl Acad Sci U S A* 104, 169-174.

Hayashi, K., Wakino, S., Sugano, N., Ozawa, Y., Homma, K., and Saruta, T. (2007). Ca<sup>2+</sup> channel subtypes and pharmacology in the kidney. *Circ Res* 100, 342-353.

Hekmat-Safe, D.S., Safe, C.R., McKinney, A.J., and Tanouye, M.A. (2002). Genome-wide analysis of the odorant-binding protein gene family in *Drosophila melanogaster*. *Genome Res* 12, 1357-1369.

Ho, M.W., Kaetzel, M.A., Armstrong, D.L., and Shears, S.B. (2001). Regulation of a human chloride channel. a paradigm for integrating input from calcium, type ii calmodulin-dependent protein kinase, and inositol 3,4,5,6-tetrakisphosphate. *J Biol Chem* 276, 18673-18680.

Hoepfner, D., van den Berg, M., Philippsen, P., Tabak, H.F., and Hettema, E.H. (2001). A role for Vps1p, actin, and the Myo2p motor in peroxisome abundance and inheritance in *Saccharomyces cerevisiae*. *J Cell Biol* 155, 979-990.

Hood, L., Heath, J.R., Phelps, M.E., and Lin, B. (2004). Systems biology and new technologies enable predictive and preventative medicine. *Science* 306, 640-643.

<http://stockcenter.vdrc.at/control/main>.

<http://www.genosphere-biotech.com/>.

<http://www.shigen.nig.ac.jp/fly/nigfly/index.jsp>.

Huang, P., Liu, J., Di, A., Robinson, N.C., Musch, M.W., Kaetzel, M.A., and Nelson, D.J. (2001). Regulation of human CLC-3 channels by multifunctional Ca<sup>2+</sup>/calmodulin-dependent protein kinase. *J Biol Chem* 276, 20093-20100.

Huang, X., Huang, Y., Chinnappan, R., Bocchini, C., Gustin, M.C., and Stern, M. (2002). The *Drosophila* inebriated-encoded neurotransmitter/osmolyte transporter: dual roles in the control of neuronal excitability and the osmotic stress response. *Genetics* 160, 561-569.

Huang, Y., and Stern, M. (2002). In vivo properties of the *Drosophila* inebriated-encoded neurotransmitter transporter. *J Neurosci* 22, 1698-1708.

Hunter, C.P. (1999). Genetics: a touch of elegance with RNAi. *Curr Biol* 9, R440-442.

Hunter, S., Apweiler, R., Attwood, T.K., Bairoch, A., Bateman, A., Binns, D., Bork, P., Das, U., Daugherty, L., Duquenne, L., *et al.* (2009). InterPro: the integrative protein signature database. *Nucleic Acids Res* 37, D211-215.

Iliadi, K.G., Avivi, A., Iliadi, N.N., Knight, D., Korol, A.B., Nevo, E., Taylor, P., Moran, M.F., Kamyshev, N.G., and Boulianne, G.L. (2008). *nemy* encodes a

cytochrome b561 that is required for *Drosophila* learning and memory. *Proc Natl Acad Sci U S A* 105, 19986-19991.

Imler, J.L., and Bulet, P. (2005). Antimicrobial peptides in *Drosophila*: structures, activities and gene regulation. *Chem Immunol Allergy* 86, 1-21.

Irizarry, R.A., Bolstad, B.M., Collin, F., Cope, L.M., Hobbs, B., and Speed, T.P. (2003). Summaries of Affymetrix GeneChip probe level data. *Nucleic Acids Res* 31, e15.

Ivanchenko, M., Stanewsky, R., and Giebultowicz, J.M. (2001). Circadian photoreception in *Drosophila*: functions of cryptochrome in peripheral and central clocks. *J Biol Rhythms* 16, 205-215.

Iversen, A., Cazzamali, G., Williamson, M., Hauser, F., and Grimmelikhuijzen, C.J. (2002). Molecular cloning and functional expression of a *Drosophila* receptor for the neuropeptides capa-1 and -2. *Biochem Biophys Res Commun* 299, 628-633.

Jankowski, A., Kim, J.H., Collins, R.F., Daneman, R., Walton, P., and Grinstein, S. (2001). In situ measurements of the pH of mammalian peroxisomes using the fluorescent protein pHluorin. *J Biol Chem* 276, 48748-48753.

Jentsch, T.J. (2007). Chloride and the endosomal-lysosomal pathway: emerging roles of CLC chloride transporters. *J Physiol* 578, 633-640.

Jentsch, T.J., Poet, M., Fuhrmann, J.C., and Zdebik, A.A. (2005). Physiological functions of CLC Cl<sup>-</sup> channels gleaned from human genetic disease and mouse models. *Annu Rev Physiol* 67, 779-807.

Jentsch, T.J., Stein, V., Weinreich, F., and Zdebik, A.A. (2002). Molecular structure and physiological function of chloride channels. *Physiol Rev* 82, 503-568.

Jimenez, F., Martin-Morris, L.E., Velasco, L., Chu, H., Sierra, J., Rosen, D.R., and White, K. (1995). vnd, a gene required for early neurogenesis of *Drosophila*, encodes a homeodomain protein. *EMBO J* 14, 3487-3495.

Johnson, O., Becnel, J., and Nichols, C.D. (2009). Serotonin 5-HT(2) and 5-HT(1A)-like receptors differentially modulate aggressive behaviors in *Drosophila melanogaster*. *Neuroscience* 158, 1292-1300.

Joseph Sambrook, D.R. (2001). *Molecular Cloning: A Laboratory Manual* (Third Edition), 3 edn (CSH Press).

Joyce, A.R., and Palsson, B.O. (2006). The model organism as a system: integrating 'omics' data sets. *Nat Rev Mol Cell Biol* 7, 198-210.

Kaiser, K. (1990). From gene to phenotype in *Drosophila* and other organisms. *Bioessays* 12, 297-301.

Kalidas, S., and Smith, D.P. (2002). Novel genomic cDNA hybrids produce effective RNA interference in adult *Drosophila*. *Neuron* 33, 177-184.

Kaneko, T., Yano, T., Aggarwal, K., Lim, J.H., Ueda, K., Oshima, Y., Peach, C., Erturk-Hasdemir, D., Goldman, W.E., Oh, B.H., *et al.* (2006). PGRP-LC and PGRP-LE have essential yet distinct functions in the drosophila immune response to monomeric DAP-type peptidoglycan. *Nat Immunol* 7, 715-723.

Karet, F.E., Finberg, K.E., Nelson, R.D., Nayir, A., Mocan, H., Sanjad, S.A., Rodriguez-Soriano, J., Santos, F., Cremers, C.W., Di Pietro, A., *et al.* (1999). Mutations in the gene encoding B1 subunit of H<sup>+</sup>-ATPase cause renal tubular acidosis with sensorineural deafness. *Nat Genet* 21, 84-90.

Kartagener, M., and Stucki, P. (1962). Bronchiectasis with situs inversus. *Arch Pediatr* 79, 193-207.

Kennerdell, J.R., and Carthew, R.W. (2000). Heritable gene silencing in *Drosophila* using double-stranded RNA. *Nat Biotechnol* 18, 896-898.

Kenyon, E., Yu, K., La Cour, M., and Miller, S.S. (1994). Lactate transport mechanisms at apical and basolateral membranes of bovine retinal pigment epithelium. *Am J Physiol* 267, C1561-1573.

Kerr, M., Davies, S.A., and Dow, J.A. (2004). Cell-specific manipulation of second messengers; a toolbox for integrative physiology in *Drosophila*. *Curr Biol* 14, 1468-1474.

Kizawa, H., Kou, I., Iida, A., Sudo, A., Miyamoto, Y., Fukuda, A., Mabuchi, A., Kotani, A., Kawakami, A., Yamamoto, S., *et al.* (2005). An aspartic acid repeat polymorphism in asporin inhibits chondrogenesis and increases susceptibility to osteoarthritis. *Nat Genet* 37, 138-144.

Knowles, M.R., Clarke, L.L., and Boucher, R.C. (1991). Activation by extracellular nucleotides of chloride secretion in the airway epithelia of patients with cystic fibrosis. *N Engl J Med* 325, 533-538.

Knust, E., and Bossinger, O. (2002). Composition and formation of intercellular junctions in epithelial cells. *Science* 298, 1955-1959.

Kondo, T., Inagaki, S., Yasuda, K., and Kageyama, Y. (2006). Rapid construction of *Drosophila* RNAi transgenes using pRISE, a P-element-mediated transformation vector exploiting an in vitro recombination system. *Genes Genet Syst* 81, 129-134.

Konopka, R.J., and Benzer, S. (1971). Clock mutants of *Drosophila melanogaster*. *Proc Natl Acad Sci U S A* 68, 2112-2116.

Kramer, F., White, K., Pauleikhoff, D., Gehrig, A., Passmore, L., Rivera, A., Rudolph, G., Kellner, U., Andrassi, M., Lorenz, B., *et al.* (2000). Mutations in the VMD2 gene are associated with juvenile-onset vitelliform macular dystrophy (Best disease) and adult vitelliform macular dystrophy but not age-related macular degeneration. *Eur J Hum Genet* 8, 286-292.

Krogh, A. (1929). The Progress of Physiology. *Science* 70, 200-204.

Kunzelmann, K., and Mall, M. (2002). Electrolyte transport in the mammalian colon: mechanisms and implications for disease. *Physiol Rev* 82, 245-289.

- Kunzelmann, K., Milenkovic, V.M., Spitzner, M., Soria, R.B., and Schreiber, R. (2007). Calcium-dependent chloride conductance in epithelia: is there a contribution by Bestrophin? *Pflugers Arch* 454, 879-889.
- Kwon, S.Y., Xiao, H., Glover, B.P., Tjian, R., Wu, C., and Badenhorst, P. (2008). The nucleosome remodeling factor (NURF) regulates genes involved in *Drosophila* innate immunity. *Dev Biol* 316, 538-547.
- Lasorsa, F.M., Pinton, P., Palmieri, L., Scarcia, P., Rottensteiner, H., Rizzuto, R., and Palmieri, F. (2008). Peroxisomes as novel players in cell calcium homeostasis. *J Biol Chem* 283, 15300-15308.
- Lasorsa, F.M., Scarcia, P., Erdmann, R., Palmieri, F., Rottensteiner, H., and Palmieri, L. (2004). The yeast peroxisomal adenine nucleotide transporter: characterization of two transport modes and involvement in DeltapH formation across peroxisomal membranes. *Biochem J* 381, 581-585.
- Leblanc, N., Ledoux, J., Saleh, S., Sanguinetti, A., Angermann, J., O'Driscoll, K., Britton, F., Perrino, B.A., and Greenwood, I.A. (2005). Regulation of calcium-activated chloride channels in smooth muscle cells: a complex picture is emerging. *Can J Physiol Pharmacol* 83, 541-556.
- Leopold, P., and Perrimon, N. (2007). *Drosophila* and the genetics of the internal milieu. *Nature* 450, 186-188.
- Levashina, E.A., Ohresser, S., Lemaitre, B., and Imler, J.L. (1998). Two distinct pathways can control expression of the gene encoding the *Drosophila* antimicrobial peptide metchnikowin. *J Mol Biol* 278, 515-527.
- Levin, M., and Palmer, A.R. (2007). Left-right patterning from the inside out: widespread evidence for intracellular control. *Bioessays* 29, 271-287.
- Lewin, R. (1986). First success with reverse genetics. *Science* 233, 159-160.
- Li, X., Baumgart, E., Dong, G.X., Morrell, J.C., Jimenez-Sanchez, G., Valle, D., Smith, K.D., and Gould, S.J. (2002). PEX11alpha is required for peroxisome proliferation in response to 4-phenylbutyrate but is dispensable for peroxisome proliferator-activated receptor alpha-mediated peroxisome proliferation. *Mol Cell Biol* 22, 8226-8240.
- Li, X., and Gould, S.J. (2002). PEX11 promotes peroxisome division independently of peroxisome metabolism. *J Cell Biol* 156, 643-651.
- Ling, K.H., Hewitt, C.A., Beissbarth, T., Hyde, L., Banerjee, K., Cheah, P.S., Cannon, P.Z., Hahn, C.N., Thomas, P.Q., Smyth, G.K., *et al.* (2009). Molecular networks involved in mouse cerebral corticogenesis and spatio-temporal regulation of Sox4 and Sox11 novel antisense transcripts revealed by transcriptome profiling. *Genome Biol* 10, R104.
- Lipicky, R.J., and Bryant, S.H. (1971). Ion content, potassium efflux and cable properties of myotonic, human, external-intercostal muscle. *Trans Am Neurol Assoc* 96, 34-38.

- Lipicky, R.J., Bryant, S.H., and Salmon, J.H. (1971). Cable parameters, sodium, potassium, chloride, and water content, and potassium efflux in isolated external intercostal muscle of normal volunteers and patients with myotonia congenita. *J Clin Invest* 50, 2091-2103.
- Liu, Y., and Lehmann, M. (2008a). Genes and biological processes controlled by the *Drosophila* FOXA orthologue Fork head. *Insect Mol Biol* 17, 91-101.
- Liu, Y., and Lehmann, M. (2008b). A genomic response to the yeast transcription factor GAL4 in *Drosophila*. *Fly (Austin)* 2, 92-98.
- Lopez-Gracia, M.L., and Ros, M.A. (2007). Left-right asymmetry in vertebrate development. *Adv Anat Embryol Cell Biol* 188, 1-121, back cover.
- MacLeish, P.R., and Nurse, C.A. (2007). Ion channel compartments in photoreceptors: evidence from salamander rods with intact and ablated terminals. *J Neurophysiol* 98, 86-95.
- MacPherson, M.R., Broderick, K.E., Graham, S., Day, J.P., Houslay, M.D., Dow, J.A., and Davies, S.A. (2004a). The *dg2* (for) gene confers a renal phenotype in *Drosophila* by modulation of cGMP-specific phosphodiesterase. *J Exp Biol* 207, 2769-2776.
- MacPherson, M.R., Lohmann, S.M., and Davies, S.A. (2004b). Analysis of *Drosophila* cGMP-dependent protein kinases and assessment of their *in vivo* roles by targeted expression in a renal transporting epithelium. *J Biol Chem* 279, 40026-40034.
- MacPherson, M.R., Pollock, V.P., Broderick, K.E., Kean, L., O'Connell, F.C., Dow, J.A., and Davies, S.A. (2001). Model organisms: new insights into ion channel and transporter function. L-type calcium channels regulate epithelial fluid transport in *Drosophila melanogaster*. *Am J Physiol Cell Physiol* 280, C394-407.
- MacPherson, M.R., Pollock, V.P., Kean, L., Southall, T.D., Giannakou, M.E., Broderick, K.E., Dow, J.A., Hardie, R.C., and Davies, S.A. (2005). Transient receptor potential-like channels are essential for calcium signaling and fluid transport in a *Drosophila* epithelium. *Genetics* 169, 1541-1552.
- Maddrell, S.H. (1991). The fastest fluid-secreting cell known: the upper Malpighian tubule cell of *Rhodnius*. *BioEssays*, 357-362.
- Mall, M., Bleich, M., Schurlein, M., Kuhr, J., Seydewitz, H.H., Brandis, M., Greger, R., and Kunzelmann, K. (1998). Cholinergic ion secretion in human colon requires coactivation by cAMP. *Am J Physiol* 275, G1274-1281.
- Manak, J.R., Dike, S., Sementchenko, V., Kapranov, P., Biemar, F., Long, J., Cheng, J., Bell, I., Ghosh, S., Piccolboni, A., *et al.* (2006). Biological function of unannotated transcription during the early development of *Drosophila melanogaster*. *Nat Genet* 38, 1151-1158.
- Mardis, E.R. (2011). A decade's perspective on DNA sequencing technology. *Nature* 470, 198-203.

- Marmorstein, A.D., Cross, H.E., and Peachey, N.S. (2009). Functional roles of bestrophins in ocular epithelia. *Prog Retin Eye Res* 28, 206-226.
- Marmorstein, A.D., and Marmorstein, L.Y. (2007). The challenge of modeling macular degeneration in mice. *Trends Genet* 23, 225-231.
- Marmorstein, A.D., Marmorstein, L.Y., Rayborn, M., Wang, X., Hollyfield, J.G., and Petrukhin, K. (2000). Bestrophin, the product of the Best vitelliform macular dystrophy gene (VMD2), localizes to the basolateral plasma membrane of the retinal pigment epithelium. *Proc Natl Acad Sci U S A* 97, 12758-12763.
- Marmorstein, L.Y., McLaughlin, P.J., Stanton, J.B., Yan, L., Crabb, J.W., and Marmorstein, A.D. (2002). Bestrophin interacts physically and functionally with protein phosphatase 2A. *J Biol Chem* 277, 30591-30597.
- Marmorstein, L.Y., Wu, J., McLaughlin, P., Yocom, J., Karl, M.O., Neussert, R., Wimmers, S., Stanton, J.B., Gregg, R.G., Strauss, O., *et al.* (2006). The light peak of the electroretinogram is dependent on voltage-gated calcium channels and antagonized by bestrophin (best-1). *J Gen Physiol* 127, 577-589.
- Marquardt, A., Stohr, H., Passmore, L.A., Kramer, F., Rivera, A., and Weber, B.H. (1998). Mutations in a novel gene, VMD2, encoding a protein of unknown properties cause juvenile-onset vitelliform macular dystrophy (Best's disease). *Hum Mol Genet* 7, 1517-1525.
- Marquez, J., de la Oliva, A.R., Mates, J.M., Segura, J.A., and Alonso, F.J. (2006). Glutaminase: a multifaceted protein not only involved in generating glutamate. *Neurochem Int* 48, 465-471.
- McGettigan, J., McLennan, R.K., Broderick, K.E., Kean, L., Allan, A.K., Cabrero, P., Regulski, M.R., Pollock, V.P., Gould, G.W., Davies, S.A., *et al.* (2005). Insect renal tubules constitute a cell-autonomous immune system that protects the organism against bacterial infection. *Insect Biochem Mol Biol* 35, 741-754.
- Melvin, J.E., Yule, D., Shuttleworth, T., and Begenisich, T. (2005). Regulation of fluid and electrolyte secretion in salivary gland acinar cells. *Annu Rev Physiol* 67, 445-469.
- Menteyne, A., Burdakov, A., Charpentier, G., Petersen, O.H., and Cancela, J.M. (2006). Generation of specific Ca(2+) signals from Ca(2+) stores and endocytosis by differential coupling to messengers. *Curr Biol* 16, 1931-1937.
- Micchelli, C.A., and Perrimon, N. (2006). Evidence that stem cells reside in the adult *Drosophila* midgut epithelium. *Nature* 439, 475-479.
- Miklos, G.L., and Rubin, G.M. (1996). The role of the genome project in determining gene function: insights from model organisms. *Cell* 86, 521-529.
- Miledi, R. (1982). A calcium-dependent transient outward current in *Xenopus laevis* oocytes. *Proc R Soc Lond B Biol Sci* 215, 491-497.
- Milenkovic, M., De Deken, X., Jin, L., De Felice, M., Di Lauro, R., Dumont, J.E., Corvilain, B., and Miot, F. (2007a). Duox expression and related H2O2

measurement in mouse thyroid: onset in embryonic development and regulation by TSH in adult. *J Endocrinol* 192, 615-626.

Milenkovic, V.M., Rivera, A., Horling, F., and Weber, B.H. (2007b). Insertion and topology of normal and mutant bestrophin-1 in the endoplasmic reticulum membrane. *J Biol Chem* 282, 1313-1321.

Milenkovic, V.M., Soria, R.B., Aldehni, F., Schreiber, R., and Kunzelmann, K. (2009). Functional assembly and purinergic activation of bestrophins. *Pflugers Arch* 458, 431-441.

Miller, F.J., Jr., Filali, M., Huss, G.J., Stanic, B., Chamseddine, A., Barna, T.J., and Lamb, F.S. (2007). Cytokine activation of nuclear factor kappa B in vascular smooth muscle cells requires signaling endosomes containing Nox1 and ClC-3. *Circ Res* 101, 663-671.

Mirza, S.P., and Olivier, M. (2008). Methods and approaches for the comprehensive characterization and quantification of cellular proteomes using mass spectrometry. *Physiol Genomics* 33, 3-11.

Mitsuuchi, Y., Kawamoto, T., Miyahara, K., Ulick, S., Morton, D.H., Naiki, Y., Kuribayashi, I., Toda, K., Hara, T., Orii, T., *et al.* (1993). Congenitally defective aldosterone biosynthesis in humans: inactivation of the P-450C18 gene (CYP11B2) due to nucleotide deletion in CMO I deficient patients. *Biochem Biophys Res Commun* 190, 864-869.

Miura, S., Kasuya-Arai, I., Mori, H., Miyazawa, S., Osumi, T., Hashimoto, T., and Fujiki, Y. (1992). Carboxyl-terminal consensus Ser-Lys-Leu-related tripeptide of peroxisomal proteins functions in vitro as a minimal peroxisome-targeting signal. *J Biol Chem* 267, 14405-14411.

Monnier, V., Girardot, F., Audin, W., and Tricoire, H. (2002). Control of oxidative stress resistance by IP3 kinase in *Drosophila melanogaster*. *Free Radic Biol Med* 33, 1250-1259.

Mourikis, P., Hurlbut, G.D., and Artavanis-Tsakonas, S. (2006). Enigma, a mitochondrial protein affecting lifespan and oxidative stress response in *Drosophila*. *Proc Natl Acad Sci U S A* 103, 1307-1312.

Mumbengegwi, D.R., Li, Q., Li, C., Bear, C.E., and Engelhardt, J.F. (2008). Evidence for a superoxide permeability pathway in endosomal membranes. *Mol Cell Biol* 28, 3700-3712.

Mustacchi, R., Hohmann, S., and Nielsen, J. (2006). Yeast systems biology to unravel the network of life. *Yeast* 23, 227-238.

Naikkhwah, W., and O'Donnell, M.J. (2012). Phenotypic plasticity in response to dietary salt stress: Na<sup>+</sup> and K<sup>+</sup> transport by the gut of *Drosophila melanogaster* larvae. *J Exp Biol* 215, 461-470.

Nelson, W.J. (2003). Adaptation of core mechanisms to generate cell polarity. *Nature* 422, 766-774.

- Neuberger, G., Maurer-Stroh, S., Eisenhaber, B., Hartig, A., and Eisenhaber, F. (2003a). Motif refinement of the peroxisomal targeting signal 1 and evaluation of taxon-specific differences. *J Mol Biol* 328, 567-579.
- Neuberger, G., Maurer-Stroh, S., Eisenhaber, B., Hartig, A., and Eisenhaber, F. (2003b). Prediction of peroxisomal targeting signal 1 containing proteins from amino acid sequence. *J Mol Biol* 328, 581-592.
- Neussert, R., Muller, C., Milenkovic, V.M., and Strauss, O. (2010). The presence of bestrophin-1 modulates the Ca<sup>2+</sup> recruitment from Ca<sup>2+</sup> stores in the ER. *Pflugers Arch* 460, 163-175.
- Nichols, C.D. (2007). 5-HT<sub>2</sub> receptors in *Drosophila* are expressed in the brain and modulate aspects of circadian behaviors. *Dev Neurobiol* 67, 752-763.
- Nilius, B., and Droogmans, G. (2003). Amazing chloride channels: an overview. *Acta Physiol Scand* 177, 119-147.
- Novarino, G., Weinert, S., Rickheit, G., and Jentsch, T.J. (2010). Endosomal chloride-proton exchange rather than chloride conductance is crucial for renal endocytosis. *Science* 328, 1398-1401.
- Nuttall, J.M., Motley, A., and Hettema, E.H. (2011). Peroxisome biogenesis: recent advances. *Curr Opin Cell Biol* 23, 421-426.
- Nuwaysir, E.F., Huang, W., Albert, T.J., Singh, J., Nuwaysir, K., Pitas, A., Richmond, T., Gorski, T., Berg, J.P., Ballin, J., *et al.* (2002). Gene expression analysis using oligonucleotide arrays produced by maskless photolithography. *Genome Res* 12, 1749-1755.
- O'Donnell, M.J., and Maddrell, S.H. (1995). Fluid reabsorption and ion transport by the lower Malpighian tubules of adult female *Drosophila*. *J Exp Biol* 198 ( Pt 8), 1647-1653.
- O'Donnell, M.J., Rheault, M.R., Davies, S.A., Rosay, P., Harvey, B.J., Maddrell, S.H., Kaiser, K., and Dow, J.A. (1998). Hormonally controlled chloride movement across *Drosophila* tubules is via ion channels in stellate cells. *Am J Physiol* 274, R1039-1049.
- Ohlstein, B., and Spradling, A. (2006). The adult *Drosophila* posterior midgut is maintained by pluripotent stem cells. *Nature* 439, 470-474.
- Opalinski, L., Kiel, J.A., Williams, C., Veenhuis, M., and van der Klei, I.J. (2011). Membrane curvature during peroxisome fission requires Pex11. *EMBO J* 30, 5-16.
- Orkin, S.H. (1986). Reverse genetics and human disease. *Cell* 47, 845-850.
- Owusu-Ansah, E., and Banerjee, U. (2009). Reactive oxygen species prime *Drosophila* haematopoietic progenitors for differentiation. *Nature* 461, 537-541.
- Palmieri, L., Rottensteiner, H., Girzalsky, W., Scarcia, P., Palmieri, F., and Erdmann, R. (2001). Identification and functional reconstitution of the yeast peroxisomal adenine nucleotide transporter. *EMBO J* 20, 5049-5059.

- Parks, D.A., and Granger, D.N. (1986). Xanthine oxidase: biochemistry, distribution and physiology. *Acta Physiol Scand Suppl* 548, 87-99.
- Petrukhin, K., Koisti, M.J., Bakall, B., Li, W., Xie, G., Marknell, T., Sandgren, O., Forsman, K., Holmgren, G., Andreasson, S., *et al.* (1998). Identification of the gene responsible for Best macular dystrophy. *Nat Genet* 19, 241-247.
- Pfeiffer, B.D., Ngo, T.T., Hibbard, K.L., Murphy, C., Jenett, A., Truman, J.W., and Rubin, G.M. (2010). Refinement of tools for targeted gene expression in *Drosophila*. *Genetics* 186, 735-755.
- Pifferi, S., Dibattista, M., Sagheddu, C., Boccaccio, A., Al Qteishat, A., Ghirardi, F., Tirindelli, R., and Menini, A. (2009). Calcium-activated chloride currents in olfactory sensory neurons from mice lacking bestrophin-2. *J Physiol* 587, 4265-4279.
- Pifferi, S., Pascarella, G., Boccaccio, A., Mazzatenta, A., Gustincich, S., Menini, A., and Zucchelli, S. (2006). Bestrophin-2 is a candidate calcium-activated chloride channel involved in olfactory transduction. *Proc Natl Acad Sci U S A* 103, 12929-12934.
- Pinckers, A., Cuyppers, M.H., and Aandekerck, A.L. (1996). The EOG in Best's disease and dominant cystoid macular dystrophy (DCMD). *Ophthalmic Genet* 17, 103-108.
- Pinton, P., Ferrari, D., Rapizzi, E., Di Virgilio, F., Pozzan, T., and Rizzuto, R. (2001). The Ca<sup>2+</sup> concentration of the endoplasmic reticulum is a key determinant of ceramide-induced apoptosis: significance for the molecular mechanism of Bcl-2 action. *EMBO J* 20, 2690-2701.
- Piwon, N., Gunther, W., Schwake, M., Bosl, M.R., and Jentsch, T.J. (2000). ClC-5 Cl<sup>-</sup> channel disruption impairs endocytosis in a mouse model for Dent's disease. *Nature* 408, 369-373.
- Planells-Cases, R., and Jentsch, T.J. (2009). Chloride channelopathies. *Biochim Biophys Acta* 1792, 173-189.
- Poggi-Travert, F., Fournier, B., Poll-The, B.T., and Saudubray, J.M. (1995). Clinical approach to inherited peroxisomal disorders. *J Inherit Metab Dis* 18 Suppl 1, 1-18.
- Pollock, V.P., Radford, J.C., Pyne, S., Hasan, G., Dow, J.A., and Davies, S.A. (2003). NorpA and itpr mutants reveal roles for phospholipase C and inositol (1,4,5)- trisphosphate receptor in *Drosophila melanogaster* renal function. *J Exp Biol* 206, 901-911.
- Predel, R., and Wegener, C. (2006). Biology of the CAPA peptides in insects. *Cell Mol Life Sci* 63, 2477-2490.
- Proenza, C., O'Brien, J., Nakai, J., Mukherjee, S., Allen, P.D., and Beam, K.G. (2002). Identification of a region of RyR1 that participates in allosteric coupling with the alpha(1S) (Ca(V)1.1) II-III loop. *J Biol Chem* 277, 6530-6535.

- Purdue, P.E., and Lazarow, P.B. (2001). Peroxisome biogenesis. *Annu Rev Cell Dev Biol* 17, 701-752.
- Qu, Z., Chien, L.T., Cui, Y., and Hartzell, H.C. (2006). The anion-selective pore of the bestrophins, a family of chloride channels associated with retinal degeneration. *J Neurosci* 26, 5411-5419.
- Qu, Z., Fischmeister, R., and Hartzell, C. (2004). Mouse bestrophin-2 is a bona fide Cl(-) channel: identification of a residue important in anion binding and conduction. *J Gen Physiol* 123, 327-340.
- Qu, Z., and Hartzell, C. (2004). Determinants of anion permeation in the second transmembrane domain of the mouse bestrophin-2 chloride channel. *J Gen Physiol* 124, 371-382.
- Qu, Z., Wei, R.W., Mann, W., and Hartzell, H.C. (2003). Two bestrophins cloned from *Xenopus laevis* oocytes express Ca(2+)-activated Cl(-) currents. *J Biol Chem* 278, 49563-49572.
- Quinn, L., Coombe, M., Mills, K., Daish, T., Colussi, P., Kumar, S., and Richardson, H. (2003). Buffy, a *Drosophila* Bcl-2 protein, has anti-apoptotic and cell cycle inhibitory functions. *EMBO J* 22, 3568-3579.
- Radford, J.C., Davies, S.A., and Dow, J.A. (2002). Systematic G-protein-coupled receptor analysis in *Drosophila melanogaster* identifies a leucokinin receptor with novel roles. *J Biol Chem* 277, 38810-38817.
- Raghu, P., Colley, N.J., Webel, R., James, T., Hasan, G., Danin, M., Selinger, Z., and Hardie, R.C. (2000). Normal phototransduction in *Drosophila* photoreceptors lacking an InsP(3) receptor gene. *Mol Cell Neurosci* 15, 429-445.
- Raychaudhury, B., Gupta, S., Banerjee, S., and Datta, S.C. (2006). Peroxisome is a reservoir of intracellular calcium. *Biochim Biophys Acta* 1760, 989-992.
- Reaume, A.G., Clark, S.H., and Chovnick, A. (1989). Xanthine dehydrogenase is transported to the *Drosophila* eye. *Genetics* 123, 503-509.
- Reddy, J.K., and Hashimoto, T. (2001). Peroxisomal beta-oxidation and peroxisome proliferator-activated receptor alpha: an adaptive metabolic system. *Annu Rev Nutr* 21, 193-230.
- Reim, I., and Frasch, M. (2005). The Dorsocross T-box genes are key components of the regulatory network controlling early cardiogenesis in *Drosophila*. *Development* 132, 4911-4925.
- RF, C. (1982). *The insects: structure and function*. (London, Hodder & Stoughton).
- Rheault, M.R., Okech, B.A., Keen, S.B., Miller, M.M., Meleshkevitch, E.A., Linser, P.J., Boudko, D.Y., and Harvey, W.R. (2007). Molecular cloning, phylogeny and localization of AgNHA1: the first Na<sup>+</sup>/H<sup>+</sup> antiporter (NHA) from a metazoan, *Anopheles gambiae*. *J Exp Biol* 210, 3848-3861.
- Richards, S., Liu, Y., Bettencourt, B.R., Hradecky, P., Letovsky, S., Nielsen, R., Thornton, K., Hubisz, M.J., Chen, R., Meisel, R.P., *et al.* (2005). Comparative

- genome sequencing of *Drosophila pseudoobscura*: chromosomal, gene, and cis-element evolution. *Genome Res* 15, 1-18.
- Ritzka, M., Stanke, F., Jansen, S., Gruber, A.D., Pusch, L., Woelfl, S., Veeze, H.J., Halley, D.J., and Tummler, B. (2004). The CLCA gene locus as a modulator of the gastrointestinal basic defect in cystic fibrosis. *Hum Genet* 115, 483-491.
- Rizzuto, R., and Pozzan, T. (2006). Microdomains of intracellular Ca<sup>2+</sup>: molecular determinants and functional consequences. *Physiol Rev* 86, 369-408.
- Roberts, D.B., Jowett, T., Hughes, J., Smith, D.F., and Glover, D.M. (1991). The major serum protein of *Drosophila* larvae, larval serum protein 1, is dispensable. *Eur J Biochem* 195, 195-201.
- Robinson, D.N., and Cooley, L. (1997). *Drosophila* kelch is an oligomeric ring canal actin organizer. *J Cell Biol* 138, 799-810.
- Rorth, P. (1996). A modular misexpression screen in *Drosophila* detecting tissue-specific phenotypes. *Proc Natl Acad Sci U S A* 93, 12418-12422.
- Rorth, P., Szabo, K., Bailey, A., Lavery, T., Rehm, J., Rubin, G.M., Weigmann, K., Milan, M., Benes, V., Ansorge, W., *et al.* (1998). Systematic gain-of-function genetics in *Drosophila*. *Development* 125, 1049-1057.
- Rosay, P., Davies, S.A., Yu, Y., Sozen, A., Kaiser, K., and Dow, J.A. (1997). Cell-type specific calcium signalling in a *Drosophila* epithelium. *J Cell Sci* 110 ( Pt 15), 1683-1692.
- Rottensteiner, H., and Theodoulou, F.L. (2006). The ins and outs of peroxisomes: co-ordination of membrane transport and peroxisomal metabolism. *Biochim Biophys Acta* 1763, 1527-1540.
- Rubin, G.M., Yandell, M.D., Wortman, J.R., Gabor Miklos, G.L., Nelson, C.R., Hariharan, I.K., Fortini, M.E., Li, P.W., Apweiler, R., Fleischmann, W., *et al.* (2000). Comparative genomics of the eukaryotes. *Science* 287, 2204-2215.
- Rucktaschel, R., Girzalsky, W., and Erdmann, R. (2011). Protein import machineries of peroxisomes. *Biochim Biophys Acta* 1808, 892-900.
- Ruddle, F.H. (1982). Reverse genetics as a means of understanding and treating genetic disease. *Adv Neurol* 35, 239-242.
- Ryder, E., Ashburner, M., Bautista-Llacer, R., Drummond, J., Webster, J., Johnson, G., Morley, T., Chan, Y.S., Blows, F., Coulson, D., *et al.* (2007). The DrosDel deletion collection: a *Drosophila* genomewide chromosomal deficiency resource. *Genetics* 177, 615-629.
- Saiki, R.K., Gelfand, D.H., Stoffel, S., Scharf, S.J., Higuchi, R., Horn, G.T., Mullis, K.B., and Erlich, H.A. (1988). Primer-directed enzymatic amplification of DNA with a thermostable DNA polymerase. *Science* 239, 487-491.
- Salkoff, L., and Wyman, R. (1981). Genetic modification of potassium channels in *Drosophila* Shaker mutants. *Nature* 293, 228-230.

- Scheel, O., Zdebik, A.A., Lourdel, S., and Jentsch, T.J. (2005). Voltage-dependent electrogenic chloride/proton exchange by endosomal CLC proteins. *Nature* 436, 424-427.
- Schena, M., Shalon, D., Davis, R.W., and Brown, P.O. (1995). Quantitative monitoring of gene expression patterns with a complementary DNA microarray. *Science* 270, 467-470.
- Schluter, A., Real-Chicharro, A., Gabaldon, T., Sanchez-Jimenez, F., and Pujol, A. (2010). PeroxisomeDB 2.0: an integrative view of the global peroxisomal metabolome. *Nucleic Acids Res* 38, D800-805.
- Schmitzova, J., Kludiny, J., Albert, S., Schroder, W., Schreckengost, W., Hanes, J., Judova, J., and Simuth, J. (1998). A family of major royal jelly proteins of the honeybee *Apis mellifera* L. *Cell Mol Life Sci* 54, 1020-1030.
- Schneider, I. (1972). Cell lines derived from late embryonic stages of *Drosophila melanogaster*. *J Embryol Exp Morphol* 27, 353-365.
- Schweikl, H., Klein, U., Schindlbeck, M., and Wieczorek, H. (1989). A vacuolar-type ATPase, partially purified from potassium transporting plasma membranes of tobacco hornworm midgut. *J Biol Chem* 264, 11136-11142.
- Schwiebert, E.M., Benos, D.J., Egan, M.E., Stutts, M.J., and Guggino, W.B. (1999). CFTR is a conductance regulator as well as a chloride channel. *Physiol Rev* 79, S145-166.
- Sharma, N., Berbari, N.F., and Yoder, B.K. (2008). Ciliary dysfunction in developmental abnormalities and diseases. *Curr Top Dev Biol* 85, 371-427.
- Shoemaker, D.D., Schadt, E.E., Armour, C.D., He, Y.D., Garrett-Engele, P., McDonagh, P.D., Loerch, P.M., Leonardson, A., Lum, P.Y., Cavet, G., *et al.* (2001). Experimental annotation of the human genome using microarray technology. *Nature* 409, 922-927.
- Simons, M., and Mlodzik, M. (2008). Planar cell polarity signaling: from fly development to human disease. *Annu Rev Genet* 42, 517-540.
- Singh, S.R., Liu, W., and Hou, S.X. (2007). The adult *Drosophila* malpighian tubules are maintained by multipotent stem cells. *Cell Stem Cell* 1, 191-203.
- Skaer, H., ed. (1993). *Development of the alimentary canal* (NY, Cold Spring Harbor Press).
- Soderberg, J.A., Birse, R.T., and Nassel, D.R. (2011). Insulin production and signaling in renal tubules of *Drosophila* is under control of tachykinin-related peptide and regulates stress resistance. *PLoS One* 6, e19866.
- Southall, T.D., Terhzaz, S., Cabrero, P., Chintapalli, V.R., Evans, J.M., Dow, J.A., and Davies, S.A. (2006). Novel subcellular locations and functions for secretory pathway  $\text{Ca}^{2+}/\text{Mn}^{2+}$ -ATPases. *Physiol Genomics* 26, 35-45.
- Sozen, M.A., Armstrong, J.D., Yang, M., Kaiser, K., and Dow, J.A. (1997). Functional domains are specified to single-cell resolution in a *Drosophila* epithelium. *Proc Natl Acad Sci U S A* 94, 5207-5212.

- Spradling, A.C., and Rubin, G.M. (1982). Transposition of cloned P elements into *Drosophila* germ line chromosomes. *Science* 218, 341-347.
- Stanewsky, R., Kaneko, M., Emery, P., Beretta, B., Wager-Smith, K., Kay, S.A., Rosbash, M., and Hall, J.C. (1998). The cryb mutation identifies cryptochrome as a circadian photoreceptor in *Drosophila*. *Cell* 95, 681-692.
- Stanton, J.B., Goldberg, A.F., Hoppe, G., Marmorstein, L.Y., and Marmorstein, A.D. (2006). Hydrodynamic properties of porcine bestrophin-1 in Triton X-100. *Biochim Biophys Acta* 1758, 241-247.
- Steinberg, S.J., Raymond, G.V., Braverman, N.E., and Moser, A.B. (1993). *Peroxisome Biogenesis Disorders, Zellweger Syndrome Spectrum*.
- Steinmeyer, K., Schwappach, B., Bens, M., Vandewalle, A., and Jentsch, T.J. (1995). Cloning and functional expression of rat CLC-5, a chloride channel related to kidney disease. *J Biol Chem* 270, 31172-31177.
- Stergiopoulos, K., Cabrero, P., Davies, S.A., and Dow, J.A. (2009). Salty dog, an SLC5 symporter, modulates *Drosophila* response to salt stress. *Physiol Genomics* 37, 1-11.
- Stewart, A.K., Yamamoto, A., Nakakuki, M., Kondo, T., Alper, S.L., and Ishiguro, H. (2009). Functional coupling of apical Cl<sup>-</sup>/HCO<sub>3</sub><sup>-</sup> exchange with CFTR in stimulated HCO<sub>3</sub><sup>-</sup> secretion by guinea pig interlobular pancreatic duct. *Am J Physiol Gastrointest Liver Physiol* 296, G1307-1317.
- Stirpe, F., and Della Corte, E. (1969). The regulation of rat liver xanthine oxidase. Conversion in vitro of the enzyme activity from dehydrogenase (type D) to oxidase (type O). *J Biol Chem* 244, 3855-3863.
- Stobrawa, S.M., Breiderhoff, T., Takamori, S., Engel, D., Schweizer, M., Zdebik, A.A., Bosl, M.R., Ruether, K., Jahn, H., Draguhn, A., *et al.* (2001). Disruption of CLC-3, a chloride channel expressed on synaptic vesicles, leads to a loss of the hippocampus. *Neuron* 29, 185-196.
- Strauss, O. (2005). The retinal pigment epithelium in visual function. *Physiol Rev* 85, 845-881.
- Stuart, L.M., Boulais, J., Charriere, G.M., Hennessy, E.J., Brunet, S., Jutras, I., Goyette, G., Rondeau, C., Letarte, S., Huang, H., *et al.* (2007). A systems biology analysis of the *Drosophila* phagosome. *Nature* 445, 95-101.
- Sun, H., Tsunenari, T., Yau, K.W., and Nathans, J. (2002). The vitelliform macular dystrophy protein defines a new family of chloride channels. *Proc Natl Acad Sci U S A* 99, 4008-4013.
- Sutherland, M.J., and Ware, S.M. (2009). Disorders of left-right asymmetry: heterotaxy and situs inversus. *Am J Med Genet C Semin Med Genet* 151C, 307-317.
- Suzuki, M. (2006). The *Drosophila* tweety family: molecular candidates for large-conductance Ca<sup>2+</sup>-activated Cl<sup>-</sup> channels. *Exp Physiol* 91, 141-147.

- Takashima, S., Mkrtchyan, M., Younossi-Hartenstein, A., Merriam, J.R., and Hartenstein, V. (2008). The behaviour of *Drosophila* adult hindgut stem cells is controlled by Wnt and Hh signalling. *Nature* *454*, 651-655.
- Tavsanli, B.C., Pappu, K.S., Mehta, S.Q., and Mardon, G. (2001). Dbest1, a *Drosophila* homolog of human Bestrophin, is not required for viability or photoreceptor integrity. *Genesis* *31*, 130-136.
- Tepass, U., and Hartenstein, V. (1994). Epithelium formation in the *Drosophila* midgut depends on the interaction of endoderm and mesoderm. *Development* *120*, 579-590.
- Terasawa, Y., Ladha, Z., Leonard, S.W., Morrow, J.D., Newland, D., Sanan, D., Packer, L., Traber, M.G., and Farese, R.V., Jr. (2000). Increased atherosclerosis in hyperlipidemic mice deficient in alpha-tocopherol transfer protein and vitamin E. *Proc Natl Acad Sci U S A* *97*, 13830-13834.
- Terhzaz, S., O'Connell, F.C., Pollock, V.P., Kean, L., Davies, S.A., Veenstra, J.A., and Dow, J.A. (1999a). Isolation and characterization of a leucokinin-like peptide of *Drosophila melanogaster*. *J Exp Biol* *202*, 3667-3676.
- Terhzaz, S., O'Connell, F.C., Pollock, V.P., Kean, L., Davies, S.A., Veenstra, J.A., and Dow, J.A. (1999b). Isolation and characterization of a leucokinin-like peptide of *Drosophila melanogaster*. *J Exp Biol* *202 Pt 24*, 3667-3676.
- Terhzaz, S., Southall, T.D., Lilley, K.S., Kean, L., Allan, A.K., Davies, S.A., and Dow, J.A. (2006). Differential gel electrophoresis and transgenic mitochondrial calcium reporters demonstrate spatiotemporal filtering in calcium control of mitochondria. *J Biol Chem* *281*, 18849-18858.
- Thoms, S., and Erdmann, R. (2005). Dynamin-related proteins and Pex11 proteins in peroxisome division and proliferation. *FEBS J* *272*, 5169-5181.
- Thummel, C. (2007). To die or not to die--a role for Fork head. *J Cell Biol* *176*, 737-739.
- Tsunenari, T., Nathans, J., and Yau, K.W. (2006). Ca<sup>2+</sup>-activated Cl<sup>-</sup> current from human bestrophin-4 in excised membrane patches. *J Gen Physiol* *127*, 749-754.
- Tsunenari, T., Sun, H., Williams, J., Cahill, H., Smallwood, P., Yau, K.W., and Nathans, J. (2003). Structure-function analysis of the bestrophin family of anion channels. *J Biol Chem* *278*, 41114-41125.
- Tzou, P., Ohresser, S., Ferrandon, D., Capovilla, M., Reichhart, J.M., Lemaitre, B., Hoffmann, J.A., and Imler, J.L. (2000). Tissue-specific inducible expression of antimicrobial peptide genes in *Drosophila* surface epithelia. *Immunity* *13*, 737-748.
- Ureta-Vidal, A., Ettwiller, L., and Birney, E. (2003). Comparative genomics: genome-wide analysis in metazoan eukaryotes. *Nat Rev Genet* *4*, 251-262.
- van den Bosch, H., Schutgens, R.B., Wanders, R.J., and Tager, J.M. (1992). Biochemistry of peroxisomes. *Annu Rev Biochem* *61*, 157-197.

van Iterson, M., t Hoen, P.A., Pedotti, P., Hooiveld, G.J., den Dunnen, J.T., van Ommen, G.J., Boer, J.M., and Menezes, R.X. (2009). Relative power and sample size analysis on gene expression profiling data. *BMC Genomics* 10, 439.

van Roermund, C.W., de Jong, M., L, I.J., van Marle, J., Dansen, T.B., Wanders, R.J., and Waterham, H.R. (2004). The peroxisomal lumen in *Saccharomyces cerevisiae* is alkaline. *J Cell Sci* 117, 4231-4237.

Vandesompele, J., De Preter, K., Pattyn, F., Poppe, B., Van Roy, N., De Paepe, A., and Speleman, F. (2002). Accurate normalization of real-time quantitative RT-PCR data by geometric averaging of multiple internal control genes. *Genome Biol* 3, RESEARCH0034.

Vasu, V.T., Hobson, B., Gohil, K., and Cross, C.E. (2007). Genome-wide screening of alpha-tocopherol sensitive genes in heart tissue from alpha-tocopherol transfer protein null mice (ATTP(-/-)). *FEBS Lett* 581, 1572-1578.

Veenstra, J.A. (2009). Peptidergic paracrine and endocrine cells in the midgut of the fruit fly maggot. *Cell Tissue Res* 336, 309-323.

Venken, K.J., and Bellen, H.J. (2007). Transgenesis upgrades for *Drosophila melanogaster*. *Development* 134, 3571-3584.

Verkman, A.S., and Galiotta, L.J. (2009). Chloride channels as drug targets. *Nat Rev Drug Discov* 8, 153-171.

Vidal, M., and Cagan, R.L. (2006). *Drosophila* models for cancer research. *Curr Opin Genet Dev* 16, 10-16.

Visser, W., van Roermund, C., Ijlst, L., Waterham, H., and Wanders, R. (2007). Metabolite transport across the peroxisomal membrane. *Biochem J* 401, 365-375.

Visser, W.F., Van Roermund, C.W., Ijlst, L., Hellingwerf, K.J., Wanders, R.J., and Waterham, H.R. (2005). Demonstration and characterization of phosphate transport in mammalian peroxisomes. *Biochem J* 389, 717-722.

Wallrath, L.L., Burnett, J.B., and Friedman, T.B. (1990). Molecular characterization of the *Drosophila melanogaster* urate oxidase gene, an ecdysone-repressible gene expressed only in the malpighian tubules. *Mol Cell Biol* 10, 5114-5127.

Wanders, R.J., and Waterham, H.R. (2006). Biochemistry of mammalian peroxisomes revisited. *Annu Rev Biochem* 75, 295-332.

Wang, J., Kean, L., Yang, J., Allan, A.K., Davies, S.A., Herzyk, P., and Dow, J.A. (2004). Function-informed transcriptome analysis of *Drosophila* renal tubule. *Genome Biol* 5, R69.

Watson, J.D., and Crick, F.H. (1953). Molecular structure of nucleic acids; a structure for deoxyribose nucleic acid. *Nature* 171, 737-738.

Wegierski, T., Steffl, D., Kopp, C., Tauber, R., Buchholz, B., Nitschke, R., Kuehn, E.W., Walz, G., and Kottgen, M. (2009). TRPP2 channels regulate apoptosis through the Ca<sup>2+</sup> concentration in the endoplasmic reticulum. *EMBO J* 28, 490-499.

- Weinert, S., Jabs, S., Supanchart, C., Schweizer, M., Gimber, N., Richter, M., Rademann, J., Stauber, T., Kornak, U., and Jentsch, T.J. (2010). Lysosomal pathology and osteopetrosis upon loss of H<sup>+</sup>-driven lysosomal Cl<sup>-</sup> accumulation. *Science* 328, 1401-1403.
- Wessing, A. (1991). Two types of concretions in *Drosophila* tubules as revealed by X-ray microanalysis: A study on urine formation. *Journal of Insect Physiology* 38, 543 - 554.
- Wessing et al., K.Z.a.F.H. (1992). Two Types of Concretion in *Drosophila* Malpighian Tubules as Revealed by X-Ray Microanalysis: A Study on Urine Formation. *J Insect Physiology* 38, 543-554.
- Wheat, C.W., Vogel, H., Wittstock, U., Braby, M.F., Underwood, D., and Mitchell-Olds, T. (2007). The genetic basis of a plant-insect coevolutionary key innovation. *Proc Natl Acad Sci U S A* 104, 20427-20431.
- Wheeler, D., Barrett, T., Benson, D., Bryant, S., Canese, K., Chetvernin, V., Church, D., Dicuccio, M., Edgar, R., Federhen, S., *et al.* (2008). Database resources of the National Center for Biotechnology Information. *Nucleic Acids Res* 36, D13-21.
- Wieczorek, H., Beyenbach, K.W., Huss, M., and Vitavska, O. (2009). Vacuolar-type proton pumps in insect epithelia. *J Exp Biol* 212, 1611-1619.
- Wieczorek, H., Brown, D., Grinstein, S., Ehrenfeld, J., and Harvey, W.R. (1999). Animal plasma membrane energization by proton-motive V-ATPases. *Bioessays* 21, 637-648.
- Wieczorek, H., Putzenlechner, M., Zeiske, W., and Klein, U. (1991). A vacuolar-type proton pump energizes K<sup>+</sup>/H<sup>+</sup> antiport in an animal plasma membrane. *J Biol Chem* 266, 15340-15347.
- Wieczorek, H., Wolfersberger, M.G., Cioffi, M., and Harvey, W.R. (1986). Cation-stimulated ATPase activity in purified plasma membranes from tobacco hornworm midgut. *Biochim Biophys Acta* 857, 271-281.
- Williams, T.A., Mulatero, P., Bosio, M., Lewicka, S., Palermo, M., Veglio, F., and Armanini, D. (2004). A particular phenotype in a girl with aldosterone synthase deficiency. *J Clin Endocrinol Metab* 89, 3168-3172.
- Wolfe, J., Akam, M.E., and Roberts, D.B. (1977). Biochemical and immunological studies on larval serum protein 1, the major haemolymph protein of *Drosophila melanogaster* third-instar larvae. *Eur J Biochem* 79, 47-53.
- Wu, J., Marmorstein, A.D., Striessnig, J., and Peachey, N.S. (2007). Voltage-dependent calcium channel CaV1.3 subunits regulate the light peak of the electroretinogram. *J Neurophysiol* 97, 3731-3735.
- Wu, X.W., Lee, C.C., Muzny, D.M., and Caskey, C.T. (1989). Urate oxidase: primary structure and evolutionary implications. *Proc Natl Acad Sci U S A* 86, 9412-9416.

Yamasaki, M., Thomas, J.M., Churchill, G.C., Garnham, C., Lewis, A.M., Cancela, J.M., Patel, S., and Galione, A. (2005). Role of NAADP and cADPR in the induction and maintenance of agonist-evoked Ca<sup>2+</sup> spiking in mouse pancreatic acinar cells. *Curr Biol* 15, 874-878.

Yang, J., McCart, C., Woods, D.J., Terhzaz, S., Greenwood, K.G., French-Constant, R.H., and Dow, J.A. (2007). A *Drosophila* systems approach to xenobiotic metabolism. *Physiol Genomics* 30, 223-231.

Yang, T., and Poovaiah, B.W. (2002). Hydrogen peroxide homeostasis: activation of plant catalase by calcium/calmodulin. *Proc Natl Acad Sci U S A* 99, 4097-4102.

Yang, Y.D., Cho, H., Koo, J.Y., Tak, M.H., Cho, Y., Shim, W.S., Park, S.P., Lee, J., Lee, B., Kim, B.M., *et al.* (2008). TMEM16A confers receptor-activated calcium-dependent chloride conductance. *Nature* 455, 1210-1215.

Yang, Z., Edenberg, H.J., and Davis, R.L. (2005). Isolation of mRNA from specific tissues of *Drosophila* by mRNA tagging. *Nucleic Acids Res* 33, e148.

Yardley, J., Leroy, B.P., Hart-Holden, N., Lafaut, B.A., Loeys, B., Messiaen, L.M., Perveen, R., Reddy, M.A., Bhattacharya, S.S., Traboulsi, E., *et al.* (2004). Mutations of VMD2 splicing regulators cause nanophthalmos and autosomal dominant vitreoretinopathy (ADVIRC). *Invest Ophthalmol Vis Sci* 45, 3683-3689.

Yeromin, A.V., Roos, J., Stauderman, K.A., and Cahalan, M.D. (2004). A store-operated calcium channel in *Drosophila* S2 cells. *J Gen Physiol* 123, 167-182.

Zaccolo, M., and Movsesian, M.A. (2007). cAMP and cGMP signaling cross-talk: role of phosphodiesterases and implications for cardiac pathophysiology. *Circ Res* 100, 1569-1578.

Zhang, S.O., Box, A.C., Xu, N., Le Men, J., Yu, J., Guo, F., Trimble, R., and Mak, H.Y. (2010a). Genetic and dietary regulation of lipid droplet expansion in *Caenorhabditis elegans*. *Proc Natl Acad Sci U S A* 107, 4640-4645.

Zhang, Y., Stanton, J.B., Wu, J., Yu, K., Hartzell, H.C., Peachey, N.S., Marmorstein, L.Y., and Marmorstein, A.D. (2010b). Suppression of Ca<sup>2+</sup> signaling in a mouse model of Best disease. *Hum Mol Genet* 19, 1108-1118.

Zsembery, A., Strazzabosco, M., and Graf, J. (2000). Ca<sup>2+</sup>-activated Cl<sup>-</sup> channels can substitute for CFTR in stimulation of pancreatic duct bicarbonate secretion. *FASEB J* 14, 2345-2356.